THE GEOLOGY AND MECHANICS OF FORMATION OF THE FORT ROCK DOME, YAVAPAI COUNTY, ARIZONA

Thesis by

Gary S. Fuis

In Partial Fulfillment of the Requirements

for the Degree of

Doctor of Philosophy

California Institute of Technology

Pasadena, California

(Submitted November 6, 1973)

ACKNOWLEDGMENTS

This study was funded by fellowship money from the National Science Foundation, project money from the National Aeronautics and Space Administration, and graduate assistantship money from the California Institute of Technology. The United States Geological Survey supplied logistical support for field work, laboratory work, including chemical analyses and preparation of thin sections, and photogrammetric work, including compilation of a topographic base map.

Three persons to whom I am most indebted for efforts in my behalf in matters of funding and other support for this study are Eugene Shoemaker, Alfred Chidester, and John McCauley, of the United States Geological Survey. Field work was facilitated in many ways by Robert Orr, former foreman of the Fort Rock Ranch, and his wife, Norma, and by William Becker, present owner of the ranch, and his wife, Joan. Arthur Dial, of the U.S. Geological Survey, was of welcome assistance in the field for several weeks near the end of the study. Jan Scott generously and patiently completed drafting of most of the illustrations in this text.

ABSTRACT

The Fort Rock dome, in Yavapai County, Arizona, is a recently discovered circular geological structure, two miles in diameter, which initially aroused interest because of its similarity to an impact crater. Features of the dome that are similar to features of an impact crater include a crater-like depression in its center underlain by brecciated Precambrian igneous and metamorphic rocks, upturned Tertiary volcanic and sedimentary rocks on its rim, radial and tangential faults, and an apron of breccia on its flanks showing a crude inversion of the pre-breccia stratigraphy. Studies by the writer have indicated that the structure is primarily a volcanic dome caused by an intrusion at depth. The crater on top is erosional in origin.

Rocks exposed in the vicinity of the Fort Rock dome range in age from Precambrian to Quaternary. Precambrian rocks include layered metamorphic rocks, cataclasites, granite, granite pegmatite, and veined rocks. These rocks are part of a broad belt of Precambrian rocks exposed in the mountains of central Arizona along the southwestern margin of the Colorado Plateau. Paleozoic sedimentary rocks, seen northeast of the dome, range in age from Cambrian to Mississippian. Tertiary volcanic rocks overlie chiefly Precambrian rocks in a large area, about 1000 square miles in extent, west and south of the dome. Numerous volcanic centers are scattered throughout this area; the Fort Rock dome is one relatively small center. Quaternary deposits include alluvium and terrace deposits.

The chief structures in the region are Basin and Range faults. Between the dome and Seligman, Arizona, to the northeast, north-south normal faults with displacements of hundreds of feet form low, linear ranges and broad valleys. In the Aquarius Mountains, west of the dome, several east-west normal faults offset rocks by hundreds of feet. On the eastern edge of Big Sandy Wash, west of the Aquarius Mountains, a north-south fault with a displacement of 1000 feet is responsible for a major escarpment in the Basin and Range Province that is continuous with the Grand Wash Cliffs to the north. Most Phanerozoic rocks in the region are relatively flat-lying. The Fort Rock dome is an anomalous area where Tertiary rocks are highly deformed.

Precambrian rocks on the Fort Rock dome are similar to older Precambrian rocks at the Grand Canyon, Arizona. Layered metamorphic rocks on the dome include amphibolite, schist, phyllonite, and gneiss. These rocks belong to the epidote-amphibolite metamorphic facies. Cataclasite bodies, which are present in the layered metamorphic rocks, appear to be granite intrusions that are crushed and foliated. Granites and granite pegmatites intrude the layered metamorphic rocks and cataclasites. They are also crushed but are not foliated. The Precambrian rocks are fractured and veined in an east-west shear zone that crosses the southern half of the dome. Veined rocks are covered by Tertiary volcanic rocks on the rim of the crater. Veined rocks in a similar shear zone several miles north of the dome are covered by Tapeats Sandstone, of Cambrian age.

Tertiary volcanic rocks lie on a mid-Tertiary erosion surface that covered most of northwestern Arizona and is responsible for much of

the topography seen today in this area. Volcanic rocks in the vicinity of the Fort Rock dome comprise chiefly two formations, here given the names Crater Pasture Formation and Fort Rock Creek Rhyodacite; the Crater Pasture Formation is the older of the two. In addition to these two formations, several lava flows and intrusive bodies are present which are younger than the Fort Rock Creek Rhyodacite, including a unit herein referred to as the basalt of Buttox Hills. Other volcanic rocks in the region include the Peach Springs Tuff, of middle Miocene age, which overlies the Fort Rock Creek Rhyodacite ten miles west of the dome, and younger Mohon Mountain volcanics, south of Trout Creek.

The Crater Pasture Formation includes a series of lava flows, agglomerates, tuffs, and associated intrusive and sedimentary rocks in the vicinity of the Fort Rock dome. The volcanic rocks range in composition from ultramafic to intermediate. In the vicinity of the dome, eleven chief subunits have been recognized. Reconnaissance mapping has indicated that volcanic rocks in an extensive area west and north of the dome are of similar age and composition and can also be included in this formation. The subunits recognized at the dome include, from oldest to youngest (where relative age is known), a limburgite flow, an olivine-trachyandesite volcanic breccia and flow, a hornblende-trachybasalt flow, a pyroxene-trachyandesite tuff and flow, three hornblende-trachyandesite flows, an olivine and hornblende trachyandesite tuff and conglomerate, a sedimentary breccia, an olivine-trachybasalt tuff and agglomerate, and an olivine-sanidine-trachybasalt flow. Most of these rocks were erupted from vents located on or near the periphery of the Fort Rock dome, and most are traceable for

distances of a mile or less. The sedimentary breccia, which in this report is referred to as the sedimentary breccia of One OClock Wash, is a local deposit on the flanks of the dome that consists of clasts eroded from the dome. This unit was deposited during uplift of the dome. The youngest unit in the formation, an olivine-sanidine-trachybasalt flow, herein referred to as the flow of Fault Canyon, was erupted from a vent on the southwest flank of the dome. This flow apparently came from a magma beneath the dome, which is believed to have been responsible for the uplift.

The Fort Rock Creek Rhyodacite includes a series of ash-flow tuffs and other massive tuffs, volcanic breccias, lava flows, and associated intrusive and sedimentary rocks in the Aquarius Mountains and vicinity. The composition of the volcanic rocks of this formation is chiefly rhyodacite. Subunits recognized are here given the names, in order from oldest to youngest, the sedimentary breccia of Noon Gorge, the Old Stage Road Member, the Three Sisters Butte Member, and the breccia and conglomerate of the Crossing. The sedimentary breccia of Noon Gorge is a local deposit on the flanks of the Fort Rock dome consisting chiefly of clasts eroded from the dome. The Old Stage Road Member is a unit chiefly of non-welded ash-flow tuff that extends throughout the Aquarius Mountains and into surrounding areas. The Three Sisters Butte Member is a unit of interbedded volcanic breccia and massive tuff which is found throughout the Aquarius Mountains. The breccia and conglomerate of the Crossing is chiefly a volcanic breccia; it occurs on the northeast flank of the Aquarius Mountains. The Old Stage Road Member, the Three Sisters Butte Member, and the breccia and conglomerate of the Crossing were erupted from a large rhyodacite center in the Aquarius

Mountains located about 2-1/2 miles southwest of the Fort Rock dome.

The basalt of Buttox Hills is a local flow that overlies ash-flow tuff on the southeast side of the dome. A dike of this unit intrudes rocks on the dome.

Quaternary units include alluvium in washes, older alluvium on terraces, and colluvium. Terrace deposits are extensive east of the Fort Rock dome. They contain abundant clasts of Paleozoic sedimentary rocks that were derived from terrane to the north and east.

Precambrian structures on the dome include folds of different amplitudes in the layered metamorphic rocks and an east-west shear zone in the southern half of the dome. The shear zone, which is characterized by fractured and veined Precambrian rocks, brings together in the dome differing rock assemblages and also rocks of slightly differing metamorphic grade. This shear zone appears to be part of a major discontinuity in Precambrian rocks that is traceable for 70 miles on an aeromagnetic map from near Ashfork, Arizona, to the western edge of the Aquarius Mountains. This discontinuity is associated with Tertiary normal faults and may be an ancient strike-slip fault zone in the Precambrian rocks.

Tertiary structures on the dome include relatively minor faults that pre-date the uplift of the dome and the dome itself, with its associated folds and faults. The dome is a structural dome. Its central part is a low, quaquaversal arch, now deeply eroded. Its edge is, in most places, a sharp monocline. Structural relief on the dome is estimated to be about 900 feet. Dips on the steep-dipping limb of the monocline, where it is sharp, vary from about 40° to about 90°(?) and average about 66°.

Most faults mapped on the dome are confined to the vicinity of the monocline, partly as a result of poor exposure and lack of structural control in the deeply eroded central part of the dome. These faults have chiefly radial and tangential strikes and steep dips, where attitudes can be determined. Normal, dip-slip movement appears to have been dominant, although radial faults may have had a strike-slip component of movement. Block rotations are observed along relatively long faults. Ages of faults, where they can be determined, range from the beginning of uplift, which was signaled by deposition of the sedimentary breccia of One OClock Wash, to after the emplacement of the ash-flow tuff of the Fort Rock Creek Rhyodacite. Major offsets, however, appear to be confined to the times of emplacement of the various units of sedimentary breccia on the flanks of the dome including the sedimentary breccia of One OClock Wash, the sedimentary breccia of Noon Gorge, and a basal sedimentary breccia in the Old Stage Road Member of the Fort Rock Creek Rhyodacite. In addition to mapped faults on the rim of the crater, abundant small faults, with displacements of inches to tens of feet, and lenses of unmineralized, open breccia were formed during doming. These are most easily seen in the Precambrian rocks in the interior of the crater.

Units of the Crater Pasture Formation older than the Fault Canyon flow are strongly uplifted and deformed on the dome, whereas the Fault Canyon flow and units of the Fort Rock Creek Rhyodacite are uplifted and deformed by much smaller amounts.

Major Tertiary structures near the dome include two west- to northwest-trending normal faults, traceable for several miles, on which movement occurred both during and after emplacement of the Fort Rock Creek Rhyodacite. Rocks on the southern and southwestern sides of these faults moved up during emplacement of the Fort Rock Creek Rhyodacite but moved down in subsequent times.

Major events in the Precambrian geologic history at the Fort Rock dome include deposition of volcanic and sedimentary rocks, metamorphism, intrusion of granites, probably at about 1725 million years before the present, re-metamorphism accompanied by intrusion of granites and granite pegmatites, probably at about 1695 million years before the present, uplift, strike-slip(?) faulting, which probably occurred prior to about 1400 million years before the present, and erosion. Major pre-volcanic events in the Phanerozoic geologic history at the dome include deposition of sedimentary rocks in times ranging from the Cambrian to the Mississippian, uplift, and erosion, in mid-Tertiary times.

The first major events in the Tertiary volcanic history at the dome include the eruption of various ultramafic to intermediate flows, tuffs, and volcanic breccias of the Crater Pasture Formation. Subsequently, during the intrusion of a large body of magma at some depth beneath the surface, overlying Precambrian rocks and volcanic rocks were domed. Erosion of the dome occurred and was coincident with eruption of volcanic rocks south of the dome. The Fault Canyon trachybasalt flow was erupted next

on the southwest flank of the dome; it apparently came from the magma beneath the dome. Uplift of the dome subsequently diminished and some collapse may have occurred.

Eruption of the Fort Rock Creek Rhyodacite began at a large center in the Aquarius Mountains southwest of the dome following extrusion of the Fault Canyon flow. Ash flows, ash and block falls(?), and volcanic mudflows, all of rhyodacite composition, were emplaced. Ash-flow tuff buried most of the terrane around the Fort Rock dome. Some faulting accompanied emplacement of the Fort Rock Creek Rhyodacite. The basalt of Buttox Hills was later erupted on the southeast side of the dome.

Ten miles east of the dome, the Peach Springs Tuff, of middle Miocene Age, was emplaced on the western flank of the Aquarius Mountains. The Mohon Mountain volcanics, south of Trout Creek, followed.

Late geologic history in the region includes formation of Basin and Range faults in Miocene to Pliocene times and cutting of the present Colorado River drainage, beginning in early to middle Pliocene times. The deep canyons of Trout Creek and other creeks south and southwest of the dome presumably were formed during the latter period of erosion. At the dome, erosion led to the carving of a crater-like depression on the dome. This depression is presently surrounded by volcanic rocks in the steep-dipping limb of the monocline on the edge of the dome. These rocks form a circular in-facing scarp, which is the rim of the depression.

A mathematical model of doming is developed in this report. The Precambrian rocks underlying the Fort Rock dome are treated as a layer of

viscous fluid. Below this layer is an inviscid magma. Intrusion of the magma into the layer of viscous fluid is modeled by applying an axisymmetric pressure distribution on the bottom of the layer. After the pressure is applied, a dome is created on the surface. This dome has a smaller amplitude than the arch created on the bottom of the layer by the intrusion. By examining layers of different thickness, h, relative to the radius, a, of the applied pressure distribution, it appears that a dome like the Fort Rock dome cannot be created unless h/a is near 1. In addition, for a cooling time of around 10^4 years for the magma that caused uplift of the Fort Rock dome, an effective viscosity for the Precambrian rocks underlying the dome is calculated to be around 4×10^{20} poises. Planes of maximum shear generated in the model are consistent in attitude and sense of displacement with most faults mapped on the Fort Rock dome. Discrepancies that are observed can be explained in several ways. The history of doming predicted by the model is consistent with the history of doming at the Fort Rock dome. It includes an initial stage of accelerating uplift followed by lesser uplift or collapse upon formation of a vent for the magma. Uplift ceases upon crystallization of the magma.

TABLE OF CONTENTS

The primary mineralization occurred during a period of hydration of the surrounding metasediments, after the growth of tremolite and before the formation of talc. Tremolite and talc formed during the metamorphism and retrograde metamorphism of the Grenville series near Balmat. The metamorphism is thought to have occurred about 1050 million years ago. The ore fluid successively deposited pyrite, then galena and iron-rich sphalerite followed by pyrrhotite and chalcopyrite. Subsequently much of the pyrrhotite was altered to marcasite. The marcasite is thought to have formed during the deposition or remobilization of anhydrite and barite. The mineralization concluded with the deposition of iron-poor sphalerite. Recurrent microbrecciation of the metasediments and ores can be correlated with the time sequence of formation of the various ore minerals in various parts of the mines. The ore fluid followed the separate zones of microbrecciation and deposited the sulfides at nearly the temperature of the country rock. On the basis of the space and time relationship between the zones of microbrecciation and different ore minerals, it is inferred that the composition of the ore fluid reaching the site of deposition of the sulfides changed with time.

The isotopic composition of lead from galena indicates that the source of the galena is compatible with the following model - a homogenized substratum in which radiogenic lead from the decay of uranium and thorium has been added to lead of meteoritic composition without disruption from the time of origin of the earth until the time of extraction of the ore fluid.

A part of the pyrrhotite found in the No. 2 mine was formed in an area containing sphalerite and pyrite. The iron content of sphalerite

(12.5 ≠ 1 percent FeS by weight) associated with pyrrhotite and pyrite is found to be significantly higher than in areas where sphalerite occurs without pyrrhotite. It is inferred that in the region containing pyrrhotite the sphalerite became saturated with FeS at the temperature of formation of pyrrhotite. From the estimates of others on similar areas, the total pressure during the deposition of the ores at Balmat is assumed to be 3 ± 1 kilobars. By use of the phase diagram for the FeS-ZnS system, the temperature of deposition of pyrrhotite is found to be 510°.

The composition of pyrrhotite was investigated by the measurement of lattice spacings. Only one specimen of pyrrhotite was found to contain the necessary hexagonal structure for use with published plots of lattice spacing versus composition. By use of the phase diagram for the FeS-FeS_2 system, a temperature of formation of pyrrhotite based on one specimen is indicated to be 340°C. The discordance in the temperature estimate using two different geothermometers is thought to be due at least in part to exsolution of pyrite from pyrrhotite at a temperature lower than that of the formation of pyrrhotite.

The variation in the iron content of sphalerite associated with pyrite is thought to be mainly due to variations in the fugacity of sulfur species rather than changes in temperature. By use of the phase diagram of the ZnS-FeS_2-S system, the temperature of formation of sphalerite (6-9 percent FeS by weight) associated with pyrite in the No. 2 mine is indicated to be greater than 320°C. Sphalerite associated with pyrite in the No. 3 mine contains 2-3 percent FeS by weight.

Calculations based on the partitioning of trace and minor elements between sphalerite and pyrite give a first approximation of the tempera-

ture at which equilibrium was approached in the No. 3 mine of 300-350°C.

Once sphalerite acquires a particular concentration of iron, it is quite resistant to change due to following geologic events. At the temperatures of formation of the sulfides at Balmat, however, reaction between sphalerite and pyrrhotite must have been comparitively rapid. Alternation of pyrrhotite to marcasite did not seem to affect the concentration of iron in sphalerite. Supergene mineralization of magnetite, hematite, and chlorite leached iron from sphalerite grains, but the leached zone is usually 0.1 millimeter thick or less and only rarely attains a thickness of one millimeter. On the other hand, the content of manganese in sphalerite from the zones of supergene mineralization is much lower than sphalerite away from the zones. The concentration of cadmium in sphalerite from both mines falls in the range 1000 to 2000 parts per million with an average value of 1400 parts per million. The content of cadmium in sphalerite does not seem to be sensitive to temperature or accompanying mineral phases or the supergene mineralization.

LIST OF ILLUSTRATIONS

I. INTRODUCTION

PURPOSE OF INVESTIGATION

The Fort Rock dome, Arizona, is a circular geological structure, two miles in diameter, discovered from the air in the early 1960's. Many features suggest it is of impact origin. It has a crater-like center underlain by brecciated Precambrian rocks, upturned volcanic flows and sedimentary rocks in its rim, radial and tangential faults, and an apron of breccia on its flanks showing, in many cases, a crude inversion of the pre-breccia stratigraphy. The record of volcanic activity in and around the feature points to a different origin, however. In 1969, the writer began a detailed study of the dome under the auspices of the U. S. Geological Survey to determine its origin.

LOCATION, ACCESSIBILITY, AND CULTURE

Fort Rock dome is located at 35° 18' N. Lat. and 113° 18' W. Long., near the western boundary of Yavapai County, Arizona (fig. 1). It lies immediately southeast of the headquarters of Fort Rock Ranch. A gravel road, maintained by the county and passable to all vehicles when dry, connects Fort Rock Ranch with Seligman, Arizona, about 30 miles to the northeast. A dirt road, maintained by the ranch and passable by jeep, connects to the northwest with a county road to Kingman, Arizona (pl. 1). Kingman is about 50 miles west. The dome is accessible from the north and east by a dirt road, maintained by the ranch that extends from the ranch headquarters to Number One Well (pl. 1). Two jeep trails extend into the interior of the dome from this road. One jeep trail enters from the north through Noon Gorge. The other passes over Two O'Clock Gap from Number One Well. The residence of W. Becker, owner of the ranch, is situated on the west flank of the dome, about 0.7 miles south of the ranch headquarters. A ranch-maintained road, passable by jeep, continues

Figure 1. Index Map Showing the Location of the Fort Rock Dome. The rectangle outlines the area of figure 3. The inset shows the location of the index map relative to Phoenix, Flagstaff, and the Arizona state boundaries.

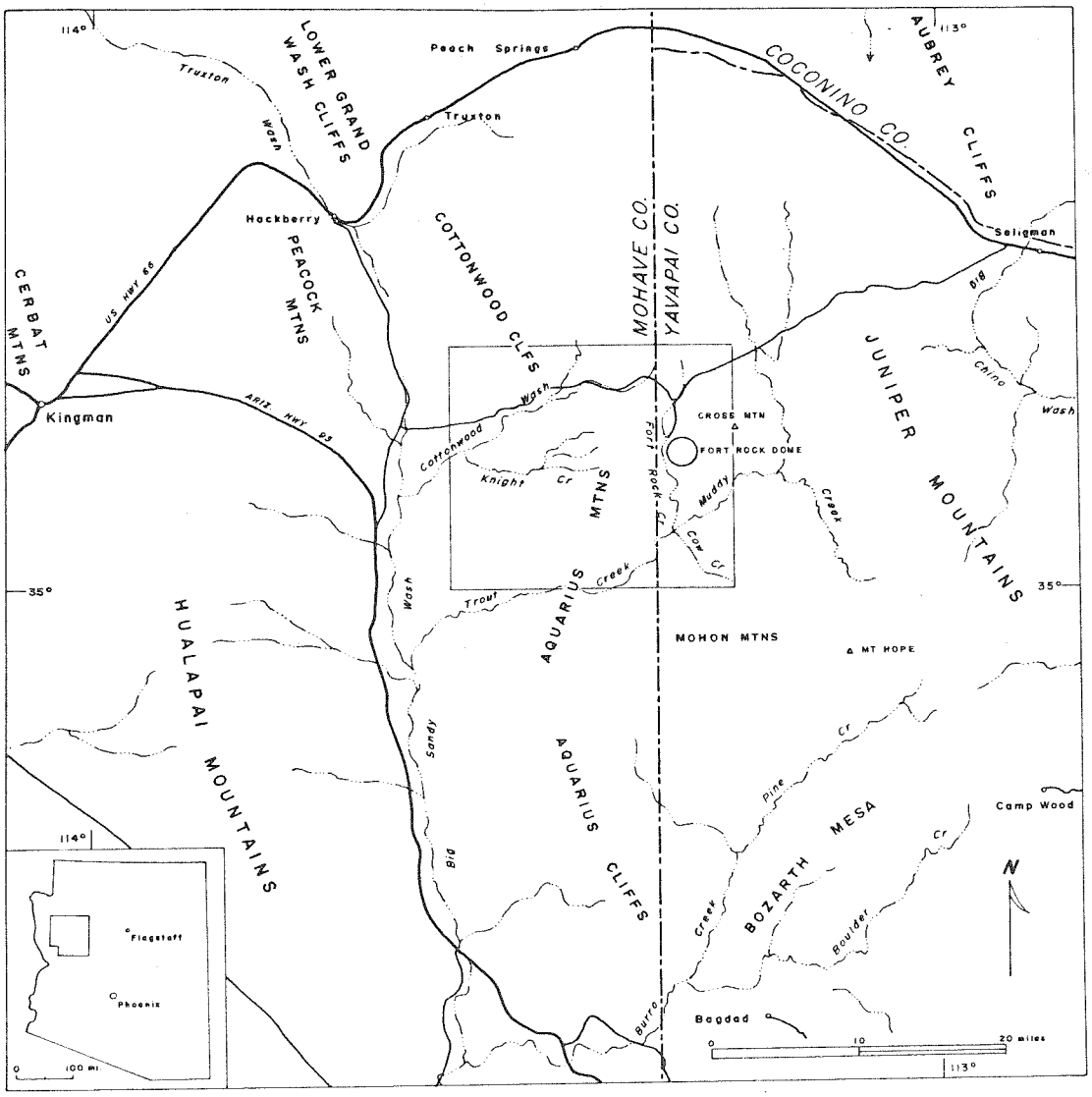
114°
113°
35°
Truxton
Wash
LOWER GRAND WASH CLIFFS
Peach Springs
Truxton
COCONINO CO.
AUBREY CLIFFS
Hackberry
PEACOCK MTNS
COTTONWOOD CLFS
MOHAVE CO.
YAVAPAI CO.
Seligman
CERBAT MTNS
US HWY 66
Kingman
ARIZ. HWY 93
Cottonwood Wash
Knight Cr
Fort Rock Wash
CROSS MTN
FORT ROCK DOME
Muddy Creek
Crow Cr
JUNIPER MOUNTAINS
Big Chino Wash
Trout Creek
AQUARIUS MTNS
MOHON MTNS
MT HOPE
HUALAPAI MOUNTAINS
Sandy Wash
Big Sandy
AQUARIUS CLIFFS
Pine Cr
Camp Wood
BOZARTH MESA
Boulder Creek
Burro
Bagdad
N
0 10 20 miles
Flagstaff
Phoenix
0 100 mi

south from the owner's house for about one mile along Fort Rock Creek before turning southwest.

A location called Fort Rock by early settlers is the site of the present Fort Rock Ranch headquarters. It was established in 1864 as a way station on the old Beale wagon road, which was a stage route between Prescott and Hardyville, Arizona (Rascoe, 1968, p. 54). (Hardyville is presently a ghost town on the Colorado River near Bullhead City, Arizona.) Remnants of this old wagon, or stage, road are still preserved as deep ruts in the white ash-flow tuff in this area and are labeled "old stage road" on the geologic map in this report (pl. 1). The name, Fort Rock, is not of military origin, but stems from a stone playhouse in which the proprietors of the way station were forced to defend themselves against a surprise attack by Hualapai Indians in the fall of 1866 (Barnes, 1960, p. 343).

PHYSICAL FEATURES

Regional

The Fort Rock dome is in the Mexican Highland section of the Basin and Range physiographic province (Fenneman, 1931). The Colorado Plateau Province lies to the north and northeast; in the area covered by figure 1, it lies roughly north of a line between the Aubrey Cliffs and the Lower Grand Wash Cliffs. The most prominent topographic feature in the vicinity of the dome is Cross Mountain (elev. 6463'), which is an 800-foot-high butte lying three miles to the northeast. The rugged Aquarius Mountains lie west and southwest of the dome. These mountains rise from an elevation of 4000 feet on the eastern edge of Big Sandy Wash, 13 miles west of the dome, to over 6000 feet several miles southwest of the dome.

Fort Rock Creek, which flows along the western flank of the dome, is the only permanent stream in the area. This stream joins Muddy Creek and Cow Creek about 5 miles south of the dome to form Trout Creek. The area south and southeast of the dome is, for the most part, a plateau into which Fort Rock, Muddy, Cow, and Trout Creeks have cut deep, spectacular canyons. Hope Mountain, 16 miles southeast of the dome, and the Mohon Mountains, 12 miles south, are prominent features rising from this plateau. The Juniper Mountains, 20 miles east of the dome, form the eastern boundary of this plateau.

Fort Rock Dome

Fort Rock dome is expressed topographically as a ring of ridges and hills (fig. 2). In the center of the dome is an elevated crater-like depression formed by erosion. The depression is divided by a drainage divide, Crater Divide (pl. 1), into two morphologically distinct halves. The southeastern half is a topographically low, gently undulating surface encircled by ridges. This low surface, referred to in this report as Crater Pasture, slopes to the southeast at a few degrees and is drained by two washes which pass through the valleys in the ridges on its southeast side. The ridges reach maximum elevations of about 5400 feet on the northeast and southwest sides of Crater Pasture. The northwestern half of the depression is broken up into a number of basins with intervening hills and ridges, and it is surrounded by a semi-circular arrangement of flatiron-like hills. Some of the hills in the interior of the depression exceed the encircling flatiron-like hills in elevation. One such hill, Ten OClock Peak, is the highest hill on the dome; it rises 450 feet to 550 feet above outlying terrain to the northwest. The northwestern half of the depression has eight drainages which exit in radial-outward directions between the

Figure 2. Air Photograph Showing the Fort Rock Dome and Nearby Features.


CROSS MTN
RANCH
FORT ROCK
DOME
THREE
SISTERS
FORT
ROCK
AQUARIUS MTNS
RHYODACITE
ERUPTIVE
CENTER
CREEK
MUDDY CREEK
N
1 mile
VVHU M 19 AMS 6 MAR 54 134
2617

flatiron-like hills. Elevation in the mapped area ranges from about 4760 feet to 5450 feet.

CLIMATE, VEGETATION, AND EXPOSURE

The climate of this region is mild, and field work usually can be conducted all year. The annual precipitation for Seligman (Green and Sellers, 1964, p. 387) is about 11". The driest months are May and June, when generally less than 1/3 inch of rain falls per month. The wettest months are July and August, when rainfall averages 1-3/4 to 2 inches per month. A second wet period occurs in the months of December through March when precipitation averages about 9/10 inch per month. The average daily temperature varies from about 36°F. in January to about 73°F. in July. The daily temperature range varies from about 30° in January to 40° in June (Green and Sellers, 1964, p. 387). Winds are from the southwest and show the highest mean velocities between April and July of around 13 miles per hour. Winds are sometimes strong.

Fort Rock dome is sparsely to densely forested with juniper and scattered piñon. The trees have been uprooted to provide better pasture on Crater Pasture and the more accessible flanks of the dome on the west, north, and east. Prominent shrubs include shrub live oak, which is very common in areas where larger trees have been uprooted, and cliffrose, or "quinine-bush." Cliffrose flourishes in areas underlain by breccia and delineates breccia outcrops well. Succulents include yucca, prickly-peak, and cholla.

The rocks of the dome are well exposed. In addition, alluvium and colluvium cover only about 35% of the area mapped.

PREVIOUS WORK

No detailed geologic investigation of Precambrian or Tertiary rocks has been carried out in the area bounded by Cross Mountain on the east, Big Sandy Wash on the west, the Cottonwood Cliffs on the north, and the Mohon Mountains on the south. Several major geologic features, including a large rhyodacite eruptive center in the Aquarius Mountains and a large volcanic center in the Mohon Mountains are unmapped geologically. Several studies and mapping projects have been carried out in the peripheral areas, however. A detailed study was conducted by Anderson and others (1955) of the geology and ore deposits of the Bagdad area, Arizona, which lies about 32 miles south of the dome. Krieger (1967) mapped, in reconnaissance, seven 15-minute quadrangles east of the Fort Rock area. Her work lies between the parallels of 34°30'N. and 35°15'N. and extends as far west as 113° W. Long. Her nearest mapping was about 16 miles east of the Fort Rock dome. Wilson (1969) completed reconnaissance mapping, for the purpose of publishing a state geologic map, in an area extending from the area mapped by Krieger to the western boundary of the state. Young (1966) studied Cenozoic geology of the Colorado Plateau between the Grand Wash Cliffs and Peach Springs, Arizona. Peach Springs is 28 miles north-northwest of the dome. Davis (1931) studied the Peacock Mountains, 25 miles northwest of the dome. Hobbs (1944) reported on a tungsten mine in Precambrian rocks in the Aquarius Mountains south of Trout Creek, about 20 miles southwest of the Fort Rock dome.

FIELD WORK

Field work was started in the Fort Rock area in the summer of 1967. Eight weeks were spent mapping, in reconnaissance, a large rhyodacite eruptive

center in the Aquarius Mountains. The Fort Rock dome was discovered on the air photographs used in this study and was also mapped in reconnaissance. (Figure 2 is one of those air photographs.) The dome had been seen earlier in the 1960's from the air and had been visited once by David Cummings of the U.S. Geological Survey. Field work was continued the following summer, during which period Precambrian rocks were investigated in an area extending from Cross Mountain westward to where these rocks are buried by Tertiary volcanic rocks in the Aquarius Mountains. Detailed field work on the dome was begun in the summer of 1969 and was completed in the fall of 1971. A total of 280 days were spent in field work on the dome.

Air photographs were used for field compilation. Initial mapping was done on Army Map Service air photographs (e.g., fig. 2 original scale, 1:62,500) enlarged five times. About one-fifth of the geology of the dome was compiled on these enlargements. In June, 1970, new air photographs were made and topographic field control was established by the U. S. Geological Survey, preparatory to making a detailed topographic map of the dome. The rest of the geology of the dome was compiled in the field on 2X enlargements of this new photography (original scale, 1:11,400). All of the geology was subsequently transferred to 4X enlargements of the new photography and was compiled photogrammetrically onto a topographic map of the dome at a scale of 1:5000. The latter task was completed by photogrammetrists at the Geological Survey Center of Astrogeology at Flagstaff, Arizona, and was edited by the writer.

Colluvium and alluvium exceeding 1 foot to 1-1/2 feet in thickness are shown on the geologic map. Bedrock underlying thinner surficial deposits can be identified with reasonable accuracy either by float or by digging shallow

pits. About 3000 pits were dug. The use of pits was essential in mapping compositional changes in breccias on the northern flank of the dome where composition is not accurately reflected in the float.

II. GEOLOGIC SETTING

Rocks exposed in the region around the Fort Rock dome range in age from Precambrian to Quaternary. The Precambrian rocks are part of a broad belt of Precambrian exposed in the mountains of central Arizona, which border the southwestern margin of the Colorado Plateau. The Precambrian rocks in the vicinity of the dome consist of layered metamorphic rocks, cataclasites, granite, and pegmatite. This assemblage resembles more closely older Precambrian rocks in the Grand Canyon than Precambrian rocks to the south and southeast.

Early to Middle Paleozoic sedimentary formations recognized in the Grand Canyon underlie Cross Mountain (fig. 3). The formations represented are the Tapeats Sandstone, Bright Angel Shale, and Muav Limestone of Cambrian age, unnamed Devonian carbonate rocks, and the Redwall Limestone of Mississippian age. Cross Mountain is the southwesternmost outcrop of these rocks in the region.

Tertiary volcanic rocks in the vicinity of the Fort Rock dome comprise a large dissected field that lies chiefly to the south and west of the dome (fig. 3). This field covers about 1000 square miles. It extends from Big Sandy Wash on the west to the Juniper Mountains on the east and from about 12 miles north of the dome to about 25 miles south of the Mohon Mountains. This field includes lava flows, pyroclastic rocks, volcanic necks, and sedimentary rocks. Numerous volcanic centers are scattered across the field. Fort Rock dome is one such center, although it is small compared to some of the others. The nearest large center is in the Aquarius Mountains about two and one-half miles southwest of the dome (figs. 2, 3). The Mohon Mountains and Hope Mountain are also large centers.

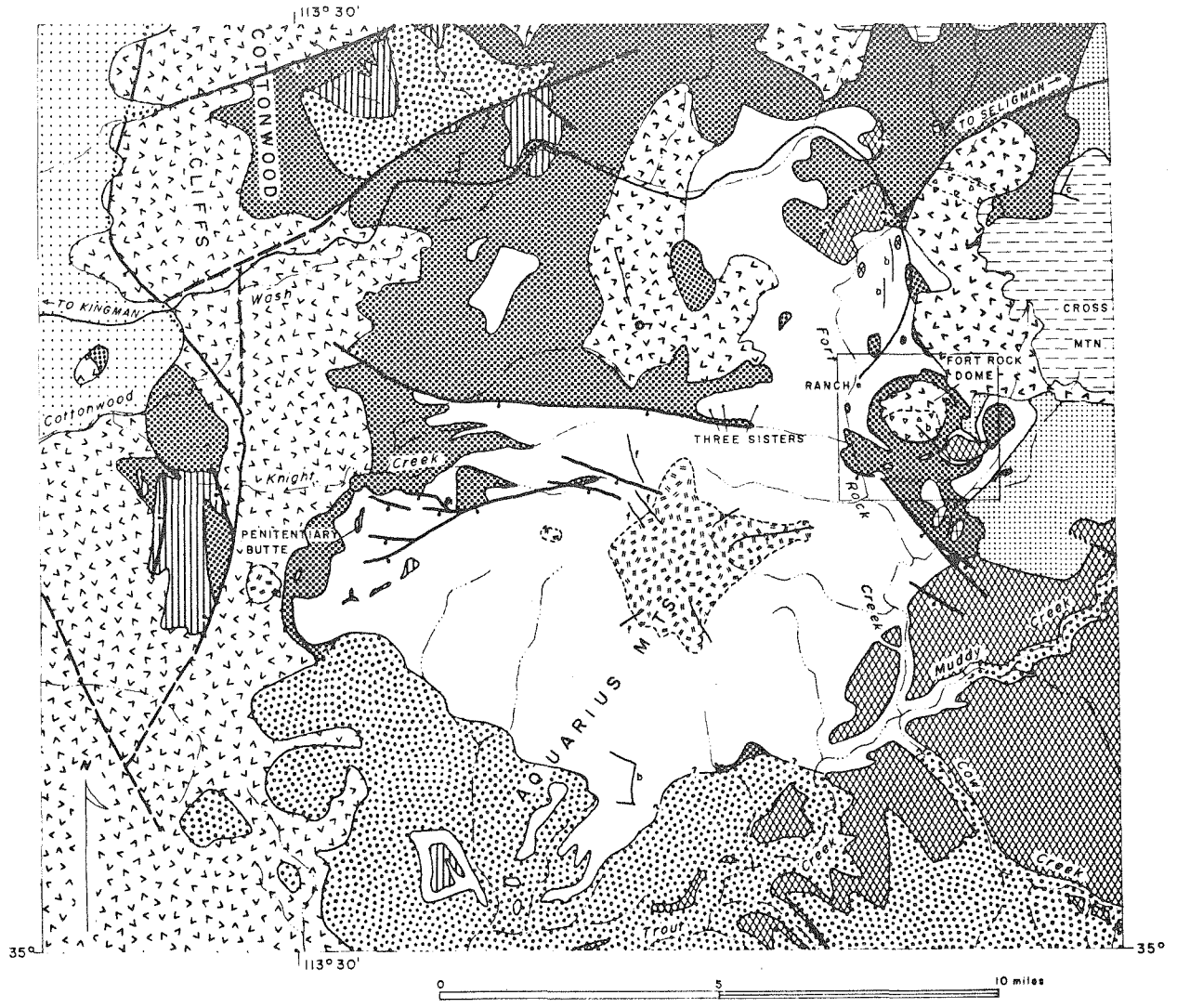

Geology by G.S. Fuis, 1967-1971

Figure 3

Reconnaissance Geologic Map of the Aquarius Mtns. and Vicinity. Square outlines area of Plate 1.

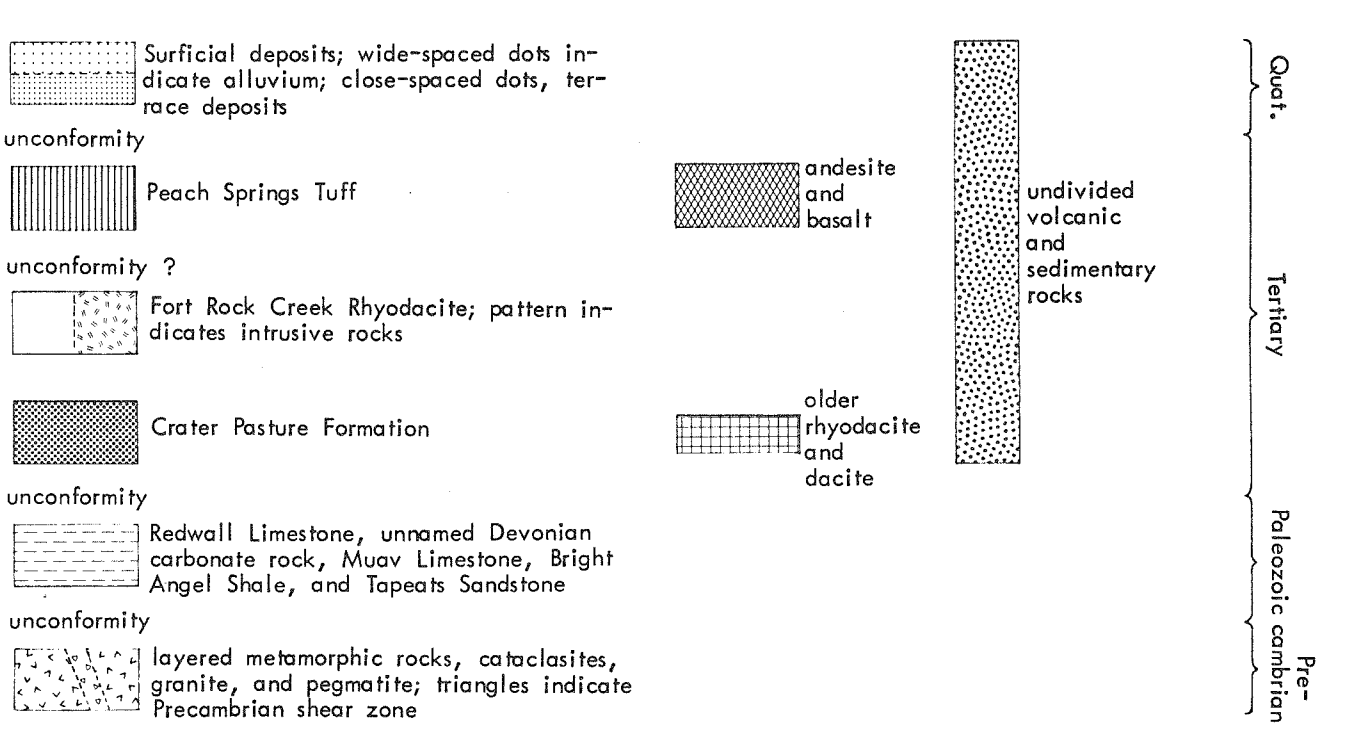

Quaternary deposits in the area include, in addition to modern alluvium and colluvium, alluvial terrace deposits, which are extensively developed east of the dome and south of Cross Mountain. The terrace deposits contain abundant Paleozoic clasts and were derived either from Cross Mountain or from Paleozoic terrane to the northeast or east.

The Fort Rock dome lies within the region of Basin and Range faulting. Between the dome and Seligman, Arizona, 30 miles to the northeast, a series of north-south trending normal faults with displacements of hundreds of feet are responsible for a series of ridges and valleys. Ten miles west of the dome one or more north-south normal faults with displacements of one thousand feet or more are responsible for the large west-facing escarpment of the Cottonwood Cliffs and Aquarius Mountains, which bounds the valley of Big Sandy Wash (fig. 3). The Hualpai Mountains on the west side of this valley are underlain by a large fault block tilted to the east.

The chief structures in the more immediate vicinity of the dome include Precambrian shear zones and Tertiary normal faults (fig. 3). The largest Precambrian shear zone is an east-west zone that runs through the Fort Rock dome. A second shear zone trends northwest-southeast in the Precambrian rocks on the northwestern side of Cross Mountain. Normal faults include several northwest-southeast trending faults south and southeast of the dome and a number of approximately east-west trending faults west of the dome in the northern and western parts of the Aquarius Mountains. The southwestern and southern sides of these faults are downthrown. In addition, two northeast-southwest trending faults bound a graben in the vicinity of the Cottonwood Cliffs.

Paleozoic and Tertiary rocks in the area around the dome are nearly flat-lying. The dome is an anomalous small area of highly deformed rocks.

III. PRECAMBRIAN ROCKS

Precambrian rocks in the area include layered metamorphic rocks and subordinate cataclasites and plutonic rocks. These rocks resemble older Precambrian rocks of the Grand Canyon described by Noble and Hunter (1916), Maxon (1961), Boyce (1972), and others. They do not resemble as closely the geographically nearer Precambrian rocks of the Yavapai Series to the south and southeast described by Anderson and others (1955), Anderson and Creasey (1958), and Anderson and others (1971).

The layered metamorphic rocks at the Fort Rock dome consist of amphibolite, schist, phyllonite and gneiss. Field relationships among various rock types are uncertain because of poor exposure. No primary sedimentary or volcanic features have been found, owing mostly to the degree of metamorphism in these rocks; however, these rocks probably represent, a metasedimentary and metavolcanic assemblage, as do most of the older Precambrian rocks of the Grand Canyon and also the rocks of the Yavapai Series to the south and southeast. Cataclasites at Fort Rock dome are small, uniform bodies with granitic compositions and distributions that suggest they are intrusive into the layered metamorphic rocks. The cataclasites may be correlative with some of the granite gneisses, e.g., the Zoroaster Granite, which are older intrusives into the amphibolites and schists in the Grand Canyon (see Noble and Hunter, 1916, p. 112). The plutonic rocks at the dome include small bodies of granite and granite pegmatite. They are intruded into both the layered metamorphic rocks and the cataclasites. They may be correlative with the younger series of granite and granite pegmatite intrusives at the Grand Canyon.

LAYERED METAMORPHIC ROCKS

Distribution and physical features. Layered metamorphic rocks in the area of the Fort Rock dome include amphibolite, schist, phyllonite and gneiss. These rocks constitute, on the average, about 75 percent of the Precambrian rocks in the area mapped. They make up a somewhat higher percentage of Precambrian rocks in the southern half of the exposure in the center of the dome and a somewhat lower percentage in the northern half. These rocks are, in general, slope-formers and are usually covered by colluvium. The best exposures are generally in gullies and washes. In places, however, metamorphic rocks underlie bouldery slopes and ridges. For example, granitic gneiss forms the ridge bounding Wedge Basin on the southeast, and forms bouldery slopes on the flanks of Ten OClock Peak, Nine OClock Hill, and Lion Ridge (northeast side). Amphibolite forms a resistant ridge between Ten OClock Peak and Crater Divide. Phyllonite forms Crater Divide southeast of Eight OClock Basin and also forms the divide between Eight OClock Basin and Ten OClock Wash.

Field Relationships. Field relationships among the various rock types within these layered metamorphic rocks are obscure because of poor exposure. Interlayering between amphibolite and schist occurs at a scale of inches in some places. In other places, areas as large as 300 feet across are composed dominantly of either amphibolite or schist. Phyllonite and gneiss occur as somewhat larger bodies of indefnitie shape, measuring up to 500 feet across. Phyllonite appears to grade in several places into bodies of cataclasite. It may represent, in part, highly foliated parts of these bodies, and, hence, may be partly intrusive in origin.

Petrography. In the petrographic descriptions below, rock types are described in order of their apparent abundance.

Amphibolite. Amphibolite appears to be the most abundant metamorphic rock in Fort Rock dome. It is a gray, medium-grained, banded rock. Black hornblende grains distributed abundantly among white plagioclase grains give a salt and pepper appearance to the hand specimen. The rock weathers to thin slabs. In one sample, it is composed of 60 percent albite, 20 percent blue-green hornblende (ferrohastingsite), 15 percent quartz, 5 percent epidote, and a trace of zircon.* Weakly developed planes of very fine-grained (75μ), crushed material, constituting a weak "cataclastic foliation", are seen parallel to the banding in this rock. All grains in the rock have ragged or irregular boundaries. Albite grains are commonly crushed to very fine grain size on their borders, giving them a ragged appearance. Where they are not crushed, they have irregular contacts with other grains. They are fractured and commonly displaced. Extinction is undulatory to patchy. Quartz grains generally occur in groups of uniform grain size and tend to be segregated into bands. Grain boundaries are irregular but not crushed.

Some recrystallization apparently took place during or after crushing. In places, grains of epidote and rarely hornblende are strung out along fractures in albite grains where there has not been any significant displacement of the grains.

Hornblende-mica schist. Hornblende-mica schist is the most poorly exposed subunit of the layered metamorphic assemblange. It is seen less commonly than amphibolite but may be equal to or even greater than amphibolite in abundance. A weakly foliated type and a strongly foliated type are recognized. The weakly foliated type appears to be more abundant.

---

*All percentages are estimates made from thin sections unless otherwise noted.

A specimen of weakly foliated schist was examined. It is a quartz-hornblende-biotite-oligoclase schist.* The rock is dark greenish brown to dark grayish brown and medium grained. In hand specimen, black hornblende grains and bronze biotite flakes are seen to be distributed abundantly among white plagioclase grains. The rock is composed of 40 percent oligoclase, 25 percent biotite, 20 percent blue-green hornblende (ferrohastingsite), 15 percent quartz, and a trace of epidote and sphene. In this specimen, ragged biotite flakes are oriented in four or five intersecting directions, which make successive angles of about 20° with each other, giving the impression of a "house of cards". Some of these directions coincide with weakly developed planes of crushed grains. Evidence for some recrystallization during crushing is stronger in this rock than in the amphibolite. Although some of the biotite is kinked, much of it, though still ragged in outline, is not. Numerous examples may be found of biotite flakes penetrating deep into cracks in the oligoclase.

A specimen of strongly foliated schist that was examined is a hornblende-albite-biotite-quartz-microcline schist. It is similar to the schist described above, but is fine-grained, strongly schistose, and has abundant quartzofeldspathic bands. It contains 35 percent microcline, 30 percent quartz, 15 percent biotite, 15 percent albite, 5 percent blue-green hornblende (ferrohastingsite(?)), and a trace of epidote and sphene. Only one major orientation of biotite flakes is seen in this specimen. Weakly developed planes of crushed grains are parallel to the foliation.

Phyllonite. Phyllonite occurs as relatively large bodies of indefinite shape in the crater. Specimens from several bodies were examined and are described below.

---

* In this report, rock names include minerals that are present in amounts of 5 percent or more; last-named minerals are most abundant.

Quartz-feldspar phyllonite underlies Crater Divide southeast of Eight OClock Basin. It is a hard, fine-grained rock that is olive-colored on fresh surfaces but commonly has a reddish weathering stain. It is characterized by minute streaks of quartzofeldspathic minerals. The phyllonite is composed of 69 percent potash feldspar, 25 percent quartz, 4 percent biotite, 2 percent epidote, and a trace of allanite and chlorite. Cataclastic foliation is strong. All grains have ragged or irregular outlines. Some feldspar occurs as small porphyroclasts. Quartz occurs in groups of grains which are strung out along the foliation. Generally, the feldspar has patchy extinction, and the quartz, undulatory extinction. Feldspar appears dominant among finer-grained crushed material. Biotite occurs as narrow stringers of small, ragged, usually bent flakes parallel to the foliation. Epidote commonly is associated with the biotite. Chlorite grades optically into biotite.

Minor recrystallization has apparently accompanied cataclastic deformation. Epidote and biotite in some cases invade cracks in feldspar. The name "phyllonite" was chosen for this rock rather than "mylonite" to reflect the small amount of recrystallization seen.

Phyllonite-gneiss underlies the divide between Ten OClock Wash and Eight OClock Basin. The rock is a biotite-epidote-albite-microcline-phyllonite-gneiss. It is an olive, fine-grained, lineated, weakly banded rock. It consists of 40 percent microcline, 39 percent albite, 12 percent epidote, 6 percent biotite, and 3 percent chlorite. No quartz is present. Microcline and albite occur both as small porphyroclasts and as finer-grained crushed material. Three or more intersecting planes which are parallel to a single direction are defined by lenses of crushed grains and by preferred orientation of biotite, chlorite, and prismatic epidote. These planes give rise to a strong lineation. The prismatic

form of epidote is an indication of recrystallization during crushing.

A hornblende-chlorite-biotite-epidote phyllonite is found in the western part of Eight OClock Basin. It is a dark, olive-brown, fine-grained rock with a very weak foliation. It contains 45 percent epidote, 35 percent biotite, 10 percent feldspar (including albite), 5 percent chlorite, 5 percent blue-green hornblende (ferrohastingsite(?)), and a trace of sphene. Feldspar occurs as prophyroclasts of medium and fine grain size. Epidote is fine-grained and is scattered throughout the rock, but it occurs in some places as medium- to fine-grained aggregates. Biotite occurs as larger (0.3mm) dark brown, largely altered (?), elongate flakes parallel to the weak foliation and as smaller (0.1mm) light brown, equant flakes of random orientation which are commonly found in aggregates. Chlorite accompanies the light-brown biotite flakes. Hornblende occurs as ragged, medium- to fine-grained prophyroclasts which are invaded by biotite. Alteration of hornblende and recrystallization of biotite, which are apparent in this rock, seem to indicate retrograde metamorphism from epidote-amphibolite facies to greenschist facies. Greenschist is found near this area, in Eight OClock Gorge.

Granitic gneiss. This rock is a hard, pink and black, medium-grained, strongly banded rock. Bands are isoclinally folded. Examples of injection banding were observed in the gneiss on the northeast flank of Lion Ridge. In a sample collected from Ten OClock Wash, the granitic bands have both sharp and gradational boundaries. Averaging light and dark bands, the specimen from Ten OClock Wash is composed of 57 percent microcline, 22 percent quartz, 13 percent oligoclast, 6 percent biotite, 2 percent hornblende (ferrohastingsite), and traces of sphene, epidote, and magnetite. The gneiss has a secondary foliation produced by cataclastic deformation which, in the sample examined,

coincides with axial planes of folds. All grains have ragged or irregular boundaries. Microcline and oligoclase occur as porphyroclasts as well as very fine-grained crushed material. The porphyroclasts are fractured and displaced and show patchy extinction. Quartz is found as irregular groups of grains of fairly even size. These groups commonly border or surround ragged feldspar porphyroclasts. Biotite occurs in two size groups. Larger-sized grains in some cases show idiomorphic or idioblastic outlines against feldspars. Fine, ragged flakes of biotite are strung out along cataclastic folia, which transect the banding where the banding is folded.

Greenschist. One outcrop of greenschist was observed in Eight OClock Gorge. This rock is medium- to coarse-grained and lineated by blades of bluish green actinolite. Porphyroclasts of pink feldspar are observable in hand specimen. It contains 71 percent actinolite, 20 percent albite (?) (heavily sericitized), 8 percent chlorite (after biotite), 1 percent epidote, and a trace of biotite. The rock is seen in thin section to be diffusely crushed.

Metamorphic facies. All of the rocks described above belong to an epidote-amphibolite metamorphic facies with the exception of the greenschist in Eight OClock Gorge and the phyllonite showing extensive retrograde greenschist metamorphism in the western part of Eight OClock Basin. All have undergone cataclastic deformation which has superimposed weak to strong cataclastic foliations. In some cases, cataclastic foliation is parallel to original banding or schistosity. In other cases, several different intersecting cataclastic foliations obscure the original rock fabric and produce a lineation in the rock. Some recrystallization of biotite and epidote accompanied cataclastic deformation. In the western and southwestern area of the crater extensive retrograde greenschist metamorphism may have accompanied cataclastic deformation.

CATACLASITES

A number of small, uniform bodies of Precambrian rock have granitic mineralogy and outcrop patterns similar to that of small intrusives but do not exhibit clear intrusive relations to the metamorphic rocks around them. Contacts are rarely exposed but appear to be concordant or gradational. Because all of these igneous-like bodies have weak to moderate cataclastic foliations and lineations, they have been termed "cataclasites". Cataclasites with distinctive physical features and petrography have been informally named after localities where they are most typically developed. These include the cataclasites of Noon Basin, Lion Ridge, Eight OClock Basin, Eight OClock Gorge, and Sams Camp Rise. Other cataclasites are distinguished only on the basis of grain size. Altogether, cataclasites constitute only a few percent of the Precambrian rocks.

Distribution. Outcrop patterns of the cataclasites differ between the northern and southern halves of the crater. (See pl. 1). The cataclasites of Noon Basin and Lion Ridge outcrop in the northern half. They are clusters of small, more or less elongate bodies. The Noon Basin cluster is elongate in an east-northeast-west-southwest direction and has a width of 400 feet and a length of 1600 feet. The Lion Ridge cluster is almost equidimensional, with a diameter of about 450 feet. Individual bodies within the Noon Basin and Lion Ridge clusters commonly have widths of about 60 feet and lengths of about 250 feet.

The cataclasites of Eight OClock Basin, Eight OClock Gorge, and Sams Camp Rise outcrop in the southern half of the crater. Each of these cataclasites consists of a relatively large, elongate body and associated smaller satellitic bodies. The main bodies of the cataclasites of Eight OClock Basin and Sams Camp Rise are each about 1300 feet in length and are 250 feet and

400 feet, respectively, in width. Both are elongate in an east-west direction. The cataclasite of Eight OClock Gorge is somewhat smaller; it is 500 feet in an east-west direction and 250 feet in a north-south direction.

Physical features. The cataclasites also differ in gross physical features between the northern and southern halves of the crater. The cataclasites of Noon Basin and Lion Ridge both form bouldery outcrops. The cataclasites of Eight OClock Basin and Sams Camp Rise, on the other hand, form low outcrops, although the former is slightly more resistant than the surrounding metamorphic rocks and forms low knobs in Eight OClock Basin. It weathers to gruss and breaks up easily under the blow of a hammer. The cataclasite of Sams Camp Rise forms low outcrops and weathers to cobble-sized, angular rocks. The cataclasite of Eight OClock Gorge outcrops as resistant angular blocks.

Field relationships. These bodies have both sharp and gradational contacts, but contacts are rarely exposed. A contact between the cataclasite of Noon Basin and adjacent schist is exposed on the divide extending south from Noon Hill. It is concordant, although two small quartz veins in the cataclasite terminate against the schist. The cataclasite of Lion Ridge appears to grade by the development of a strong foliation and lineation and increase in biotite into poorly resistant phyllonite. The main body of the cataclasite of Eight OClock Basin also grades on its eastern border into phyllonite. Contacts on the north, south, and west sides of this body, however, appear sharp. The cataclasite of Eight OClock Gorge exhibits a concordant contact with gneiss in a gully near the contact with Tertiary volcanic rocks on the southeast side of Eight OClock Gorge. The cataclasite of Sams Camp Rise grades by the development of a strong foliation and a slight increase in biotite content into mylonite and phyllonite. Distinction between the

mylonite and the phyllonite is arbitrary at best. The mylonite was mapped as part of this cataclasite, and the phyllonite was mapped as part of the layered metamorphic rocks. By a marked increase in mafic mineral content and development of strong foliation, the cataclasite of Sams Camp Rise appears to grade into gneiss, schist or amphibolite.

Petrography. A cataclastic fabric characterizes all of these rocks. One or more foliations are commonly developed by the alignment of lenticular grains and of stringers of grains less than about 0.5 mm across. The foliation is enhanced by alignment of biotite, although in most bodies, biotite occurs in amounts less than 5 percent. The development of two intersecting foliations gives rise to a lineation. Generally one foliation is stronger than the other. Feldspar occurs as porphyroclasts, although in the cataclasite of Eight OClock Gorge, some feldspar porphyroclasts are seen. Porphyroclasts have boundaries which are crushed and ragged. They are commonly fractured and, in places, displaced and have undulatory to patchy extinction. Porphyroblasts seen in the cataclasite of Eight OClock Gorge are grains of microcline containing a complete or partial ring of quartz inclusions. Quartz grains in the cataclasites occur in groups of relatively uniform grain size and generally do not show strongly undulatory extinction. Biotite is ragged and locally bent and kinked.

Distinctions among the various cataclasites are based on color and fabric and to a lesser extent on mineralogic composition. Mineralogic compositions are tabulated in Table 1.

The cataclasite of Noon Basin is a dark brown, medium-grained rock having the composition of a granite. It is characterized by scattered, coarse-grained, twinned augens of microcline and relatively abundant (4 percent) black biotite. It has a weak foliation and lineation, which is best seen on a

TABLE I. Estimated Modal Composition of Cataclasites. Estimates are made from thin sections.

Mineral	cataclasite of Noon Basin	cataclasite of Lion Ridge	cataclasite of Eight OClock Basin	cataclasite of Eight OClock Gorge: quartz-monzonitic rock	cataclasite of Eight OClock Gorge: granodioritic rock	cataclasite of Sams Camp Rise
	Percent					
Quartz	15	25	39	25	40	35
Microcline	55	43	33	32	10	55
Plagioclase	25	30	27	28	45	9
Biotite	4	1-1/2	1/2	*	2	3/4
Muscovite	tr	tr	1/2	tr	--	tr
Chlorite	tr	--	tr	--	3	tr
Epidote	tr	tr	--	--	--	tr
Allanite	tr	--	--	--	--	tr - 1/4
Sphene	tr	tr	--	tr	tr	--
Zircon	tr	--	--	--	--	--
Apatite	--	tr	--	--	--	--
Opaque min.	tr	1/2	tr	*	--	1/4
				*Biotite + Opaque Minerals 15		
Total	99	100	100	100	100	100
Plagioclase is	oligoclase	albite	albite	albite	albite	albite

fresh surface.

The cataclasite of Lion Ridge is a red, medium- to fine-grained rock, having the composition of a quartz monzonite. It is characterized by rare augens like those of the Noon Basin cataclasite. Fresh surfaces are mottled pink by microcline and red brown to olive by finely divided biotite. Foliation is weak to moderate. Moderately foliated specimens contain a few percent biotite (cf. Table I).

The cataclasite of Eight OClock Basin is a white, medium-grained rock, having the composition of a leucocratic quartz monzonite. A strong lineation is developed by parallel alignment of stringers of quartz grains and finely divided biotite.

The cataclasite of Eight OClock Gorge includes two rock types. The more dominant has the composition of a quartz monzonite. This rock is characterized by pink, medium-grained microcline augens in a fine-grained, dark, red-brown matrix. The second rock type has the composition of a granodiorite. This rock consists of close-spaced plagioclase augens in a scant, dark green, fine-grained matrix. The quartz-monzonitic rock is poorly foliated, but the grandodioritic rock is moderately well foliated. The relationship between these two rock types is unknown.

The cataclasite of Sams Camp Rise is of differing appearance in hand specimen. One specimen that was examined is dark pink, medium-grained, and unfoliated. Another specimen is mottled pink and olive, is medium-grained, and is weakly foliated. Still another has an olive color on a fresh surface, generally masked by a red weathering stain, and is fine-grained, well foliated, and lineated by streaks of fine-grained biotite. The latter specimen has been

termed a mylonite. Strongly foliated specimens of this unit contain a few percent biotite (cf. Table I). This cataclasite has the mineralogic composition of a granite.

Several bodies of cataclasite have been distinguished only on the basis of grain size. The largest is a body southwest of Thunder Camp. It is undistinctive topographically and petrographically. It is a medium- to fine-grained, poorly to moderately foliated granitic rock. A more distinctive cataclasite in this group is found in several locations, but its largest outcrop is at the head of Ten OClock Wash. It is a white, coarse-grained, weakly banded rock, consisting dominantly of white feldspar.

Some recrystallization is indicated in most of the cataclasites by invasion of biotite into fractures in feldspar. In the Eight OClock Gorge cataclasite, some recrystallization to form microcline porphyroblasts is indicated.

GRANITE AND GRANITE PEGMATITE

Granite and granite pegmatite clearly intrude the layered metamorphic rocks and some of the cataclasites in Fort Rock dome. Like the older rocks, these intrusives are crushed, but only in the granite are there instances where cataclastic foliation is developed. Both the granite and granite pegmatite are leucocratic and resistant to weathering, and they tend to occur in close association with one another. These characteristics help distinguish the granite from the cataclasite in places where the granite is foliated.

Distribution and physical features. Granite is most abundant in the exposure of Precambrian rocks northeast of the dome and in the northwest quadrant of the exposure inside the dome (pl. 1). It tends to form small bodies and irregular dikes. The rock is more resistant than the surrounding metamorphic

rocks and underlies hills, spurs, and irregular ridges. The largest body underlies Ten OClock Peak, which is the highest hill in the area mapped. Outcrops of granite are generally bouldery or blocky.

Granite pegmatite in the area mapped is almost exclusively confined to the northern half of the dome and the exposure northeast of the dome (pl. 1). It forms narrow, linear to irregularly shaped dikes. Three swarms of larger dikes can be identified. The largest swarm is found on Noon Hill, on the hill south of Noon Hill, and on One OClock Hill. The second largest swarm occurs in the vicinity of Crater Divide just north of the center of the dome. A smaller swarm occurs on the west flank of the small knob extending southwest of Lion Ridge. The pegmatites are more resistant to weathering than the metamorphic rock they intrude and underlie topographic ribs, ridges, and hills. Outcrop of pegmatite is blocky; very coarse crystals in the rock weather to sharp, angular faces.

Field relationships. Granite and granite pegmatite clearly intrude the layered metamorphic rocks. In addition, granite pegmatite intrudes the cataclasites of Noon Basin and Lion Ridge. The virtual lack of pegmatite in the southern half of the crater, unfortunately, precludes determining the age of this rock relative to the cataclasites in that area, although the pegmatite is almost certainly younger.

The pegmatite and granite occur, in most places, in close association. In some cases, the pegmatite intrudes the granite, and in other cases, it grades texturally into the granite. In cases of either intrusion or gradation, mixtures of nearly equal proportions of both rocks are observed in some localities and are mapped as "mixed granite and granite pegmatite". This mixed

unit is formally defined to include mixtures of between 30 percent and 70 percent of either component. Mixtures falling outside of this range are mapped simply as "granite" or "granite pegmatite". Mixture occurs on the scale of inches to tens of feet. The smaller scale mixtures are typical of gradation of pegmatite into granite. The unit of "mixed granite and granite pegmatite" is only common in the exposure northeast of the dome .

Petrography.

Granite. The granite on Ten OClock Peak is a very hard, pink, fine-grained, lineated (or streaked) rock. Lineation is developed in all minerals that can be observed in hand specimen. Finely divided biotite gives rise to black streaks or specks, depending on the orientation in which the rock is viewed. Stringers of feldspar and quartz grains give rise to light-colored streaks. The rock is a leucogranite and contains 60 percent microcline, 39 percent quartz, 1/2 percent albite or oligoclase, 3/4 percent biotite, 1/4 percent opaques, and traces of muscovite, epidote, and zircon. In thin section, the rock is seen to be crushed, but lineation does not show up as strongly in thin section as it does in hand specimen. Most of the biotite forms sharply defined, undeformed flakes, which may be evidence for some recrystallization of the rock. Rare strings of quartz inclusions which are found in microcline grains and are parallel to the lineation of the rock may be additional evidence for recrystallization. These strings of inclusions suggest crystalloblastic growth of microcline.

A specimen of granite from near the center of the dome is white (fresh surface) to light brown (weathered surface), medium-grained, and poorly to moderately foliated. Albite content reaches about 20 percent and there is a trace of garnet.

A few of the rocks mapped as granite are leucocratic quartz monozonites and granodiorites.

Granite pegmatite. Granite pegmatite is pink and massive with a grain size varying from medium to very coarse. Crystals of microcline with dimensions up to several inches are characteristic. These large crystals are frequently graphically intergrown with quartz and sometimes appear to be a mosaic. Quartz is occasionally segregated into large white bodies within the pegmatite. Since this rock is of variable grain size and since mineral segregation occurs on several scales, it is difficult to determine the overall mineral percentages. One medium-grained specimen that was examined contains 40 percent quartz, 40 percent microcline, 19-1/2 percent plagioclase, 1/2 percent biotite, and traces of muscovite and opaques. All pegmatites show crushing, but cataclastic foliation is rare. Feldspar, especially microcline, forms porphyroclasts, some of which are inches long. These porphyroclasts either have boundaries which are crushed and ragged or are irregular. Irregular boundaries occur adjacent to groups of quartz grains, which have fairly uniform grain size. Feldspars are more commonly fractured and displaced in the pegmatites than in the cataclasites and show rotation of internal grain segments. Displacements and rotations have the effect of breaking up grains into mosaics; hence, the mosaic-like appearance of large microcline crystals in hand specimens. The fractures in the grains are occupied by very fine-grained crushed material but are frequently invaded by coarser-grained quartz, which may be evidence for some recrystallization during deformation.

A minor outcrop of flaser granite, mapped in the southern half of the crater near the crest of Buffalo Ridge, may be a sheared granite pegmatite.

The rock is a pink, coarse-grained granite consisting of microcline augens in a rust-colored matrix. The contacts of this rock are intrusive.

VEINED ROCKS

Numerous small faults and fractures in the Precambrian rocks that occupy shear zones have been veined by epidote, hematite, quartz, and other minerals. Veins have thicknesses ranging from microns to several centimeters. In places, veins are so dense that the original rock can no longer be distinguished, and a separate geologic map unit, "veined rock", is used.

Distribution and physical features. Veined rock occurs in an east-west zone which occupies the southern half of Fort Rock dome and also in a half-mile wide, northwest-southeast zone on the northwestern side of Cross Mountain (fig. 3). Veined rock tends to break up along veins during weathering and forms small (one- to several-inch), angular float. This weathering characteristic distinguishes it from most of the rest of the Precambrian rock, which weathers to blocks and boulders. Outcrops of veined rock are generally topographically low. Where quartz is the chief vein mineral, low ridges may be found.

Field relationships. Within the shear zones, the spatial density of veins can be mapped. Several levels of vein density were defined and mapped in Fort Rock dome (fig. 4). The levels are defined as follows:

"low density"	veins spaced farther than 10 cm apart
"moderate density"	veins spaced 1 cm to 10 cm apart
"high density"	veins spaced 1 mm to 1 cm apart
"very high density"	veins spaced closer than 1 mm; identity of the original rock obscured in most places

Owing to poor exposure of veined rocks in the dome, mapping of these levels was based largely on float. In a given small area, say, 20 feet by 20 feet, the highest possible level was mapped if 20 percent or more of the float (or 10 percent or more of the outcrop, where outcrop is seen) had a vein density of that level. The rest of the float in this small area had either lower or higher levels of vein density than the level that was mapped, but less than 20 percent of the float had higher levels. At some localities, it was found that adjacent small areas would be mapped as different levels. At these localities, "mixed" levels were mapped. Only one mixed level occurs in the dome, "mixed high and very high density" veined rock. The level designated "very high density" was mapped as a geologic unit (pl. 1). The levels defined above are seen in an easily mappable, regular sequence on the east end of the rise north of Sams Camp Rise. This area was used as a reference for mapping levels in the rest of the shear zone in the crater.

A discussion of the outcrop pattern of the various levels of vein density is found below in a discussion of the structure of the shear zone in Fort Rock dome.

Petrography. Veins vary in width from 20 microns to one or two centimeters. Vein minerals include, in order of abundance, olive-green epidote, clear to milky quartz, dark red to specular hematite, pinkish orange adularia, bluish black chlorite (rare), and sericite (rare). Fractures are continuous through many grains in the rock and, generally, extend throughout a hand specimen. They cut both porphyroclasts and finer-grained cataclastically granulated material in the rock. They commonly offset grains and other fractures, although offsets are usually small (less than 1 cm). In some cases,

the fractures are zones of crushing and diffuse to heavy mineralization. In other cases, they are cracks lined with druzy vein minerals. In cases where crushing occurs, the fractures are distinguished from older cataclastic foliation in the host rock in that they a) are localized (or bounded by two, more or less discrete planes), b) have a broad grain-size distribution, with a minimum granulation size much smaller than seen in the host rock (less than a few microns), and c) are mineralized. Zones of crushing are mineralized by only epidote or hematite. Fractures lined by druzy vein minerals contain any of the minerals listed above.

Paragenesis of vein minerals. The following are examples of paragenesis of vein minerals in rocks of Fort Rock dome. In each example, the level of vein density in the particular rock sample that was examined is given first, followed by a numbered sequence of events that can be recognized in the rock. The oldest event is listed first.

A. Rock with a "moderate density" of veins.
    1. Fracturing and veining by very fine-grained epidote
    2. Fracturing and veining by druzy quartz followed by druzy epidote.

B. Rock with a "moderate density" of veins.
    1. Fracturing and veining simultaneously by adularia, chlorite, and sericite.

C. Rock with a "high density" of veins.
    1. Fracturing and veining by epidote.
    2. Fracturing and veining by hematite.

D. Rock with a "high density" of veins.

1. Fracturing and veining by epidote, including some druzy epidote.
2. Fracturing and veining by quartz and/or adularia(?)

E. Rock with a "high density" of veins.

1. Fracturing with extensive crushing and mineralization by very fine-grained epidote.
2. Fracturing and veining by clear quartz.
3. Fracturing and veining by druzy milky quartz followed, but in some cases preceded by, druzy adularia(?).

F. Rock with a "high density" of veins.

1. Fracturing with extensive crushing and mineralization by epidote.

G. Rock with a "very high density" of veins.

1. Fracturing with some crushing and mineralization by epidote.
2. Fracturing and veining by hematite and quartz.
3. Fracturing and veining by druzy quartz followed by druzy adularia(?); simultaneous filling of hair-like veins by quartz.
4. Fracturing with crushing and mineralization by hematite.

H. Rock with a "very high density" of veins.

1. Fracturing with extensive crushing and mineralization by very fine-grained epidote in one case and hematite in another; relative ages of epidote and hematite mineralization unknown.
2. Fracturing and filling of hair-like veins by quartz; associated or somewhat younger fracturing and veining by milky quartz followed by druzy adularia(?).

3. Minor fracturing and filling of hair-like veins by clear quartz.

Summary. The oldest event in most of the examples of vein-mineral paragenesis is fracturing, generally with crushing, and veining by epidote or, less commonly, hematite. The next event involves open fracturing and filling of the fractures by druzy quartz, minor adularia, and, rarely, epidote. An event succeeding these two events in at least one rock involves fracturing, with some crushing, and veining by hematite. The oldest event in this sequence is suggestive of higher pressures and temperatures than the second event because of the crushing involved and the abundance of epidote. Pressures in the second event apparently frequently dropped below local rock strengths, as evidenced by open cracks. A potential reversion to higher pressures is suggested by the third event.

IV. TERTIARY VOLCANIC AND SEDIMENTARY ROCKS

Tertiary rocks in the vicinity of the Fort Rock dome comprise chiefly two formations. The older formation is here given the name, Crater Pasture Formation; the younger is given the name, Fort Rock Creek Rhyodacite. In addition to these two formations, several lava flows of varying extent and isolated intrusive bodies are present which are younger than the Fort Rock Creek Rhyodacite (see fig. 3). Ten miles west of Fort Rock dome, the Peach Springs Tuff, of middle Miocene age, overlies the Fort Rock Creek Rhyodacite. The Mohon Mountain volcanics, south of Trout Creek, are younger than the Peach Springs Tuff.

The Crater Pasture Formation is the oldest Tertiary unit exposed in this area. It consists of lava flows, agglomerates, tuffs, and associated sedimentary and intrusive rocks. Rocks range in composition from ultramafic to intermediate; they include shonkinite, limburgite, trachybasalt and trachyandesite. The lava flows originated from numerous scattered vents and generally extend laterally for distances of a mile or less.

The Fort Rock Creek Rhyodacite conformably overlies the Crater Pasture Formation. It consists chiefly of ash flow tuff and volcanic breccia. The ash and clasts in these deposits are rhyodacite and, less commonly, rhyolite. Most of the ash and clasts were erupted from a large, complex volcanic vent in the Aquarius Mountains, 2-1/2 miles southwest of Fort Rock dome (fig. 3). Individual ash flow and volcanic breccia units within the Fort Rock Creek Rhyodacite extend over distances of more than 5 miles.

The scattered flows, dikes, and plugs which post-date the Fort Rock Creek Rhyodacite range from mafic to intermediate in composition. In the area

mapped (pl. 1), the basalt of Buttox Hills is one of these units. It forms a flow, dike, and plug. The flow is of dimension comparable to flows in the Crater Pasture Formation. Beyond the area mapped, more extensive flows are exposed. The plateau south of the dome (fig. 3) is largely underlain by basaltic lava flows which are stratigraphically above the Fort Rock Creek Rhyodacite.

Ten miles west of the dome, the Peach Springs Tuff, of middle Miocene age, unconformably(?) overlies the Fort Rock Creek Rhyodacite (fig. 3). The tuff caps a number of buttes in the western Aquarius Mountains and is also preserved on downdropped fault blocks on the edge of Big Sandy Wash and in the vicinity of the Cottonwood Cliffs. This tuff comprised a regional sheet which can be traced as far north as the Grand Wash Cliffs and as far west as the Black Mountains in western Arizona (Young and Brennan, in press). It is overlain by the Mohon Mountain volcanics (Young and Brennan, loc. cit.).

The Tertiary volcanic and sedimentary rocks a Fort Rock dome lie on a mid-Tertiary erosion surface, parts of which are preserved in many places in the surrounding region. Cross Mountain formed a prominent butte on this ancient surface that rose at least 800 feet above the surrounding terrain. South and west of Cross Mountain, a rolling to hilly surface was developed on Precambrian rocks which had a relief comparable to that of the present surface on these rocks. The surface at the site of present Fort Rock dome is discussed later and is shown on paleogeographic Map 1 (fig. 9).

The mid-Tertiary erosion surface has been recognized in the Prescott-Jerome area, along the Mogollon Rim, in the Seligman-Ashfork area, and on the eastern and western Hualapai Plateau. Present topography in the Seligman-Ashfork area and on the eastern and western Hualapai Plateau is apparently

similar to the mid-Tertiary topography.

In the Prescott-Jerome area, the mid-Tertiary surface has been described by Krieger (1965) and Anderson and Creasey (1958). It is overlain by gravel and basalt of the Hickey Formation. A basalt flow in the Hickey Formation has a reported potassium-argon age of 10 to 11 million years (McKee and Anderson, 1971; Damon, 1968, p. 49). Gravels filling a broad ancient valley under the Mount Floyd volcanic field north and northeast of Seligman, Arizona, have been described by Koons (1948, 1964). The oldest basalt overlying these gravels has a reported potassium-argon age of 14 million years (McKee and McKee, 1972). Similar gravels on the eastern Hualpai Plateau (Koons, 1948; 1964) are overlain in one location by the basalt of Blue Mountain, which has a reported age of 14 million years (Damon, oral comm.). On the western Hualpai Plateau, deep canyons were present in the mid-Tertiary erosion surface which were later filled by thick deposits of alluvial and colluvial deposits and locally by volcanic rocks (Young, 1966). Most of the volcanic rocks in this area post-date the gravels and include, from oldest to youngest, basalts or andesites, the Peach Springs Tuff, and younger basalts or andesites. The Peach Springs Tuff has a reported potassium-argon age of 18 million years (Damon, 1964, p. 19). (A summary of Cenozoic erosion, sedimentation, and volcanism in the above areas is given by McKee and others (1964).

CRATER PASTURE FORMATION

Crater Pasture Formation is a new name applied here to a series of lava flows, agglomerates, tuffs, and associated intrusive and sedimentary rocks in the vicinity of the Fort Rock dome. Composition of the volcanic rocks ranges from ultramafic to intermediate. The name, Crater Pasture, is taken from an informal name used by local inhabitants for a fenced area enclosing the dome,

which constitutes most of the area mapped (pl. 1). As used in this report, however, the name, Crater Pasture, refers to that part of the physiographic crater inside the dome southeast of Crater Divide.

The Crater Pasture Formation is subdivided into eleven informal members in or near the dome. Reconnaissance mapping (fig. 3) has indicated that other volcanic rocks in an extensive area west and north of the dome are of similar age and composition and can be included under this formational name. The informal members are listed below with the oldest at the bottom. Rock-unit names such as flow and agglomerate, refer to the major rock unit(s) of each member. Geographic names are derived from features in and near the outcrop areas. The general rock type in each member is listed in parentheses after the name. Relative ages are unknown in the two pairs of members at the bottom of the list.

flow of Fault Canyon (olivine-sanidine trachybasalt)

tuff and agglomerate of Cinder Basin (olivine trachybasalt)

sedimentary breccia of One OClock Wash (dominantly clasts of hornblende trachyandesite and clasts of Precambrian rocks)

tuff and conglomerate of Hidden Pasture (olivine, hornblende trachyandesite)

flow of Lion Ridge (hornblende trachyandesite)

flow of Buffalo Ridge (hornblende trachyandesite)

flow of Annex Ridge (hornblende trachyandesite)

flow of Meadow Dam (hornblende trachybasalt); tuff and flow of Two OClock Gap (pyroxene trachyandesite)

flow of Eight OClock Gorge (limburgite); volcanic breccia and flow of Road End Gap (olivine trachyandesite)

In addition to the informal members, the Crater Pasture Formation includes a basal tuffaceous sandstone, a pyroxene trachyandesite sandstone and conglomerate,

and four separate intrusive bodies, three of which appear related to three of the informal members.

Type Section

The section exposed in Eight OClock Gorge, which cuts through the southwest rim of the crater, is chosen as the type section for the Crater Pasture Formation. The base of the section is located in NW 1/4, SW 1/4, NW 1/4, sec. 10, T. 20 N., R. 10 W. The section extends to the southwest through the gorge and down the wash to its junction with Fort Rock Creek. A total of between 500 feet and 600 feet of this formation is exposed in the gorge, depending on the wall in which the section is measured. Another 60 feet of the youngest flow in the formation is exposed farther down the wash.

In the gorge, the Crater Pasture Formation overlies Precambrian rocks, and all rocks in the formation dip about 50° to the southwest. Rocks in this formation underlie the rim of the crater on the southeast side of the gorge, but on the northwest side, they underlie a flatiron-like escarpment on the flank of a hill of granite pegmatite and other Precambrian rocks. Five units are present in the type section, the flow of Eight OClock Gorge, the flow of Meadow Dam, the flow of Buffalo Ridge, the sedimentary breccia of One OClock Wash, and the flow of Fault Canyon.

The basal contact of the Crater Pasture formation is well exposed (and slightly faulted) in a gully in the southeast wall of the gorge. Here, a few inches of buff to orange tuffaceous sandstone overlies Precambrian gneiss and cataclasite and is in turn overlain by black, massive, amygdaloidal limburgite of the Eight OClock Gorge flow. The limburgite varies in thickness in the gorge from about 30 feet on the southeast wall to about 70 feet on the northwest wall. Just above the flow is a thin, orange, fine-grained tuffaceous sandstone.

The Eight OClock Gorge unit is overlain by gray hornblende trachybasalt of the Meadow Dam flow; the contact is well exposed in the northwest bank of the wash. The Meadow Dam flow is about 135 feet thick here. It has excellent flow cleavage throughout, except in its basal few feet. It is overlain by about a foot of maroon volcanic sandstone and conglomerate in the northwest wall of the gorge.

Blue-gray hornblende trachyandesite of the Buffalo Ridge flow, 205 feet in thickness, overlies the Meadow Dam flow and the thin sandstone and conglomerate unit. Two to three feet of trachyandesite lapilli tuff, made up of yellow-brown clasts with abundant hornblende, occur at the base of the flow. The flow has flow cleavage near its base, is massive in its central and upper parts, and has a rough brownish, varnished, aa top.

Structural complications are seen in the Buffalo Ridge flow in Eight OClock Gorge. On the northwest wall, two bodies of breccia are exposed. One body extends upward from the base of the flow to deep within the flow; the other body is found in the central part of the flow. The breccia in both bodies is locally reddened and is thought to be flow breccia. Both breccia bodies are exposed only a few feet above the wash bottom and are shown on the geologic map (pl. 1). Another structural complication is the presence of three shingle-like thrust faults in the upper part of the flow. The apparent thickness of the flow is increased by these faults in the vicinity of a sharp kink in the gorge. This kink appears to be controlled by the upper fault. All of these faults apparently formed open fissures which were later filled by the sedimentary breccia of One OClock Wash.

Past the kink in the gorge, the gorge walls diminish sharply in height on the flank of the dome. The flank is underlain in part by two breccia units.

The older breccia is the One OClock Wash sedimentary breccia of the Crater Pasture Formation. The younger is the Noon Gorge sedimentary breccia, which is a member of the Fort Rock Creek Rhyodacite. The basal contact of the One OClock Wash breccia is exposed in the northwestern wall of the gorge and is highly irregular owing to the rugged topography on the top of the flow, which had been offset by thrusting prior to deposition of the breccia. The thickness of the breccia, consequently, varies from a few feet to about 200 feet in this area. The breccia consists of gray, red-brown, and yellow-brown clasts of Buffalo Ridge flow, a trace or more of black to light green ash, and a trace of clasts of Precambrian rock. The contact between this breccia and Noon Gorge sedimentary breccia is subtle and poorly exposed. It trends steeply down the hillside on the northwest side of the wash, intersecting the wash only about 50 feet downstream from the last outcrop of Buffalo Ridge flow. On the southwest side of the wash, essentially all the breccia exposed belongs to the Noon Gorge sedimentary breccia. The One OClock Wash sedimentary breccia on this side of the wash forms only a few isolated pockets on top of the thrust plates in the Buffalo Ridge flow.

Three hundred feet farther down the wash, the One OClock Wash sedimentary breccia is overlain by a higher member of the Crater Pasture Formation, the Fault Canyon flow, although its contact with the flow is not exposed. At this location, beds are relatively flat-lying, as they lie beyond the structural flank of Fort Rock dome. The Fault Canyon flow is a black, olivine-sanidine trachybasalt. It forms the walls of a shallow canyon extending from this location to the junction of Eight OClock Wash with Fort Rock Creek. On top of the flow, pockets of distinctive agglomerate are seen which consist of vesicular grayish-brown clasts in a fine-grained, white, tuffaceous matrix.

The contact between the Fault Canyon flow or the agglomerate and the overlying Noon Gorge breccia of the Fort Rock Creek Rhyodacite is well exposed in the northwest bank of the wash at the point where outcrop of the flow is first encountered. It is also exposed in a small gully on the same side of the wash just around the bend in the wash at this point. Farther down the wash, the Fault Canyon flow is directly overlain by the pumice-rich Old Stage Road Member of the Fort Rock Creek Rhyodacite.

Reference Section

A reference section for the Crater Pasture Formation is designated in Six Thirty Wash, which cuts into the southern rim of the crater. The base of this section is located in the SW 1/4, NW 1/4, SE 1/4, sec. 10, T. 20 N., R. 10 W.; it is 800 feet west of Road End Gap, on Buffalo Ridge. The reference section extends southeastward into Six Thirty Wash and on down the wash to its junction with Six OClock Wash. The total exposed thickness of the Crater Pasture Formation in this section is about 800 feet.

In Six Thirty Wash the rocks of the Crater Pasture Formation dip about 75° to the south. At the base of the section these rocks underlie the rim of the crater. Six units are exposed, the volcanic breccia and flow of Road End Gap, the flow of Annex Ridge, the flow of Buffalo Ridge, the sedimentary breccia of One OClock Wash, the agglomerate and tuff of Cinder Basin, and the flow of Fault Canyon.

The basal contact of the Crater Pasture Formation with Precambrian rocks runs precisely along the crest of Buffalo Ridge in this area and can easily be exposed by digging. The basal Crater Pasture unit here is the Road End Gap volcanic breccia and flow, which is estimated to be 300 feet thick in this section. Rock of this unit is olivine trachyandesite. The volcanic breccia

consists of black, vesicular clasts in a reddened matrix. Flow rock varies from light grayish brown to black; the black variety is commonly vesicular. Flow rarely shows flow cleavage and is generally massive. In this locality, flow commonly grades into volcanic breccia; however, colluvium is fairly thick on the Road End Gap rocks and internal contacts are difficult to follow.

At the head of Six Thirty Wash, on its east bank, is a good exposure of the contact between the Road End Gap breccia and flow and the overlying Annex Ridge flow. The upper part of the Road End Gap unit is a sedimentary breccia, with clasts of Road End Gap trachyandesite up to 2 feet across. This breccia grades upward into a conglomerate with clasts no larger than 1 centimeter across. The next higher unit is a bedded sedimentary breccia containing fragments of the Road End Gap unit, yellow-brown hornblende-bearing trachyandesite ash and lapilli, and clasts of Precambrian rock. The contact between the Annex Ridge and the Road End Gap units is placed at the base of this breccia. Above this breccia are thin beds of volcanic breccia, sedimentary breccia, conglomeratic sandstone, tuff, and finally flow. The Annex Ridge flow is approximately 350 feet thick and is exposed for about 400 feet on the northeast side of the wash. On this side of the wash, the flow is light gray to very light gray in color and is commonly brecciated. On the southwest bank of the wash and in the bed of the wash, the upper part of the flow is soft, light brown rock in contrast to the rock on the northeast side of the wash.

On the slope on the southwest side of the wash, the Buffalo Ridge flow is exposed, but it pinches out against the Annex Ridge flow before it reaches the wash. The geologic map (pl. 1) provides a cross-section of this relationship owing to the high dip of all units. In a low saddle west of the

contact between the Road End Gap and Annex Ridge units in Six Thirty Wash, the Road End Gap unit is in contact with the Buffalo Ridge unit. The sedimentary breccia and conglomerate in the upper part of the Road End Gap unit are missing here, however. The Buffalo Ridge flow is a somewhat darker blue-gray than the Annex Ridge flow, but both flows are characterized by abundant hornblende laths. The basal contact of the Buffalo Ridge flow swings southeastward from the saddle to a position above and parallel to the wash. Some reddened breccia is associated with the contact in this area in addition to characteristic yellow-brown ash. The top of the Buffalo Ridge flow is dark, varnished aa.

One OClock Wash sedimentary breccia overlies both the Buffalo Ridge and Annex Ridge flows in this area. In the wash it forms a small flatiron over the Annex Ridge flow with a dip of about 30° to the south. The breccia is seen to contain, in the wash, clasts of Annex Ridge flow, some of which are larger than 4 feet across. About 100 feet down the wash from the basal contact of the breccia, it contains clasts of Precambrian rocks and Road End Gap(?) olivine trachyandesite.

At a bend in Six Thirty Wash, 140 feet south of the Annex Ridge flow, the One OClock Wash breccia is in contact with an agglomeratic unit in the overlying Cinder Basin tuff and agglomerate member of the Crater Pasture Formation. The contact is here covered by alluvium. Trachybasalt agglomerate, with bombs exceeding 10 feet in dimension, is exposed from the bend in the wash to junction of Six Thirty and Six OClock Washes. Agglomerate is also exposed in a gully which joins Six Thirty Wash from the west at this bend. The basal contact of the Cinder Basin tuff and agglomerate extends to the west from this bend under colluvium, through a low saddle. The contact also extends to the east,

under colluvium, and is exposed in Six OClock Wash. Overlying the agglomerate on the hill south of the bend is an orange volcanic sandstone and sedimentary breccia, which is part of the Cinder Basin unit. This deposit is exposed both on the north side of the hill and on the south side of the hill, in Six OClock Wash. It contains clasts of Annex Ridge(?) flow (up to 4 feet across) and Precambrian rocks in addition to trachybasalt clasts. Taken together the agglomerate and sedimentary units in the Cinder Basin member have a thickness of about 65 feet in the vicinity of this hill.

The hill is capped by black, poorly banded trachybasalt of the Fault Canyon flow, which, in this area, forms a low, north-facing escarpment on the flank of the dome.

Basal Tuffaceous Breccia and Sandstone

Distribution and physical features. In a few isolated localities along the contact between the Crater Pasture Formation and Precambrian rocks, tuffaceous breccia and sandstone (cs) are exposed. The thickest deposit, 30 feet, is found in Nine OClock Wash. In Four OClock Wash, a shallow excavation in the wash bottom revealed more than 4 feet of such deposits. In the southeast wall of Eight OClock Gorge, basal tuffaceous sandstone deposits are about a foot thick. At the base of the Road End Gap volcanic breccia and flow, a thin, bedded, dark-olive tuff is found in many localities which is too thin to map separately but which contains ash that is petrographically similar to ash found elsewhere in the basal breccia and sandstone. These basal deposits are poorly resistant to erosion and difficult to map separately, but they are important locally in determining structure in the rim.

Petrography. The lower part of the basal tuffaceous sandstone and breccia in Nine OClock Wash is a breccia consisting of crudely bedded clasts of

Precambrian rocks, up to 6 inches across, in a matrix of moderately sorted sandstone. The sandstone contains a trace of red-brown ash and is cemented by caliche. This breccia is about 20 feet thick and grades upward into a maroon, moderately well sorted, thick-bedded, tuffaceous sandstone consisting dominantly of red-brown ash. In Four OClock Wash, the lower part of the basal unit is a breccia which shows an increase in both sorting and ash-content from base to top. It is about 3 feet thick and is overlain by a 1-foot-thick bed of red, moderately well sorted, tuffaceous sandstone succeeded by a 6-inch-thick bed of olive-brown tuff.

The ash in these deposits is yellow-brown to dominantly red-brown in thin section and is microvesicular. It contains abundant (15 to 30 percent) serpentinized olivine grains which occur as phenocrysts, microphenocrysts, and (rarely) groundmass grains in a glassy to opaque matrix. The ash in the deposits in Eight OClock Gorge contain rare pyroxene phenocrysts and commonly has a groundmass of plagioclase laths and yellow-brown to red-brown glass. The ash in the Four and Nine OClock Wash deposits contains no pyroxene and has a dark, dusty to opaque matrix.

In addition to mafic ash, the bed of breccia in Four OClock Wash contains a trace of felsic volcanic clasts up to 1 centimeter in size. These clasts contain small phenocrysts and microphenocrysts of sanidine, plagioclase, biotite and hornblende in a groundmass of sparse feldspar laths and cryptocrystalline felsic minerals. These clasts are either latite or rhyodacite and are petrographically similar to the rhyodacite intrusive body (rf) in the gully at the head of Five OClock Wash.

Volcanic Breccia and Flow of Road End Gap

Distribution, stratigraphy, and physical features. The volcanic breccia and flow of Road End Gap is exposed in the southeastern and southern parts of

the rim of the crater from the southwest flank of Three OClock Hill to the crest of Buffalo Ridge. It consists of volcanic breccia (crb) interlayered with five relatively small flows (cr1 to cr5 numbered in order of age). There is a successive increase in maximum flow thickness from flow 1 (30 feet to 65(?) feet) to flow 2 (65 feet to 110(?) feet) to flow 3 (215(?) feet), and there is also a successive shift southward of the centers of the outcrop areas of these three flows. Flows 4 and 5 are west of the first three flows and have maximum thickness of 10 feet and 35 feet respectively. The Road End Gap unit as a whole is thickest near the head of Six Thirty Wash where it may be as much as 300 feet thick. The section exposed in Road End Gap is representative but not complete.

The volcanic breccia and flow of Road End Gap is more colorful than the rest of the Crater Pasture units; the rocks are black, red, red-orange, and yellow-brown. It also tends to be less resistant to erosion and more commonly covered by colluvium than the adjacent flows in the formation. Except for a few outcrops of its flows, it rarely forms the blocky outcrops that are typical of other volcanic units.

Relationship to other units. This unit overlies Precambrian rocks and pockets of the basal tuffaceous sandstone and breccia of the Crater Pasture Formation. It terminates on the crest of Buffalo Ridge before reaching the flow of Eight OClock Gorge; hence, its age relative to this unit is unknown. It is overlain on its northeastern edge by pockets of tuff of the Two OClock Gap unit, which are too small to be shown on the geologic map (pl. 1). It is overlain in several places, including its northeastern edge, by deposits of a pyroxene-trachyandesite sandstone and breccia of the Crater Pasture Formation. In most places, it is overlain by Annex Ridge flow. Its western part is

overlain by Buffalo Ridge flow. A vent for the Buffalo Ridge flow cuts this unit, as does a sill of the Fault Canyon unit.

Source. The thickest section of the Road End Gap unit and also the thickest sections of flows 2 and 3, which are the major flows in the unit, are located on the southern rim of the crater. Unless these thicknesses merely represent fillings of a local depression, the vent for the Road End Gap lavas probably lies to the south of this area.

Petrography. The volcanic breccia (crb) consists of black, vesicular clasts in a tan to reddish matrix. Clasts rarely exceed a foot or so across. Flows 1 and 4 consist of rock which is medium gray on fresh surfaces, grayish brown on weathered surfaces, nonvesicular, and has flow cleavage. Rocks of flows 2 and 5 are dark brownish red or dark tan on fresh surfaces, reddish-orange on weathered surfaces, and have no flow cleavage. Flow 3 is either black and vesicular or medium gray and non-vesicular. All rock in the Road End Gap unit contains red-brown-rimmed phenocrysts of olivine up to 3 millimeters across.

Flow 1 contains plagioclase, sanidine, olivine, augite, opaque minerals, and apatite and has a color index of about 35 (Table 2). Recognizable sanidine is subordinate to plagioclase but exceeds 10 percent of the total rock. On the basis of its color index, lack of quartz, and presence of more than 10 percent sanidine, the rock is classified as an olivine trachyandesite.* The presence of sanidine in the groundmass, suggested by chemical and normative analyses (Table 3) was confirmed using an electron microprobe. The sanidine occupies interstices between plagioclase laths and tends to contain abundant apatite needles. Plagioclase has a composition, as indicated by probe analysis, ranging

*The rock classification by Williams and others (1954) is used in this text for the naming of all igneous rocks.

TABLE 2. Modal Composition of Rocks of the Crater Pasture Formation

Unit sampled (map label)	crl	cef	cmf	ctf	caf	cbf	clf	cff
Sample number	190	A_o	227	178b	154c	235	154f	406b
Points Counted	989	500	501	972	991	500	1001	500
Mineral				Percent				
Glass	--	6.2	--	--	--	--	--	--
Plagioclase	18.3	6.0	7.6	11.2	14.9	20.0	20.9	0.6
Sanidine	14.3	--	13.2	14.4	25.3	14.8	12.8	57.2
Indefinite feldspar	28.9	18.4	29.8	35.4	35.7	40.0	29.1	--
Olivine*	8.3	6.8	5.2	2.0	--	--	--	9.6
Clinopyroxene*	22.3	32.2	19.4	19.4	1.0	3.4	16.6	17.8
Orthopyroxene*	--	--	--	1.3	--	--	--	--
Hornblende *	--	--	16.8	10.0	16.3	14.6	11.6	--
Biotite*	--	2.6	2.0	--	--	--	0.2	3.0
Apatite	0.7	0.4	0.6	0.7	2.8	tr	1.5	1.4
Zircon	--	--	0.2	--	--	--	--	--
Opaque minerals	4.5	18.6	2.4	5.1	3.9	5.8	7.2	7.8
Analcite	--	0.6	--	--	--	--	--	--
Calcite	--	2.2	--	--	--	--	--	--
Secondary minerals	2.2	--	3.0	0.1	--	--	0.2	2.6
Unknown minerals	--	6.0	--	--	--	1.4	--	--
Total	99.5	100.0	100.2	99.6	99.9	100.0	100.1	100.0
Color index **	35.1	66.2	46.0	37.8	21.2	23.8	35.6	38.2
Plagioclase/Total feldspar	>30.3	>24.6	> 15.0	> 18.3	> 19.6	> 26.7	> 33.3	1.4
Sanidine/Total feldspar	>23.0	> 0(?)	> 26.1	> 23.6	> 33.3	> 19.8	> 20.4	98.6

*. Includes alteration products, if any

** Sum of olivine, pyroxenes, hornblende, biotite, opaques, and dark unknown minerals

TABLE 2 continued

Sample location	
190	northwest side of Four OClock Hill
A_o	northwest bank of wash in Eight OClock Gorge
227	southeast end of Meadow Dam flow on Buffalo Ridge
178b	base of Two OClock Gap flow northwest of Two OClock Gap
154c	northeast bank of Four OClock Wash
235	base of Buffalo Ridge flow on top of Buffalo Ridge
154f	northeast bank of Four OClock Wash
406b	center of cliff in Fault Canyon flow on north side of Six OClock Wash east of Cinder Basin

from sodic labradorite to oligoclase. Olivine occurs as phenocrysts up to 3 mm in diameter and averages about 0.6 mm. It is altered to brown vermiculite(?) on its rims. Diopsidic augite is equally distributed in volume percent between phenocrysts (commonly glomerophenocrysts) and groundmass. The phenocrysts are similar in size to those of olivine. An unidentified, secondary mineral of low index, low birefringence, light brown color, and cryptocrystalline to radial-fibrous habit is commonly found in interstices between plagioclase laths and is generally occluded by red hematite dust and apatite needles. The texture of the rock is pilotaxitic.

In contrast to rock of flow 1, clasts of the volcanic breccia (crb) have a groundmass consisting of light yellow-brown to dark red-brown glass, subaligned plagioclase laths, a felt of diopsidic augite prisms and apatite needles, and opaque minerals. Crystalline phases have sharp relief and definition against the glass. Rock of flow 2 is similar to rock of the volcanic breccia except that cyptocrystalline material, which is heavily occluded by red hematite dust, occurs in the groundmass in the place of glass.

Chemical Composition. In three chemically analyzed samples of this unit (Table 3), silica, recalculated on a water-free and calcium-carbonate-free basis, ranges from 56 percent to 58 percent, well within the range of intermediate composition (52 percent to 66 percent). Potash averages around 3 percent, and normative potassium feldspar averages around 19 percent. A lower limit of 10 percent modal or normative potassium feldspar is used by Williams and others (1954, p. 97) for trachyandesite. Chemical and modal data are, thus, in accord in classifying rock of this unit as a trachyandesite.

Flow of Eight OClock Gorge

Distribution, stratigraphy, and physical features. The flow of Eight OClock Gorge crops out in the southwestern and western rim of the crater from the middle

TABLE 3. Chemical and Normative Composition of Rocks of the Crater Pasture Formation. (*) denotes a single clast from a clastic unit.

Unit sampled (map label)	crb	crl	cr2	cef	cef
Sample number	189	190	195a	Ao	294
Oxide		Weight percent			
SiO_2	54.5	56.2	56.6	47.2	49.0
Al_2O_3	14.0	13.9	13.7	12.5	13.0
Fe_2O_3	4.2	3.6	4.0	6.3	5.8
FeO	2.79	3.24	2.25	3.33	3.61
MgO	7.7	7.4	7.4	6.7	8.1
CaO	6.4	6.6	5.6	11.6	10.3
Na_2O	2.7	3.2	2.9	1.8	2.1
K_2O	2.6	3.1	3.6	2.9	3.0
TiO_2	1.03	1.02	0.93	1.78	0.11
P_2O_5	0.37	0.34	0.36	0.64	0.76
MnO	0.11	0.11	0.10	0.14	0.15
H_2O+	1.54	0.72	1.19	1.83	1.97
H_2O-	1.30	0.67	0.96	1.52	1.09
CO_2	0.19	<0.05	<0.05	1.41	0.56
Total	99.4	100.1	99.6	99.7	99.6
Normative mineral[1]					
Qz	7.53	4.36	6.63	2.44	--
Or	15.98	18.56	21.84	18.41	18.62
Ab	23.77	27.44	25.19	16.37	18.67
An	19.15	14.61	14.11	18.77	18.06
Co	--	--	--	--	--
Dp	7.89	12.81	9.34	22.55	20.99
Hy	16.45	14.19	14.58	7.47	11.33
Ol	--	--	--	--	1.45
Mt	6.33	5.29	5.01	6.48	8.83
Ht	--	--	0.65	2.30	--
Il	2.04	1.96	1.81	3.63	0.22
Sph	--	--	--	--	--
Rut	--	--	--	--	--
Ap	0.88	0.78	0.84	1.57	1.82
Total	100.00	100.00	100.00	100.00	100.00
Color index	32.70	34.25	31.40	42.44	42.82
An/(Ab +An)	44.62	34.74	35.90	53.42	49.18
Or/(Or +Ab +An)	27.13	30.63	35.72	34.38	33.64
SiO_2 (H_2O-, $CaCO_3$-free)	56.68	56.93	58.09	50.70	51.46

[1]Normative minerals are calculated after subtracting $CaCO_3$ from the oxides.

TABLE 3 continued

Unit sampled (*map label*)	cmf	cm1	cm2	ctb	ctf
Sample number	227	439	440	148	178b
Oxide		Weight percent			
SiO_2	51.8	51.8	50.0	52.3	54.9
Al_2O_3	13.8	15.1	14.7	15.0	15.3
Fe_2O_3	7.5	8.7	6.9	5.3	5.1
FeO	0.99	0.60	1.2	1.80	2.16
MgO	6.7	4.5	4.6	6.4	5.8
CaO	8.1	6.2	8.7	7.2	6.7
Na_2O	3.4	3.3	2.9	2.9	3.8
K_2O	2.3	2.5	3.1	2.8	2.4
TiO_2	1.25	1.6	1.2	0.85	1.25
P_2O_5	0.66	0.74	0.99	0.49	0.44
MnO	0.13	0.14	0.13	0.11	0.10
H_2O+	1.26	2.4	1.6	2.42	1.05
H_2O-	1.47	2.4	1.8	2.19	0.96
CO_2	0.26	<0.05	1.6	<0.05	<0.05
Total	99.6	100.0	99.4	99.8	100.0
Normative mineral					
Qz	2.56	6.95	5.19	4.10	4.70
Or	14.12	15.53	19.84	17.39	14.48
Ab	29.89	29.35	26.58	25.80	32.84
An	16.21	19.99	19.44	20.66	17.98
Co	--	--	--	--	--
Dp	15.05	3.44	7.27	10.53	10.14
Hy	10.35	10.18	9.03	11.87	10.05
Ol	--	--	--	--	--
Mt	--	--	0.88	3.89	3.74
Ht	7.79	9.14	6.86	2.89	2.63
Il	2.46	1.65	2.47	1.70	2.43
Sph	0.01	2.00	--	--	--
Rut	—	--	--	--	--
Ap	1.56	1.77	2.44	1.17	1.02
Total	100.00	100.00	100.00	100.00	100.00
Color index	35.66	26.41	26.52	30.87	28.98
An/(Ab +An)	35.17	40.51	42.24	44.47	35.39
Or/(Or +Ab +An)	23.44	23.94	30.13	27.24	22.18
SiO_2 (H_2O-, $CaCO_3$-free)	53.79	54.42	54.12	54.97	56.05

TABLE 3 continued

Unit sampled (map label)	caf	cam	cis	cis'
Sample number	154c	167	326a	328
Oxide		Weight percent		
SiO_2	55.3	56.2	56.0	52.1
Al_2O_3	16.8	16.9	16.3	16.0
Fe_2O_3	6.5	6.8	6.9	7.1
FeO	1.17	<0.05	0.86	0.95
MgO	2.6	2.9	3.1	3.5
CaO	5.4	5.9	5.2	3.9
Na_2O	4.0	4.1	3.6	2.4
K_2O	3.2	2.9	3.1	3.1
TiO_2	1.12	0.96	1.15	1.04
P_2O_5	0.64]	0.57	0.71	0.66
MnO	0.12	0.11	0.12	0.15
H_2O+	1.27	1.80	1.42	2.80
H_2O-	1.41	1.12	0.95	4.19
CO_2	<0.05	<0.05	0.12	0.44
Total	99.5	100.3	99.5	99.3
Normative mineral				
Qz	7.27	7.47	10.34	17.45
Or	19.53	17.61	18.91	20.28
Ab	34.96	35.65	31.45	22.49
An	19.05	19.68	19.79	13.57
Co	--	--	--	4.66
Dp	3.35	2.78	0.84	--
Hy	5.14	6.13	7.58	9.65
Ol	--	--	--	--
Mt	0.95	--	--	0.59
Ht	6.06	6.99	7.12	7.45
Il	2.20	0.24	2.14	2.19
Sph	--	2.11	0.15	--
Rut	--	--	--	--
Ap	1.51	1.33	1.67	1.66
Total	100.00	100.00	100.00	100.00
Color index	17.68	18.25	17.83	19.88
An/(Ab +An)	35.27	35.57	38.62	37.64
Or/(Or +Ab +An)	26.56	24.14	26.96	36.00
SiO_2 (H_2O-, $CaCO_3$-free)	57.10	57.74	57.80	57.67

TABLE 3 continued

Unit sampled (map label)	cbf	cbi	cbf	cbf(?)	cic
Sample number	235	232	291a	291c	429
Oxide		Weight percent			
SiO_2	56.0	54.1	55.7	53.9	55.6
Al_2O_3	15.8	16.3	16.1	16.0	16.5
Fe_2O_3	6.6	5.2	7.5	5.2	6.4
FeO	1.25	2.44	0.03	2.72	1.2
MgO	3.4	4.3	4.0	4.4	2.7
CaO	5.7	6.9	6.9	7.6	5.3
Na_2O	3.9	3.7	4.3	4.2	3.7
K_2O	3.2	2.9	2.7	2.7	2.9
TiO_2	1.10	1.13	1.05	1.25	1.2
P_2O_5	0.74	0.75	0.71	0.65	0.76
MnO	0.11	0.13	0.14	0.13	0.09
H_2O+	0.91	0.86	0.84	0.58	1.6
H_2O-	1.00	0.69	0.39	0.32	1.6
CO_2	0.20	0.29	0.29	0.44	<0.05
Total	99.9	99.7	100.7	100.1	99.55
Normative mineral					
Qz	7.90	5.51	4.85	2.35	10.44
Or	19.39	18.00	16.16	16.25	17.79
Ab	33.84	33.52	36.86	36.21	32.51
An	16.58	18.13	16.88	17.16	20.62
Co	--	--	--	--	--
Dp	4.82	7.23	6.39	10.97	1.19
Hy	6.45	7.01	7.13	6.07	6.43
Ol	--	--	--	--	--
Mt	1.23	3.64	--	5.67	0.71
Ht	5.92	2.97	7.59	1.38	6.15
Il	2.14	2.32	0.37	2.82	2.37
Sph	--	--	2.14	--	--
Rut	--	--	--	--	--
Ap	1.73	1.67	1.64	1.51	1.80
Total	100.00	100.00	100.00	100.00	100.00
Color index	20.56	23.18	23.61	26.52	16.85
An/(Ab +An)	32.88	35.10	31.41	32.15	38.81
Or/(Or +Ab +An)	27.78	25.85	23.12	23.35	25.09
SiO_2 (H_2O-, $CaCO_3$-free)	57.41	56.24	56.40	54.89	57.71

TABLE 3. continued

Unit sampled (map label)	clf	clf	cie	chh	ch
Sample number	154f	171	NE	166a	165
Oxide		Weight percent			
SiO_2	54.8	54.9	52.4	50.3	51.5
Al_2O_3	16.0	16.1	16.0	14.8	12.6
Fe_2O_3	6.3	5.6	6.6	6.2	7.2
FeO	1.71	2.16	1.62	1.35	0.90
MgO	3.7	4.4	4.6	4.8	6.1
CaO	7.1	7.8	7.4	8.1	8.1
Na_2O	3.8	3.8	3.8	1.9	1.4
K_2O	2.9	2.8	2.8	2.2	2.2
TiO_2	1.11	1.13	1.19	1.05	1.11
P_2O_5	0.59	0.59	0.54	0.56	0.44
MnO	0.13	0.13	0.13	0.12	0.12
H_2O+	0.75	0.31	0.78	3.49	2.97
H_2O-	1.21	0.44	1.42	4.25	4.84
CO_2	<0.05	0.06	<0.05	0.29	<0.05
Total	100.1	100.2	99.3	99.4	99.5
Normative mineral					
Qz	5.51	4.08	1.64	11.76	14.31
Or	17.47	16.66	17.05	14.29	14.19
Ab	32.78	32.38	33.13	17.67	12.93
An	18.39	18.74	18.90	27.88	23.58
Co	--	--	--	--	--
Dp	10.57	12.41	11.90	7.98	13.34
Hy	4.49	5.28	6.28	9.44	10.39
Ol	--	--	--	--	--
Mt	2.27	4.14	2.26	1.87	0.08
Ht	4.51	2.78	5.24	5.52	7.80
Il	2.15	2.16	2.33	2.19	2.30
Sph	--	--	--	--	--
Rut	--	--	--	--	--
Ap	1.37	1.35	1.27	1.40	1.09
Total	100.00	100.00	100.00	100.00	100.00
Color index	24.49	26.77	28.02	27.00	33.91
An/(Ab + An)	35.95	36.66	36.32	61.21	64.59
Or/(Or + Ab + An)	25.45	24.58	24.68	23.88	27.98
SiO_2 (H_2O^-, $CaCO_3$-free)	55.84	55.27	53.98	55.27	56.18

TABLE 3. continued

Unit sampled (map label)	ch	ch*	cct	cct*	cca
Sample number	286	289a1	250	240	409
Oxide			Weight percent		
SiO_2	49.4	52.9	50.6	47.2	49.5
Al_2O_3	14.5	16.1	13.2	12.1	14.6
Fe_2O_3	9.6	7.5	8.2	7.5	9.5
FeO	0.36	1.20	1.10	2.53	0.68
MgO	5.6	4.1	5.7	7.2	4.5
CaO	5.2	7.4	9.2	11.2	5.8
Na_2O	1.1	1.5	2.2	2.9	2.4
K_2O	0.8	1.9	3.0	1.5	3.1
TiO_2	1.29	1.22	1.51	1.52	1.6
P_2O_5	0.27	0.41	1.27	1.08	1.4
MnO	0.15	0.10	0.15	0.15	0.15
H_2O+	5.03	2.79	1.41	1.98	3.0
H_2O-	6.22	2.56	1.84	1.86	3.4
CO_2	0.20	0.32	0.23	0.38	<0.05
Total	99.7	100.0	99.6	99.1	99.6
Normative mineral					
Qz	24.73	18.16	6.61	0.56	9.10
Or	5.37	11.96	18.51	9.39	19.66
Ab	10.58	13.52	19.44	26.01	21.80
An	25.85	33.65	18.05	16.51	21.07
Co	3.97	--	--	--	0.11
Dp	--	0.33	14.79	25.20	--
Hy	15.85	10.72	7.96	7.32	12.03
Ol	--	--	--	--	--
Mt	--	0.70	--	4.49	--
Ht	10.91	7.50	8.56	4.85	10.19
Il	1.23	2.47	2.76	3.06	1.89
Sph	--	--	0.30	--	--
Rut	0.82	--	--	--	0.72
Ap	0.70	0.99	3.02	2.61	3.42
Total	100.00	100.00	100.00	100.00	100.00
Color index	28.80	21.72	34.38	44.92	24.83
An/(Ab + An)	70.96	71.34	48.15	38.83	47.15
Or/(Or + Ab + An)	12.85	20.22	33.05	18.10	31.44
SiO_2 (H_2O-, $CaCO_3$-free)	56.13	56.32	52.80	50.00	53.09

TABLE 3. continued

Unit sampled (map label)	ccl	ccd	ccm*	cff	cff
Sample number	414	410	416a	406a	246
Oxide			Weight percent		
SiO_2	51.9	49.3	62.4	54.1	52.4
Al_2O_3	13.3	13.7	15.4	13.3	13.4
Fe_2O_3	8.9	9.3	4.7	5.6	5.4
FeO	0.36	0.88	0.92	1.4	1.36
MgO	5.5	6.0	2.0	6.2	6.3
CaO	4.3	8.3	5.0	6.5	7.9
Na_2O	1.8	2.7	3.5	2.1	1.7
K_2O	2.8	1.7	3.5	5.5	5.9
TiO_2	1.2	1.5	0.86	0.95	1.02
P_2O_5	0.54	1.3	0.42	0.74	0.69
MnO	0.09	0.13	0.05	0.03	0.10
H_2O+	3.4	2.3	0.73	1.5	0.90
H_2O-	5.1	2.8	0.47	2.0	1.21
CO_2	<0.05	<0.05	0.08	<0.05	1.05
Total	99.2	99.9	100.0	99.9	99.3
Normative mineral					
Qz	16.35	7.08	17.67	3.50	2.10
Or	18.25	10.60	20.95	33.72	36.78
Ab	16.80	24.11	30.00	18.44	15.18
An	19.64	21.37	16.19	11.03	12.15
Co	0.87	--	--	--	--
Dp	--	9.14	4.79	13.55	13.57
Hy	15.11	11.53	2.82	9.73	10.26
Ol	--	--	--	--	--
Mt	--	--	0.64	1.93	1.85
Ht	9.81	9.81	4.32	4.48	4.42
Il	1.05	2.26	1.65	1.87	2.04
Sph	--	0.97	--	--	--
Rut	0.77	--	--	--	--
Ap	1.36	3.12	0.97	1.75	1.66
Total	100.00	100.00	100.00	100.00	100.00
Color index	26.74	33.71	14.23	31.57	32.14
An/(Ab + An)	53.89	46.99	35.05	37.43	44.46
Or/(Or + Ab + An)	33.37	18.90	31.20	53.37	57.37
SiO_2 (H_2O-, $CaCO_3$-free)	57.23	52.00	63.19	56.11	55.26

TABLE 3. continued

Unit sampled (map label)	cff	cip	unmapped rocks from Crater Pasture Formation		
Sample number	280a	331	459b	459c	334
Oxide			Weight percent		
SiO_2	55.9	41.5	48.6	46.4	49.4
Al_2O_3	13.8	10.3	12.5	12.1	13.1
Fe_2O_3	5.8	5.6	9.7	5.9	8.6
FeO	1.33	6.54	0.92	4.1	1.41
MgO	5.3	14.9	6.9	11.4	7.4
CaO	6.6	11.5	8.8	9.8	9.6
Na_2O	1.8	2.7	2.0	2.9	3.2
K_2O	6.3	0.9	3.5	1.2	1.6
TiO_2	0.98	2.99	2.0	1.9	1.80
P_2O_5	0.69	0.77	0.89	0.86	0.89
MnO	0.10	0.18	0.16	0.15	0.14
H_2O+	<0.01	1.96	2.2	2.5	2.04
H_2O-	1.12	0.62	1.8	0.81	1.18
CO_2	0.18	0.33	<0.05	<0.05	0.13
Total	99.9	100.8	100.0	100.0	100.5
Normative mineral					
Qz	5.28	--	1.99	--	1.22
Or	37.86	5.46	21.56	7.34	9.75
Ab	15.49	7.75	17.64	25.39	27.94
An	11.16	13.69	15.43	17.03	17.19
Co	--	--	--	--	--
Dp	12.76	29.48	16.44	21.37	19.31
Hy	7.51	--	10.29	2.52	10.06
Ol	--	ol 19.16 ne 8.50	--	11.87	--
Mt	1.80	8.33	--	8.48	--
Ht	4.65	--	10.11	0.25	8.87
Il	1.89	5.83	2.38	3.73	3.38
Sph	--	--	2.04	--	0.19
Rut	--	--	--	--	--
Ap	1.60	1.80	2.11	2.03	2.09
Total	100.00	100.00	100.00	100.00	100.00
Color index	28.61	62.80	41.26	48.22	41.81
An/(Ab + An)	41.89	63.83	46.65	40.15	38.09
Or/(Or + Ab + An)	58.68	20.29	39.46	14.74	17.77
SiO_2 (H_2O-, $CaCO_3$-free)	56.83	42.58	50.64	47.98	50.94

TABLE 3. continued

	Sample location
189	northwest side of Four OClock Hill
190	" "
195a	" "
Ao	northwest bank of wash in Eight OClock Gorge
294	top of Nine OClock Hill
227	southeast end of Meadow Dam flow on Buffalo Ridge
439	east bank of Fort Rock Creek south of Eight OClock Wash
440	high cliffs on west side of Fort Rock Creek south of Eight OClock Wash
148	near base of Two OClock Gap flow northwest of Two OClock Gap
178b	base of Two OClock Gap flow northwest of Two OClock Gap
154c	northeast bank of Four OClock Wash
167	northeast end of Hidden Pasture
326a	dike on north side of Six OClock Hill northeast of Road End Gap
328	gully at head of Five OClock Wash
235	base of Buffalo Ridge flow east of high point on Buffalo Ridge
232	boot-shaped intrusive body on Buffalo Ridge
291a	reddened base of Buffalo Ridge flow on Noon Hill
291c	massive upper part of Buffalo Ridge flow on Noon Hill
429	dike southeast of Crater Divide in southern half of Crater
154f	base of flow on northeast bank of Four OClock Wash
171	base of flow on east wall of Noon Gorge west of One OClock Hill fault
NE	northeasternmost intrusive body on southeastern edge of Eight OClock Basin
166a	northern end of Hidden Pasture
165	" "
286	east side of Noon Hill
289a1	" "
250	head of Cinder Basin Wash
240	head of Tyria Wash
409	east side of Cinder Basin
414	east bank of wash in Fault Canyon

410	Cinder Basin near head of Fault Canyon
416a	east wall of Fault Canyon
406a	north bank of Six OClock Wash east of Cinder Basin
246	head of Tyria Wash
280a	north bank of Eight OClock Wash
331	low saddle at northeast end of mound at bend in powerlines
459b	east side of large wash southeast of Number One Well
459c	" "
334	wash on north side of hill underlying Indian ruins

of Buffalo Ridge to the northern flank of Nine OClock Hill. This unit consists of flow and minor infolded agglomerate (cef) and a thin overlying deposit of sandstone and granule conglomerate (ces). Maximum thicknesses are 70 feet for the flow and 10 feet for the sandstone. This unit is thickest and best exposed in the vicinity of Eight OClock Gorge.

The flow (cef) is poorly resistant to weathering and is generally covered by colluvium. Where it crops out, it forms low, black, grussy outcrops. The sandstone (ces) is generally nonresistant, but does form a ledge on the northeast flank of Nine OClock Hill.

Relationship to other units. The Eight OClock Gorge flow overlies Precambrian rocks and pockets of basal tuffaceous breccia and sandstone of the Crater Pasture Formation. It is overlain by the flow of Meadow Dam in the southeast and by a pyroxene-trachyandesite sandstone and conglomerate of the Crater Pasture Formation in the northeast.

Source. This unit is thickest in the vicinity of Eight OClock Hill and Eight OClock Gorge. This area may have been the site of an old valley which the flow followed to the northeast. The source of the flow is presumed to be west of Eight OClock Hill.

Petrography. The flow (cef) is black with white calcite amygdules up to 1 cm across and abundant red-brown pseudomorphs of olivine phenocrysts up to 5 millimeters across. It is massive; no flow cleavage is present. It contains brown glass, plagioclase, sandine(?), pseudomorphs after olivine, augite, biotite, apatite, opaque minerals, analcite, and calcite (Table 2). The rock is a limburgite (Williams and others, 1954, p. 74). In thin section, olivine is seen to be completely altered, and its pseudomorphs range in size from 50 μ to 5 mm. The pseudomorphs are rimmed by very fine-grained red and yellow-brown

minerals which may be iddingsite and vermiculite, respectively. The interior of the grains are serpentine. Augite occurs as microphenocrysts ranging in size from 50 μ up to 0.5 mm. These microphenocrysts generally have distinctive hour-glass zonation and commonly occur in stellate to cruciform clusters. The groundmass consists of brown glass, arborescent opaque microlites, or scopulites, plagioclase laths, anhedral, low-birefringent feldspar, tiny biotite flakes, and apatite needles. The scopulites are generally arranged in fan-like clusters and plagioclase laths are intergrown with them. Rarely, plagioclase forms larger laths arranged in a more or less regular, criss-cross pattern, or "house-of-cards". Much of the anhedral feldspar, which appears as low-birefringent patches in the glass and in interstices between scopulites, probably is sanidine. Biotite flakes commonly are arranged in a "house-of-cards" pattern in the glass. A trace of analcite is associated with the calcite amygdules. The 6 percent of "unknown minerals" reported in the modal analysis (Table 2) refers to apparent hematite alteration of the scopulites and of biotite.

In another sample of the Eight OClock Gorge flow, plagioclase occurs predominantly as lath-like microphenocrysts and the arborescent form of the scopulites is suppressed.

The sandstone and granule conglomerate (ces) has colors of orange, maroon, and olive-buff. It consists dominantly of red-brown, microvesicular ash which contains pseudomorphs of olivine phenocrysts and microphenocrysts and also microphenocrysts of augite, commonly seen in stellate to cruciform clusters. The ash most commonly has an occluded, glassy matrix, but holocrystalline ash is also seen.

Chemical composition. In two chemically analyzed samples of the Eight OClock Gorge flow (Table 3), silica, recalculated on a water-free and calcium-

carbonate-free basis, is about 51 percent, or within the range of basic composition (45 percent to 52 percent). Potash content, about 3 percent in these samples, is relatively high for the silica content, and is reflected in high normative potassium feldspar (about 18 percent) and in the presence(?) of sanidine in the groundmass of the rocks.

Flow of the Meadow Dam

Distribution, stratigraphy, and physical features. The flow of Meadow Dam underlies a low hill on the west side of Meadow Dam and a large hill south of the dam, where it forms high cliffs on the west side of Fort Rock Creek. It also crops out for about a thousand feet along the base of low cliffs on the east side of the creek below the dam. Additionally, this unit is exposed in the rim of the crater, where it is tilted to the southwest. In the rim, it crops out from near the crest of Buffalo Ridge to near the top of Eight OClock Hill.

The unit consists chiefly of two flows, or two parts of one flow, which can be distinguished in outcrops along Fort Rock Creek. A lower flow (cml) is separated from an upper flow (cm2) by a thin (agglomeratic(?)) volcanic breccia (cmm). Where there is no breccia separating the upper from the lower flow, the unit is mapped as undivided flow (cmf). In the rim of the crater, the unit is mapped as undivided flow, although it has been correlated with the lower flow. (See pl. 3). Here, flow overlies a thin basal unit (cmb) consisting of volcanic breccia and minor sandstone. The rim of the crater provides the only exposure of the base of the Meadow Dam unit.

The maximum thickness of the flow of Meadow Dam in the rim of the crater is 135 feet. In the large hill south of the dam, the maximum thickness

of the upper flow is 135 feet, and the lower flow may be as much as 250 feet thick.

The flow of Meadow Dam is relatively resistant to erosion and tends to form blocky outcrops. The upper flow is the most resistant part of this unit and is responsible for the high cliffs on the west side of Fort Rock Creek.

Relationship to other units. In the rim of the crater, the Meadow Dam flow overlies the Eight OClock Gorge flow and is overlain by pockets of a pyroxene trachyandesite sandstone of the Crater Pasture Formation and by the Buffalo Ridge flow. Along Fort Rock Creek, the Meadow Dam flow is overlain by pockets of conglomerate of the Cinder Basin unit and by the Fault Canyon flow. On the southwest, west and northwest sides of the large hill south of Meadow Dam, it is overlain by and, in one place, faulted against the Old Stage Road Member of the Fort Rock Creek Rhyodacite.

Source. The large hill south of Meadow Dam apparently represents the thickest accumulation of the Meadow Dam flow; the vent for the flow probably underlies the hill. Outcrop of this flow in the rim of the crater may represent a lobe which, like the Eight OClock Gorge flow, flowed northeast up an old valley in Precambrian rocks.

Petrography. Outcrops of this unit along Fort Rock Creek are massive; whereas outcrops in the rim of the crater show flow cleavage. All rock in this unit is medium gray on fresh surfaces and brownish gray on weathered surfaces. None of the flow is vesicular, although the upper flow has calcite-filled vugs. Phenocrysts of hornblende are abundant. They are altered red-brown or dark gray and are in some cases difficult to distinguish from the groundmass. Phenocrysts of green diopsidic(?) augite are also present but sparse.

The rock is made up of plagioclase, sanidine, clinopyroxene, altered olivine, altered hornblende, biotite, opaque minerals, and accessory minerals (Table 2). On the basis of its high color index, 46, the absence of quartz, and the presence of more than 10 percent sanidine, the rock is classified as a trachybasalt (Williams, 1954, p. 57), or, in particular, a hornblende trachybasalt. In the sample examined, most hornblende grains are totally altered to a mixture of granular opaque minerals, pyroxene and brown biotite. The outlines of the original grains are preserved but their centers are ragged. Two generations of hornblende grains are present. One-third of the hornblende occurs as larger stubby prisms up to one centimeter in width; two-thirds occur as smaller prisms and needles less than 1 mm in length. Clinopyroxene, including both augite and pigeonite, occurs rarely as phenocrysts, abundantly as microphenocrysts, which range in size from 20μ to 0.5 mm and, in some cases occur in clumps, and abundantly as groundmass grains. It is approximately equally distributed in volume percent between microphenocrysts and groundmass. Olivine, completely altered to red-brown biotite, occurs as microphenocrysts up to 0.2 mm in diameter. Plagioclase occurs as subhedral, poorly twinned laths, arranged in sheaf-like masses which sweep around phenocrysts. Sanidine(?) occupies interstices, but the identity of this mineral has not been confirmed by probe analysis. Secondary minerals are represented by a pinkish-brown crystocrystalline mineral of high negative relief. No large petrographic differences appear to be present among the various parts of this unit, although the upper flow (cm2) is somewhat finer grained than the rest.

Chemical composition. In three chemically analyzed samples (Table 3), silica, recalculated on a water-free and calcium-carbonate-free basis, averages

54 percent, which falls at the low end of the intermediate range of composition (52 percent to 66 percent). Potash and normative potassium feldspar average 2-1/2 percent to 17 percent, respectively.

Tuff and Flow of Two OClock Gap

Distribution, stratigraphy, and physical features. The tuff and flow of Two OClock Gap consists chiefly of basal tuff and, locally, tuff breccia (ctb) overlain by flow (ctf). The tuff reaches a maximum thickness of perhaps 50 feet on Outer Hill, where it is most extensively exposed. It is exposed in the rim of the crater as a thin bed which extends as far as One OClock Wash, on the northwest,and Four OClock Wash on the south. The flow is confined to the southeastern end of Lion Ridge, just northwest of Two OClock Gap, where it probably reaches a thickness of about 125 feet. The flow has a vuggy zone (ctz) on its northeastern flank which may be a flow-top zone.

The tuff (ctb) thins abruptly to the southwest across the Upper Two OClock Gap fault. On the southeastern end of Lion Ridge adjacent to the flow (crf), the tuff is as much as 50 feet thick. Across the fault on the small knob extending southwest of Lion Ridge, the tuff is at most a few feet thick. In Two OClock Gap, the tuff is also thinner on the southwest side of the fault. These consistent stratigraphic changes across the Upper Two OClock Gap fault can be attributed to movement on the fault during or after emplacement of the tuff.

The tuff (ctb) is poorly resistant to erosion; its presence is revealed only by uprooted trees in many locations. The flow (ctf) is relatively resistant and, in a few locations, forms blocky outcrops.

Relationship to other units. The tuff and flow of Two OClock Gap overlies Precambrian rocks everywhere where it is mapped (pl. 1), but in the

vicinity of Four OClock Wash, it occurs in pockets too small to map on top of the volcanic breccia of the Road End Gap unit. It is overlain by Lion Ridge flow in most places and by Annex Ridge flow on the southern flank of Three OClock Hill. Unmapped pockets of the tuff (ctb) in the vicinity of Four OClock Wash are overlain in places by a pyroxene-trachyandesite sandstone and conglomerate of the Crater Pasture Formation.

Source. A vent for the tuff (ctb) is probably located in the vicinity of Outer Hill, where the tuff is thickest. The flow (ctf) must overlie its own vent on the southeastern end of Lion Ridge, as the flow is entirely restricted to this area.

Petrography. The basal tuff (ctb) is characterized by lapilli which weather to an olive-green and contain rare green pyroxene phenocrysts up to several millimeters across. Other clast colors include olive-buff, olive-gray, and charcoal gray. Most clasts are microvesicular. In addition, the tuff includes a few percent of clasts of Precambrian rock. Most of the Precambrian rocks appear to be of local derivation, and, in fact, many may have come from Precambrian exposures on the southwestern wall of the Upper Two OClock Gap fault. Some of the Precambrian clasts, however, appear deformed in the tuff and hence may be xenoliths subsequently stripped of enclosing magma. The flow (ctf) is nonvesicular and flow cleavage is developed poorly at its base. It varies in color from light bluish gray to light maroon on fresh surfaces and has a varnished exterior. The vuggy zone (ctz) is charcoal gray.

Rock of the flow is made up of plagioclase, sanidine, altered olivine, clinopyroxene, orthopyroxene, hornblende, opaque minerals, and apatite (Table 2). The rock is a pyroxene trachyandesite. Its color index is about 38. Sanidine, which occurs as an interstitial mineral in amounts exceeding 14 percent

was identified with the electron microprobe. Plagioclase, has a composition ranging from sodic labradorite to sodic andesine, as indicated by the microprobe. In the modal analysis, about 3/4 of the pyroxene phenocrysts counted, or about 1 percent of the rock, are orthopyroxene, including enstatite and hypersthene, as determined by microprobe analysis. The remainder of the phenocrysts are augite. Orthopyroxene constitutes less than 1/6 of the pyroxene microphenocrysts, however. These grains range in size from 0.1 mm to 0.5 mm. Groundmass pyroxene grains, or grains smaller than 0.1 mm, are apparently all augite. Rims of augite and altered olivine are found around some orthopyroxene grains. Olivine and hornblende occur in the rock as microphenocrysts. The olivine is altered red-brown and in places attains sizes as large as 0.15 mm. The hornblende occurs as needles and shows rim alteration to granular opaque minerals and pyroxene. Fresh hornblende occurs only in the cores of the larger needles, which in some cases reach 1 mm in length. The texture of the rock is pilotaxitic.

In contrast to the flow rock, clasts of the tuff that were examined in thin-section have fresh hornblende and a glassy matrix which varies in color from yellow-brown to occluded reddish brown.

Chemical composition. In two chemically analyzed samples (Table 3), recalculated silica averages 55-1/2 percent, well within the range of intermediate composition. Potash content, averaging about 2-1/2 percent, and normative potassium feldspar content, averaging about 6 percent, are similar to contents in the Meadow Dam hornblende trachybasalt and in the Road End Gap olivine trachyandesite.

Pyroxene-Trachyandesite Sandstone and Conglomerate

Distribution and physical features. A minor unit of light maroon to red-orange pyroxene-trachyandesite sandstone and granule conglomerate (cp), is found in a few places around the rim of the crater. In the north wall of Four OClock Wash, about 40 feet of this unit is exposed. In many places on Four OClock Hill along the contact between the Road End Gap volcanic breccia and flow and the Annex Ridge flow, a few inches of this sandstone and conglomerate can be exposed by digging. Discontinuous outcrops are seen on Six OClock Hill and Buffalo Ridge. The unit is exposed continuously from Eight OClock Gorge to the top of Nine OClock Hill, attaining a thickness of at least 25 feet and possibly 90 feet on Eight OClock Hill. Except for local ledges, it is poorly resistant to erosion.

Relationship to other units. This sandstone and conglomerate overlies the volcanic breccia and flow of Road End Gap in the southeastern and southern parts of the rim of the crater. In the vicinity of Four OClock Wash it also overlies local pockets of tuff of the Two OClock Gap unit. In the southwestern and western parts of the rim, it overlies the Meadow Dam flow and the Eight OClock Gorge flow. It is overlain by the Annex Ridge flow in the southeast and south and by the Buffalo Ridge flow in the southwest and west.

Petrography. The sandstone and conglomerate are well bedded and moderately well sorted. They consist dominantly of microvesicular gray, red, and red-orange ash which contains abundant microphenocrysts of altered olivine scattered phenocrysts of augite, and rare phenocrysts of (olivine-rimmed) orthopyroxene. A few clasts contain abundant microphenocrysts of hornblende. The matrix of the ash is dominantly red-brown, dark, occluded glass which contains abundant tiny laths of plagioclase. Ash from this unit differs from ash in

lower tuffaceous sandstone units (cs and ces) in containing no olivine phenocrysts and in containing pyroxene almost exclusively as phenocrysts.

In outcrops on Six OClock Hill and Buffalo Ridge, this unit is a breccia; it contains coarse clasts, including blocks, of Road End Gap olivine trachyandesite. The matrix between these clasts is pyroxene-trachyandesite ash.

Flow of Annex Ridge

Distribution, stratigraphy, and physical features. The flow of Annex Ridge underlies the southeastern quadrant of the crater rim. It attains a maximum thickness of about 400 feet, as measured on Six OClock Hill and pinches out abruptly on Three OClock Hill and at Six Thirty Wash. It is a steep-sided dome, viewed nearly in cross section on the geologic map (pl. I) owing to its high dip. The flow also underlies Annex Ridge, southeast of the rim and crops out in many places around the base of the Buttox Hills and the hills farther east, beyond the area mapped.

This flow has been subdivided into a basal facies (cab), a lower flow (caf), a flow-top zone (caz), and an upper flow (cam). The lower flow (caf) is the unit which underlies the rim of the crater. The upper flow (cam) constitutes all outcrops of the Annex Ridge unit southeast of the crater rim, including outcrops on Annex Ridge.

A dike-like intrusive body on the north flank of Six OClock Hill (cis) and a similar intrusive, which is largely altered to clay minerals, in the gully at the head of Five OClock Wash (cis') are petrographically similar to the Annex Ridge flow and are correlated with it.

The lower flow (caf) is slabby and is somewhat less resistant to erosion than the adjacent Lion Ridge and Buffalo Ridge flows; consequently, Four OClock Hill and Six OClock Hill, which are underlain by this flow, are

low areas in the rim of the crater. The upper flow (cam) is massive and is more resistant than the lower flow.

Relationship to other units. The Annex Ridge overlies the Road End Gap volcanic breccia and flow in most places. Locally, it overlies a pyroxene-trachyandesite sandstone and conglomerate of the Crater Pasture Formation and pockets of tuff of the Two OClock Gap unit. At the northern tip of its outcrop area it overlies Precambrian rocks in a few places. In the rim of the crater, it is overlain by Lion Ridge flow on the north and Buffalo Ridge flow on the west. On the flanks of the dome and beyond, it is overlain in different places by the Hidden Pasture tuff and conglomerate, the One OClock Wash sedimentary breccia, the Cinder Basin tuff and agglomerate, and the Fault Canyon flow, of the Crater Pasture Formation, and by the Noon Gorge sedimentary breccia, the Old Stage Road Member, and an unnamed rhyodacite-bearing sandstone, conglomerate, and breccia (fs), of the Fort Rock Creek Rhyodacite. It is intruded by a dike of the basalt of Buttox Hills and by a dike of trachybasalt of the Fault Canyon unit.

Source. The upper flow (cam) probably overlies a major vent for the Annex Ridge flow in the region southeast of the crater rim. The Annex Ridge flow appears to have been extruded as a viscous dome in two stages, which are represented by the upper and lower flows (caf and cam). (See pl. 3). The small intrusive body on the north flank of Six OClock Hill (cis) may occupy a small vent for this unit.

Petrography. The basal facies (cab), is characteristically a soft, buff to light pinkish brown, (pyro-)clastic to microvuggy rock. It contains phenocrysts and microphenocrysts of black hornblende as does all rock of the Annex Ridge flow. In Six Thirty Wash this basal unit also includes volcanic and tuffaceous

sedimentary rocks. The lower flow (caf) is light bluish gray to very light gray on both weathered and fresh surfaces. It is nonvesicular, and has flow cleavage, which is best developed toward the base of the flow. The flow-top zone (caz), is characterized by microvugs, some microbrecciation, a light pinkish brown color on fresh surfaces, and a brownish weathering rind with a rough, "warty" appearance. The "warty" appearance comes largely from the selective preservation of hornblende phenocrysts during weathering. Hornblende phenocrysts in the flow-top zone have, in many localities, resistant, brownish-red to scarlet rims. Crude vertical partings in the flow-top zone distinguishes it, albeit faintly, from the overlying flow (cam), which is very similar in all respects but is massive.

A sample of the lower flow (caf) contains plagioclase, sanidine, hornblende, opaque minerals, apatite, and almost no pyroxene. The rock is a hornblende trachyandesite. Its color index is about 21. Analysis by electron microprobe confirmed the presence of interstitial sanidine. All of the plagioclase analyzed was sodic labradorite, but the grains studied were all sharp laths greater than 5 μ in width. Further probe analysis might well reveal andesine and oligoclase. Hornblende occurs as phenocrysts up to nearly 1 cm in length. All hornblende is altered on the rim to very fine granular opaque minerals; in the larger grains the core is altered to augite, plagioclase, opaque minerals, and vermiculite(?). This alteration of the core gives the hornblende phenocrysts the appearance of rotted wood. Zoning, with up to three zones, is observed in a number of hornblende grains. Radial (spoke-like) strings of very fine-granular opaque minerals is also seen. Hornblende microphenocrysts are present which are sharply distinguished from the phenocrysts in size and shape. These grains have lengths less than 0.5 mm and are needle-like. They are

almost totally altered to opaque minerals. About one third of the hornblende occurs as microphenocrysts; the rest occurs as phenocrysts. About one-fourth of the apatite in this rock occurs as stubby prisms up to 0.25 mm in length. These have a purple to violet tinge and characteristic striations parallel to their long axes. The rest of the apatite occurs as needles in the ground mass. The texture of the rock is pilotaxitic.

The dike-like intrusive body (cis) consists of blue-gray rock with abundant prisms of black hornblende. In thin section the rock is identical to the modally analyzed sample of the Annex Ridge flow except that the hornblende is olive-green in color and unaltered. The altered intrusive (cis') is similar to the dike-like body (cis) except that the feldspar in the ground mass has been totally altered to clay minerals. Outlines of plagioclase laths are still plainly visible. The hornblende in this rock is unaltered.

Chemical composition. In two chemically analyzed samples of the Annex Ridge flow (Table 3), recalculated silica averages about 57 percent, well within the intermediate range of composition. Potash is about 3 percent, and normative potassium feldspar is between 18 and 19 percent. In silica content and normative potassium feldspar content, rock of this unit is most similar to the olivine trachyandesite of the Road End Gap unit. Color index, however, which averages about 18, is about half of that of rocks of the Road End Gap.

Rock from the dike-like body (cis) is chemically similar to rock of the Annex Ridge flow (Table 3). Rock from the altered intrusive (cis'), however, is depleted in lime and soda, reflecting alteration of its feldspar to clay (montmorillonite(?)). Depletion of lime and soda is the reason for lower normative albite, anorthite, and diopside and higher normative quartz in this rock.

Flow of Buffalo Ridge

Distribution and physical features. The flow of Buffalo Ridge outcrops continuously in the rim of the crater from the head of Six Thirty Wash to Wedge Basin. In Six Thirty Wash, it pinches out abruptly against the steep side of the Annex Ridge flow. North of Buffalo Ridge, the flow thins somewhat more gradually. A block of petrographically similar rock rests, somewhat jumbled, on top of deposits of the Hidden Pasture tuff and conglomerate on Noon Hill and is correlated with the flow of Buffalo Ridge.

The Buffalo Ridge flow is divided into five subunits, a basal facies (cbb), an intrusive breccia (cbt), which is an equivalent of the basal facies, the major flow (cbf), with a flow-top zone (cbz), and a massive intrusive body (cbi), which is an equivalent of the flow. The intrusive bodies of this unit (cbt and cbi) are exposed on Buffalo Ridge. The extrusive material of the unit (comprised by cbb, cbf, and cbz) attains a maximum thickness, atop Buffalo Ridge, of about 330 feet.

A dike in the vicinity of Crater Divide (cic) and a small intrusive body at the south end of Eight OClock Basin (cic') are petrographically similar to rock of the Buffalo Ridge unit and are correlated with it.

The flow, flow-top, and massive intrusive body (cbf, cbz, and cbi), are resistant to erosion and tend to form blocky, often varnished, outcrops. This unit is responsible for the presence of Buffalo Ridge and the series of flatiron-like hills which form the rim of the crater to the north of Buffalo Ridge.

Relationship to other units. In order from south to north, the Buffalo Ridge flow overlies the Road End Gap volcanic breccia and flow, which its vents also cut, the Meadow Dam flow, a pyroxene-trachyandesite sandstone and conglomerate of the Crater Pasture Formation, the Eight OClock Gorge flow, and

Precambrian rocks. It is overlain in different places on the flank of the dome by the One OClock Wash sedimentary breccia and the Cinder Basin tuff and agglomerate of the Crater Pasture Formation and by the Noon Gorge sedimentary breccia and the Old Stage Road Member of the Fort Rock Creek Rhyodacite. It is intruded by a dike of trachybasalt related to the Fault Canyon flow.

Blocks of this Buffalo Ridge flow are embedded in a conglomeratic bed (chc) at the top of the exposed section of the Hidden Pasture unit on Noon Hill; it would appear that the Hidden Pasture unit is younger than the Buffalo Ridge flow. The blocks embedded in this unit probably were deposited prior to a landslide which brought the large jumbled body of Buffalo Ridge flow to rest on top of the Hidden Pasture deposits in this location.

A tiny fragment of hornblende trachyandesite similar to that of the Buffalo Ridge flow was identified in the basal clastic unit (clb) of the Lion Ridge flow, suggesting that the Lion Ridge flow is younger than the Buffalo Ridge flow.

Source. The intrusive breccia (cbt) and the massive intrusive body (cbi) occupy vents for the Buffalo Ridge unit on Buffalo Ridge. These intrusives can be traced continuously into their extrusive equivalents, and represent the only explicit sources for any of the Crater Pasture extrusives except the Fault Canyon flow (which has an explicit source at the head of Tyria Wash). The intrusive breccia penetrates the Road End Gap volcanic breccia and flow and, in many places, follows the bedding in this unit. This breccia can be traced laterally into tuff of the basal facies (cbb). The massive intrusive body (cbi) occupies a boot-shaped bent on the inner flank of Buffalo Ridge and a vent of indefinite shape on the crest of the ridge where massive hornblende trachyandesite can be traced continuously into the flow (cbf). A patch of flow breccia on the southwestern side of Buffalo Ridge, near the head of Tyria Wash is associated with

changes in flow-banding attitudes in its vicinity; this breccia may occupy still another vent. The small dike in the vicinity of Crater Divide (cic) and the small intrusive body at the south end of Eight OClock Basin (cic') may have been minor sources for the Buffalo Ridge unit. Small concealed vents may also lie west of the rim of the crater.

Petrography. The basal facies (cbb) includes tuff, minor tuffaceous sandstone, and local flow-base breccia. The tuff is characterized by moderately sorted, microvesicular, yellow to buff-weathering, coarse ash and lapilli containing abundant black hornblende prisms. The tuff contains rare accidental clasts of Precambrian rocks and Road End Gap olivine trachyandesite. The intrusive equivalent of the basal facies (cbt) is a breccia consisting of yellow to buff-weathering lapilli-sized clasts of Buffalo Ridge rock mixed with abundant maroon-colored fragments of Road End Gap olivine trachyandesite. The latter fragments were apparently reddened during intrusion of the breccia. They range in amount from less than 10 percent of the breccia up to almost 100 percent of the breccia. The breccia is distinguishable from the basal facies in its lack of sorting and in its high content of these xenoliths. The flow (cbf) varies from a blue-gray rock with flow cleavage, at the base of the flow, to a massive, medium-gray rock with a varnish exterior, in the middle and upper parts of the flow. The middle and upper parts of the flow are microvesicular and have largely altered hornblende phenocrysts. The flow-top zone (cbz) is a brownish, microvuggy rock. The intrusive equivalent of the flow (cbi) is a massive, medium to dark gray rock which weathers gray-buff.

A sample of flow (cbf) from atop Buffalo Ridge (Table 2) is petrographically similar to rock of the Annex Ridge flow. It has a slightly higher color index, 24. The hornblende content of this rock resembles that of the Annex

Ridge flow in every way except that microphenocrysts make up only about a quarter of the hornblende. Groundmass clinopyroxene (3-1/2 percent) and opaque minerals (6 percent) are more abundant in this rock than in the Annex Ridge rock, but apatite microphenocrysts (trace) and groundmass apatite grains (trace(?)) are less abundant.

In Eight OClock Gorge, rock of the flow (cbf) is somewhat more mafic than the sample described above. It contains a trace of small clinopyroxene phenocrysts and also abundant (5 to 10 percent) groundmass pyroxene. Microphenocrysts of hornblende and apatite are much diminished in number compared to the sample from Buffalo Ridge. This rock is transitional in its petrography to rock of the Lion Ridge flow, to be discussed below.

Rock from the northern end of the Buffalo Ridge flow, in Wedge Basin, is similar to the modally analyzed rock from Buffalo Ridge. It contains no phenocrysts of clinopyroxene; however, it does contain abundant (5 to 10 percent) groundmass pyroxene.

The large block of flow on Noon Hill preserves the gross stratigraphy of the Buffalo Ridge flow, with an identifiable basal facies in at least two places. Attitudes of flow banding within the block, however, are not consistent, leading to the conclusion that the block is broken and structurally disarrayed. Most of the rock in this block resembles rock atop Buffalo Ridge with its characteristic abundant hornblende microphenocrysts, its trace of purplish apatite microphenocrysts, and its low pyroxene content. Other rock in this block resembles the more mafic rock of the Buffalo Ridge flow seen in Eight OClock Gorge or rock of the Lion Ridge flow.

The dike near Crater Divide (cic) consists of blue-gray rock with abundant black hornblende prisms. In thin section the hornblende is olive-green and is

unaltered. The rock resembles the modally analyzed rock from Buffalo Ridge except that it does not contain hornblende microphenocrysts. The intrusive body at the south end of Eight OClock Basin (cic') is a breccia containing abundant contact-metamorphosed clasts of Precambrian rocks and multi-colored clasts of altered hornblende trachyandesite. The latter clasts contain abundant phenocrysts of hornblende which have been totally altered to a light yellow-green clay mineral. The groundmass, like the groundmass of the altered intrusive body in the gully at the head of Five OClock Wash (cis'), has been completely altered to clay minerals, but outlines of plagioclase laths are still plainly visible.

Chemical composition. Three chemically analyzed samples of the Buffalo Ridge flow, samples 235, 232, and 29la (Table 3), are closely similar in chemistry and also resemble the hornblende trachyandesite of the Annex Ridge flow. These samples have slightly less silica, averaging 56-1/2 percent, and slightly higher color indices, averaging 22-1/2, than the Annex Ridge flow. One of these samples, 29la, is from the jumbled block of Buffalo Ridge flow on Noon Hill. Another sample from this jumbled block, 29lc, is chemically (and petrographically) similar to the hornblende trachyandesite of the Lion Ridge flow (Table 3).

Dike rock (sample 429) is chemically similar to rock from Buffalo Ridge, although its lower modal hornblende content is reflected in a lower normative color index.

Flow of Lion Ridge

Distribution, stratigraphy, and physical features. The flow of Lion Ridge crops out in several large areas on the rim of the crater between Noon Gorge and Four OClock Hill. On One OClock Hill and Lion Ridge, the flow constitutes a band of outcrop of fairly uniform width, thinning out in Noon Gorge and

pinching out against the Two OClock Gap unit on the southeast end of Lion Ridge. On a small knob extending southwest from Lion Ridge near its southeast end, the Lion Ridge flow forms two northwest-southeast-trending strips of outcrop which terminate on the northwest side of the knob and converge in Two OClock Gap. Two faults, the Upper and Lower Two OClock Gap faults, are responsible for the repetition of the Lion Ridge flow in this area. Blocks have been faulted successively downward toward the southwest, or toward the interior of the crater. A similar repetition of the Lion Ridge flow, caused by these two faults, is seen on Outer Hill. The Lion Ridge flow is also present on Three OClock Hill where it is apparently continuous, under the colluvium in Two OClock Gap, with flow in the lower fault block on both Outer Hill and on the small knob southwest of Lion Ridge. The flow pinches out against the Annex Ridge Flow on the east side of Four OClock Hill.

A basal facies (clb), a reddened flow-base zone (clr), and a flow-top zone (clz), have been recognized in this unit. The unit is about 150 feet thick at the head of One OClock Wash; its maximum thickness is probably attained on Three OClock Hill where it may be as much as 200 feet thick.

An intrusive body in Eight OClock Basin (cie) is petrographically similar to the Lion Ridge flow and is correlated with it.

The Lion Ridge flow is resistant to weathering and tends to form blocky, varnished outcrops. It is responsible for the presence of One OClock Hill, Lion Ridge, Outer Hill, and Three OClock Hill.

Relationship to other units. In order from south to north, the Lion Ridge flow overlies the Annex Ridge flow, the tuff and flow of Two OClock Gap, and Precambrian rocks. It is overlain in Four OClock wash by the Old Stage Road Member of the Fort Rock Creek Rhyodacite, and on Lion Ridge by the One OClock Wash sedimentary breccia.

The field relationship of the Lion Ridge flow to the Hidden Pasture tuff and conglomerate is problematical. In the east wall of Noon Gorge, a jumbled block of Lion Ridge flow rests on Hidden Pasture deposits in a fashion similar to that of the block of Buffalo Ridge flow across the gorge. No blocks of Lion Ridge flow were actually observed to be embedded in the Hidden Pasture deposits, however, as was seen across the gorge. In Hidden Pasture, Hidden Pasture deposits conspicuously overlie Annex Ridge flow on the southeast side of Four OClock Hill and appear to overlie the tip of the Lion Ridge flow, although excavating in this location would be necessary to determine whether this deposit overlies or underlies the flow. On Outer Hill a distinctive blue-gray hornblende trachyandesite tuff underlies Lion Ridge flow. This tuff resembles a distinctive tuff (chh) of the Hidden Pasture unit, although it has been mapped as part of the basal facies (clb) of the Lion Ridge flow. At the southeastern tip of Outer Hill, some blocks of Lion Ridge flow, along with the distinctive basal blue-gray tuff, overlie Hidden-Pasture-like deposits (cu) but have been interpreted tentatively as a landslide. In summary, the Lion Ridge flow appears to be older than the Hidden Pasture tuff and conglomerate. Like the Buffalo Ridge flow, it has been thrust over these deposits in some places by landsliding.

Source. A major vent for the Lion Ridge flow may be located beneath Three OClock Hill, where the flow is apparently thickest. A second vent beneath Lion Ridge may have been the source for the northern segment of the flow, which is geographically higher than and somewhat removed from the postulated Three OClock Hill vent. A relatively thicker sequence of basal tuff-breccia (clb) on Outer Hill may indicate the presence of a small vent in that area. The small plug in Eight OClock Basin (cie) may have also been a source for this unit.

Petrography. The rocks of the Lion Ridge flow are similar to those of the Buffalo Ridge flow. The basal facies (clb) includes tuff, minor tuff-breccia, and minor flow-base breccia. The tuff is yellow-buff to pink and is moderately sorted. On Outer Hill, the basal tuff is blue-gray and moderately well sorted. The reddened flow-base zone (clr) resembles the overlying part of the flow (clf) but has a distinctive reddish to lavender color which makes it a useful mapping unit. The main part of the flow (clf) is dark blue-gray at its base and has well developed flow cleavage. In its middle and upper parts, the flow is medium to dark gray and massive with varnished surfaces. The base of the flow is nonvesicular, whereas the middle and upper parts are sparsely vesicular. Generally, the vesicles are flattened. The flow-top zone (clz) is dark steel gray on a fresh surface, has microvugs, and shows some microbrecciation. Largely altered hornblende prisms are present throughout this flow; they are less altered toward the base and toward the top of the flow.

This flow is a hornblende trachyandesite. It is similar to the Annex Ridge and Buffalo Ridge hornblende trachyandesites but contains considerably more pyroxene and also more opaque minerals (Table 2). The hornblende in this sample has a thick alteration rind consisting of fine-granular opaque minerals and pyroxene. The cores of the hornblende grains generally are altered to opaque minerals, pyroxene, feldspar, and biotite. The pattern of alteration in the core resembles rotted wood. Unlike the hornblende in the Buffalo Ridge and Annex Ridge flows, the hornblende of the Lion Ridge flow occurs chiefly as phenocrysts, which range in size up to 1/2 cm across.

Microphenocrysts of hornblende are rare. Augite occurs as small phenocrysts, generally less than 1 mm in size, as glomerophenocrysts, and as ground mass grains. Phenocrysts and glomerophenocrysts of augite make up only about 1-1/2 percent of the rock. These grains are occasionally found as inclusions in the hornblende. Analysis of the groundmass with the electron microprobe confirmed the presence of interstitial sanidine and indicates a range in plagioclase composition from sodic labradorite to oligoclase. Apatite in this rock occurs as needles in the ground mass and only very rarely as purplish microphenocrysts of the type found in the Buffalo Ridge and Annex Ridge hornblende trachyandesites. The texture of the rock is pilotaxitic.

Rock from the intrusive body in Eight OClock Basin (cie) is somewhat similar to the Lion Ridge flow but contains half again to twice as much hornblende (15 percent to 20 percent). The hornblende in this rock is, furthermore, olive green and fresh except for some "worm-hole" core alteration.

Chemical composition. Two modally analyzed samples of the Lion Ridge flow (Table 3) show recalculated silica to be about 55-1/2 percent, which is lower than an average of value for the Buffalo Ridge hornblende trachyandesite (56-1/2 percent) or for the Annex Ridge hornblende trachyandesite (57 percent). A lower silica content in this flow is reflected in a higher normative color index, which averages 25-1/2. Potash averages about 3 percent, and normative potassium feldspar averages 17 percent; both are slightly lower than they are in the Buffalo Ridge and Annex Ridge flows.

The intrusive body (sample NE) is somewhat more basic than any of the samples of the Lion Ridge flow; it has a recalculated silica content of 54 percent.

Tuff and Conglomerate of Hidden Pasture

Distribution, stratigraphy, and physical features. The tuff and conglomerate of Hidden Pasture crops out in several relatively small areas on the Fort Rock structure. In Hidden Pasture, up to 75 feet of tuff and conglomerate overlies the Annex Ridge flow on the southeast side of Four OClock Hill. Another outcrop area is in the vicinity of Noon Gorge, where as much as 90 feet of tuff and conglomerate occupies an ancient valley or hollow in the Precambrian rock. The deposits in the Noon Gorge area were tilted and faulted during doming and their upper beds incorporate landslide material which was emplaced during doming. Two small outcrops of the Hidden Pasture unit are also found on the east flank of Short Hill.

This unit is poorly resistant to erosion and is generally covered by colluvium. Where it does crop out, however, it is fairly distinctive. It consists of tuff, tuffaceous sandstone, and fine-pebble conglomerate. Yellow and olive-brown tuffs occur at several horizons. The tuffaceous sandstone and conglomerate are characterized by light gray to light brown overall colors and multicolored clasts. Two distinctive beds in the unit have been mapped, a blue-gray hornblende trachyandesite tuff (chh), found in Hidden Pasture and in the Noon Gorge area, and a fine-pebble conglomerate (chc), found in the Noon Gorge area.

Relationship to other units. In Hidden Pasture, tuff and conglomerate of this unit overlie the Annex Ridge flow and(?) Lion Ridge flow and are overlain by ash-flow tuff of the Fort Rock Creek Rhyodacite. In the Noon Gorge area, Hidden Pasture deposits overlie Precambrian rocks. In the east wall of Noon Gorge, these deposits are seen to be conformably overlain by the sedimentary

breccia of One OClock Wash. In most places in the Noon Gorge area, however, they are in fault contact with either Precambrian rock or overlying landslide blocks of Buffalo Ridge and Lion Ridge flow.

Source. A unit of undivided Hidden Pasture and Cinder Basin deposits (cu) has been mapped in a number of scattered locations from the northeast flank of Annex Ridge to the southeast corner of Outer Hill. Similar deposits are also found farther east, beyond the area mapped, and appear to be associated with a large trachybasalt eruptive center located about 3/4 mile east of the dome. (See fig. 3). Ash from an outcrop on the southeast flank of Outer Hill and also from an outcrop farther east is petrographically identical to Hidden Pasture ash. At least some of the Hidden Pasture ash probably originated from the large trachybasalt center to the east. Some also could be derived from the Cinder Basin eruptive center to be discussed below.

Petrography. Beds in this unit vary in thickness from millimeters to several tenths of a meter. Sorting varies from moderate to good; the tuffs are the best sorted. Two chief petrographic types of ash are present in the tuffs, one is hornblende trachyandesite, and the other is olivine trachyandesite. The first type constitutes the hornblende-trachyandesite tuff (chh) and the second constitutes yellow tuffs which are found at several horizons in the section. Sandstone and conglomerate in this unit contain mixtures of these two types of ash and also ash which is petrographically transitional between the two.

Hornblende trachyandesite tuff (chh). This tuff forms a thin bed (less than one foot thick) of well sorted blue-gray to blue-green microvesicular ash which contains abundant euhedral hornblende prisms. In thin section the hornblende is greenish brown, which distinguishes it from the brown variety of hornblende found in the Annex Ridge, Buffalo Ridge and Lion Ridge flows. Subhedral

groundmass hornblende granules are also seen. Tiny phenocrysts of clinopyroxene are present but rare. In addition to hornblende granules the groundmass contains plagioclase laths, pyroxene prisms, and abundant apatite prisms in a clear, glassy to cryptocrystalline matrix.

Yellow tuff. This tuff consists of yellow, yellow-brown, and olive-brown to black, microvesicular ash. In thin section it is seen to contain rare phenocrysts and microphenocrysts of clinopyroxene and abundant microphenocrysts of red-brown, altered olivine. The groundmass is yellow-brown, red-brown, or occluded glass, which is commonly altered to clay minerals; plagioclase laths are generally present. This ash is olivine trachyandesite.

Fine-pebble conglomerate (chc). This unit contains rounded, fine pebbles which weather out to form a characteristic pebbly float. The pebbles are various colors including light gray to charcoal gray, light brown to red-brown, and, more rarely, yellow and bluish green. Typically, the pebbles are microvesicular and devoid of phenocrysts or microphenocrysts. They are composed of glass, tiny laths of plagioclase and tiny grains of hornblende(?) and/or altered olivine. The texture of the ash is pilotaxitic. Ash in the matrix of the conglomerate includes other petrographic types with abundant olivine and clinopyroxene microphenocrysts.

Other deposits. The remaining beds in the Hidden Pasture unit are gray to brownish sandstone and conglomerate. In hand specimen, multicolored clasts are seen which contain either hornblende, green pyroxene, red-brown olivine, or any combination of these. Hornblende occurs both as small phenocrysts and as microphenocrysts; pyroxene occurs dominantly as phenocrysts, attaining sizes of several millimeters, but is rare; olivine occurs mostly as microphenocrysts and generally is abundant.

All deposits in this unit are cemented by tridymite and potassium feldspar.

Chemical composition. In Table 3, the samples are hornblende-trachyandesite tuff (chh), 166a, olive to yellow tuff, 165, yellow tuff, 286, and a clast from a conglomerate, 289al. Silica in these samples, recalculated to eliminate the large quantities of water and lesser quantities of calcium carbonate which are present, averages about 56 percent. Potash ranges from 1 percent to 2 percent and is low compared to potash in all older rocks of the Crater Pasture Formation. Normative potassium feldspar contents are correspondingly low; nevertheless, all but the sample of yellow tuff, 286, contain more than 10 percent normative potassium feldspar and are trachyandesites. In the sample of yellow tuff, 286, and the clast from the conglomerate, 289al, depletion(?) of soda and potash relative to silica and alumina may reflect the alteration to clay minerals seen in these samples. This depletion(?) of soda and potash results in lower normative albite and orthoclase and higher normative quartz in these samples relative to other trachyandesites of the Crater Pasture Formation. A depletion of soda and lime was seen in the sample of the altered hornblende trachyandesite dike rock (cis') in the gully at the head of Five OClock Wash.

Sedimentary Breccia of One OClock Wash

Distribution and physical features. The sedimentary breccia of One OClock Wash is a local deposit on the flanks of Fort Rock dome which was formed during uplift of the dome. It is distributed around three-fourths of the periphery of the dome in outcrops of varying size and thickness. The most extensive outcrop is found on the northern flank of the crater where this breccia crops out continuously from near Two OClock Gap to Wedge Basin. Thicknesses

of preserved breccia in this area are estimated at 75 feet in One OClock Wash, 200 feet on Noon Hill, and 240 feet on Short Hill. From Wedge Basin counterclockwise around the crater to Six OClock Wash, the breccia is exposed chiefly in the walls of the valleys which cut into the flank of the dome. In Eight OClock Gorge, it ranges in thickness between a few feet and 200 feet. In the vicinity of Six Thirty Wash, it is about 60 feet thick.

The One OClock Wash breccia is poorly resistant to weathering; it is covered by colluvium in almost all places except where it is made up of coarse angular blocks. Where outcrops are seen, they are generally in the banks of washes or in local places which have been washed clean of colluvium on the flank of the dome. Cliffrose or "quinine bush" grows preferentially on soil underlain by this breccia (and other clastic units) and is of help in locating outcrops of this unit. Often it is necessary to dig shallow pits, one to two feet deep, to determine the presence and nature of the breccia. Hundreds of pits were dug in the hills on the north side of the crater. Float from this unit consists, in most places, of a mixture of dark volcanic rocks and light-colored, pink and orange Precambrian rocks.

Relationship to other units. The One OClock Wash sedimentary breccia overlies the Hidden Pasture tuff and conglomerate in Noon Gorge, the Lion Ridge flow and the tuff and flow of Two OClock Gap on Lion Ridge, the Buffalo Ridge flow on Noon Hill, Ten OClock Hill, Nine OClock Hill, Eight OClock Hill, and Buffalo Ridge, the Annex Ridge flow in Six OClock Wash and vicinity, and Precambrian rocks in Noon Gorge, on Short Hill, and in Wedge Basin. It is overlain by the tuff and agglomerate of Cinder Basin in Six OClock Wash and in a number of nearby places to the west. Throughout most of its area of outcrop, it is overlain by the Noon Gorge sedimentary breccia of the Fort Rock Creek Rhyodacite and locally by the Old Stage Road Member of the Fort

Rock Creek Rhyodacite.

The contact of the One OClock Wash sedimentary breccia with the underlying Hidden Pasture tuff and conglomerate can be readily studied in the east wall of Noon Gorge by digging shallow pits. The contact appears to be gradational over a narrow interval. Ash content diminishes upward, and clasts of recognizable flow rock, which are the chief constituent of the breccia, increase. The gradation takes place over an interval of about 50 feet on the ground. There is some alternation of ash-rich and clast-rich lithology within this interval.

Near its contact with underlying volcanic flow rock, the sedimentary breccia locally includes small bodies of authigenic breccia, which are indicated by the symbol, ⅄, on the geologic map (pl. I). These bodies include discrete fillings of large cracks, such as those created by the Eight OClock Gorge faults and the Eight OClock Hill fault. They also include rock in the uppermost part of some flows in which there is widespread filling of small cracks or in which extensive open brecciation is observed accompanied by inclusion of small amounts of foreign ash. Defined in this fashion, the One OClock Wash breccia includes rock in the uppermost parts of the Buffalo Ridge flow in Ten OClock Wash and Nine OClock Wash; it includes rock in the uppermost part of the Lion Ridge flow in Four OClock Wash. Bodies of authigenic breccia grade upward into (allogenic) sedimentary breccia in most locations.

Provenance and clast content. The One OClock Wash sedimentary breccia consists of clasts eroded from the dome during its uplift and also of varying small amounts of olivine-trachyandesite ash. Clasts eroded from the dome include both volcanic and Precambrian rocks, and their compositions reflect the source areas on the dome from which they were derived. The Lion

Ridge flow apparently underlay most of the roof of the dome; clasts of this flow are generally most abundant in the breccia. Clasts of the Lion Ridge flow cannot be distinguished in all cases, however, from clasts of the Buffalo Ridge flow. Clasts of Precambrian rocks generally are second in abundance in breccia. Volume percentages of these clasts have been contoured on the geologic map (pl. I). The variation in abundance of Precambrian clasts represents the only stratigraphic variation observable in the breccia. Two patterns of variation can be seen. In the vicinity of Lion Ridge, Eight OClock Gorge, and Six OClock Wash, the content of Precambrian rocks is essentially nil in the basal part of the breccia and increases relatively smoothly in successively higher parts of the breccia. Between Noon Hill and Wedge Basin, the content of Precambrian rock is initially high at the base of the breccia, becomes lower somewhat higher in the section, and then increases rather smoothly in still higher parts of the breccia. The first pattern probably reflects progressive erosion of a source area on the dome in which volcanic rocks initially overlay Precambrian rocks; the second pattern probably reflects progressive erosion of a source area on the dome in which Precambrian rocks were initially exposed but outcrops of volcanic rocks occurred in nearby high areas on the dome.

Block patches also have been mapped in the breccia. A block patch is defined to be an area containing five or more blocks of volcanic flow rock, each of which is four or more feet across, which together constitute 30 percent or more of the patch. Clasts as large as 17 feet are seen in some locations. These block patches probably originated as disaggregated landslide blocks, similar to the blocks of flow still largely intact atop Noon Hill and in the east wall of Noon Gorge. Block patches are confined to the northern flank of the crater.

Lithology. The breccia is unbedded and unsorted; it contains angular to subangular clasts. In a few localities, lenticular clasts show a weak preferred orientation which is interpreted as bedding. In most outcrops which are not in the vicinity of block patches, clasts do not exceed one foot in size, and most of the breccia is made up of clasts an inch or smaller in size. Clasts of Precambrian rocks tend to be smaller than clasts of volcanic rocks. Where the breccia is relatively fine-grained and made up mostly of volcanic clasts, it has an overall pinkish brown color. In these rocks, there is a continuous gradation in clast size from silt to large clasts; a "matrix" is not easily distinguishable from larger clasts. Induration is strong enough in some instances that the rock fractures through its clasts, although in most instances it is possible to break clasts out of the breccia. The volcanic clasts have different colors. Larger ones are medium gray to maroon, and smaller ones (one centimeter or less in size) have additional colors of red-brown, yellow-brown, pink, and light gray Mafic to intermediate* ash is present everywhere in the finer-grained part of the breccia. This ash occurs in amounts rarely exceeding a trace. It is identical petrographically to olivine-trachyandesite ash in the Hidden Pasture tuff and conglomerate and also to olivine-trachybasalt ash in the Cinder Basin tuff and agglomerate, which is discussed below. The ash is most easily observed in thin section, but can also be seen in hand specimen on close crutiny. In hand specimen, it shows up as tiny green, yellow, and olive-brown clasts which are less than one millimeter across. Some of these tiny clasts are small pyroxene phenocrysts, some are small serpentinized olivine phenocrysts, and most are

* Mafic is used here to refer to dark-colored rock, ideally rock with a color index greater than 40, although color index cannot be determined in glassy specimens. Intermediate here refers to moderately dark-colored rock, or rock with a color index between 10 and 40. Felsic refers to light-colored rock, or rock with a color index less than 10.

microvesicular ash containing green and red-brown speck-like microphenocrysts. The breccia is cemented by tridymite and potassium feldspar(?).

Tuff and Agglomerate of Cinder Basin

Distribution, stratigraphy, and physical features. In the mapped area, tuff and agglomerate of Cinder Basin is exposed in several inliers in the overlying Fault Canyon flow and along the base of the Fault Canyon flow from Annex Ridge to the head of Tyria Wash. It also forms a few narrow outcrops at the base of the Fault Canyon flow in Fort Rock Creek. The outcrop belt of the Cinder Basin unit extends well beyond the mapped area (pl. 1) to the south and southeast.

The Cinder Basin tuff and agglomerate is divided into several intertonguing subunits. (See the explanation for the geologic map, pl. 1). The principal subunits are tuff (cct), agglomerate (cca), and sedimentary breccia (ccb). Several small flows (ccl, cc2, and cc3) and a dike (ccd) have also been mapped, as well as a distinctive bed of sedimentary breccia (ccm) which contains a mixture of rhyodacite, dacite and trachybasalt clasts. The three principal subunits are found throughout the outcrop area of the Cinder Basin tuff and agglomerate, whereas the minor subunits are local in occurrence.

None of the subunits of the Cinder Basin tuff and agglomerate are resistant to erosion, although the agglomerate, the minor flows, and the dike tend to be more resistant than the tuff and sedimentary breccia . Where it is exposed as inliers in the overlying Fault Canyon flow, this unit forms basins, of which Cinder Basin is one.

Relationship to other units. The Cinder Basin tuff and agglomerate overlies the One OClock Wash sedimentary breccia in Six OClock Wash and in nearby places to the west. On the southwest flank of Buffalo Ridge it overlies the

Buffalo Ridge flow in a few places. It overlies the Annex Ridge flow on the south side of Six OClock Hill and along the west flank of Annex Ridge. In Fort Rock Creek, thin lenses of this unit overlie the flow of Meadow Dam. The Cinder Basin unit is overlain in most places by Fault Canyon flow; it is also cut by vents for the Fault Canyon flow on the southwest flank of Buffalo Ridge. Locally on the flank of the dome, it is overlain by the Noon Gorge breccia and the Old Stage Road Member of the Fort Rock Creek Rhyodacite.

The contact of the Cinder Basin tuff and agglomerate with the underlying One OClock Wash sedimentary breccia is not exposed but may be gradational over a narrow interval. In Six OClock Wash, over a distance of about twenty feet on the ground, one passes from the One OClock Wash sedimentary breccia, which contains only a trace of ash, to a tuffaceous breccia assigned to the Cinder Basin unit, that contains 40 percent or more ash. Beds of sedimentary breccia in the Cinder Basin unit probably correlate with parts of the One OClock Wash sedimentary breccia at other locations around the dome.

Some rocks of the Cinder Basin tuff (cct) may be present in a unit mapped as undivided Crater Pasture Formation (cu) found in a large area extending northeastward from the northeast flank of Annex Ridge. The undivided unit consists of blue-green tuff and associated sedimentary rocks. It is not clear whether these beds belong to the Hidden Pasture tuff and conglomerate or to the Cinder Basin tuff and agglomerate.

Source for volcanic units. The agglomerate (cca) of the Cinder Basin unit forms two hills beneath the Fault Canyon flow. One hill is between Six OClock Wash and Annex Wash. Parts of the flanks of these hills are exposed as inliers in the flow. The hills are probably cinder cores located over vents from which the agglomerate (cca) and possibly the tuff (cct) and some of the

small flows (ccl and cc2) were derived. The youngest of the small flows (cc3) may have been fed by the dike (ccd).

Provenance for sedimentary units. Where it outcrops on or near the southern flank of the dome, the sedimentary breccia (ccb) contains abundant clasts similar to those in the sedimentary breccia of One OClock Wash, which are clearly derived from the dome. The small outcrop of sedimentary breccia in Cinder Basin, however, is devoid of these clasts; it contains only ash and angular clasts of trachybasalt. This area apparently was not supplied by a drainage from the dome.

The sedimentary breccia that contains a mixture of rhyodacite, dacite, and trachybasalt clasts (ccm) was probably derived in part from an area to the southeast, in which two intrusive(?) bodies of rhyodacite and dacite are located (fig. 3). Rocks of these intrusives are petrographically similar to the rhyodacite and dacite clasts in the breccia.

Petrography. Rocks of the Cinder Basin tuff and agglomerate are characterized by pseudomorphs of olivine phenocrysts and microphenocrysts. Commonly the pseudomorphs are light green serpentine, but in some specimens they are very fine-grained red-brown minerals. The altered phenocrysts occur in sizes up to several millimeters and are relatively sparse; the altered microphenocrysts occur in sizes up to 0.5 mm and are abundant. In rocks of most subunits, clinopyroxene is present as phenocrysts, microphenocrysts, and groundmass grains but is somewhat less abundant than olivine and much less visible in hand specimen. A trace of biotite is present in most rocks and is locally visible in hand specimen. Color, texture, and groundmass composition differ from subunit to subunit.

Tuff (cct). The subunit designated Cinder Basin tuff includes tuff,

agglomeratic tuff, sandstone, and conglomerate. Tuff, sandstone and conglomerate are in most places well bedded and moderately to moderately well sorted, whereas agglomeratic tuff is massive and unsorted. These deposits have colors of light bluish green, maroon, yellow, and white. In thin section of the tuff, ash grains are seen to be chiefly light-brown glass, occluded red-brown glass, or pale brown altered glass. Some tuffs consist mostly of glassy ash, and some, mostly of altered ash. Scattered bombs in the agglomeratic tuff are as large as 5 feet across. They are vesicular, banded, and are dark bluish gray to reddish gray in color. Bombs contain, on the average, 1/2 percent serpentinized olivine phenocrysts, 15 percent serpentinized olivine microphenocrysts, 1/2 percent clinopyroxene phenocrysts, 10 percent clinopyroxene microphenocrysts, 20 percent groundmass clinopyroxene, 15 percent plagioclase laths (less calcic than An_{44}), 8 percent opaque minerals, a trace of biotite phenocrysts and the remaining 30 percent cryptocrystalline interstitial minerals. Sanidine is probably present among the interstitial minerals; normative potassium feldspar is calculated to be about 18.5 percent (Table 3, sample 250). This rock is a trachybasalt, if one uses a modal color index of 40 to separate trachybasalts from trachyandesites.

A minor unit mapped as granule and fine-pebble conglomerate (ccc) is a distinctive sedimentary bed in the tuff, consisting of red to multicolored, rounded clasts of olivine trachybasalt and olivine trachyandesite. Some beds of this conglomerate contain ash similar to ash of the fine-pebble conglomerate of the Hidden Pasture unit (chc).

None of the deposits mapped as tuff (cct) contain more than 10 percent foreign clasts. A deposit with more than 10 percent foreign clasts was mapped as sedimentary breccia (ccb).

Agglomerate (cca). This subunit consists of bombs up to 10 feet across. The bombs are microvesicular and gray or vesicular and banded in colors red-brown and dark gray. They are embedded in a lighter colored red-brown matrix of ash. The bombs are similar in petrography to the bombs described in the tuff, but olivine is altered to hematite(?) and biotite(?) and tends to weather out of the rock leaving prismatic holes lined by alteration products. A trace of embayed hornblende phenocrysts is also present. A zone of welded agglomerate (ccw) has been mapped in places where the bombs become difficult to distinguish from the matrix and from each other. In this zone of welding both the matrix and bombs are bluish gray in color.

Sedimentary breccia (ccb). This subunit consists of breccia and sandstone. It is composed dominantly of clasts of olivine trachybasalt but contains more than 10 percent foreign clasts, including hornblende-trachyandesite clasts and Precambrian rocks. The breccia is orange in color. Most of the foreign clasts apparently were derived by erosion of the dome although some could have been accidental clasts in the eruption of the trachybasalt. On the south flank of the dome the foreign clasts are up to 4 feet across.

Minor subunits. Three small flows have been mapped in the Cinder Basin unit. The lowest of these (ccl) is found in Fault Canyon. It is a massive, vesicular, light-maroon-colored rock. It contains no pyroxene except for a possible trace in the groundmass. Serpentine pseudomorphs of olivine phenocrysts and microphenocrysts are found in abundance (15 percent total). This flow has a lower abundance of mafic minerals than other trachybasalts in the unit. The middle flow (cc2) is also found in Fault Canyon. It is a dark bluish gray, sparsely vesicular rock similar to rock of the agglomerate (cca). It occurs at the same stratigraphic horizon as the agglomerate and may be a spatter flow

related to the agglomerate. A third flow (cc3) crops out in Cinder Basin. It is a nonvesicular, dark gray rock similar to rock of a dike (ccd), also found in Cinder Basin. The rock of the dike contains phenocrysts and abundant microphenocrysts of clinopyroxene, and fairly abundant tiny anhedral flakes of biotite. The groundmass consists dominantly of pyroxene, opaque minerals, plagioclase(?) laths, and apatite with interstitial anhedral grains of feldspar.

A sedimentary breccia (ccm) has been mapped in Fault Canyon that is distinguished from the other sedimentary breccia (ccb) by its clast content. This breccia is a massive, unsorted pinkish buff rock containing clasts of olivine trachybasalt (and olivine trachyandesite(?)), rhyodacite, and dacite; it is referred to here as mixed breccia. Olivine-trachybasalt clasts dominate among the visible clasts in the breccia and occur in relatively dark colors of gray, brown, red-brown, yellow-brown, and maroon. These clasts range in size up to 5 inches across but generally are about 1/2 inch across. Rhyodacite clasts make up most of the matrix of the breccia but are found in sizes up to 10 inches across. These clasts include gray-white, gray, and red nonvesicular clasts as well as scattered fragments of white pumice. They are similar to rocks of the overlying Fort Rock Creek Rhyodacite. They contain 10 to 15 percent phenocrysts and microphenocrysts of plagioclase, 2 percent biotite, 2 percent clinopyroxene, and rare phenocrysts of sanidine and quartz(?). The groundmass is cryptocrystalline. Dacite clasts constitute less than 15 percent of the breccia. They are dark maroon and are up to 10 inches across. They are slightly more mafic than the rhyodacite clasts. One dacite clast that was examined contains 25 percent plagioclase (less calcic than An_{48}), 5(?) percent potassium feldspar, 3 percent clinopyroxene, 2 percent biotite, 1 percent pseudomorphs after olivine (red and opaque minerals), 3 percent opaque minerals, and

a cryptocrystalline groundmass with a few percent opaque dust. The feldspar and pyroxene in this rock occur bimodally as phenocrysts and microphenocrysts. Biotite and pseudomorphs after olivine occur as microphenocrysts, which are seen as brown specks in hand specimen.

Chemical composition. Exclusive of dacite sample, 416a, from the mixed sedimentary breccia (ccm), the range in recalculated silica content among rocks of the Cinder Basin unit is 50 percent to 57 percent (Table 3). Four of the rocks in this range have recalculated silica contents between 50 percent and 53 percent; these rocks are near the division, 52 percent, between intermediate and basic rocks. Sample 414 of the minor flow (ccl) has a recalculated silica content of 57 percent, reflecting its low modal abundance of mafic minerals. On the average, rocks of the Cinder Basin unit are more basic than any older unit of the Crater Pasture Formation except the flow of Eight OClock Gorge. Potash content in these rocks averages about 2-1/2 percent, and normative potassium feldspar averages 15 percent.

Flow of Fault Canyon

Distribution, stratigraphy, and physical features. The flow of Fault Canyon covers much of the southwestern part of the map (pl. 1). The flow is approximately bounded by Fort Rock Creek on the west, the flank of the Fort Rock dome on the north, and Annex Ridge on the east. It extends about a mile to the southeast beyond the area mapped. The Fault Canyon flow probably attains a maximum thickness of about 200 feet in the vicinity of Tyria Wash. Several minor subdivisions have been recognized in addition to the major flow (cff). They include an agglomerate (cfa) on top of the flow, dikes and other intrusive bodies (cfi), intrusive tuff-breccia or breccia (cft), and a flow-base zone (cfb).

The Fault Canyon flow is resistant to erosion; it forms high cliffs along the eastern side of Fort Rock Creek and along eastern tributaries of Fort Rock Creek.

Relationship to other units. Throughout most of its outcrop area, the Fault Canyon flow overlies the Cinder Basin tuff and agglomerate. Locally, along Fort Rock Creek, it overlies the flow of Meadow Dam. It probably overlies the One OClock Wash sedimentary breccia in the vicinity of Eight OClock Wash, but the contact is covered here by the Noon Gorge sedimentary breccia. The Fault Canyon flow is overlain in places along the flank of the dome by the Noon Gorge sedimentary breccia and the Old Stage Road Member of the Fort Rock Creek Rhyodacite. Elsewhere it is overlain only by the Old Stage Road Member of the Fort Rock Creek Rhyodacite.

Source and relationship to doming. One vent for the Fault Canyon flow is exposed at the head of Tyria Wash. An associated dike northeast of this vent and two small sills in the vicinity of Road End Gap may have been small vents for the flow. Topographically high areas on the flow on either side of Six OClock Wash may overlie concealed vents.

Intrusive contacts at the head of Tyria Wash dip moderately to shallowly to the northeast under Buffalo Ridge; it appears that this lava was erupted from a magma chamber beneath the dome (pl. 2). Extrusion of the Fault Canyon flow is closely associated in time with uplift of the Fort Rock dome. Sedimentary breccias formed by erosion of the dome both underlie and overlie the flow. Conclusions drawn from a study of structure of the dome and of the Fault Canyon flow (p. 167 ff) are that the flow was extruded near the end of doming. The interpretation in this report is that the magma which was the source for the Fault Canyon flow was responsible for the uplift of the dome.

Petrography. The flow (cff), is massive and nonvesicular to sparsely vesicular. It is black, dark brownish gray, medium brownish gray, or greenish gray in color. In Six OClock Wash, Tyria Wash, and other canyons, it is greenish gray and jointed at its base and brownish gray and massive at its top. Joints at the base of the flow occur in two or more directions, and in places, are spaced as close as one to two centimeters. Red stain commonly occurs along one of the joint sets.

The Fault Canyon flow is characterized by abundant microphenocrysts and scattered glomerophenocrysts of altered olivine. Microphenocrysts are easily seen under a hand lens and are yellow-brown to red-brown in color. The glomerophenocrysts are either yellowish green with a yellow-brown rim or are red-brown. Green pyroxene phenocrysts, glomerophenocrysts, and microphenocrysts also are abundant but are much less easily seen in hand specimen.

Petrographic analysis of a sample of the flow (cff) (Table 2) shows this rock to be made up of sanidine and mafic minerals; the rock has a color index of about 38. In its lack of plagioclase, this rock resembles the trachybasalts of the Navajo country described by Williams (1936, p. 148). It is here given the name of olivine-sanidine trachybasalt. Sanidine occurs as subhedral laths, averaging 0.1 mm in length, and as anhedral grains. The mafic minerals include augite, pigeonite, altered olivine, altered biotite, and opaque minerals. In the sample examined, augite occurs as clear, euhedral to subhedral phenocrysts, up to 1 mm, and microphenocrysts, averaging 0.2 mm; pigeonite occurs as yellow-green overgrowths on the augite and as anhedral groundmass granules. Pigeonite is over twice as abundant as augite. In other samples of this flow, augite and pigeonite are not easily distinguished optically, but small grains of pigeonite can be identified. Olivine in the sample studied occurs as altered microphenocrysts

averaging 0.2 mm in length. Alteration minerals include opaque minerals plus a small amount of a translucent brown mineral. In other samples, olivine characteristically is altered to serpentine. Biotite in the sample analyzed occurs as microphenocrysts of the same sizes as altered olivine. It is completely altered to granular opaque material; in many cases it is hard to distinguish from the altered olivine. In some samples, biotite is absent, but in others it is more plentiful than in the sample analyzed and occurs both as largely altered phenocrysts and microphenocrysts and as unaltered grains, some of which can be seen to protrude into vesicles.

Agglomerate (cfa) occurs in thin, scattered patches on top of the flow (cff). It consists of dark brown, vesicular bombs and other clasts of olivine-sanidine trachybasalt in a matrix of fine-grained white ash which contains abundant tiny biotite flakes. In addition to biotite, the white ash is seen in thin section to contain plagioclase, sanidine, and quartz grains. The ash probably is rhyodacite or dacite. In several localities, the ash has been metamorphosed to a hard, very fine-grained hornfels adjacent to bombs of trachybasalt. The ash may have been a thin regional deposit laid down very shortly after extrusion of the Fault Canyon flow. It was incorporated into an agglomerate in a subsequent eruption of bombs.

The intrusive bodies (cfi) of the Fault Canyon flow are identical petrographically to the flow (cff). The body at the head of Tyria Wash has a contact aureole, 6 inches to 1 foot thick, of bright yellow, chert-like hornfels. This hornfels is contact-metamorphosed tuff (cct) of the Cinder Basin unit adjacent to the intrusion.

Intrusive tuff-breccia or breccia (cft) contains red scoria, a few bomb-like clasts, abundant angular clasts, and, adjacent to one of the sills, accidental clasts of Annex Ridge Flow. The largest body of tuff-breccia is associated with

the intrusive body (cfi) at the head of Tyria Wash.

The flow-base zone (cfb) is characterized by vugs and/or breccia. It is found at the base of the flow (cff) and also at the base of faint flow lobes within the flow.

Chemical composition. The Fault Canyon flow is easily distinguishable on a chemical basis from all other rocks of the Crater Pasture Formation. It contains about twice as much potash and normative potassium feldspar as other rocks of the formation. Potash averages 6 percent; normative potassium feldspar averages 36 percent. Although this rock has been classified as a trachybasalt, its recalculated silica content averages 56 percent, which is well into the intermediate range of composition.

Miscellaneous Units

In the vicinity of Fort Rock dome are outcrops of rocks of the Crater Pasture Formation which cannot be correlated with certainty with rocks mapped on the dome. Many of these rocks are petrographically different from rocks on the dome. Outcrops of these rocks which are located within a distance of one diameter of Fort Rock dome are described briefly below. One of these outcrops appears on the geologic map (pl. 1, map unit cip).

Intrusion near the powerlines. An outcrop of dark-colored intrusive (or extrusive) rock (cip) is found at the northern tip of the area mapped. This outcrop continues northwestward for about 3/4 mile parallel to the powerlines. It is located on the edge of a low escarpment of Precambrian granitic rock which forms the eastern boundary of a large basin drained by Fort Rock Creek and underlain largely by ash-flow tuff of the Fort Rock Creek Rhyodacite (fig. 3). The intrusive is apparently overlain in the mapped area by the Noon Gorge sedimentary breccia of the Fort Rock Creek Rhyodacite; 1/2 mile to the northwest it is

overlain by ash-flow tuff. In a few places to the northwest, it is overlain by tuff and conglomerate containing intermediate to mafic ash and clasts.

In the mapped area, rock of this intrusive body is poorly resistant to weathering; it underlies a low saddle between a hill of Noon Gorge sedimentary breccia and the escarpment of Precambrian rock. Where gullies have cut into it , it forms gruss. Surface float consists of detached blocks. Farther northwest this rock forms a resistant ridge.

Rock of this intrusive is massive, nonvesicular, and black (brownish on a weathered surface) with abundant visible red-brown olivine phenocrysts. It is classified as a shonkinite. In thin section it is seen to contain 15 percent olivine, 50 percent augite, 5 percent opaque minerals, 3 percent biotite, 27 percent orthoclase, and a trace of analcite. Olivine occurs as phenocrysts, up to 3 mm across, and as microphenocrysts. The olivine phenocrysts are altered to a red-brown mineral on their rims, and a few microphenocrysts are totally altered to chlorite. Augite occurs in a continuous size-distribution from groundmass grains to phenocrysts. The augite occurs as distinctive elongated prisms. Biotite occurs as ragged, poikilitic flakes up to 0.5 mm across. Orthoclase also forms anhedral poikilitic grains up to 0.5 mm across. Petrographically this rock is similar to the flow of Eight OClock Gorge, which is a limburgite; it is more mafic, however, and is not glassy.

The recalculated silica content for a sample of this body (Table 3, sample 331) is about 42-1/2 percent which is well within the range of ultrabasic composition (less than 45 percent). This rock is the only sample of the Crater Pasture Formation that is undersaturated in silica.

Other rocks. Other outcrops of Crater Pasture rocks which are not definitely correlated with rocks mapped on the dome are numbered below in order of their occurrence in a clockwise sense around the dome, beginning in the east.

1. A large body of olivine-trachybasalt flow and agglomerate underlies a basin about 0.8 miles in diameter which is located 3/4 mile east of Fort Rock dome (fig. 3). These rocks form a high hill in the center of this basin and also two smaller adjoining hills. In some locations on the edge of the basin, these rocks are overlain by tuff and conglomerate similar to the tuff and conglomerate of Hidden Pasture on Fort Rock dome. A source for the ash of these deposits may lie somewhere in the vicinity of this basin. In most places on the edge of the basin, the trachybasalt is overlain by ash-flow tuff of the Fort Rock Creek Rhyodacite.

The rocks of this body of olivine trachybasalt are both vesicular and nonvesicular. Vesicular rocks are dark bluish-gray, charcoal-gray, light brownish gray, or red in color; nonvesicular rocks are dark gray or black. Color and texture vary markedly over distances of feet to tens of feet. Petrographically, this olivine trachybasalt is similar to the shonkinite intrusive under the powerlines, (cip), only it is slightly finer-grained. Olivine occurs as phenocrysts, up to 1 mm across, and microphenocrysts. In vesicular samples, olivine is totally altered to red-brown minerals on its rims and to serpentine in its interior. Clinopyroxene occurs only as groundmass grains. Interstitial minerals include potassium feldspar, analcite, and a mineral of moderate birefringence and high negative relief.

Two chemically analyzed samples of this olivine trachybasalt (Table 3) have recalculated silica contents averaging 49 percent, which is in the range of basic composition. One of these rocks has less than 10 percent normative

potassium feldspar and is technically not a trachybasalt.

2. A massive hornblende-trachyandesite body, which is similar in hand specimen to the massive hornblende-trachyandesite flow (cam) of the Annex Ridge unit, crops out in a small inlier in the terrace gravels about one mile southeast of the dome (fig. 3). This flow differs from the flow of Annex Ridge in containing scattered green pyroxene phenocrysts.

3. A massive pyroxene-trachyandesite flow, similar in hand specimen to the flow (ctf) of the Two OClock Gap unit on Fort Rock dome, crops out beneath agglomerate and minor flows of the Cinder Basin unit about one mile south-southeast of the dome. Its outcrop area is about 0.8 mile long and 0.25 mile wide and straddles the major drainage in this area. A deep canyon cuts the flow on the south but does not expose its base; the flow is at least 75 feet thick in this area.

4. A small outcrop of hornblende-trachyandesite flow, similar in hand specimen to the Buffalo Ridge flow (cff) on Fort Rock dome, is exposed beneath Cinder Basin extrusives on the northeast side of the Fort Rock Creek fault south of the dome.

5. An agglomerate composed of red to charcoal gray bombs underlies a low mound, about 200 feet across, located one quarter mile southwest of the Fort Rock Ranch headquarters (fig. 3). The agglomerate is overlain by ash-flow tuff of the Fort Rock Creek Rhyodacite. The rock is an aphanitic trachyandesite. In thin section it is composed of tiny plagioclase laths, opaque minerals, and glass.

6. An agglomerate composed of brown to red-brown bombs underlies a large hill, 0.3 miles across, located one half mile northeast of the ranch (fig. 3, pl. 1, the hill underlying the Indian ruins). Two low mounds northeast

of this hill are composed of similar agglomerates. This agglomerate is overlain by ash-flow tuff of the Fort Rock Creek Rhyodacite.

The rock of the agglomerate is olivine trachybasalt. It is petrographically similar to both the shonkinite intrusive body under the powerlines (cip) and the olivine trachybasalt flow and agglomerate east of Fort Rock dome. It contains 15 percent olivine, 40 percent clinopyroxene, 10 percent plagioclase, 30 percent potassium feldspar, 3 percent opaque minerals, and 2 percent calcite. Olivine ranges in size from 0.1 mm to 1 mm; it is totally altered to biotite. Clinopyroxene occurs only in the groundmass as prisms up to 0.2 mm. Plagioclase occurs as scattered laths. Potassium feldspar is anhedral and fills interstices between other minerals. Calcite fills scattered vesicles. The rock has a recalculated silica content of nearly 51 percent and a normative potassium feldspar content of nearly 10 percent (Table 3).

7. A pyroxene-trachyandesite lapilli tuff and tuff-breccia, similar in hand specimen to the tuff (ctb) of the Two OClock Gap unit on Fort Rock dome, underlies a low mound, 350 feet across, located beneath the powerlines one half mile north of the dome. This tuff and tuff breccia is overlain by ash-flow tuff of the Fort Rock Creek Rhyodacite.

FORT ROCK CREEK RHYODACITE

Fort Rock Creek Rhyodacite is a new name applied here to a series of ash-flow tuffs and other massive tuffs, volcanic breccias, lava flows, and associated intrusive and sedimentary rocks in the Aquarius Mountains. The composition of volcanic rocks in these units is chiefly rhyodacite, although rhyolite is present in some units.

This formation is subdivided into two formal members and two informal members, which are listed below with the oldest at the bottom.

breccia and conglomerate of the Crossing
Three Sisters Butte Member (chiefly
massive tuff and breccia)
Old Stage Road Member (chiefly ash-
flow tuff)
sedimentary breccia of Noon Gorge

In addition to these members, the formation includes, in the vicinity of Fort Rock dome, a rhyodacite intrusive body and an unnamed unit of rhyodacite-bearing sedimentary breccia and rhyodacite sandstone.

Type Section

The easternmost butte of the three buttes called the Three Sisters (figs. 2 and 3) is the type section for the Fort Rock Creek Rhyodacite. This butte is located about 2-1/4 miles west-southwest of the Fort Rock Ranch headquarters. The type section was measured and described on the north side of this butte beginning at a 20-foot high, white bluff located in the NW 1/4, NE 1/4, SE 1/4, sec. 6, T.20 N., R.10 W. The traverse followed in describing this section runs southward up the low bluff and then west-southwestward from the top of the bluff for about 0.2 miles along a low rise. At the end of the rise, the traverse runs southward again for about 0.3 miles up a topographic rib to the top of the butte, which is located between the NW 1/4 and

the SW 1/4 of SE 1/4, SE 1/4, sec. 6, T.20 N. R. 10 W.

At the base of each of the Three Sisters, the Fort Rock Creek Rhyodacite rests on intermediate to mafic lava flows, agglomerates, and volcanic breccias of the Crater Pasture Formation. The contact between the two formations dips gently to the east and has local relief of several tens of feet. Most beds in the Fort Rock Creek Rhyodacite also dip gently to the east or are horizontal. Locally steeper dips are seen at the base of the section.

Three members are present in the type section, the Old Stage Road Member, the Three Sisters Butte Member, and the breccia and conglomerate of the Crossing. The Old Stage Road Member and the Three Sisters Butte Member are defined in the type section.

Section Measured at the Easternmost Butte of the

Three Sisters, Mohave County, Arizona

	Feet
Fort Rock Creek Rhyodacite	
massive tuff; similar to unit 5 of Three Sisters Butte Member below. Indian ruins atop the butte are built on this unit.	15
	preserved
breccia and conglomerate of the Crossing	
2. poorly resistant breccia; unexposed; blocks of gray to red rhyodacite up to 2 m across occur in the colluvium covering this unit; the presence of pumice in the breccia would account for lack of resistance to weathering.	25.0
1. resistant breccia; forms the cap rock of the butte; poorly sorted; crudely bedded; contains chiefly blocks of red to gray rhyodacite; contains a trace of clasts of Precambrian rocks and dark brown to gray rocks from the Crater Pasture Formation; contains no observable pumice; mode, 10 cm at the base, 0.5 m in the middle, 10 to 15 cm at the top; maximum clast, size 3 m	41.5
Total breccia and conglomerate of the Crossing	66.5
unconformity(?); contact has relief of less than 1 to 2 cm where exposed	

Three Sisters Butte Member

8. sandstone; light gray-brown, very fine-grained to very coarse-grained, moderately well to well sorted; bed thickness varies from 1 mm to 1 cm; contains chiefly grains of gray rhyodacite; contains 1% grains of Precambrian rock. Total thickness varies from 7 cm to 0.4 m 1.0
7. massive tuff; similar to unit 5 of this member. The upper 100 feet are covered by colluvium and may include breccias similar to units 4 or 6 of this member. Four feet below the top is a light gray-brown sandstone with a thickness of 1 to 15 cm. 169.0
6. breccia; pumiceous; crudely bedded; grades into unit 7; contains mostly gray rhyodacite clasts and white pumice; contains a trace of clasts of Precambrian rocks and clasts of dark brown to gray rocks from the Crater Pasture Formation; mode, 12 cm at the base, 7 cm at the top; maximum clast size, 0.6 m. 12.5
5. massive tuff; white, unsorted, massive; grades upward into pumiceous breccia and includes ill-defined lenses of rock transitional to pumiceous breccia. Clasts between about 2 mm and 6 cm make up over half of the rock: 35% to 45% of the rock is white pumice in this size range, 15% to 35% is gray rhyodacite accessory clasts in this size range, and a trace is accidental clasts of Precambrian rocks and accidental clasts of dark brown to gray rocks from the Crater Pasture Formation in this size range. The rest of the rock is matrix, which consists of clasts of all compositions that are less than 2 mm across. Mode, ill-defined; matrix not sharply differentiable in grain size from the larger clasts; pumice generally smaller than accessory and accidental clasts; maximum clast size, about 0.3 m. . . 23.5
4. breccia*; pumiceous; largely unexposed; grades upward and laterally into massive tuff; contains mostly clasts of gray rhyodacite and white pumice; contains a trace of clasts of Precambrian rocks and clasts of dark brown to gray rocks from the Crater Pasture Formation; mode, 5 cm to 10 cm; maximum clast size, 0.4 m. 46.0
3. fine pebble conglomerate; moderately to moderately well sorted, pumiceous; contains 75% gray to red rhyodacite pebbles, 17% white pumice, 5% pebbles of Precambrian rocks, and 3% pebbles of dark brown to gray rocks from the Crater Pasture Formation; mode, 0.5 cm. 1.0

* The following arbitrary limit was used to separate units described as massive tuff from units described as breccia. A massive tuff contains less than 35% accessory and accidental clasts which are greater than 2 mm across; a breccia contains more than 35% of these clasts. The remaining parts of both the massive tuff and breccia consists of clasts of all compositions less than 2 mm across. Defined in this fashion, massive tuff is similar except for its field relationships to ash-flow tuff.

2. resistant breccia; dark red, slabby, moderately to moderately well sorted; contains mostly red rhyodacite clasts, contains a trace of clasts of Precambrian rocks; mode, 1 to 1-1/2 cm; maximum clast size, 3 cm. 0.25

1. *sandstone; light brown, very fine-grained to very coarse-grained, moderately to moderately well sorted; bed thickness varies from 1 mm to 5 mm; contains 90% grains of gray to red rhyodacite, 7% white pumice, and 3% clasts of Precambrian rock 0.25

Total Three Sisters Butte Member 335

Old Stage Road Member

9. ash-flow tuff; similar to unit 5 of this member. One and a half feet above its base is a horizon containing abundant cobble-sized, angular clasts of rhyodacite, Precambrian rocks, and rocks from the Crater Pasture Formation 8.3

8. interbedded ash-flow tuff, ash-fall lapilli tuff, and sandstone; ash-flow tuff similar to but finer-grained than lower beds of ash-flow tuff; mode, less than 0.5 cm; grades into sandstone by reduction of clast size and increase in sorting; typical bed thickness 0.3 m; ash-fall lapilli tuff, similar to but finer-grained than lower beds of ash-fall tuff; mode, 0.5 cm to 1 cm; average bed thickness 0.15 m; sandstone, white, pumiceous, nonfissile; average bed thickness several centimeters. . . 3.5

7. ash-flow tuff; similar to unit 5 of this member; shows same subtle gradation in clast size from finer clasts (3/4 cm) at the base to coarser clasts (1 cm) at the top 17.0

6. ash-fall lapilli tuff; white to pinkish brown, moderately to moderately well sorted, bedded with bed thickness varying from 0.3 m at the base to about 2 cm at the top; contains 75% white pumice, 10% gray to red rhyodacite accessory clasts, 12% accidental clasts of dark brown to gray rocks from the Crater Pasture Formation, and 3% accidental clasts of Precambrian rocks; mode, 10 cm. 2.7

* Units 1 through 4 of the Three Sisters Butte Member occur on an outlier, several hundred feet across, located on the low, northeast-southwest-trending rise above the white bluff at the base of the section. The outlier is about half of the way between the bluff and the topographic rib on the north side of the butte. At the north end of the topographic rib, one finds at the base of the Three Sisters Butte Member a 3-inch-thick, fine-grained well-sorted, resistant, dark gray sandstone. Neither units 2 nor 3 are visible, although excavation might reveal them. The sandstone is overlain by unit 4.

On the east side of the butte, in an area not measured in the type section, the basal sandstone of the Three Sisters Butte Member, unit 1, is about 12 feet thick.

5. ash-flow tuff; white, unsorted, massive, nonwelded. Clasts between about 2 mm and 15 mm in size make up a little over half the rock: 25% of the rock is white pumice in this size range, 25% is gray to red rhyodacite accessory clasts in this size range, 3% is accidental clasts of Precambrian rocks in this size range, and a trace is accidental clasts of dark brown to gray rocks from the Crater Pasture Formation in this size range. The other half of the rock is constituted by pinkish gray matrix, which includes all clasts less than 2 mm in size. Mode, 3/4 cm at the bottom, 1 cm at the top; maximum clast size, about 5 cm..... 6.0

4. ash-fall lapilli tuff; white to pinkish brown, moderately to moderately well sorted, massive; base of unit slightly better sorted and contains less pumice than top; top grades into ash-flow tuff; contains 80% white pumice, 15% gray to red rhyodacite accessory clasts, 5% clasts of Precambrian rocks, and one percent clasts of dark brown to gray rocks from the Crater Pasture Formation; mode, 2 cm; 1.5

unconformity; angular; dips of beds on either side differ by a few degrees; contact has only a few centimeters relief.....

3. sandstone; light gray, very fine-grained to very coarse-grained, moderately well sorted, fissile, pumiceous; bed thickness varies from one millimeter to several centimeters; lower beds thicker regularly toward the east; upper beds are cross-laminated and indicate a westerly current direction; contains subequal amounts of white pumice and gray to red accessory rhyodacite grains, 3% grains of Precambrian rocks, and less than 1% grains of dark brown to gray rocks from the Crater Pasture Formation..... 11.0

2. sandstone; white, very fine-grained to very coarse-grained moderately sorted, nonfissile, pumiceous; bed thickness varies from 1 mm to 0.3 m..... 5+

1. sedimentary breccia; massive; contains 70% clasts of Precambrian rocks, 20% gray to red rhyodacite clasts 10% clasts of dark brown to gray rocks from the Crater Pasture Formation; mode, 1.5 cm to 2 cm. ..... 2+*

Total Old Stage Road Member	57+
Total Fort Rock Creek Rhyodacite	392+ preserved

* This unit is in fault contact with the overlying sandstone. Fault displacements in this area are generally small, and missing section is probably only a few feet thick at most.

Crater Pasture Formation

2. sedimentary breccia; massive; contains clasts of olivine trachybasalt(?) in an orange, sandy matrix; clast colors include red, yellow-brown, and dark gray; mode, several centimeters. ..... ~ 1
1. volcanic breccia and agglomerate; red; olivine trachybasalt ..... ~20

Reference Section

Penitentiary Butte, 9 miles west-southwest of Fort Rock dome (fig. 3), is a reference section for the Fort Rock Creek Rhyodacite. This section was measured and described on the west side of the butte beginning in the SW 1/4, SW 1/4, SW 1/4, sec. 18, T.20 N., R.11 W. and proceeding northeastward up the side of the butte to the northern end of the cap rock of the butte.

In the vicinity of Penitentiary Butte the Fort Rock Creek Rhyodacite rests on lava flows, agglomerates and tuffs of the Crater Pasture Formation. The contact has a few hundred feet of relief. Most beds in the Fort Rock Creek Rhyodacite are approximately horizontal although locally steeper dips are found at the base of the section.

The Old Stage Road Member and the Three Sisters Butte Member constitute the section here. Unfortunately, the section was described several years before these members were formally defined and has not been revisited to determine the exact contact between them. The division of the section indicated below must, therefore, be regarded as tentative.

The Peach Springs Tuff overlies the Fort Rock Creek Rhyodacite at Penitentiary Butte. It forms the cap rock of the butte.

Section Measured at Penitentiary Butte, Mohave County, Arizona

Peach Springs Tuff

2. ash-flow tuff; lower 3 ft. partially welded, bedded; bed thickness up to 1-1/2 ft.; beds internally massive; gray with scattered white pumice; pumice is progressively flattened

and rock is progressively hardened toward the top; upper 40 feet welded, unbedded; pinkish brown to light gray on a fresh surface, varnished exterior; lower part (6 ft.) has irregular horizontal partings, spaced one to several cm apart, which make the rock crumbly and poorly resistant to weathering; upper part (34 ft.) massive and resistant to weathering. In hand specimen, the tuff contains about 5% clear phenocrysts of feldspar (up to 5 mm in length; mode, 1 mm), about 2% pumice (in lower 3 ft., white, friable; mode, 1 cm; in upper 40 ft. gray, hardened, flattened; mode, 5 cm, maximum size, 0.3 m), a trace of mafic minerals and a trace of accessory clasts in a lithic matrix with abundant black specks* 43

preserved

1. ash-fall tuff or sandstone; pinkish white, moderately well sorted, bedded; bed thickness, 1 mm to 5 mm; faint laminations within beds; contains chiefly glass shards (average size 0.3 mm); contains scattered, unoriented white pumice (up to several mm across). 4

Total Peach Springs Tuff 47

preserved

Fort Rock Creek Rhyodacite

Three Sisters Butte Member

3. massive tuff and breccia; slope largely colluviated; an exposure of massive tuff occurs about 80 ft. above the base; the upper 50 ft. is apparently breccia. This unit is probably similar to a combination of units 4 and 5 of the Three Sisters Butte Member in the type section 373
2. lapilli tuff or conglomerate; white, poorly resistant to weathering, bedded, pumiceous 20
1. resistant conglomerate or breccia; forms small ledge; contains gray to red clasts of rhyodacite and a trace of clasts of Precambrian rocks and clasts of dark gray to brown rocks of the Crater Pasture Formation; mode, 10 cm, coarser at base; maximum clast size, 1 m at base, 0.3 m at top; top includes 10-cm-thick red, resistant cap of somewhat finer-grained breccia..... 10

Total Three Sisters Butte Member 403

Old Stage Road Member

8. ash-flow tuff; white, unsorted, massive, contains abundant white pumice and red to gray accessory clasts of rhyodacite; contains only a trace of clasts of Precambrian rocks and clasts of dark brown to gray rocks from the Crater Pasture Formation; mode for accessory clasts varies from 1.5 cm to 7 cm; coarser accessory clasts found in diffuse lenses up to

*In thin section, this rock is seen to contain 4% sanidine (up to 5 mm in length; mode, 0.75 mm; subhedral to anhedral), 1/2% plagioclase (same size and shape as sanidine), 1/2% biotite and hornblende, and a trace of clinopyroxene, opaque minerals, and sphene. The bulk of the rock is welded, devitrified glass shards (up to 5 mm in length; mode, 0.15 mm; axiolitic structure in some) and interstitial opaque minerals. Normative quartz in this rock is 27-1/2% (Table 4). The rock is a rhyolite.

25 ft. thick; one such lens occurs at the base..... 90

7. ash-flow tuff; white, unsorted, massive, contains abundant white pumice and red to gray accessory clasts of rhyodacite; contains only a trace of clasts of Precambrian rocks and clasts of dark brown to gray rocks of the Crater Pasture Formation; mode for accessory clasts varies from 1.5 cm to 7 cm; coarser accessory clasts occur in a 20-foot-thick diffuse lens at the top; uppermost 4 ft. stratified..... 71
6. ash-flow tuff; similar to unit 1 below but contains only a trace of clasts of Precambrian rocks and clasts of rocks of the Crater Pasture Formation; includes a 10-cm-thick pumiceous sandstone at the top..... 15
5. ash-flow tuff; similar to unit 1 below; includes a discontinuous thin (less than 3-cm-thick) bed of pumiceous sandstone at the top..... 17
4. ash-flow tuff; similar to unit 1 below; includes two thin (less than 3-cm-thick) beds of pumiceous sandstone, occurring one foot apart, at the top and a bed of ash-fall lapilli tuff (a few tenths meter thick) at the base..... 11
3. ash-flow tuff; similar to unit 1 below; includes a bed of ash-fall lapilli tuff (few tenths meter thick) at the base.... 22
2. ash-flow tuff; similar to unit 1 below..... 45
1. ash-flow tuff; white, unsorted, massive. Clasts between 2 mm and 30 mm make up 80% of the rock: 75% of the rock is white pumice in this size range; 4% of the rock is gray to dark red accessory clasts of rhyodacite in this size range; and 1% of the rock is accidental clasts of Precambrian rocks and clasts of dark brown to gray rocks from the Crater Pasture Formation in this size range; mode, 1/2 cm for pumice, 1.5 cm for other clasts. The rest of the rock is constituted by light pinkish-gray matrix, which includes all clasts less than 2 mm; matrix contains biotite books and clear feldspar grains..... 13

Total Old Stage Road Member 284
Total Fort Rock Creek Rhyodacite 687

Crater Pasture Formation

1. agglomerate; dark gray to black bombs in a scant red-orange matrix of ash..... 25+

Sedimentary Breccia of Noon Gorge

Distribution and physical features. The sedimentary breccia of Noon Gorge is a local unit of the Fort Rock Creek Rhyodacite found on or near the flanks of the Fort Rock dome. Distribution of this breccia is similar to that of the One OClock Wash sedimentary breccia of the Crater Pasture Formation, which it overlies. It is distributed around three-fourths of the periphery of the

TABLE 4. Chemical and Normative Composition of Rocks of the Fort Rock Creek Rhyodacite and Other Units. (*) denotes a single clast from a clastic unit.

Unit sampled (map label)	fnb*	fnt*	fob*	fot	fot
Sample number	325a	452b	300	318	332
Oxide			Weight percent		
SiO_2	58.5	47.0	73.7	67.0	66.1
Al_2O_3	13.1	15.2	14.1	14.2	13.5
Fe_2O_3	2.8	9.1	1.0	1.6	1.9
FeO	3.10	1.2	0.14	0.52	0.54
MgO	6.4	4.3	0.3	1.2	2.0
CaO	5.7	6.1	1.2	2.2	2.2
Na_2O	3.2	1.6	4.2	3.4	2.8
K_2O	3.9	2.8	4.8	3.9	3.8
TiO_2	0.99	1.8	0.09	0.25	0.39
P_2O_5	0.34	1.1	0.06	0.08	0.13
MnO	0.10	0.14	0.05	0.10	0.07
H_2O^+	1.18	5.3	0.16	3.02	3.06
H_2O^-	0.38	4.2	0.19	1.79	2.90
CO_2	0.35	<0.05	0.41	0.15	0.10
Total	100.0	99.8	100.4	99.4	99.5
Normative mineral[1]			Weight percent		
Qz	7.43	11.73	29.42	28.03	30.24
Or	23.60	18.32	28.62	24.45	24.07
Ab	27.73	15.00	35.86	30.53	25.40
An	10.11	25.26	3.01	10.02	10.10
Co	--	1.20	0.91	0.98	1.43
Dp	11.26	--	--	--	--
Hy	13.00	11.86	0.75	3.17	5.34
Ol	--	--	--	--	--
Mt	4.16	--	0.36	1.36	0.90
Ht	--	10.08	0.76	0.76	1.42
Il	1.93	3.14	0.17	0.50	0.79
Sph	--	--	--	--	--
Rut	--	0.34	--	--	--
Ap	0.79	2.77	0.14	0.19	0.32
Total	100.00	100.00	100.00	100.00	100.00
Color index	30.34	25.41	2.05	5.79	8.45
An/(Ab + An)	26.71	63.02	7.74	24.72	28.45
Or/(Or + Ab + An)	38.41	31.12	42.41	37.62	40.41
SiO_2 (H_2O^-, $CaCO_3$-free)	59.89	52.03	74.35	71.08	70.85

[1] Normative minerals are calculated after subtracting $CaCO_3$ from the oxides.

TABLE 4. continued

Unit sampled (map label)	fov	fit	rf	bf	Peach Springs Tuff
Sample number	333	187a	207	205	5
Oxide			Weight percent		
SiO_2	70.3	66.6	67.1	47.4	67.0
Al_2O_3	10.8	14.8	15.9	15.5	13.8
Fe_2O_3	1.4	1.7	2.2	7.6	1.0
FeO	0.36	1.26	0.54	2.70	0.22
MgO	1.2	1.2	1.0	5.7	1.3
CaO	2.5	3.2	2.3	10.4	1.4
Na_2O	1.7	4.1	3.8	3.5	3.6
K_2O	2.7	4.1	4.1	1.4	4.4
TiO_2	0.26	0.44	0.33	1.83	0.21
P_2O_5	0.11	0.20	0.19	0.98	0.04
MnO	0.07	0.06	0.07	0.15	0.08
H_2O^+	4.37	1.62	0.57	1.22	3.53
H_2O^-	3.39	0.53	1.90	1.62	3.15
CO_2	0.06	0.06	0.07	0.19	0.44
Total	99.2	99.9	100.1	100.2	100.2
Normative mineral					
Qz	47.54	20.43	24.23	--	27.67
Or	17.47	24.83	24.87	8.54	28.11
Ab	15.76	35.56	33.01	30.57	32.94
An	12.36	10.13	9.98	23.18	4.22
Co	1.04	--	1.69	--	1.82
Dp	--	3.46	--	17.31	--
Hy	3.27	1.74	2.56	2.58	3.50
Ol	--	--	--	2.83	--
Mt	0.70	2.53	1.04	4.01	0.39
Ht	1.05	--	1.54	5.08	0.81
Il	0.54	0.86	0.64	3.59	0.43
Sph	--	--	--	--	--
Rut	--	--	--	--	--
Ap	0.27	0.47	0.44	2.30	0.10
Total	100.00	100.00	100.00	100.00	100.00
Color index	5.56	8.58	5.78	35.40	5.13
An/(Ab + An)	43.96	22.17	23.22	43.13	11.36
Or/(Or + Ab + An)	38.33	35.21	36.65	13.71	43.07
SiO_2 (H_2O^-, $CaCO_3$-free)	76.98	68.25	68.86	48.91	72.44

TABLE 4 continued

	Sample location
325a	north side of Noon Hill
452b	north side of One OClock Hill near the road
300	north bank of Ten OClock Wash
318	basal bed of ash-flow tuff on northwest side of hill east of Short Hill*
332	bed of ash-flow tuff above basal bed in vicinity of Old Stage Road Butte*
333	Old Stage Road Butte
187a	southeast flank of Three OClock Hill
207	west end of gully at head of Five OClock Wash
205	base of Buttox Hills basalt flow on southwest side of Buttox Hills
5	partially welded ash-flow tuff from lower part of low cliff on top of Penitentiary Butte

*Visible accessory and accidental fragments (generally greater than 2 mm across) were removed by hand from these samples after the samples were disaggregated.

dome in outcrops of varying size. The most extensive outcrops occur on the northern flank of One OClock Hill and Lion Ridge. In this area, the Noon Gorge breccia attains an estimated thickness of about 50 feet. Although thinner than the parts of the One OClock Wash sedimentary breccia which are preserved here (estimated thickness, 75 feet), the Noon Gorge sedimentary breccia crops out over a somewhat larger area because of its lower dip. From Noon Gorge in a counterclockwise direction around the crater to the southwest flank of Buffalo Ridge, this breccia crops out as a narrow belt high on the flank of the dome adjacent to theOne OClock Wash breccia. The chief exposures of this unit are in valleys cut into the flank of the dome. Estimated maximum thicknesses are 30 feet on Noon Hill, 75 feet on Short Hill, 100 feet in Eight OClock Gorge, and 15 feet at the head of Tyria Wash. In addition to outcrops high on the flank of the dome, a large inlier of Noon Gorge breccia occurs in the overlying Old Stage Road Member about 1500 feet north of Wedge Basin, and a large outlier of the unit occurs at the northern edge of the mapped area.

Like the One OClock Wash breccia, the Noon Gorge breccia is poorly resistant to weathering and is in most places covered by colluvium. Uprooted trees, which are numerous on the lower part of the flank of the dome, were frequently used to determine the presence and character of this breccia. Shallow excavations were often needed elsewhere. Float from this unit consists of gray clasts of volcanic rocks and clasts of pink, orange, and black Precambrian rocks.

Relationship to other units. The Noon Gorge sedimentary breccia, in most places on the dome, overlies the One OClock Wash sedimentary breccia. Locally, it overlies the Buffalo Ridge flow, the Fault Canyon flow, the Cinder Basin tuff and agglomerate, and the Annex Ridge flow. On the lower flank of

the dome, north of Lion Ridge, it overlies Precambrian rocks. This unit is overlain by sedimentary breccia, sandstone, ash-fall tuff, and ash-flow tuff of the Old Stage Road Member.

The contact of the Noon Gorge sedimentary breccia with the underlying One OClock Wash sedimentary breccia is nowhere exposed. In mapping this unit, the contact was drawn between outcrops in which the lithology of the breccia contrasted in the manner set forth in Table 5 below. The contact appears to be gradational on the flanks of Lion Ridge, One OClock Hill (east of the One OClock Hill fault), Noon Hill, Short Hill, and in Wedge Basin, where the lithology of the breccia above and below the contact is similar. The contact appears sharper west of the One OClock Hill Fault on One OClock Hill, in Ten OClock Wash, and in Eight OClock Wash.

Provenance and clast content. Like the underlying One OClock Wash sedimentary breccia, the Noon Gorge sedimentary breccia consists chiefly of clasts eroded from the dome during its uplift, including clasts of volcanic and Precambrian rocks. Volume percentages of Precambrian clasts in this breccia were contoured on the geologic map (pl. 1) as they were in the underlying One OClock Wash breccia. In general, the volume percentage of Precambrian clasts increases in a smooth fashion from the upper part of the One OClock Wash breccia to the lower part of the Noon Gorge breccia, and it continues to increase upward through the Noon Gorge breccia. This pattern of increase in Precambrian clasts in the breccia probably reflects the widening of the exposure of Precambrian rocks on the dome as the covering of volcanic rock was being stripped back by erosion.

TABLE 5. Contrasts between the Lithology of the Sedimentary Breccia of One OClock Wash (Crater Pasture Formation) and the Sedimentary Breccia of Noon Gorge (Fort Rock Creek Rhyodacite)

Sedimentary breccia of One OClock Wash	Sedimentary breccia of Noon Gorge
1) Contains a trace or more mafic to intermediate ash distributed through the rock; contains no felsic volcanic clasts (rhyolite or rhyodacite).	1) Contains a trace to a few percent mafic to intermediate ash distributed through the rock; contains a few beds rich in this ash; contains in many localities traces of felsic volcanic clasts (rhyolite and/or rhyodacite); on the north flank of the dome, contains distinctive black olivine-trachyandesite clasts which are thought to be detrital clasts from the Road End Gap volcanic breccia and flow.
2) Massive.	2) Massive to very crudely bedded.
3) Unsorted; clasts commonly not easily distinguished from the matrix; the matrix contains a continuous clast-size distribution from silt size on up; up to 5% tridymite and potassium feldspar(?) cement.	3) Unsorted to poorly sorted; clasts easily distinguished from the matrix. the matrix is sandy and contains little silt; up to 20% tridymite and potassium feldspar(?) cement; small cavities abundant.
4) Moderately well indurated and poorly resistant to erosion; clasts do not break out easily.	4) Poorly indurated and very poorly resistant to erosion; clasts break out relatively easily.

TABLE 5 continued

Sedimentary breccia of One OClock Wash	Sedimentary breccia of Noon Gorge
5) In most areas, characterized by clasts 1 inch in size or smaller, although much larger clasts are present; block patches abundant.	5) In most areas characterized by clasts 6 inches in size or smaller, although much larger are present; block patches rare
6) Clasts angular to subrounded	6) Clasts angular.
7) Pinkish brown with multicolored clasts: gray, red-brown, yellow-brown.	7) Gray clasts and light brown to buff matrix; matrix commonly has white specks (rhyodacite and/or rhyolite).

Distinctive black clasts of olivine trachyandesite are found in the Noon Gorge breccia from Noon Hill to the north side of Lion Ridge. Their lowest occurrence coincides with the basal contact of the breccia through most of the area in which they are found and they are thus useful in mapping the basal contact of this unit. These clasts are petrographically and chemically similar to rock of the Road End Gap volcanic breccia and flow (see below). They have been interpreted as detrital clasts derived from this unit by erosion during uplift of the dome. The Road End Gap volcanic breccia and flow presently crops out only on the southern rim of the crater. In order for this unit to have been a source for the clasts in the breccia, a lobe of volcanic breccia (or flow) must have originally extended northward more than half way across the site of the present crater.

Block patches, defined as they were in the One OClock Wash sedimentary breccia, are found in a few locations in the Noon Gorge sedimentary breccia.

Source for volcanic ash. In addition to detrital clasts from Fort Rock dome, the Noon Gorge sedimentary breccia contains small amounts of mafic to intermediate ash and also small amounts of felsic volcanic clasts. Locally, mafic and intermediate ash are concentrated in tuffaceous beds in the breccia. Two such beds have been mapped. A tuffaceous sandstone and conglomerate (fnt) consisting chiefly of dark-colored olivine-trachyandesite (or olivine-trachybasalt) clasts occurs in the breccia at one locality on the northern flank of One OClock Hill. Bomb-like clasts from this subunit are petrographically similar to the shonkinite intrusive body (cip) 1500 feet to the northeast and also to a body of olivine-trachybasalt agglomerate 4300 feet to the west-northwest (underlying the hill with Indian ruins on top in pl. 1). The latter body may have been

the source for ash and clasts in this bed, as the shonkinite intrusive appears to be overlain by the Noon Gorge breccia. A tuffaceous granule and fine-pebble conglomerate (fnc) consisting chiefly of light-colored trachyandesite ash was mapped in isolated localities on the southwestern and southern flanks of the dome. The source for this ash is unknown. Rhyolite and/or rhyodacite clasts scattered through the breccia most likely had their source in the large rhyodacite eruptive center in the Aquarius Mountains to the southwest; they apparently represent the onset of volcanism in that center. Sedimentary breccia containing more than about 1/2 percent of these clasts is mapped as a subunit (fob) of the overlying Old Stage Road Member.

Lithology. The breccia is unbedded to poorly bedded, and unsorted to poorly sorted; it contains angular clasts. In most outcrops which are not in the vicinity of block patches, clasts do not exceed one foot in size, and most of the breccia is made up of clasts 6 inches or smaller in size. Owing to slightly better sorting in this breccia than in the One OClock Wash sedimentary breccia, the matrix is in most locations sandy and contains little silt. The matrix is commonly light pinkish brown, light gray-brown, or buff. The larger volcanic clasts in the breccia, which are light to medium gray, stand out against the matrix. Because of its sandy matrix, this breccia is in most locations not as well indurated as the One OClock Wash sedimentary breccia; individual clasts break out easily. This breccia is abundantly cemented by tridymite and potassium feldspar(?); small cavities are abundant. The lithology of the Noon Gorge breccia is contrasted with that of the One OClock Wash breccia in Table 5.

Petrography of clasts and ash. The distinctive black olivine trachyandesite clasts that occur in the breccia on the north side of the crater are dark gray to black on fresh surfaces and gray-brown to yellow-brown on weathered

surfaces with abundant red-brown grains of olivine (up to 1 mm across). They are vesicular to nonvesicular. In thin section they contain 6 percent olivine, 12 percent clinopyroxene, 25 percent plagioclase, 55 percent reddish brown glass, and 2 percent opaque minerals. Olivine occurs as small phenocrysts and microphenocrysts with light-brown rim alteration. Clinopyroxene occurs chiefly as microphenocrysts and groundmass prisms. The plagioclase laths, pyroxene prisms, and opaque minerals have sharp relief and definition against the reddish-brown glass. The modal composition of this rock and the distinctive appearance of its groundmass makes it petrographically very similar to rock of the Road End Gap volcanic breccia and flow. Its chemistry (Table 4, sample 325a) is also similar. Its recalculated silica content, 59 percent, is most similar to that of the sample of flow 2 (195a) of the Road End Gap unit.

A few percent of mafic to intermediate ash is commonly present in the matrix of the breccia in most places. In hand specimen, it shows up as small grains, rarely larger than 2 mm, which are green, yellow-green, buff, gray-brown, and olive-brown in color and contain tiny orange (altered olivine) specks. Petrographically, this ash is identical to the olivine-trachyandesite ash in the Hidden Pasture tuff and conglomerate and in the One OClock Wash sedimentary breccia below.

A bomb-like clast that was taken from the tuffaceous sandstone and conglomerate (fnt) on the northern flank of One OClock Hill is an olivine trachyandesite or olivine trachybasalt. In hand specimen, it is dark brownish gray and vesicular. In thin section it is seen to contain 5 percent altered olivine, 25 percent clinopyroxene, 25 percent plagioclase, 40 percent cryptocrystalline interstitial feldspar, and 5 percent opaque minerals. Olivine is altered to brown material on its rim and serpentine in its interior; it occurs as

microphenocrysts up to 0.5 mm in length. Clinopyroxene occurs as prisms generally less than 0.3 mm in length and tiny (5 μ) orange groundmass granules. Plagioclase occurs as laths in the groundmass. The habit and abundance of clinopyroxene makes this rock petrographically similar to the shonkinite intrusive body (cip) to the north and to the trachybasalt agglomerate to the west. This rock has a recalculated silica content of about 52 percent (Table 4).

Light gray trachyandesite ash constitutes most of the subunit mapped as tuffaceous granule and fine-pebble conglomerate (fnc). An unmapped thin bed of this unit in Eight OClock wash was examined in thin section. It contains scattered phenocrysts and microphenocrysts of hornblende (up to 1 mm), and 5 percent tiny (50 μ) red-brown pseudomorphs after olivine in a glassy, microvesicular matrix containing feldspar microlites.

A trace of felsic clasts are scattered through the breccia in most places. In hand specimen, these clasts are white to light gray and range in size from specks to about 1 cm. They are characterized by small white feldspar phenocrysts, scattered biotite books and rarer hornblende prisms. In thin section, they are seen to contain rare plagioclase phenocrysts, as much as 25 percent microphenocrysts of sanidine (stubby laths up to 0.1 mm in length), scattered biotite, and rare hornblende grains. The matrix is glassy to cryptocrystalline.

Old Stage Road Member

Distribution, stratigraphy, and physical features. The Old Stage Road Member is named after the old Beale wagon, or stage, road, which is preserved as deep ruts in ash-flow tuff on the northern flank of Fort Rock dome and in other places. This member is defined in the type section on the easternmost butte of the Three Sisters.

This member crops out over most of the area mapped as Fort Rock Creek Rhyodacite on the reconnaissance geologic map of the region (fig. 3). Outcrops extend from Penitentiary Butte on the west to near Cross Mountain on the east and from near the Kingman-Seligman county road on the north to near Trout Creek on the south. This member is 284 feet thick at Penitentiary Butte and 57 feet thick at the easternmost butte of the Three Sisters. It is thickest in areas where it fills basins in underlying rocks, and it thins to feather edges on the flanks of high hills on underlying rocks.

The Old Stage Road Member consists in most places of a basal pumiceous sandstone or tuff (fos), or, on the flanks of Fort Rock dome, a basal sedimentary breccia (fob), overlain by beds of ash-flow tuff (fot) interlayered with thin, unmapped beds of ash-fall lapilli tuff and sandstone. In the vicinity of Fort Rock Creek, lens-shaped regions (fov) within the beds of ash-flow tuff have undergone vapor-phase crystallization and have been mapped. Minor units which have been mapped include a lapilli breccia (fol) which occurs in the southwestern part of the area mapped and boulder patches (fop) which are found on the southeast flank of the dome.

The basal pumiceous sandstone or tuff (fos) is generally poorly resistant to weathering, as it is thinly bedded and commonly fissile. In some places it weathers to slabs and has been quarried for building stone. Several buildings on the Fort Rock Ranch have been built with this stone. Ash-flow tuff (fot) is generally moderately resistant to weathering owing to its massive character; it tends to form low white bluffs. The zone of vapor-phase crystallization in the ash-flow tuff (fov) is resistant to weathering and underlies numerous low buttes in the vicinity of Fort Rock Creek.

Relationship to other units. In the northeastern part of its outcrop area, the Old Stage Road Member overlies chiefly rocks of the Crater Pasture Formation and Precambrian rocks (fig. 3). In most places on the flanks of Fort Rock dome, it overlies the Noon Gorge sedimentary breccia of the Fort Rock Creek Rhyodacite. In the western and southern parts of its outcrop area, it overlies rocks of the Crater Pasture Formation and undivided volcanic and sedimentary rocks. This member is overlain in the area west, south, and southeast of the Three Sisters by the Three Sisters Butte Member of the Fort Rock Creek Rhyodacite. In the area north of the ranch it is locally intruded and capped by younger andesite. In the area immediately southeast of the Fort Rock dome it is overlain by rhyodacite-bearing sedimentary breccia and rhyodacite sandstone and by the basalt of Buttox Hills. In a large area east and southeast of the dome, it is overlain by Quaternary terrace deposits.

On the flanks of Fort Rock dome, the contact between the basal unit (fob) of the Old Stage Road Member and the sedimentary breccia of Noon Gorge (fnb) is gradational. The gradation is characterized either by a gradual increase in the content of felsic volcanic clasts or by alternation of rhyodacite-poor sedimentary breccia and tuff or pumiceous sandstone. In One OClock Wash, a gradual increase in the content of rhyolite and/or rhyodacite clasts is seen in the Noon Gorge breccia. The contact with the basal sedimentary breccia of the Old Stage Road Member is placed at the point where the content of these clasts exceeds about 1/2 percent by volume. On the northwest side of Eight OClock Wash rhyodacite-poor sedimentary breccia is interbedded at intervals with thin beds of white tuff and pumiceous sandstone. The percentage of rhyodacite and/or rhyolite fragments in the breccia follows a cyclic pattern whereby it is initially high (5 percent or more) above each tuff or sandstone

bed and decreases upward to as little as a trace. There is an overall increase in rhyodacite and/or rhyolite fragments in the breccia upward through the sequence. The sequence is overlain by ash-flow tuff. The contact between the Noon Gorge unit and the basal sedimentary breccia of the Old Stage Road Member is placed, in this locality, at the base of the first pumiceous sandstone in the sequence.

Lithology. The basal sandstone (fos) is generally white, pumiceous, and fissile. The basal sedimentary breccia (fob) on the flank of the dome is generally similar in lithology to breccia of the underlying Noon Gorge unit, except that it is poorly sorted to moderately sorted, crudely bedded to well bedded, and contains varying amounts of white felsic specks and larger light gray, reddish gray, and dark red felsic volcanic clasts (up to 2 inches across; commonly 1 cm across). Locally, this sedimentary breccia includes pumiceous sandstone or tuff equivalent to the basal sandstone or tuff (fos) elsewhere. Ash-fall tuff in this member, which is not mapped separately, is well-bedded, well sorted and is composed of white lapilli of pumice and up to 50 percent lapilli-sized clasts of rhyodacite and/or rhyolite, Precambrian rocks, and rocks of the Crater Pasture Formation. Ash-flow tuff (fot) is massive, unsorted, non-welded and contains 10 to 25 percent white pumice, a trace to 35 percent red to gray rhyodacite and/or rhyolite accessory fragments, a trace to 10 percent accidental clasts of Precambrian rocks, and a trace to 10 percent accidental clasts of rocks from the Crater Pasture Formation. The remaining fraction of the tuff is matrix consisting of ash less than 2 mm across. The matrix has an overall color of gray to light pinkish gray. Parts of the ash-flow adjacent to Fort Rock dome which contain more than about 35 percent detrital clasts from the dome

and/or rhyodacite accessory clasts are mapped as part of the basal unit (fob). Ash-flow tuff which has undergone vapor-phase crystallization (fov) is mapped in places where 50 percent or more of the pumice in the tuff is crystallized, cavities occur in place of the pumice. Crystallized ash-flow tuff is porous; yellow-brown in color, and very hard. The lapilli breccia (fol) is massive and consists chiefly of angular lapilli of rhyodacite and/or rhyolite. It appears to grade by decrease in lapilli and increase in ash into ash-flow tuff, generally crystallized ash-flow tuff (fov). Like the crystallized ash-flow tuff, this rock is very hard. Boulder patches (fop) are defined in the same way as block patches in the Noon Gorge and One OClock Wash sedimentary breccias. The boulders in these patches are dark gray to dark red rhyodacite containing abundant (20 to 25 percent) white plagioclase phenocrysts, up to 5 mm across, and fairly abundant (5 percent) black biotite books and hornblende prisms, up to 2 mm in largest dimension.

Petrography. A 1-1/2 inch fragment of rhyolite from the basal unit on Fort Rock dome (fob) was examined. It is light gray and banded. In thin section it is seen to contain 1 percent oligoclase phenocrysts, up to 2 mm in length, 1/2 percent sanidine phenocrysts, up to 2 mm in length, 1/2 percent biotite phenocrysts, up to 1.5 mm across, 25 percent sanidine microphenocrysts averaging 0.1 mm in length, 3 percent biotite microphenocrysts, and a trace of quartz microphenocrysts. The matrix is cryptocrystalline.

A specimen of the lowest bed of ash-flow tuff at Fort Rock dome contains 20 percent white pumice and almost no visible accessory or accidental fragments in a uniformly fine-grained gray matrix. The pumice is up to 3 cm across but averages 1/2 cm across. In terms of identifiable grains in thin section, the rock is rhyodacite. Pumice fragments are seen to contain scattered

phenocrysts of sanidine, plagioclase, biotite, and quartz, listed in order of abundance. The order of abundance of these grains in the matrix, where they are plentiful, is plagioclase, sanidine, quartz, and biotite. The overall volume percentages of grains is 1-3/4 percent plagioclase, 1-1/2 percent sanidine, 1 percent quartz, and 1/2 percent biotite. The matrix also contains scattered clasts of Precambrian rocks, olivine trachyandesite, and rhyolite similar to the small fragment described above. It is difficult to separate Precambrian xenocrysts from volcanic crystals; the overall percentages of various crystal fragments given above includes some contamination from Precambrian rocks.

A specimen of a higher bed of ash-flow tuff at Fort Rock dome contains 25 percent white pumice, 5 percent accessory fragments, and 2 percent accidental fragments in a light pinkish gray matrix of heterogeneous grain size. Pumice and accessory and accidental fragments are up to 3 cm across but average 1/2 cm across. In terms of identifiable grains in thin section, this tuff is also a rhyodacite. Pumice is seen to contain scattered phenocrysts of quartz, biotite, hornblende, plagioclase, and sanidine (rare), listed in order of abundance. The order of abundance in the matrix, where these grains are plentiful, is quartz, plagioclase, sanidine, biotite, and hornblende. The overall volume percentages of grains is 1-1/4 percent quartz, 1 percent plagioclase, 1/2 percent sanidine, 1/4 percent biotite, and 1/8 percent hornblende. The matrix also contains scattered clasts of Precambrian rocks, olivine trachyandesite, and rhyolite similar to the one described above. In other specimens of ash-flow tuff, some of the accessory fragments contain abundant phenocrysts of plagioclase and probably are rhyodacite rather than rhyolite.

A sample of vapor-phase-crystallized ashflow (fov) contains 25 percent cavities by volume. Most cavities are at least partly lined by tridymite and

potassium feldspar(?). These minerals occur as small (25μ) clear, low-birefringent, low-index tablets showing striations parallel to their longest dimensions. In some cases, the tablets are intergrown in a bladed, radial habit on the cavity walls; in other cases, they occur as shingle-like aggregates. In areas where cavities are thickly lined with tridymite and potassium feldspar(?), the matrix of the rock is finely crystalline, and accessory fragments are recrystallized to relatively coarse, interbladed aggregates of these minerals. Where cavities are only thinly or partly lined by these minerals, the matrix is glassy.

Chemical composition. A chemically analyzed sample of a rhyolite clast from the basal breccia on Fort Rock dome (fob) has a recalculated silica content of about 74 percent (Table 4). Its normative potassium feldspar content is about 28-1/2 percent, which constitutes 42-1/2 percent of the total normative feldspar in the rock. In an average rhyolite (Nockolds, 1954), normative potassium feldspar is 32 percent and is about 51-1/2 percent of the total normative feldspar. For comparison, in an average rhyodacite, normative potassium feldspar is 18 percent and is 26-1/2 percent of the total normative feldspar. The rhyolite clast from the basal breccia is, thus, chemically most similar to the average rhyolite.

A sample of the lowest bed of ash-flow tuff of the Old Stage Road Member, sample 318 (Table 4), and a sample of a higher bed of ashflow tuff, sample 332, are chemically similar. Both have a recalculated silica content of about 71 percent. Normative potassium feldspar in both rocks is about 24 percent and constitutes 37-1/2 percent to 40-1/2 percent of the total normative feldspar. Comparing these rocks chemically to the average rhyolite and the average rhyodacite (Nockolds, 1954), it is seen that they are intermediate between the two.

A sample of vapor-phase crystallized ashflow-tuff, sample 333 (Table 4), is high in silica and low in alkali oxides compared to sample 332, which was

collected nearby. Recalculated silica is about 77 percent in this rock. Alkali oxides are reduced by 0.6 to 0.7 times that of the sample 332. These differences presumably reflect a leaching of alkalis during vapor-phase crystallization.

Three Sisters Butte Member

Distribution, stratigraphy, and physical features. The Three Sisters Butte Member crops out over most of the area of the Fort Rock Creek Rhyodacite that is southwest of the Fort Rock Creek fault and south of the east-west fault between Knight Creek and the Three Sisters. The only location where this member occurs on the opposite sides of these faults is at the Three Sisters. This member is 403 feet thick at Penitentiary Butte and 335 feet thick at the eastern-most butte of the Three Sisters.

This member consists chiefly of interbedded volcanic breccia (ftb) and massive tuff (ftt) which are laterally and vertically gradational into one another. In the type section and reference section, relatively thin beds of sandstone and conglomerate are locally present at or near the base of the member. In addition, deposits of ash-fall lapilli tuff (ftl) are thick enough to map in some places.

The Three Sisters Butte Member is poorly resistant to erosion and forms steep-sided hills covered by colluvium which is made up of angular rhyodacite lapilli and blocks. Volcanic breccia (ftb) forms resistant ledges in some locations. At Penitentiary Butte and throughout most of the vicinity of Knight Creek, a resistant ledge of volcanic breccia occurs at the base of this member. Massive tuff (ftt) is rarely exposed. Where it does crop out, it rarely forms bluffs like those which characterize ash-flow tuff of the underlying Old Stage Road Member.

Relationship to other units. Throughout most of its outcrop area, the Three Sisters Butte Member overlies the Old Stage Road Member. In the vicinity of Trout Creek it locally overlies older rocks. It is overlain at the Three Sisters and in a large area south of Three Sisters and southwest of the Fort Rock Creek fault by the breccia and conglomerate of the Crossing. It is capped at Penitentiary Butte and several other nearby buttes by the Peach Springs Tuff.

The contact between the Three Sisters Butte Member and the Old Stage Road Member was chosen in the type section at the base of a thin (0.5-foot-thick sandstone which separates ash-flow tuff from a sequence consisting chiefly of interbedded volcanic breccia and massive tuff. On the east side of the butte on which the type section was described, this sandstone is considerably thicker (12 feet). At Penitentiary Butte the contact was not studied but has been tentatively placed at the base of a 10-foot ledge-forming breccia (locally a conglomerate) that divides the Fort Rock Creek Rhyodacite into sections similar to those in the type section. Along Fort Rock Creek, the contact appears to be in part gradational. Here, a lapilli breccia (fol), assigned to the Old Stage Road Member, grades downward into vapor-phase-crystallized ash-flow tuff (fov) of the Old Stage Road Member and upward into volcanic breccia (ftb) of the Three Sisters Butte Member.

Lithology. In general, the volcanic breccia (ftb) are poorly sorted and weakly indurated. Where it is moderately sorted, it is commonly strongly indurated, and forms a ledge. As a ledge-former it is dark red on a fresh surface and dark red to buff on a weathered surface. In general, clasts in the breccia are angular to locally subrounded. The mode varies from 1 cm to 12 cm but commonly is 5 cm. Maximum clast size is around 0.3 m. Clasts are chiefly

red to gray rhyodacite, which contains abundant (25 percent) white plagioclase phenocrysts, up to 5 mm across, and fairly abundant (5 percent) biotite books and hornblende prisms, up to 2 mm in largest dimension. The matrix in these rocks is glassy to lithic. None of the clasts were studied in thin section, but the petrography is similar to that of a rhyodacite intrusive (fit) on Three OClock Hill, which was studied in thin section and is described below. Only a trace of clasts of Precambrian rocks and clasts of rocks from the Crater Pasture Formation is found in the breccia.

The massive tuff (ftt) resembles lithologically ash-flow tuff (fot) of the underlying Old Stage Road Member except that accessory clasts are more heterogeneous in size and include large clasts similar to those found in beds of volcanic breccia, into which the massive tuff grades. Additionally, clasts of Precambrian rocks and clasts of rocks from the Crater Pasture Formation are rare in the massive tuff (generally a trace to 1 percent), whereas these clasts are fairly abundant (generally a few percent) in ash-flow tuff of the Old Stage Road Member.

Breccia and Conglomerate of the Crossing

Distribution and physical features. The breccia and conglomerate of the Crossing forms the cap rock of the Three Sisters and caps an irregular east-west escarpment south of the Three Sisters (fig. 2). The latter escarpment swings to the southeast near Fort Rock Creek and is parallel to the creek in the vicinity of the Crossing. On the east side of the creek, the breccia and conglomerate of the Crossing underlies the top of a high hill bounded on the east by Fault Canyon. The unit crops out over most of the area between the escarpment and the large eruptive center in the Aquarius Mountains.

The breccia and conglomerate of the Crossing is characterized by very coarse, angular, gray to red blocks of rhyodacite, reaching sizes of 15 feet across.

The unit is poorly resistant to weathering except where it forms the cap rock of the Three Sisters . Generally it is covered by coarse colluvium

Relationship to other units. This unit overlies the Three Sisters Butte Member. It is overlain at the Three Sisters by small outcrops of massive tuff similar to massive tuff in the Three Sisters Butte Member.

At the Three Sisters, the basal contact of the breccia and conglomerate of the Crossing is seen to be sharp; it is probably unconformable. In a cliff on the north side of a wash which joins Fort Rock Creek from the southwest below the Crossing (fig. 2), the contact is unconformable on top of massive (ash-flow) tuff of the Three Sisters Butte Member. In cross section B-B' (pl. 2), the contact is interpreted to be an unconformity. Here the breccia and conglomerate of the Crossing is interpreted to fill an ancient valley in the top of the Three Sisters Butte Member at the site of present-day Fort Rock Creek.

Lithology. Except for local conglomerate beds, this unit is poorly to moderately poorly sorted and consists of angular clasts. The mode varies from 10 cm to 0.5 m. Clasts are gray to red rhyodacite, which appear to be petrographically similar to rock of the small intrusive (fit) on Three OClock Hill, described below.

Miscellaneous Units

Rhyodacite Intrusion on Three OClock Hill. An intrusive body of rhyodacite (fit) crops out on the south-eastern flank of Three OClock Hill. It is elongated in a northeast-southwest direction; its length is 330 feet, and its width is 150 feet. Outcrop consists of blocks of rhyodacite up to 5 feet across which appear to be parts of disaggregated blocks as large as 20 feet across. Although contacts are not exposed, this body is assumed to be an intrusion

because of its isolated occurrence.

The rock is gray to red-brown with abundant white phenocrysts of plagioclase, black books of biotite, and black prisms of hornblende. It is massive to locally banded. In terms of grains that can be identified in thin section, the rock is a dacite, although it is chemically a rhyodacite. In thin section, it is seen to contain 30 percent oligoclase, 6 percent hornblende, 5 percent biotite, 1/2 percent sanidine, a trace of quartz, a trace of augite, a trace of hypersthene, and the remainder glass. Oligoclase occurs as euhedral to broken or rounded phenocrysts up to 4 mm in length and as smaller fragments in the glassy matrix. Sanidine occurs as broken or rounded microphenocrysts up to 0.5 mm and also as smaller fragments in the matrix. Biotite and hornblende occur as books and prisms, often broken, up to 3 mm in maximum dimension. Quartz occurs as embayed microphenocrysts, 0.5 mm across. Augite occurs as microphenocrysts, 0.5 mm across, partly altered to hornblende. Hypersthene occurs as small grains, 0.1 mm across, in the matrix. The glass of the matrix was analyzed using an electron microprobe and was found to contain 77 percent silica, 12 percent alumina, 3-1/2 percent potash, 1 percent soda, 1/2 percent each of lime and iron oxide, and about 5 percent water(?). This glass has the composition of a mixture of quartz and sanidine.

A chemically analyzed whole-rock sample contains 68 percent recalculated silica (Table 4). Normative potassium feldspar content is about 25 percent, and normative potassium feldspar is about 35 percent of the total normative feldspar. Chemically, the rock is most similar to the average rhyodacite (Nockolds, 1954).

Sedimentary breccia, sandstone, and conglomerate. A thin deposit of rhyodacite-bearing sedimentary breccia and rhyodacite sandstone and conglomerate

overlies ash-flow tuff of the Old Stage Road Member in the Buttox Hills. It varies in thickness from a feather edge to 30 feet at most. It is rarely exposed but is characterized by abundant float of massive rhyodacite (including boulders), Precambrian rocks, and rocks from the Crater Pasture Formation. Clasts in this deposit are derived from units on the dome and on the flank of the dome to the northwest and north. Rhyodacite clasts appear to be petrographically similar to rhyodacite of the intrusion (fit) on the flank of Three OClock Hill. This deposit is overlain by the basalt of Buttox Hills.

Source for the Fort Rock Creek Rhyodacite

The Fort Rock Creek Rhyodacite is distributed around a large eruptive center in the Aquarius Mountains (fig. 3). Some units in this formation can be traced to extrusive rocks on the flanks of the eruptive center; others cannot, although the center has only been studied in reconnaissance by the author. In addition to the large eruptive center, several smaller intrusive bodies in the western part of the Aquarius Mountains were sources for parts of the Fort Rock Creek Rhyodacite. Rocks within this formation were emplaced chiefly as ash flows, ash and block falls, and volcanic mudflows.

Aquarius-Mountains Eruptive Center. The Aquarius-Mountains eruptive center is a complex body of massive intrusive rocks, shown by a hashure pattern on the reconnaissance geologic map (fig. 3), flanked by pumiceous agglomerate, volcanic breccia, and lava flows. Radiating dikes cut all rocks in this center.

Stratigraphy in the agglomerate, breccia, and lava flows on the flanks of the center is complicated owing to rapid facies changes, intrusion of dikes, and faulting. Two sequences of rocks can be recognized in these extrusives,

however; these sequences are similar to one another. The oldest sequence consists of a basal pumiceous agglomerate overlain by a lava flow. The agglomerate appears to grade into the flow through a zone where its clasts become compressed, welded, and ultimately indistinguishable from one another and from overlying banded flow rock. The second sequence overlies the first and consists of a basal volcanic breccia overlain by a lava flow. As in the first sequence, the breccia becomes indistinguishable from overlying flow rock in a zone of welding near its top.

These two sequences of extrusive rocks on the flanks of the eruptive center can be correlated, in part, with the two chief members of the Fort Rock Creek Rhyodacite, the Old Stage Road Member and the Three Sisters Butte Member. A resistant, volcanic breccia (ftb) at the base of the Three Sisters Butte Member, traceable throughout most of the vicinity of Knight Creek has been tentatively traced to breccia on the western flank of the eruptive center which overlies rocks of the older sequence and underlies rocks of the younger sequence. On the northwestern flank of the eruptive center, the lava flow in the younger sequence is underlain on its distal (northwestern) end by massive tuff of the Three Sisters Butte Member and is also overlain by breccia and massive tuff of this member. The Three Sisters Butte Member, thus, correlates at least in part, with the younger sequence. The Old Stage Road Member correlates in a similar fashion with the older sequence, although none of its beds of ash-flow tuff can be traced directly into the eruptive center.

Minor intrusive bodies. Three relatively small bodies of intrusive breccia and banded rocks occur to the west of the large eruptive center. One body, located one mile west (fig. 3), is a rhyodacite neck that intrudes the part of the Three Sisters Butte Member which is preserved at that location.

This neck may have been a source for a higher part of this member. A second body, located three miles west of the center, near Knight Creek, was the source for a local sequence of rhyolitic sandstone, tuff, volcanic breccia, and flow, all of which is older than the Old Stage Road Member. The largest intrusive body is located about 1-1/2 miles southwest of Penitentiary Butte. It is a rhyodacite neck which rises 1000 feet above surrounding Precambrian rocks. It does appear to be related to any nearby deposits of the Fort Rock Creek Rhyodacite.

Mode of emplacement of extrusive rocks.

Pumiceous sandstone or tuff. The basal pumiceous sandstone or tuff (fos) of the Old Stage Road Member blankets underlying topography and is very evenly bedded with little channeling. Cross-lamination is seen in scattered localities. The sandstone or tuff probably was emplaced as an ash fall that was reworked in varying amounts by wind but was not reworked significantly by water.

Ash-flow tuff. The beds of massive tuff (fot) in the Old Stage Road Member were emplaced as ash-flows. They are homogeneous over large distances; they fill basins and thin to a feather edge on the flanks of high hills; and they were emplaced with entrapped steam, as is indicated by zones of vapor-phase crystallization. (Refer to Ross and Smith, 1961).

Volcanic breccia. A resistant volcanic breccia (ftb) at the base of the Three Sisters Butte Member in the vicinity of Knight Creek has the characteristics of a flow. It is relatively homogeneous over a large area, and it thins to a feather edge on the flanks of high hills. This breccia may have been emplaced as a lahar, or volcanic mudflow. The breccia and conglomerate of the Crossing (fc) may likewise represent a volcanic mudflow on the northeast flank of the eruptive center.

Massive tuff. Some of the massive tuff (ftt) of the Three Sisters Butte Member may have been emplaced as ash flow, but unlike ash-flow tuff of the underlying Old Stage Road Member, beds cannot be traced for large distances laterally; they grade into beds of volcanic breccia (ftb). No zones of vapor-phase crystallization are observed; therefore, evidence of emplacement with entrapped steam is lacking. This tuff and associated volcanic breccia were probably emplaced chiefly as massive ash and block falls. Local ash flows and volcanic mudflows may have occurred in addition.

MISCELLANEOUS UNITS

Rhyodacite Intrusive Body in Gully at Head of Five OClock Wash

A body of rhyodacite (rf) is located in the western part of the gully at the head of Five OClock Wash. At its eastern end, this body is seen to be intrusive into Precambrian rocks.

The rhyodacite is light gray and contains abundant white phenocrysts of plagioclase, black books of biotite, and black prisms of hornblende. In thin section, it is seen to contain 12 percent oligoclase phenocrysts, a trace of small phenocrysts of sanidine, 3 percent biotite books, and 1 percent hornblende prisms. In its matrix, the rock contains 25 percent microphenocrysts of sanidine, 30 percent microphenocrysts of quartz, 2 percent opaque minerals, a trace of apatite prisms, and 27 percent crystocrystalline minerals. Oligoclase phenocrysts are euhedral to broken and rounded and are as large as 5 mm in length. Biotite and hornblende are as large as 2 mm in maximum dimension. In the matrix, sanidine occurs as relatively sharp, stubby, rectangular grains averaging 0.1 mm across. Quartz occurs as indistinct equant grains about 0.1 mm across

which are heavily occluded with dust and are difficult to identify.

The microcrystalline, occluded quartz grains in this rock may have formed during contact metamorphism by nearby intrusive bodies of the basalt of Buttox Hills. Contact metamorphism in adjacent Precambrian rocks is seen in a conversion of microcline to sanidine and in oxidation of mafic minerals.

Except for apparent contact-metamorphic features, this rhyodacite is petrographically similar to tiny fragments found in the basal tuffaceous breccia and sandstone (cs) of the Crater Pasture Formation in Four OClock Wash. On this basis, this rhyodacite body is thought to be older than the Crater Pasture Formation.

A chemically analyzed specimen of this rock has a recalculated silica content of 69 percent. Normative potassium feldspar is about 25 percent and constitutes 36-1/2 percent of the total normative feldspar in the rock. Chemically, the rock is intermediate between the average rhyodacite and the average rhyolite (Nockolds, 1954).

Basalt of Buttox Hills

Distribution, stratigraphy, and physical features. The basalt of Buttox Hills underlies the Buttox Hills, parts of a narrow ridge to the east, and part of Three OClock Hill to the north. It also forms a dike, which is roughly parallel to Five OClock Wash, and a series of plugs, which are aligned with the dike inside the crater. The dike varies in width from a few feet to 200 feet, and the distance from the southeast end of the dike to the northwestern-most plug is nearly 1 mile. The maximum preserved thickness of basalt flow in the Buttox Hills is about 75 feet.

This unit consists of flow (bf), intrusive (bi), tuff and tuff-breccia (bt), and undivided basalt (bu). The flow and intrusive rocks are generally resistant

to erosion and are responsible for the presence of Buttox Hills, a narrow ridge to the east, a small knob south of Sams Camp. The tuff and tuff-breccia are poorly resistant to erosion.

Relationship to other units. In most places, this unit overlies a rhyodacite-bearing sedimentary breccia and rhyodacite sandstone and conglomerate (fs) of the Fort Rock Creek Rhyodacite. Locally it overlies ash-flow tuff of the latter formation or Annex Ridge flow of the Crater Pasture Formation. The dike of Buttox Hills basalt intrudes ash-flow tuff, Annex Ridge flow, and Precambrian rocks. In a concealed body of tuff-breccia northwest of the dike and 400 feet southwest of Sams Camp, fragments of basalt are seen to include small clasts of rhyodacite which are identical in hand specimen to rhyodacite of the intrusive body in the gully at the head of Five OClock Wash. Contact metamorphism of both the rhyodacite and Precambrian rocks in the area between the end of the dike and the concealed body of tuff-breccia appears related to intrusion of the basalt.

This basalt is overlain on the narrow ridge east of Buttox Hills by terrace deposits.

Source. Intrusive basalt (bi), characterized by irregular contacts and steep-dipping banding, where banding is present, occurs in the northwestern parts of the Buttox Hills. Relatively flat-lying basalt flow (bf) occurs in the southeastern parts of these hills and on the narrow ridge to the east. The flow can be traced continuously into the intrusive body. The dike may have also been a small source for the flow. Bodies of tuff and tuff-breccia (bt) in the northwestern part of the Buttox Hills probably are partly intrusive and partly extrusive in nature. A thin blanket of reddened tuff which underlies the flow to the southeast can be traced continuously, except where it is covered by colluvium, into these bodies of tuff and tuff-breccia. These bodies probably also were

the source for the patch of tuff on the east flank of Three OClock Hill.

Petrography. Flow (bf) and intrusive rock (bi) are steel gray on weathered surfaces and dark gray to black on fresh surfaces. Near the base of the flow and near the edges of the intrusive bodies, the rock has flow cleavage and bands of tiny vesicles. The tuff and tuff-breccia contain red to olive-brown vesicular ash, lapilli and (rare) bombs of basalt, and as much as 5 percent angular fragments of Precambrian rocks (up to several inches across), Annex Ridge flow (up to more than 1 foot across), and olivine trachyandesite (up to several inches across).

In thin section a sample of the flow (bf) is seen to contain 1 percent pseudomorphs of olivine phenocrysts, 23 percent clinopyroxene grains (all sizes), 12 percent pseudomorphs of olivine microphenocrysts, 49 percent groundmass labradorite, and 15 percent opaque minerals. The pseudomorphs of olivine are constituted by red-brown to red minerals on their edges and serpentine in their centers. The phenocrysts reach a size of 1 mm across. The microphenocrysts are distinctive in that they are uniform in size, about 0.1 mm across. These tiny grains can be seen as red specks in hand specimen. Clinopyroxene is distributed in continuous sizes from 1 mm down to groundmass grains. About 3 percent of the clinopyroxene occurs as grains greater than 0.1 mm. The larger grains are diopsidic augite. Glomerophenocrysts of clinopyroxene are common. The composition of the plagioclase was determined by microprobe analysis. The texture of the rock is intergranular to pilotaxitic.

In rock of the dike and rock of the small plugs northwest of the dike, clinopyroxene commonly occurs abundantly (10 percent) in sizes greater than 0.1 mm and the total content of olivine pseudomorphs is only about 5 percent.

Chemical composition. A sample of the Buttox Hills basalt contains 49 percent recalculated silica, which is well within the range of basic composition. Potash is only 1.4 percent. This rock is chemically similar to an average alkali basalt (Nockolds, 1954).

V. QUATERNARY SEDIMENTS

Quaternary sediments in the vicinity of Fort Rock dome include alluvium, of several ages, and colluvium. On the geologic map (pl. 1), two units are distinguished. The unit labeled Qal includes all but the oldest alluvium in the area. It includes modern alluvium in washes and older alluvium on low terraces on the flanks of the dome. It does not include alluvium which underlies high terraces in the area. The unit labeled Qc includes all surficial cover not mapped as Qal, chiefly colluvium but, locally, high terrace deposits. Alluvium (Qal) is shown on the geologic map where it exceeds a thickness of about 1/2 foot; colluvium and high terrace deposits (Qc) are shown where they exceed a thickness of 1 foot to 1-1/2 feet.

Alluvium is distinguished from colluvium by composition and sorting. It contains clasts which have been transported some distance and which are in many locations foreign to local rock types. For example, on the west and northwest flanks of the dome, alluvial fans contain chiefly clasts of Precambrian rocks from the interior of the crater, whereas colluvium is composed chiefly of rocks of the Crater Pasture Formation from nearby areas on the rim and flank. Additionally, alluvium is better sorted than colluvium. Its finest particles are silt, whereas the finest particles in the colluvium are clay. Colluvium also contains abundant caliche.

High terrace deposits in the area generally contain abundant clasts of Paleozoic rocks, chiefly dark red fragments of Tapeats Sandstone. Locally these deposits are cemented by caliche or calcite and are well indurated. An extensive area east of Fort Rock dome is underlain by these high terrace deposits. Within the area mapped (pl. 1), these deposits occur on the

northern flank of One OClock Hill, on the northeastern flank of Lion Ridge, and in the area east of Three OClock Hill. The clasts in these deposits were derived from Cross Mountain or from terrane to the east and northeast underlain by Paleozoic rocks.

VI. STRUCTURE

Structures of several different ages can be observed at the Fort Rock dome and in the area nearby. Precambrian structures include folds and veined fractures. Tertiary structures include small faults which predate the Fort Rock dome, the Fort Rock dome itself, with its associated folds and faults, and large normal faults, which accompanied and followed rhyodacite eruption in the area.

PRECAMBRIAN STRUCTURES

On the Fort Rock dome, Precambrian structures have been deformed somewhat, but in most cases it is possible to distinguish them from younger structures. A large fold or fault is apparent in the vicinity of Lion Ridge, but the rotation of attitudes that occurred during doming must be removed, using a stereonet, in order to observe this structure clearly. Small folds are seen in layered metamorphic rocks. These are unaffected by doming except for rotation. A broad shear zone in the Precambrian rocks crosses the southern half of the crater. This zone is characterized by fractured and veined rocks. Fractures are in most cases distinct from the largely unmineralized fractures and open-breccia lenses which were formed during doming.

Folds

A large structure in the Precambrian rocks is apparent in the vicinity of Lion Ridge (pl. 1). In the exposure of Precambrian rocks northeast of the crater, the foliation dips, on the average, about 75° to the west-northwest. In rocks in the northern half of the crater, however, the foliation presently dips about 60° to the south. The effect of doming can be removed from attitudes inside the

crater by rotating each attitude, using a stereonet, in a direction counter to the rotation caused by doming; the amount of rotation necessary is determined from the cross sections (pls. 2 and 3). This procedure leaves the strike of the foliation of rocks inside the crater essentially unchanged but steepens the dip to an average of 75° to 80° to the south (fig. 4). A large difference in attitude between rocks inside and outside of the crater remains, reflecting a structure that predates the formation of the dome. This structure might be a fold or a fault. It is also possible that two different foliations were developed in the rocks, in which case no large structure is required to explain the observations. If a large fold is present, its axis must lie beneath Lion Ridge, where the two sets of attitudes are separated by less than 900 feet. More of the Precambrian rocks northeast of the crater must be mapped to interpret this structure fully.

Small folds, measuring one to several inches in amplitude, are observable in the layered metamorphic rocks. These folds are most easily seen in the well exposed gneiss in the northwest quadrant of the crater interior. They are largely isoclinal and may reflect larger scale isoclinal folding. The lack of observable units in the layered metamorphic rocks, however, prevents the recognition of larger folds. Some folds can be observed in which foliation locally follows the margins of pegmatites.

Shear Zone

A broad shear zone crosses the southern half of Fort Rock crater. This zone is characterized by Precambrian rocks that have been fractured and veined. These rocks are covered by Tertiary volcanic rocks on the rim of the crater, and 4 miles north of the crater, rocks in a similar shear zone are covered by Tapeats Sandstone, of Cambrian age. Minor hematite-veined fractures seen in

Figure 4. Precambrian Structures on the Fort Rock Dome.

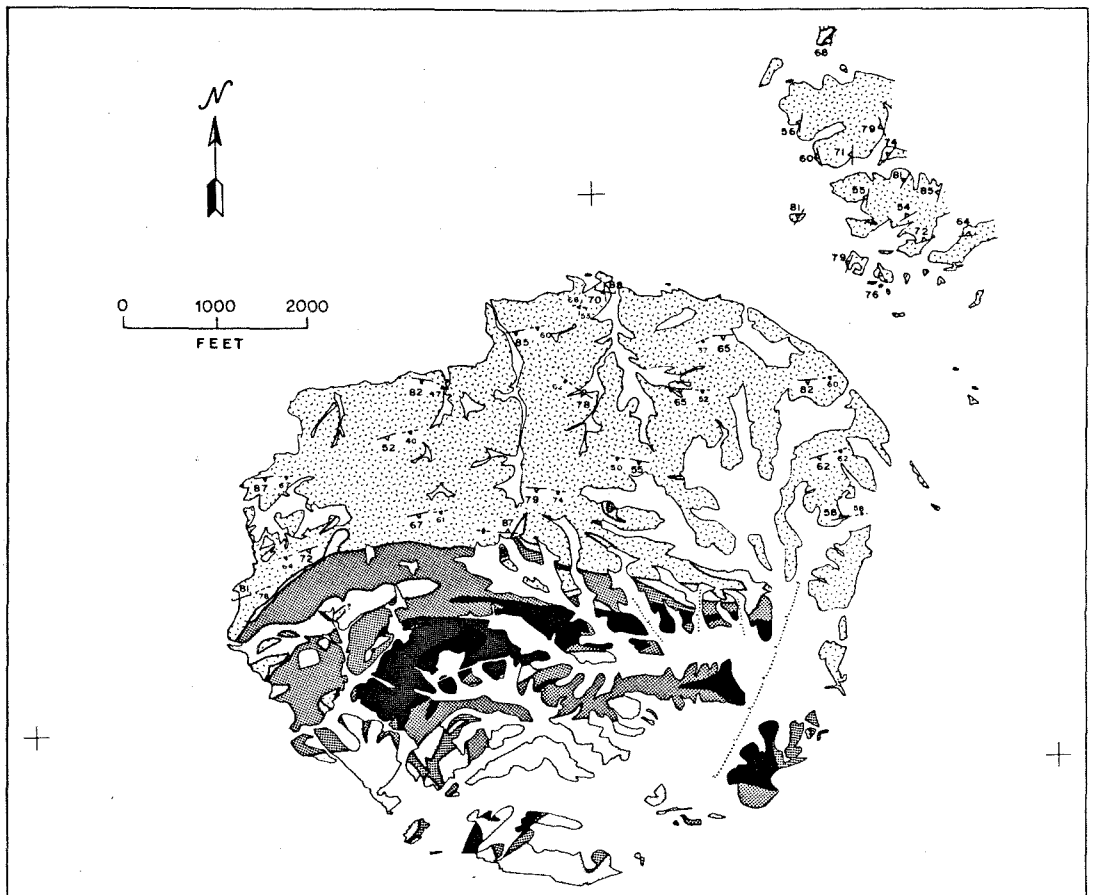

EXPLANATION

Outcrops of Precambrian rocks appearing on the geologic map (pl. 1) are shown here.

Attitudes

- present foliation
- present attitude of axial planes of small folds
- foliation prior to doming; estimated rotations which occurred during doming have been removed
- attitude of axial planes of small folds prior to doming

Levels of Vein Density

- low density . . . . . veins spaced farther than 10 cm apart
- moderate density . . . . veins spaced 1 cm to 10 cm apart
- high density. . . . . veins spaced 1 mm to 1 cm apart
- very high density . . . . veins spaced closer than 1 mm; identity of original rocks obscured in most places; appears on geologic map (pl. 1) as "veined rocks" (pЄv)
- mixed high and very high density

places in the Tapeats Sandstone indicate minor renewed movement in the latter zone in Phanerozoic time.

The spatial density of veined fractures in the shear zone in Fort Rock crater has been mapped (fig. 4). Isopleths, marking the divisions between different levels of vein density, trend largely east-west in the center of the crater, swing around to the southwest in the western and southwestern part of the crater and appear to be discontinuous in the eastern part. From north to south across the shear zone there is a fairly regular increase in the density of veins from low to very high, followed by a more erratic decrease in density to moderate. Moderate density of veins prevails through most of the exposed Precambrian rocks in the southern part of the crater. Rock type influences, to some extent, the observed density of veins. In Eight OClock Basin, the cataclasite of Eight OClock Basin forms an elongate pocket of moderate vein density within a zone of high vein density.

The shear zone may be part of a major Precambrian fault zone. Discontinuity across this zone can be seen in the rocks in the crater. Rocks in the northern part of the crater generally are different from those in the southern part. Pegmatites are abundant north of the shear zone, for example, but are nearly absent in the south. No Precambrian unit that was mapped can be traced across the zone. In addition, rocks of slightly differing metamorphic grade may have been brought into contact along this shear zone. North of the zone, the layered metamorphic rocks belong entirely to the epidote-amphibolite facies, whereas within the shear zone, some rocks of greenschist facies are found.

A discontinuity of large proportions passing through the vicinity of the Fort Rock dome is apparent on an aeromagnetic map of Arizona (Sauck and Sumner, 1970).

The dome lies on a line bounding a series of positive magnetic anomalies that trends west-southwest from the vicinity of Ashfork, Arizona, to the western border of the Aquarius Mountains. The anomalies have low gradients and bear no direct relationship to volcanic rocks in the region; they are apparently due to differences in the properties of the Precambrian basement rocks (Shoemaker and others, in press). Linear margins on the anomalies imply linear discontinuities of rock type which probably correspond to an ancient fault zone. Tertiary volcanic rocks are offset by minor west-trending and west-southwest-trending normal faults in places along the margins of the anomalies. Faults in the northwestern part of the Aquarius Mountains and in the southern part of the Cottonwood Cliffs (fig. 3) are examples. Such normal faults are believed to have been formed by renewed movement on the ancient system of faults (Shoemaker and others, in press).

The shear zone exposed at Fort Rock dome may be similar in structure to the Shylock fault zone which is exposed for a distance of about 50 miles between Black Canyon and Mingus Mountain in central Arizona. The Shylock fault zone trends north-south and is covered at the north end by Tapeats Sandstone of Cambrian age. This structure separates Precambrian rocks of widely differing composition at its north end and rocks of similar composition but differing metamorphic grade at its south end. A minimum of 5 miles right lateral displacement can be documented at its north end, although displacement may be less at its south end (Anderson, 1967; Anderson and Creasey, 1958, p. 77). A pronounced linear boundary of aeromagnetic anomalies is present along the entire exposed length of the fault zone. Movement along this fault zone produced foliation and fissility in the rocks that were sheared, whereas movement along the shear zone at Fort Rock dome produced only brittle fractures that were subsequently veined.

TERTIARY PRE-DOME FAULTS

A number of faults on the rim of the crater offset rocks as young as the Two OClock Gap tuff and flow of the Crater Pasture Formation but are either covered or intruded by younger rocks in this formation. These faults predate the uplift of the dome. One fault, on Four OClock Hill, may have been ancestral to the Four OClock Hill fault, which formed during doming. The Upper Two OClock Gap fault is a pre-dome fault which experienced movement during doming in a direction opposite to its pre-dome movement.

The Road End Gap volcanic breccia and flow is offset by three faults that are covered by the Annex Ridge flow. On Six OClock Hill, a north-trending fault offsets this unit by as much as 75 feet stratigraphically. An east-west fault on Four OClock Hill offsets the unit by about 50 feet stratigraphically, and another fault, which trends west-northwest and lies about 400 feet farther northeast on the same hill, offsets the unit and is accompanied by change in attitude of rocks on either side. Rocks along these faults are displaced down on the east, north, and northeast, respectively. No fault scarps are preserved beneath the Annex Ridge flow; the Road End Gap unit is thinner on upthrown sides of the faults, indicating a period of erosion between faulting and emplacement of the Annex Ridge flow. A reverse-facing fault-line scarp is, however, preserved along the east-west fault on Four OClock Hill, as there is a small buried hill on the downthrown side of this fault beneath the Annex Ridge flow. The east-west fault is closely associated geographically and in its trend with the structurally complex, southwesternmost part of the Four OClock Hill fault. The Four OClock Hill fault offsets the Annex Ridge and Lion Ridge flows and apparently was formed during doming. The east-west fault may have been ancestral to this fault.

The Eight OClock Gorge flow is offset by two faults that are covered by the Buffalo Ridge flow. On the top of Nine OClock Hill, this flow is offset by an east-west fault which has a stratigraphic displacement of about 70 feet. A smaller fault in this unit is seen near the top of Eight OClock Hill. No scarps are preserved on these faults beneath the Buffalo Ridge flow.

Atop Buffalo Ridge, the Road End Gap unit is offset by a number of faults that are associated with intrusive bodies that fed the Buffalo Ridge flow. Five small, north-trending faults east of the boot-shaped intrusion of massive hornblende trachyandesite (cbi) atop this ridge, drop the Road End Gap unit successively down in the direction of the intrusion. On the west side of the boot-shaped intrusion, a 60-foot by 50-foot block of the Road End Gap unit is dropped down along an east-west and a north-south fault, which are both intruded by intrusive breccia (cbt). Farther west, three similar-sized blocks have been faulted successively down to the west in the direction of another intrusive body. On the northwest side of the latter body, a block of Road End Gap volcanic breccia has been dropped and rotated parallel to the margin of the intrusion such that the basal contact of the breccia now strikes perpendicular to Buffalo Ridge. All of this faulting adjacent to Buffalo Ridge intrusives seems to represent collapse of wall rock into eruptive vents.

In Two OClock Gap, an abrupt thinning of the Two OClock Gap tuff is seen across the Upper Two OClock Gap fault. In order to explain the thinning, it is estimated that prior to emplacement of the Lion Ridge flow, the rocks in the southwest wall of the fault moved up relative to those on the northeast by an amount ranging from 50 feet, along the northwestern exposure of the fault, to 30 feet, along the southeastern exposure. Later movement on this fault during doming took place in the opposite direction.

FORT ROCK DOME

The Fort Rock dome is a structural dome. The central part of the dome is a low quaquaversal arch, 1-1/2 miles in diameter which has been almost entirely removed by erosion. The edge of the dome is in most places a monocline. Most faults shown on the geologic map are related in origin to the dome. They are confined to the vicinity of the monocline, partly as a result of poor exposure and lack of structural control in the deeply eroded central part of the dome. In addition to the mapped faults, abundant small faults, with displacements of inches to feet, and lenses of unmineralized, open breccia occur everywhere in the structure. These features are also related in origin to doming. All units of the Crater Pasture Formation older than the Fault Canyon flow are strongly uplifted and deformed on the dome; the Fault Canyon flow and units of the Fort Rock Creek Rhyodacite are uplifted and deformed by much smaller amounts.

The Monocline

Volcanic rocks older than the Fault Canyon flow in the rim of Fort Rock crater have dips that range from 43° to 90°(?) and average about 66° (Table 6). In one or two places, it can be seen that these rocks form the steep-dipping limb of a monocline. This monocline nearly encircles in dome. In most places, the low-dipping inner limb of the monocline has been removed by erosion and the low-dipping outer limb is buried beneath younger units.

On Nine and Ten OClock Hills, the entire monocline is exposed. The structure is best observed on the northeast wall of Ten OClock Wash, where it is defined by the contact of the Buffalo Ridge flow on Precambrian rocks.*

* It should be noted that attitudes of flow cleavage in volcanic rocks can not, in general, be used to determine structure. On Ten OClock Hill, flow cleavage dips steeply (40° or more) into the contact between the flow and the

TABLE 6. Dips of Volcanic Units Older than the Fault Canyon Flow on the Dome

Location	Dip (degrees)	Dip obtained from
Nine OClock Wash	52	basal tuffaceous sandstone (cs) of Crater Pasture Formation
	68, 50	pyroxene trachyandesite sandstone (cp) of Crater Pasture Formation
Eight OClock Gorge	51	basal contact of Buffalo Ridge flow (cbf)
	52	basal tuffaceous sandstone (cs) of Crater Pasture Formation
Six Thirty Wash	74, 80	sandstone within basal facies (cbb and cab) of Buffalo Ridge and Annex Ridge flows
Six OClock Hill, near Road End Gap	52	basal tuffaceous sandstone (cs) of Crater Pasture Formation
Hidden Pasture	55, 50 73, 56	tuff and tuffaceous sandstone (ch) of Hidden Pasture tuff and conglomerate
Four OClock Wash	56	basal tuffaceous sandstone (cs) of Crater Pasture Formation from a pit in the bottom of the wash
Three OClock Hill, southwest flank	76	basal contact of Crater Pasture Formation exposed in pit
One OClock Wash	90(?)	basal contact of Lion Ridge flow (clf)
Noon Hill, east side	90(?)	isopleths in One OClock Wash sedimentary breccia (cob)
	43, 63, 90	hornblende trachyandesite tuff and tuffaceous sandstone (chh) of Hidden Pasture tuff and conglomerate

In this wall, the low-dipping outer limb of the monocline is exposed just above the bottom of the wash and dips about 15° to the northwest. The steep-dipping limb lies between the elevations of 5100 feet and 5200 feet and dips about 60° to the northwest. The low-dipping inner limb lies above 5200 feet, and dips about 28° to the northwest. The monocline can be viewed in its entirety by standing on Nine OClock Hill and looking to the northeast. It can also be seen on the southwest wall of Ten OClock Wash by standing on Ten OClock Hill. On the southwest wall, the steep-dipping limb lies approximately between the elevations of 5200 feet and 5300 feet. The monocline is, thus, warped or possibly displaced along a concealed fault in the vicinity of the wash. The initial surface on the Precambrian rocks over which the Buffalo Ridge flow was emplaced at this locality was somewhat hilly, and structural interpretation must be made with caution here.

The only other location where the low-dipping inner limb of the monocline is well preserved is Four OClock Hill. On top of this hill, contacts of the Road End Gap volcanic breccia and flow on Precambrian rocks and of the Annex Ridge flow on Road End Gap rocks dip as low as 7° to the southeast. Hidden Pasture deposits on the southeast side of this hill, which dip 55° to the southeast, are on the steep-dipping limb of the monocline.

Cross sections A-A', B-B', C-C', and D-D' (pls. 2 and 3) show the monocline in profile at various locations around the dome. In cross section

Precambrian rocks near the top of the hill. This phenomenon is also seen on Outer Hill, on the top of Four OClock Hill, and on the small knob extending southwest of the southeastern end of Lion Ridge. There is, furthermore, a tendency in most places for the attitudes of flow cleavage to change directions from the bottom to the top of a flow. This phenomenon can be easily seen, for example, in rocks on the southwest side of the Upper Two OClock Gap fault on Outer Hill.

D-D' (pl. 3) enough ground control on the inner limb of the monocline on Ten OClock Hill and on Four OClock Hill is available to project contacts inward and reconstruct the form of the now-eroded central part of the dome. Cross section C-C' (pl. 3) is also well controlled by exposures in Eight OClock Gorge and on Lion Ridge. In the southeast wall of Eight OClock Gorge, a double monocline is present; here the flank of the dome has a structural terrace. As shown in the cross section, the flank of the dome has collapsed near Lion Ridge. Reconstruction of the dome above ground in the remaining two cross sections, A-A' and B-B' (pls. 2 and 3), is somewhat conjectural and is done with the aid of cross sections C-C' and D-D'. The structural relief of the Fort Rock dome, measured on the contact between Precambrian and Tertiary rocks, is about 900 feet.

The structural relief of the monocline, where it is sharply developed, varies greatly from place to place. In the vicinity of Eight OClock Gorge, the relief is about 700 feet. On Ten OClock Hill, the relief is only about 150 feet. On the southeast end of Lion Ridge, apparently no monocline was formed, as there is no evidence for it in the collapsed flank of the dome. The structural relief on the monocline, where it is sharp, appears to be inversely correlated to the elevation of Precambrian rocks at the margins of the dome; the monocline is highest where the Precambrian is lowest. Beyond Buffalo Ridge, where the monocline has sizeable relief, Precambrian rocks occur well below the surface at an estimated elevation of between 4600 feet and 4700 feet (pl. 3). Just northwest of Ten OClock Hill, where the monocline is small, Precambrian rocks have an estimated elevation of between 4800 feet and 4900 feet (pl. 3). Northeast of Lion Ridge, where no monocline was formed, Precambrian rocks crop out at the surface at an elevation of 5200 feet. Estimated

elevations of the Precambrian rocks at the margins of the dome define a pre-volcanic surface on these rocks which sloped away to the west, southwest, and south from a high area in the vicinity of present-day Lion Ridge. The most sizeable monocline is thus developed in lava flows that were emplaced at the lowest elevations on this sloping surface.

Development of a sharp monocline may be related to inhomogeneity in the basement rocks, as well as to the pre-volcanic topography on these rocks. Rocks in the Precambrian shear zone in the southern half of the crater are fractured and veined. The monocline is well developed in this area. The northern half of the crater is characterized by an abundance of relatively competent intrusive bodies. In this half, the monocline is poorly and irregularly developed.

The asymmetry of the monocline is illustrated in a structure contour map of the dome (fig. 5). The monocline is well developed along the southern margin of the dome but diminishes in amplitude and sharpness in both directions around the dome. To the east, it diminishes rapidly, as it encounters a relatively steep initial slope on the basement; it dies out abruptly on Three OClock Hill. To the west, it gradually gives way to a broad monocline interrupted by a small, sharp monocline, as is seen in the vicinity of Ten OClock Peak.

Along the north side of the dome, control for the structure contour map is somewhat sketchy. Noon Hill appears to be underlain by a sharp monocline. This monocline is offset successively on the west by two faults. West of these faults the monocline is very broad. The monocline is also offset by several faults east of Noon Hill. Between the One OClock Hill fault and a fault farther east, the monocline is anomalously broad. East of the latter fault, the monocline is again sharp but becomes gradually broader along Lion Ridge. It

Figure 5. Structure Contour Map of the Fort Rock Dome

EXPLANATION

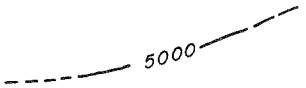

contour on contact between Precambrian and Tertiary rocks; short dashed above present ground surface; long dashed below present ground surface where uncertain; elevation given in feet above sea level

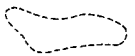

intruded area

fault; queried where uncertain; names abbreviated:

EHF	Eight OClock Hill fault
FHF	Four OClock Hill fault
LTGF	Lower Two OClock Gap fault
NGF	Noon Gorge fault
OHF	One OClock Hill fault
SHF	Short Hill fault
THF	Three OClock Hill fault
UTGF	Upper Two OClock Gap fault
WBF	Wedge Basin fault

geographic locations abbreviated:

BR	Buffalo Ridge
EB	Eight OClock Basin
EG	Eight OClock Gorge
FH	Four OClock Hill
LR	Lion Ridge
NB	Noon Basin
NH	Noon Hill
SH	Six OClock Hill
TG	Two OClock Gap
TH	Three OClock Hill
TP	Ten OClock Peak
WB	Wedge Basin

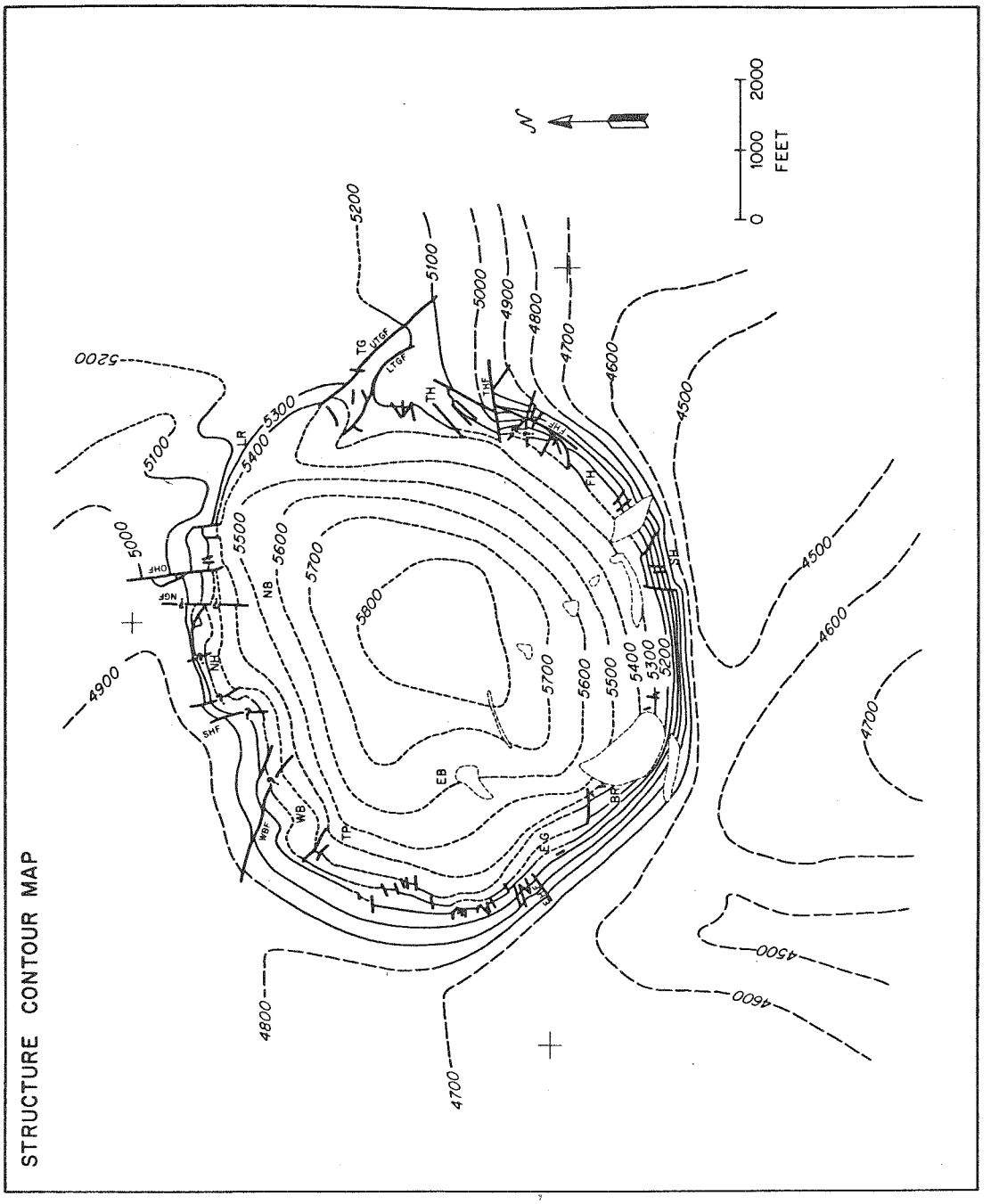
STRUCTURE CONTOUR MAP
N
0 1000 2000
FEET
5200
5100
5000
4900
4800
4700
4600
4500
5300
5400
5500
5600
5700
5800
TG
VTGF
LTGF
TH
THF
FH
JH
JR
OHF
NGF
NB
WB
SHF
WBF
TP
EB
BF
EG

dies out at Two OClock Gap.

A topographic map of the pre-volcanic surface on the Precambrian rocks can be constructed using the structure contour map for undeformed areas outside the dome and using a few inferences about the initial topography inside the dome. The topographic relief on this surface can be subtracted from the structural relief in figure 5 to determine the vertical uplift which occurred during doming. Figure 6 shows contours of equal uplift of Precambrian rocks within the dome. This map is similar in its configuration to the structure contour map but with contours shifted southwestward. If one considers the center of the 5800-foot contour on the structure contour map to be the center of the dome and the center of the 900-foot contour on the uplift map to be the center of the uplift, then the latter center is shifted about 1000 feet southwest of the former.

Mapped Faults

Most faults shown on the geologic map (pl. 1) offset rocks younger than the Two OClock Gap tuff and flow in the rim of the crater. Where ages can be determined, these faults occurred during or shortly after uplift of the dome. These faults have chiefly radial and tangential strikes. Dips are steep where they can be determined. Block rotations are observable along faults that can be traced for large distances.

Assemblages of faults differ significantly among the east, north, west, and south sides of the dome. On the east side of the dome, tangential faults, also traceable for relatively long distances, are found. Radial and subradial faults, also traceable for relatively long distances, offset these faults in places. On the north side of the dome, relatively long radial and subradial faults occur.

Figure 6. Uplift Map of the Fort Rock Dome

EXPLANATION

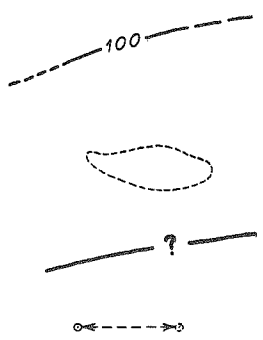

contour of locations on the dome showing equal amounts of uplift; short dashed above present ground surface; long dashed below present ground surface where uncertain; uplift given in feet.

intruded area

fault; queried where uncertain; names abbreviated as in fig. 5 .

dashed circle, center of Structure Contour Map (fig. 5); solid circle, center of Uplift Map; dashed arrow shows spatial difference between the two centers.

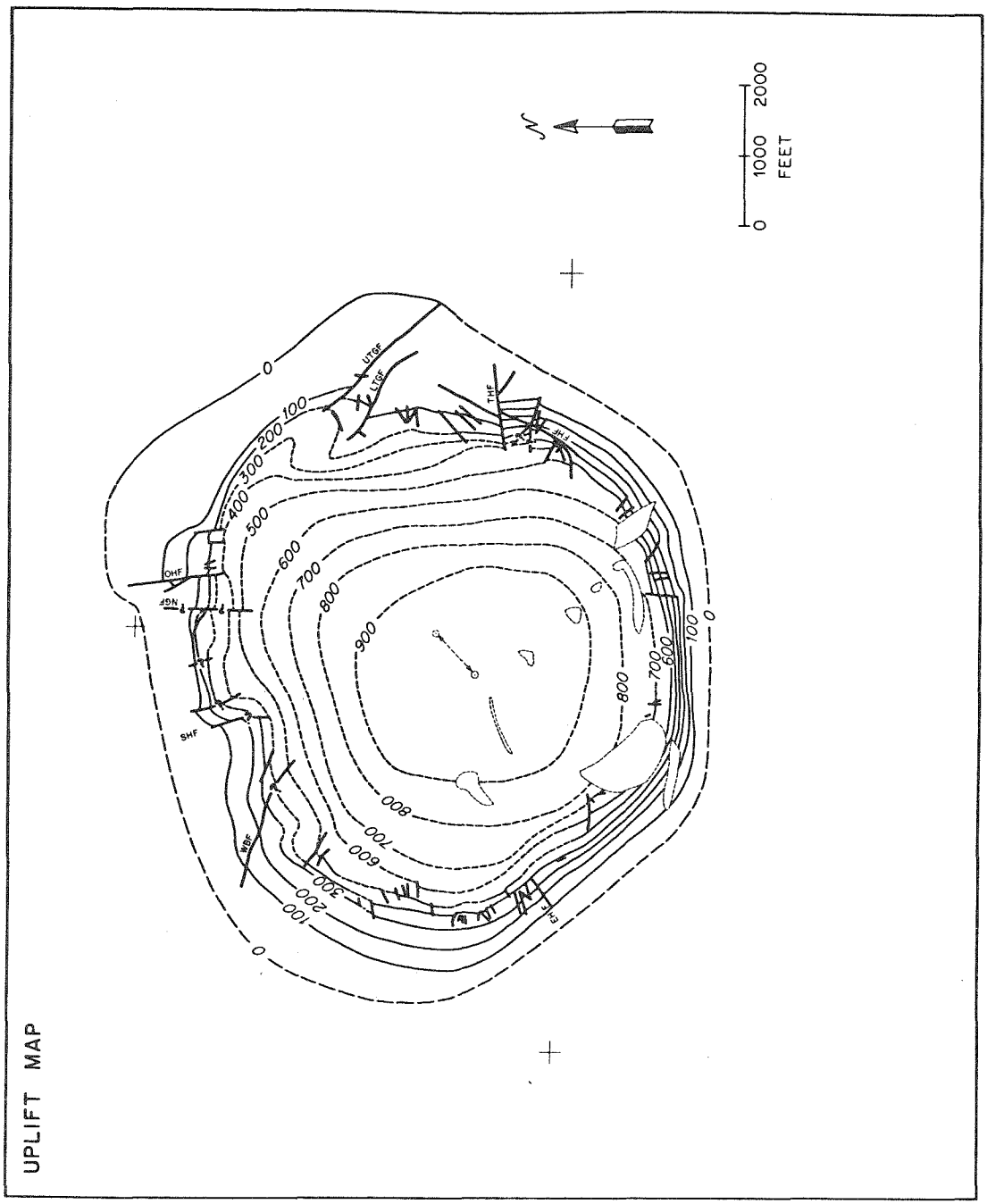
UPLIFT MAP
N
0
1000
2000
FEET
0
100
200
300
400
500
600
700
800
900
UTGF
LTGF
THF
OHF
NGF
SHF
WGF
EHF

On the west side, relatively short radial faults are found and are numerous compared to faults in other areas on the dome. On the south side of the dome, relatively short radial faults occur but are rare.

Faults on the east side of the dome. Tangential faults, traceable for up to 2000 feet, occur on the east side of the dome. These faults include the Upper Two OClock Gap fault, the Lower Two OClock Gap fault and the Four OClock Hill fault. In addition, three tangential faults traceable for a few hundred feet, at most, are parallel to the Four OClock Hill fault near its northern end. The Three OClock Hill fault and a fault in Four OClock Wash, offset the Four OClock Hill fault.

The Upper Two OClock Gap fault trends southeast-northwest from the south side of Outer Hill to the saddle between Lion Ridge and the small knob on the southwest side of this ridge. This fault offsets the contact of Tertiary volcanic rocks on Precambrian rocks by about 20 feet along its northwestern exposure and by less than 5(?) feet along its southeastern exposure. The contact of Lion Ridge flow (clf) on Two OClock Gap tuff (ctb) is offset along this fault by as much as 70 feet on the northwest and by 25 feet on the southeast. All contacts are offset relatively downward on the southwest. In addition to offset, there is a persistent angular discordance between contacts on either side of this fault. The angular discordance varies from 18° in the northwest to 7° in the southeast. Units on the southwest side of this fault have been rotated to the southwest relative to units on the northeast side. The fact that younger units are offset by greater amounts than older units along this fault implies a history of faulting. Early movement occurred between emplacement of the Two OClock Gap tuff and flow and the Lion Ridge flow, as noted earlier. Rocks on the northeast side of the fault were displaced relatively

down. Movement after emplacement of the Lion Ridge flow occurred in the opposite direction and apparently involved rotation.

The Lower Two OClock Gap fault is exposed on the west side of Outer Hill and along the southwest flank of the small knob southwest of Lion Ridge. It probably extends beneath the colluvium in Two OClock Gap but has been queried here, as the resulting fault is quite crooked. This fault offsets all contacts by about 35 feet along its northwestern exposure and by about 15 feet along its southeastern exposure. Displacement is relatively down on the southwest.

The Four OClock Hill fault extends north-northeastward from the top of Four OClock Hill to the east side of Three OClock Hill. Displacement is nil at either end and is as great as 250 feet on the north bank of Four OClock Wash. The displacement changes abruptly across several radial and subradial faults which offset the Four OClock Hill fault. The largest displacement occurs along the segment of the fault between the Three OClock Hill fault and a concealed fault in Four OClock Wash. Angular discordance is observed in the flow cleavage in the Annex Ridge flow on either side of this fault (pl. 1). Rocks on the northwest side of the fault on Four OClock Hill and on Three OClock Hill south of the Three OClock Hill fault have apparently been rotated to the east relative to rocks on the southeast side of the fault. Structure at the southwest end of the fault is complicated by en eschelon faults and by the presence of older faults. The Four OClock Hill Fault may be, in part, a reactivated pre-dome fault.

Faults on the north side of the dome. Radial and subradial faults, traceable for as much as 2000 feet, occur on the north side of the dome. These faults

include the One OClock Hill fault, the Noon Gorge fault, the Short Hill fault, the Wedge Basin fault, and others.

The One OClock Hill fault trends north-south and is located high on the west flank of One OClock Hill. Rocks on the west side of the fault have been either downthrown with respect to rocks on the east side or moved left-laterally along the fault, or both. Along the southern exposure of the fault, rocks on the west side have steep dips (60°), whereas rocks on the east side have moderate dips (30°), as inferred from isopleths within the One OClock Wash sedimentary breccia. Along the northern exposure of the fault, rocks on both sides of the fault appear to have low dips (15°). On the structure contour map (fig. 5), the contact of Tertiary rocks on Precambrian rocks is interpreted to form a broad monocline on the east side of the One OClock Hill fault; on the west side, it is interpreted to form a sharp monocline. The writer's conception of this fault is shown in figure 7.

The Noon Gorge fault is a concealed north-south fault in Noon Gorge. Rocks on the east side have been either downthrown with respect to rocks on the west side or moved right laterally along the fault. Dips within units on opposite sides of the fault are similar. On the structure contour map (fig. 5), this fault is interpreted to offset the axes of the monoclines on either side.

The Short Hill fault is an apparent fault that trends north-south to northwest-southeast along the crest of Short Hill. It is similar to the One OClock Hill Fault in that rocks on the west side have been either downthrown or moved left laterally along the fault; they also dip more steeply than rocks on the east side along the southern exposure of the fault.

The Wedge Basin fault can be traced along the northeastern edge of Wedge Basin. Toward its southeastern end, rocks on the northeast side appear

Figure 7. Writer's Conception of the One OClock Hill Fault.

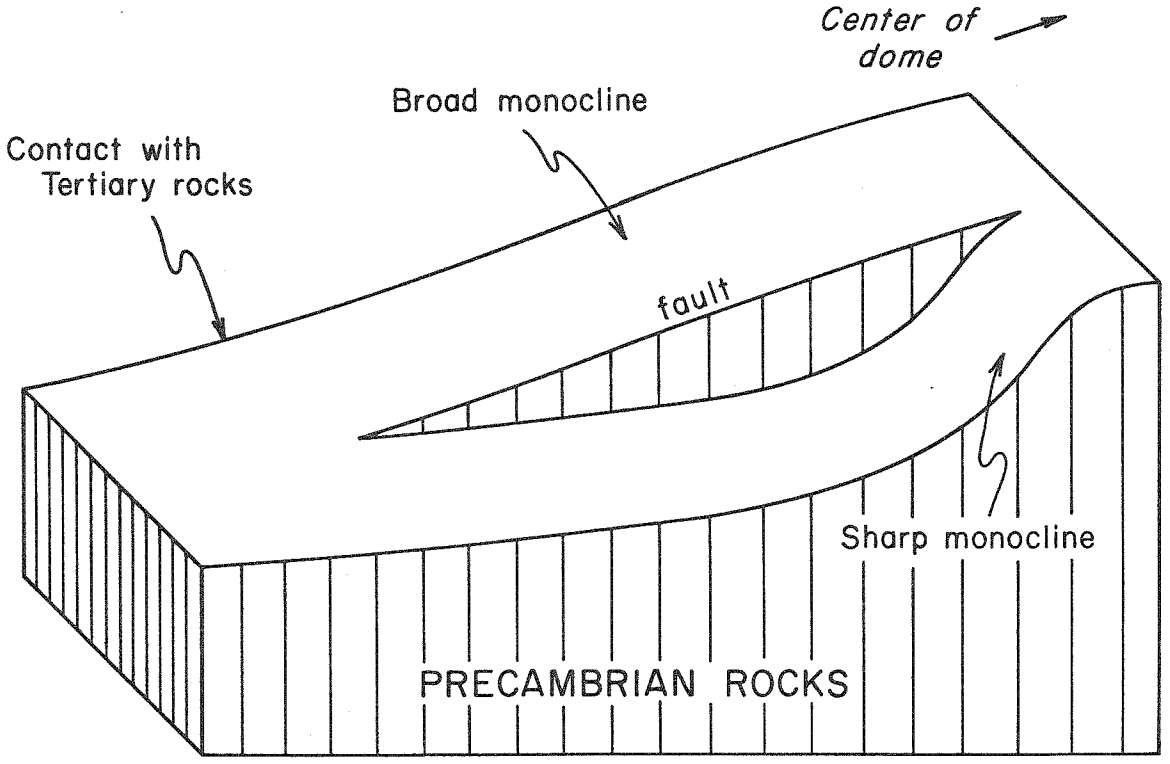
Center of dome
Broad monocline
Contact with Tertiary rocks
fault
Sharp monocline
PRECAMBRIAN ROCKS

to be downthrown, whereas toward its northwestern end rocks on the southwest side are downthrown. Excellent exposures of the fault in the wash draining Wedge Basin show it to be a normal fault with a displacement of 10 to 20 feet in this area.

Faults on the west and south sides of the dome. Except for the Eight OClock Gorge faults, faults on the west side of the dome have radial and subradial trends. Generally, they are more numerous and traceable for shorter distances (hundreds of feet) than faults on other sides of the dome. They have normal and/or strike-slip offsets. One of the largest faults on this side of the dome is the Eight OClock Hill fault, which trends northeast-southwest and is located on the northwest wall of Eight OClock Gorge. Rocks on its southeast side are downthrown or offset left laterally along the fault. Most other faults on Eight OClock Hill show a similar sense of displacement. Faults on Nine OClock Hill, on the other hand, are downthrown on the north or show right lateral movement. Rocks in the region between Eight and Nine OClock Hills, were, thus, uplifted slightly more or moved slightly more toward the edge of the dome than rocks on either side. (See fig. 5).

The Eight OClock Gorge faults are exposed as three breccia-filled fissures in the upper part of the Buffalo Ridge flow in Eight OClock Gorge. The fissures strike tangentially to the dome and dip steeply to the southwest. Rocks on their southwest sides have moved relatively up. They are reverse faults.

Faults on the south side of the dome which are not associated with intrusion of the Buffalo Ridge and which do not predate emplacement of the Annex Ridge flow are rare. The largest is an east-west fault at the northwest end of Buffalo Ridge, which is traceable for about 350 feet. Four or five

radial and subradial faults of similar length occur on the rim of the crater in the vicinity of Five OClock Wash.

Ages of faults. Several faults in the rim of the crater have well determined ages that range from the beginning of doming to well after major doming was finished. Other faults which cut rocks younger than the Two OClock Gap tuff and flow do not have well known ages but are presumed to be related to doming because of their local extent and because they have radial or tangential trends.

The Eight OClock Hill fault and the Eight OClock Gorge faults are the oldest faults related to doming. These faults offset the Buffalo Ridge flow, but are covered (and locally filled) by One OClock Wash sedimentary breccia; fault scarps are preserved beneath the breccia. These faults occurred at the beginning of doming.

The Short Hill fault offsets most of the section of the One OClock Wash sedimentary breccia on Short Hill, but is covered by 50 feet of this unit. The isopleth pattern in the breccia is suggestive of a low fault scarp preserved beneath the upper 50 feet. This fault occurred during the major part of doming, which is represented by the emplacement of the One OClock Wash breccia.

The youngest unit offset by the One OClock Hill fault is the lower part of the basal sedimentary breccia (fob) of the Old Stage Road Member. The fault is covered by a higher part of this basal breccia. Movement thus occurred after the major part of the uplift of the dome was over. Possible coarsening of the Noon Gorge sedimentary breccia on the west side of the fault may or may not indicate earlier movement on this fault. The Noon Gorge fault, which is concealed by alluvium, is probably the same age as the One OClock Hill fault. Another fault, atop Noon Hill, is covered by the basal sedimentary

breccia of the Old Stage Road Member and occurred at about the same time as the One OClock Hill fault.

The Wedge Basin fault offsets ash-flow tuff of the Old Stage Road Member; it occurred well after doming was finished but caused only minor offset.

Ages of the Lower Two OClock Gap fault, the Four OClock Hill fault, and the latest movement on the Upper Two OClock Gap fault are unknown and must be inferred from the geologic history of the dome (see p. 189) or from a model of doming (see p. 267). The Three OClock Hill fault and a concealed fault in Four OClock Wash offset the Four OClock Hill Fault. Although these faults are younger than the Four OClock Hill fault, they may be very close in age.

Unmapped Faults and Breccia Lenses

Numerous small faults, wi th displacements of inches to feet, and lenses of largely unmineralized, open breccia occur on the dome. These small structural features are most abundant and most easily observed in the Precambrian rocks but also are seen in the volcanic rocks. Their distribution on the dome and their occurrence in both the Precambrian and Tertiary rocks indicates that they are related in origin to the dome.

The average spatial density of small faults and the maximum thicknesses of breccia lenses were recorded in traverses through Noon Basin, Eight OClock Gorge, Eight OClock Basin, and the Precambrian rocks northeast of Lion Ridge. The faults and breccia lenses were observable only in the banks and bottoms of washes where recent floods had locally removed all surficial cover. In most cases, exposures were in the form of narrow strips parallel to the washes. Generally, the faults and lenses of breccia that were seen were those oriented nearly perpendicular to the strip of outcrop; these faults and breccia lenses almost invariably had

steep dips. The total number of faults seen in a given strip of outcrop was divided by the length of that outcrop to give a density measured in number of faults per foot. The fault density and breccia-lens thickness are plotted versus distance from the center of the dome (fig. 8), where the center of the dome is determined from the structure contour map (fig. 5).

The dome is well defined by fault density and by breccia-lens thickness. Beyond the crater the density of faults is low, generally less than one fault per 10 feet of outcrop; there are virtually no breccias. Inside the crater, the density of faults is commonly between one and five faults per 10 feet of outcrop. Breccia lenses are numerous and range from a few inches in maximum thickness to as much as 80 feet. Fault density and maximum breccia-lens thickness generally decrease from the rim of the crater toward the center; however, because of thick deposits of alluvium in the center of the crater, no data are available here. In addition, fault density and the number of breccia lenses measuring, say, one foot or more in thickness are higher in the region of Eight OClock Gorge and Eight OClock Basin than in the region of Noon Basin.

The fact that small faults are more numerous and that breccia-lenses are thicker toward the edges of the dome is consistent with the fact that a monocline is found on the edge of the dome in most places. Rock deformation was presumably highest in the vicinity of the monocline. The fact that small faults and thick breccia lenses are most numerous in the southwestern part of the dome is consistent with the fact that the best developed monocline occurs in that area.

Uplift and Tilting of the Fault Canyon Flow and Units of the Fort Rock Creek Rhyodacite

Rocks of the Fault Canyon flow and the Fort Rock Creek Rhyodacite are not as strongly uplifted and tilted on the dome as rocks of the Crater Pasture

Figure 8. Average Spatial Density of Small Faults and Maximum Thicknesses of Breccia Lenses on the Fort Rock Dome. The number of faults seen in a given outcrop is divided by the length of that outcrop to give an average spatial density measured in number of faults per foot. In the figure the number of faults per 10 linear feet of outcrop is plotted. (Outcrops tend to occur as narrow strips in the bottom and banks of washes.) Faults spaced closer than 6 inches apart were considered a single fault zone. Symbols are

- • maximum thickness of a breccia lens (upper plot); average spatial density of small faults (lower plot)
- 20 | dimensions of an outcrop if the outcrop is entirely breccia (upper plot)
- ↕ minimum or maximum fault density (lower plot)
- (•) fault density determined from only one fault (lower plot)
- ↧ upper limit on fault density; no faults were seen in the given outcrop (lower plot)

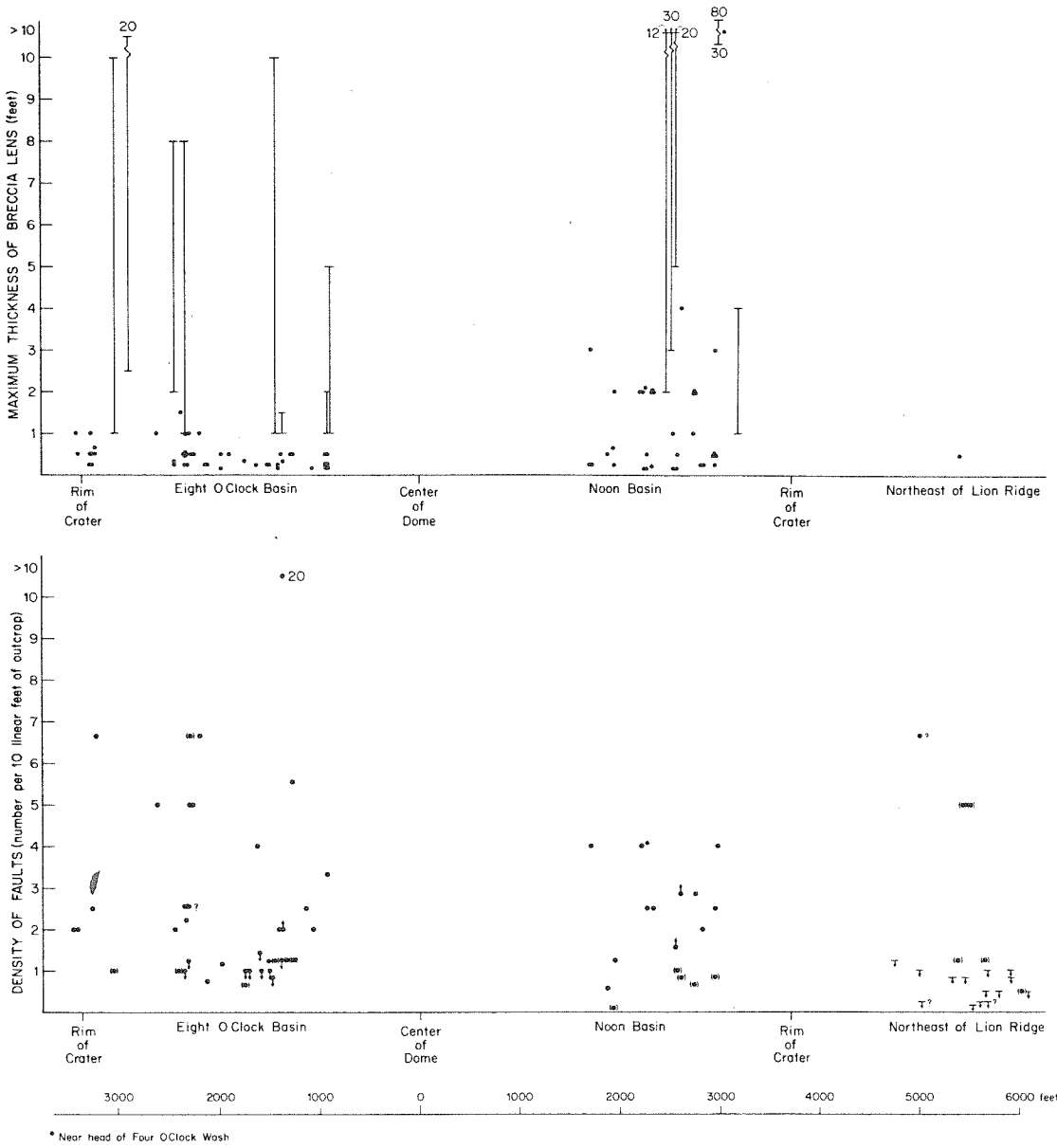

* Near head of Four O Clock Wash

Formation that are older than the Fault Canyon flow. These rocks may not, in fact, be uplifted or tilted at all.

The topography on the Fault Canyon flow after it was extruded (fig. 9, Map 9) consisted chiefly of lobate spurs extending away from feeder vents. A slightly anomalous long narrow ridge extending northwest from the main feeder vent is probably best explained by uplift, of the order of 25 feet, adjacent to the dome subsequent to extrusion of the flow. Explanations that do not involve uplift, however, are possible. For example, additional vents could underlie this ridge.

The basal contact of the Noon Gorge sedimentary breccia dips on the average about 33° away from the dome; the maximum dip is 45° (Table 7). Dips on the basal contact of the overlying Old Stage Road Member and on sandstone beds within this unit range from 6° to 34°, depending on how high on the flank of the dome the dip is measured. Generally, dips are steeper higher on the flanks of the dome. Most of the dips on the base of the Noon Gorge sedimentary breccia could be explained as initial dips, assuming that the angle of repose of the One OClock Wash sedimentary breccia was between 30° and 40° at the time the Noon Gorge breccia was deposited. Although this unit probably was, indeed, deposited on a steep slope, it is reasonable to believe that some subsequent tilting took place. Perhaps as much as 5° to 10° of the present dips on the steep limb of the monocline (Table 6) is attributable to continued uplift of the dome after emplacement of the Noon Gorge unit. Dips on the base of the Old Stage Road Member and on sandstones within this unit are all easily explainable as initial dips on the dome.

TABLE 7. Dips of Units in the Fort Rock Creek Rhyodacite on the Dome

Location	Dip (degrees)*	Dip obtained from
Wash between Noon Hill and Short Hill	32	basal contact of Noon Gorge sedimentary breccia
	10 (11→ 8)	basal contact of Old Stage Road Member
	10	sandstone in Old Stage Road Member
Wash on west side of Short Hill	33	basal contact of Noon Gorge sedimentary breccia
	14	sandstone in Old Stage Road Member
Wash draining Wedge Basin	34 (43→ 29)	basal contact of Noon Gorge sedimentary breccia
	32	basal contact of Old Stage Road Member
	32, 17	sandstone in Old Stage Road Member
Ten OClock Wash	30	basal contact of Noon Gorge sedimentary breccia
Nine OClock Hill, west side	20 → 12 → 6	sandstone in Old Stage Road Member
Eight OClock Hill, southwest side	12 → 16, 27 → 23 → 14 → 9	sandstone in Old Stage Road Member
Eight OClock Gorge	38 (36 → 45)	basal contact of Noon Gorge sedimentary breccia
	17 (22 → 12)	basal contact of Old Stage Road Member
Buffalo Ridge, southwest side	15	sandstone in Old Stage Road Member
	34	sandstone in Old Stage Road Member
	18	sandstone in Noon Gorge sedimentary breccia
Four OClock Wash	14	sandstone in Old Stage Road Member

*The number preceding a set of parentheses is an average dip for the given location. The numbers in parentheses are a selected dip higher on the flank of the dome (left) and a selected dip lower on the flank of the dome (right). Arrows point to dip(s) measured (successively) lower on the flank of the dome.

LARGE NORMAL FAULTS

Large normal faults near the Fort Rock dome include the Fort Rock Creek fault (pl. 1, fig. 3) and an east-west fault south of the Three Sisters (fig. 3). The youngest unit offset by Fort Rock Creek fault is a basalt which postdates the Fort Rock Creek Rhyodacite. The youngest unit offset by the fault south of the Three Sisters is the Fort Rock Creek Rhyodacite. The downthrown sides of these two faults are the southwest and south sides, respectively. Units within the Fort Rock Creek Rhyodacite appear to thin abruptly on the downthrown sides of both faults, suggesting that early movements on the faults took place during emplacement of the Fort Rock Creek Rhyodacite in directions opposite to the presently observed displacements.

On the Fort Rock Creek fault, the displacement of rocks of the Crater Pasture Formation is estimated to be about 150 feet in the area southeast of Fault Canyon (pl. 3; cross section A-A'). Maximum displacement of rocks of the Fort Rock Creek Rhyodacite is unknown at this location but probably is several hundred feet. The fault passes into a monocline on the hill west and northwest of Fault Canyon (pl. 2). West of the hill, the fault offsets rocks of the Crater Pasture Formation by more than 25 feet and dies out about 1000 feet northwest of the point where it crosses Fort Rock Creek. The southeastern part of the fault consists of two branches (fig. 3). Displacement is small on the northeastern branch. The southwestern branch offsets young (post-Fort Rock Creek Rhyodacite) basalt by as much as 100 feet.

On the fault south of the Three Sisters, the displacement of rocks of the Crater Pasture Formation varies from zero to 400 feet. South of the Three Sisters this displacement is zero. Two miles east of the point where a tributary to Knight Creek crosses the fault (fig. 3), the displacement is 400 feet.

One half mile west of the tributary, the displacement is again zero. Farther west displacement is small but reversed, with the downthrown side on the north. South of the Three Sisters, the breccia and conglomerate of the Crossing, which caps the Three Sisters, is displaced 300 feet downward across the fault.

VII. GEOLOGIC HISTORY

Geologic history at the Fort Rock dome can be divided broadly into early geologic history, which includes events that predate eruption of Tertiary volcanic rocks, Tertiary volcanic history, which began in mid-Tertiary times and probably ended in Miocene times, and late geologic history, which includes events younger than the Tertiary volcanism.

The major events in the early geologic history at the Fort Rock dome include, in Precambrian times, deposition of volcanic and sedimentary rocks, metamorphism, intrusion, uplift, faulting, and erosion and, in Phanerozoic times, deposition of sedimentary rocks, uplift, and erosion. Major events in the Tertiary volcanic history at the dome include eruption of the Crater Pasture Formation, during which uplift of the dome occurred, eruption of the Fort Rock Creek Rhyodacite, which was accompanied by some large-scale faulting, and eruption of the basalt of Buttox Hills. In addition, other volcanic rocks were erupted at some distance from the dome after the eruption of the Fort Rock Creek Rhyodacite. The major events in the late geologic history at the dome are large-scale normal faulting in Miocene to Pliocene times, and extensive erosion in early to middle Pliocene and younger times, including excavation of a crater-like depression on the dome.

EARLY GEOLOGIC HISTORY

The oldest geologic event that can be inferred from rocks on the Fort Rock dome is the deposition in early Precambrian times of a sequence of volcanic and/or sedimentary rocks. These rocks were subsequently deeply buried, folded, and metamorphosed to epidote-amphibolite facies. The layered metamorphic rocks that were produced were then intruded by a number of

relatively small bodies of granitic rocks. Both the layered metamorphic rocks and the granitic intrusive rocks were next subjected to cataclastic deformation. Near the end of the episode of cataclastic deformation, these rocks were in some areas intruded by granites and then by swarms of pegmatites. Uplift and erosion ensued. At some time during the uplift, shearing and veining occurred, which probably was produced by large-scale (strike-slip?) faulting. The shear zone that passes through the Fort Rock dome probably was part of an active fault zone that extended from near Ashfork, Arizona, to the western edge of the Aquarius Mountains, a distance of about 70 miles. Prior to deposition of the Tapeats Sandstone, in Cambrian times, a surface of very low relief was produced on the faulted metamorphic and plutonic rocks.

The timing of the Precambrian events at the Fort Rock dome was probably similar to the timing of Precambrian events at the Grand Canyon. At the Grand Canyon, volcanic and sedimentary rocks were buried, folded and metamorphosed to produce layered metamorphic rocks. These rocks were then intruded by the Zoroaster granite and other granites which have reported uranium-lead ages of around 1725 million years before the present (Pasteels and Silver, 1965; Silver, oral communication). These rocks were subsequently metamorphosed at about 1695 million years before the present and were intruded at about the same time by pegmatites (Pasteels and Silver, 1965). Uplift and erosion occurred next. There is evidence that large-scale strike-slip faulting may have occurred at about this time (Shoemaker and others, in press). Erosion continued, and a surface of very low relief, the Arizonan Plain (Maxon, 1961), was produced. Subsidence was next, followed by deposition of rocks of the Grand Canyon Supergroup, which are not present at the Fort Rock dome. This deposition apparently began no earlier than 1400 million years ago (Elston and others, 1973; Elston, written communication) and no later than 1150 million

years ago (L. T. Silver, oral communication). Uplift, tilting, normal and reverse faulting, and erosion occurred next. A surface of very low relief was present on the Precambrian rocks at the time the Tapeats Sandstone was deposited, in Cambrian times.

Early Phanerozoic events at the Fort Rock dome, recorded at nearby Cross Mountain, were subsidence and the deposition of Paleozoic sedimentary rocks. In Cambrian times, the Tapeats Sandstone, Bright Angel Shale, and Muav Limestone were deposited. Unnamed carbonate rocks were deposited in Devonian times. In Mississippian times, the Redwall Limestone was deposited. Younger Paleozoic units probably were deposited but were subsequently removed by erosion. Likewise, Mesozoic and early Tertiary units may have been deposited, but have not been preserved.

In mid-Tertiary times, uplift and erosion occurred. An erosional surface was formed over a wide area in northwestern Arizona. In the vicinity of the Fort Rock dome, Cross Mountain was a butte on this surface. West and south of Cross Mountain, Phanerozoic rocks were completely removed by erosion. The topography that was developed on underlying Precambrian rocks was similar to topography seen today on these rocks. At the Fort Rock dome, the pre-volcanic erosion surface that was produced sloped to the west, southwest, and south away from a high area in the vicinity of present-day Lion Ridge (fig. 9, Map I). Local relief was about 700 feet. A northeast-trending valley apparently was cut in the vicinity of present-day Eight OClock Gorge. This valley extended well inside the limits of the present crater.

Figure 9. Maps I through 10, Showing Paleogeology and Paleotopography at the Fort Rock Dome

EXPLANATION

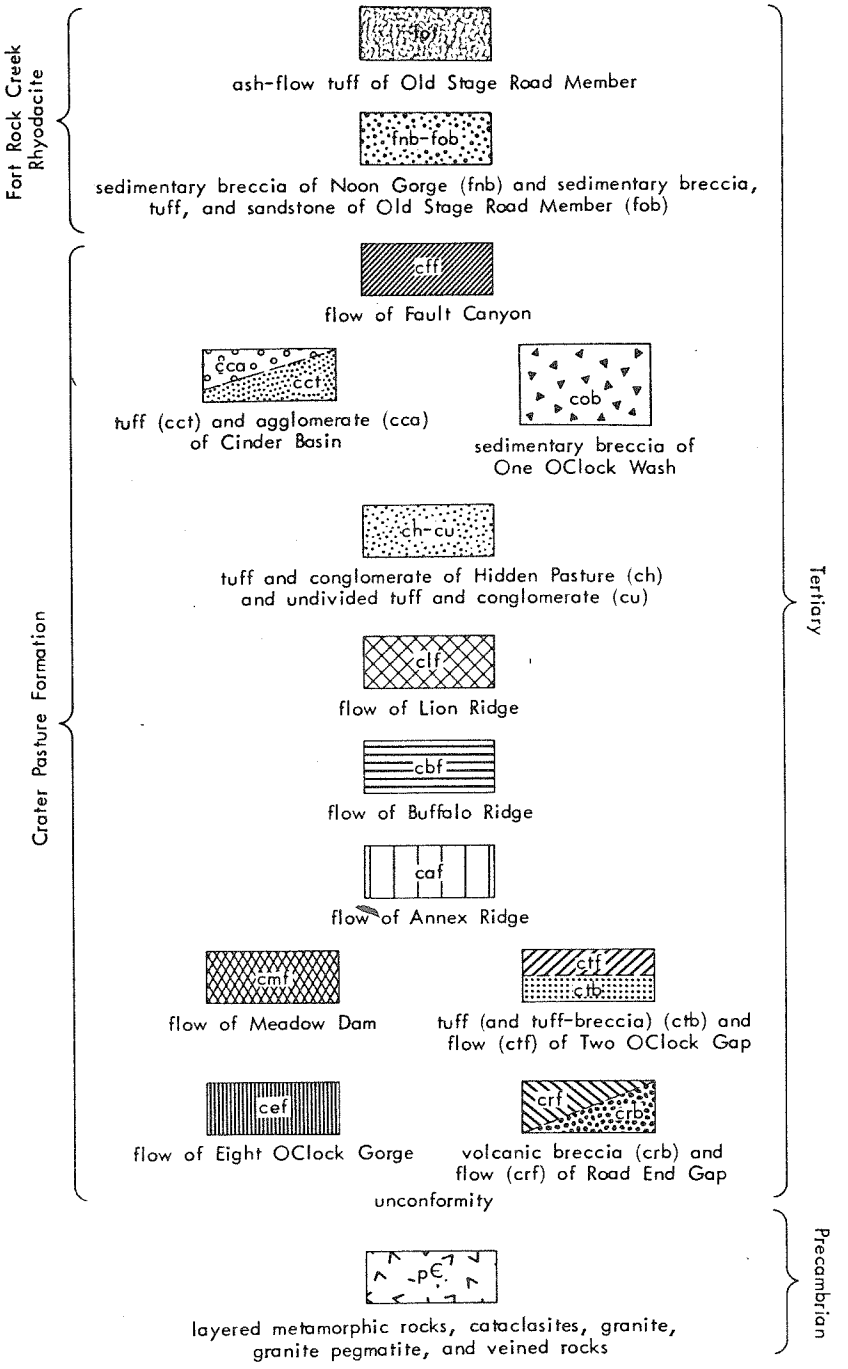

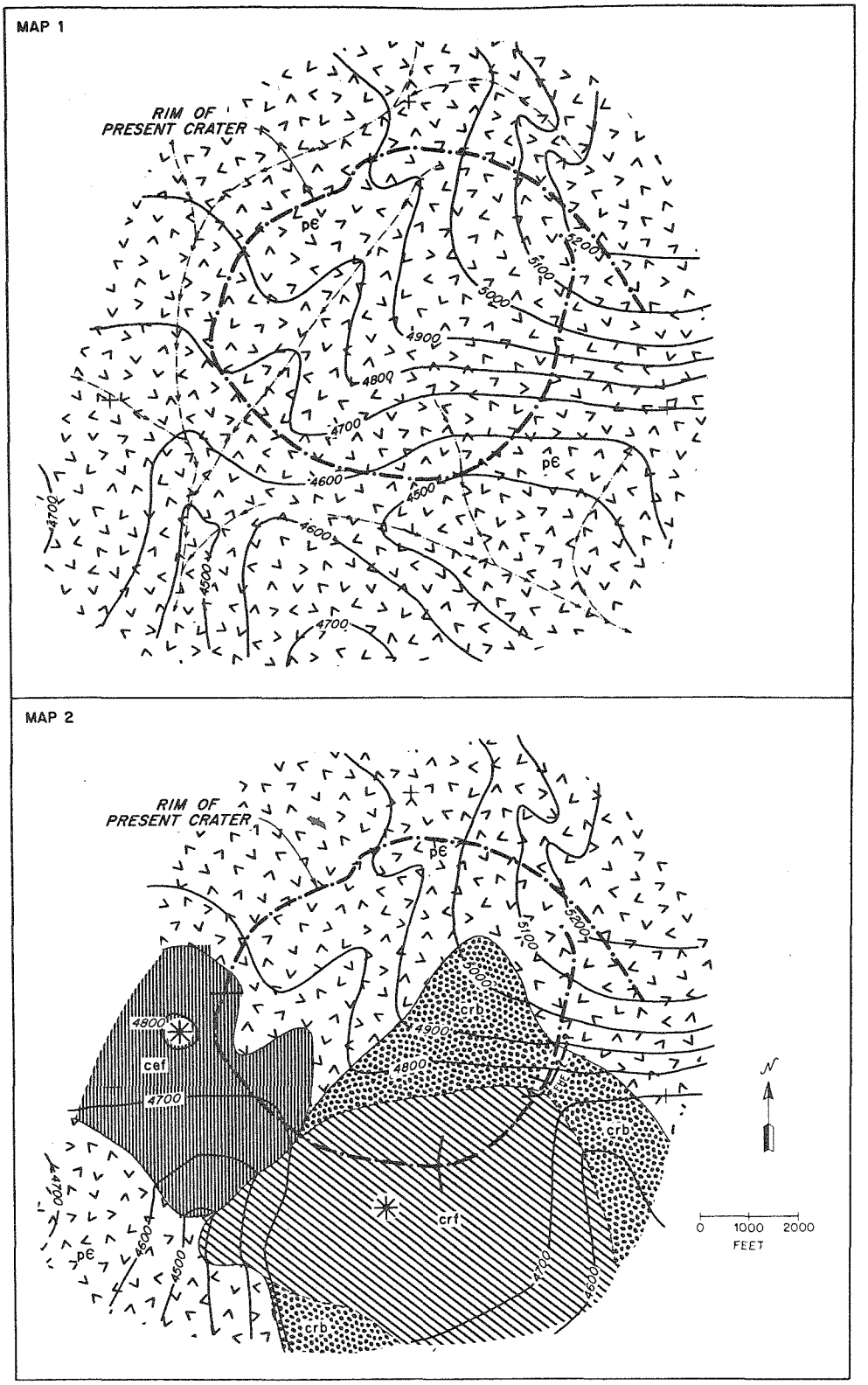
MAP 1
RIM OF PRESENT CRATER
pε
4700
4600
4500
4900
5000
5100
5200
MAP 2
RIM OF PRESENT CRATER
pε
4800
cef
4700
crb
4900
4800
crf
5000
5100
5200
4600
4500
4700
N
0 1000 2000
FEET

MAP 3

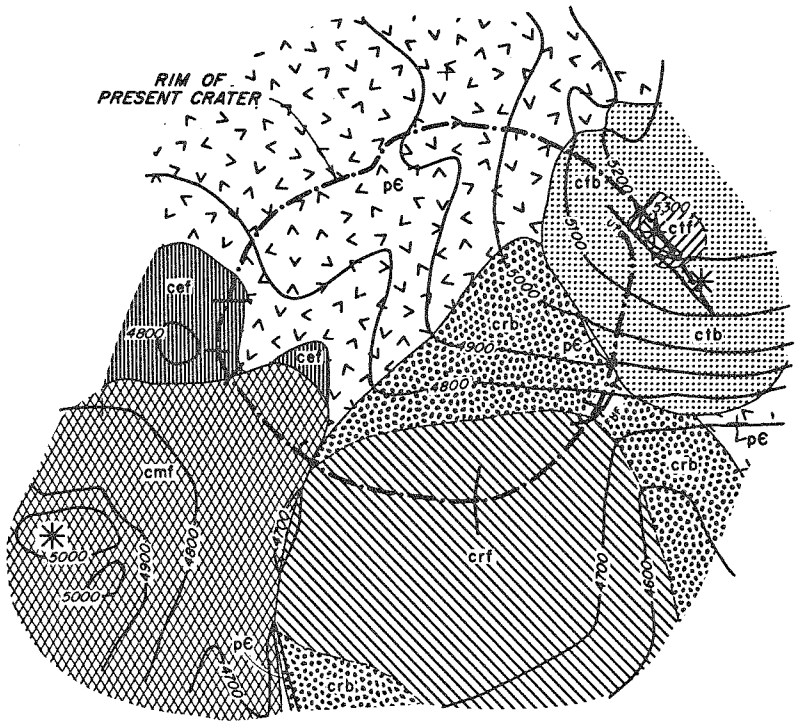
RIM OF PRESENT CRATER
pε
ctb
5200
5300
5100
ctf
cef
4800
4900
crb
5000
cmf
4600
4700
crf

MAP 4

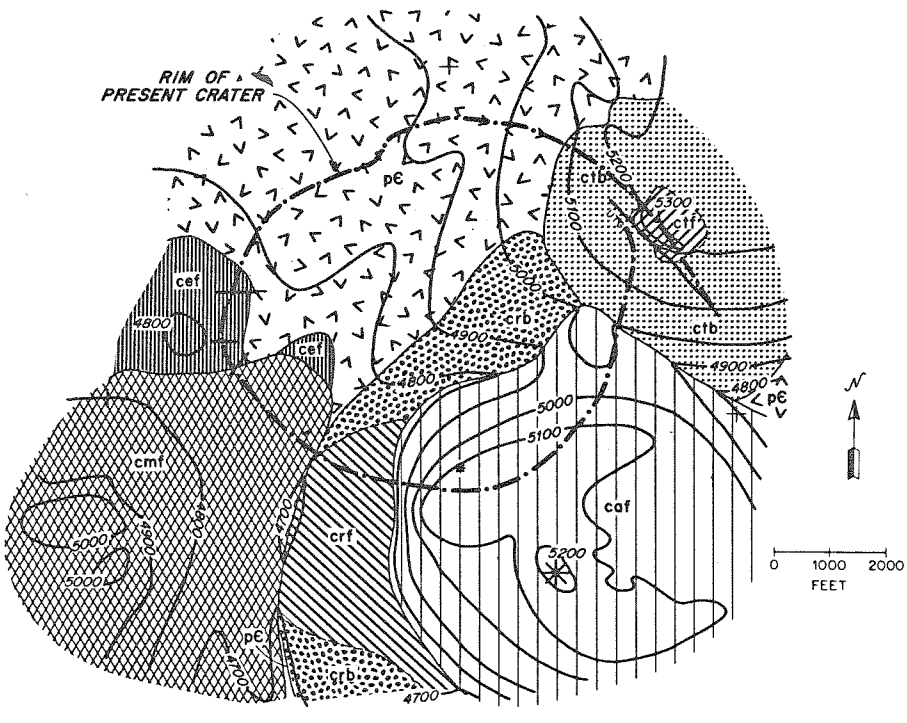
RIM OF PRESENT CRATER
pε
ctb
5200
5300
5100
ctf
cef
4800
4900
crb
5000
caf
cmf
4600
4700
crf
N
0
1000
2000
FEET

MAP 5

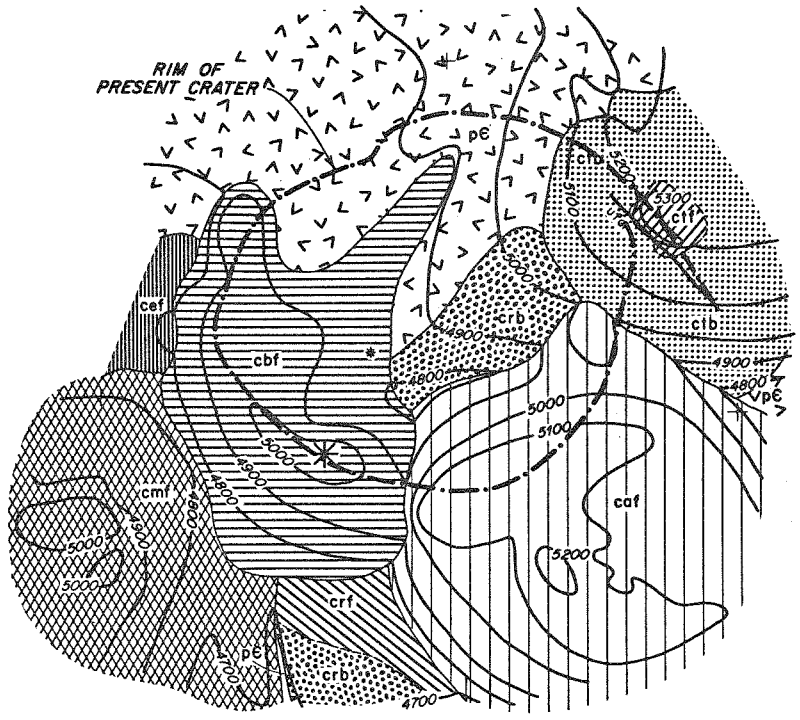
RIM OF
PRESENT CRATER
pε
ctb
5300
ctf
5200
5100
5000
4900
4800
cef
cbf
crb
caf
cmf
crf
4700

MAP 6

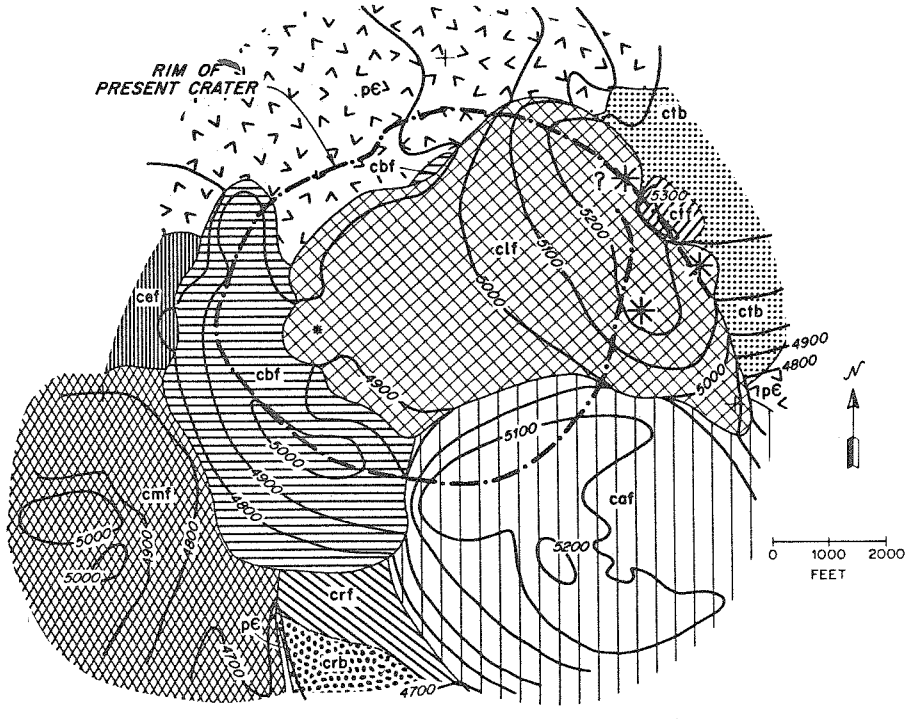
RIM OF
PRESENT CRATER
pε
ctb
cbf
5300
ctf
5200
5100
5000
4900
4800
cef
clf
caf
cmf
crf
crb
4700
N
0 1000 2000
FEET

MAP 7

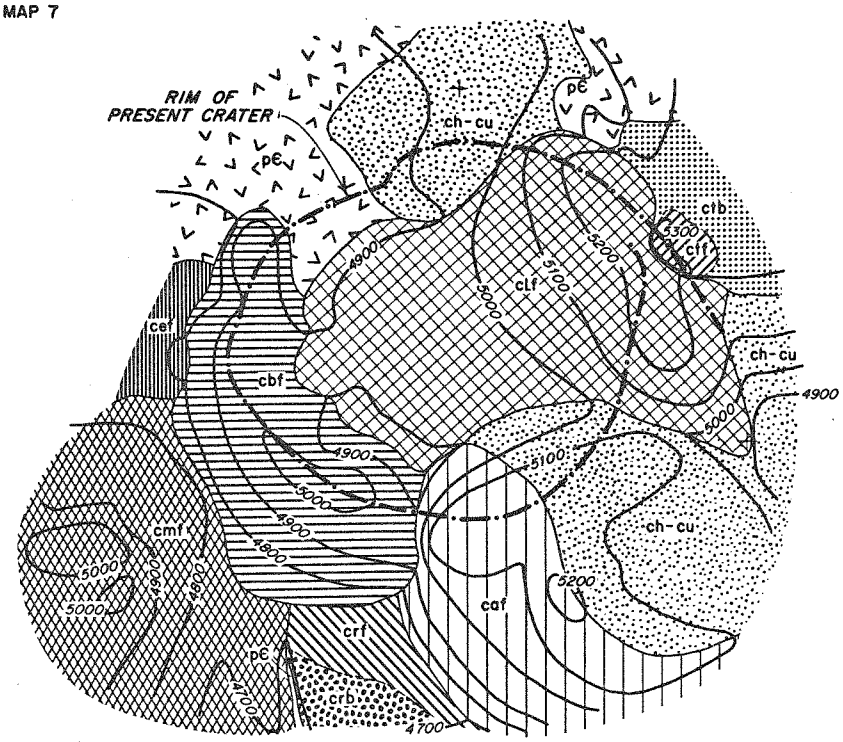
RIM OF
PRESENT CRATER
pe
ch-cu
ctb
ctf
clf
cef
cbf
cmf
caf
crf
crb
4900
5000
5100
5200
5300
4800
4700

MAP 8

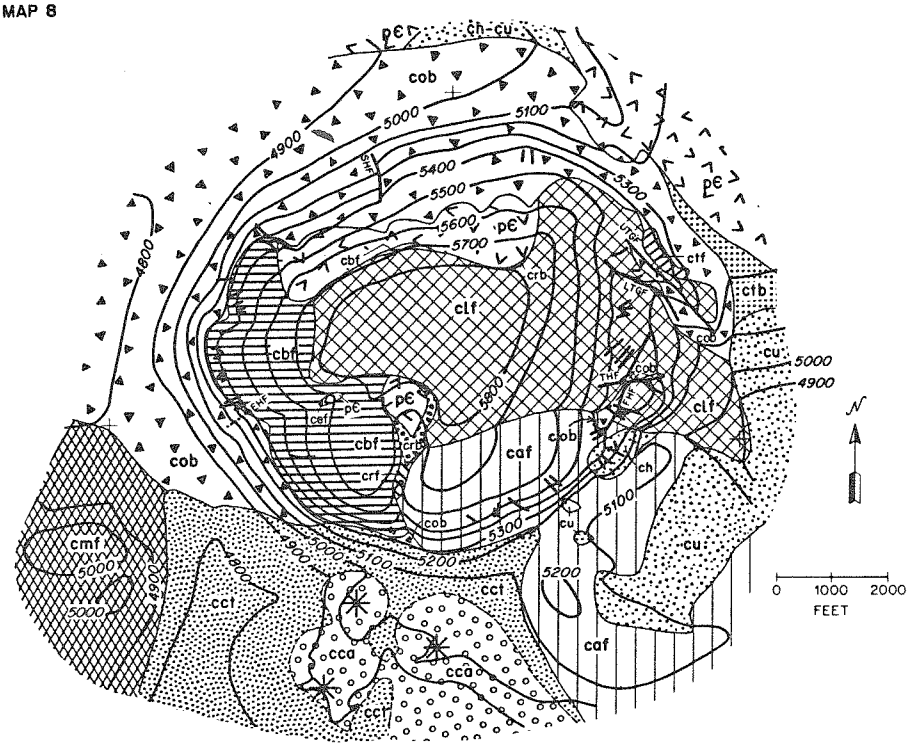
pe
ch-cu
cob
cbf
cef
crb
crf
clf
ctf
ctb
caf
cmf
ccf
cca
cu
THF
5000
5100
5200
5300
5400
5500
5600
5700
4900
4800
N
0
1000
2000
FEET

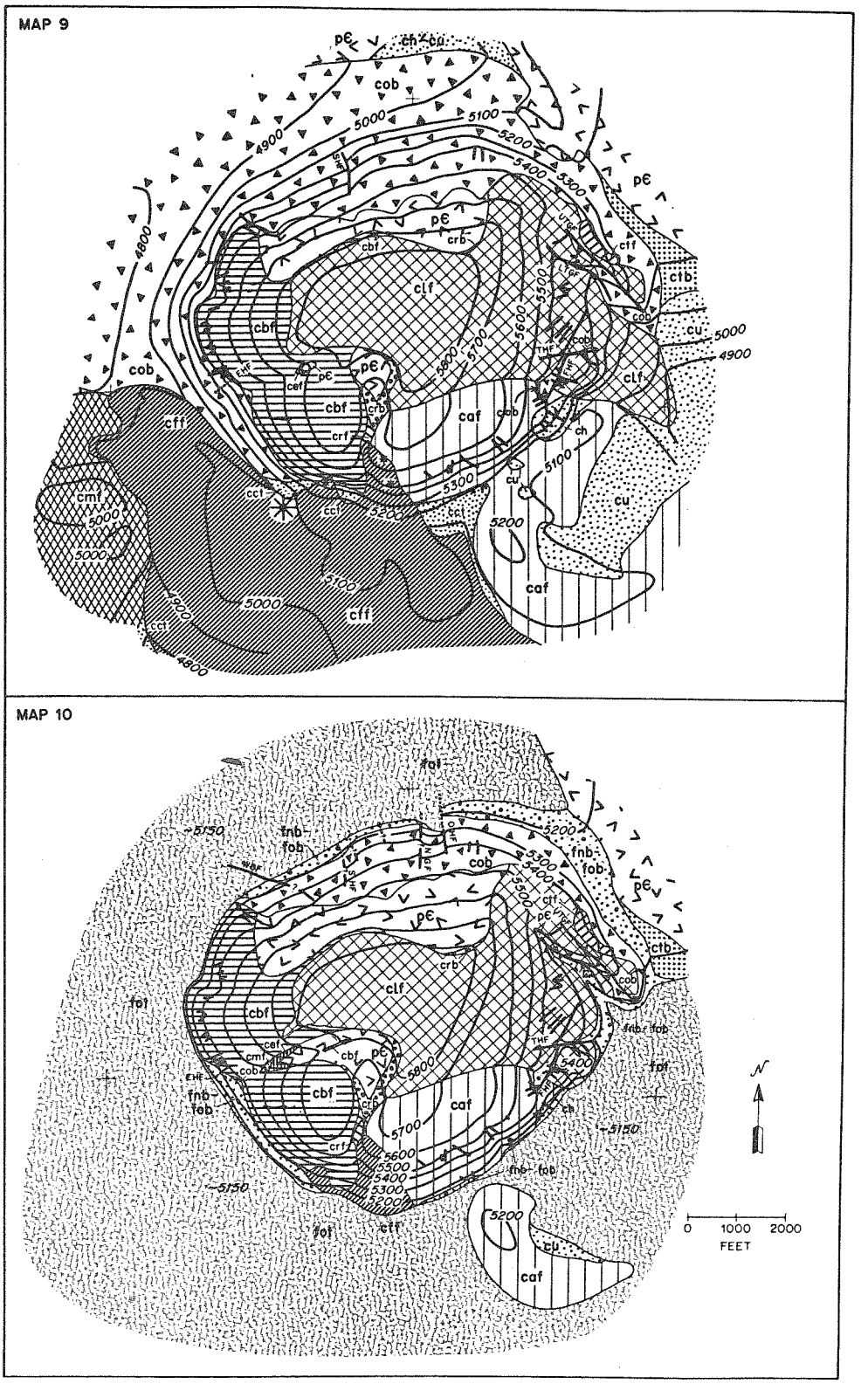
MAP 9
pε
ch
cu
cob
5000
5100
4900
5200
5400
5300
cff
cbf
clf
crb
ctb
5500
5600
5700
5800
caf
cmf
cct
ccf
crf
THF
EHF
MAP 10
fof
fnb
fob
wbf
~5150
0
1000
2000
FEET

TERTIARY VOLCANIC HISTORY

Beginning of Volcanism and Eruption of the Crater Pasture Formation

Volcanism in the vicinity of the Fort Rock dome apparently began with the intrusion of one or more small rhyodacite plugs (rf). One plug was intruded inside the limits of the present crater and is seen today at the head of Five OClock Wash. A period of minor(?) erosion followed and fragments of this rhyodacite were deposited in the thin tuffaceous basal sandstone (cs) of the Crater Pasture Formation. Mafic ash in this sandstone signaled the beginning of eruption of rocks of the Crater Pasture Formation.

The first major volcanic units to be erupted in the vicinity of the Fort Rock dome were the volcanic breccia (crb)* and flow (crf) of Road End Gap, which is an olivine trachyandesite, and the flow (cef) of Eight OClock Gorge, which is a limburgite (fig. 9, Map 2). The vent for the Road End Gap unit is located south of the rim of the present crater. Volcanic breccia (crb) was apparently deposited well to the north inside the limits of the present crater, because probable clasts of this unit are now found in beds of sedimentary breccia on the north flank of the Fort Rock dome. The vent for the Eight OClock Gorge flow is west of the rim of the present crater. A lobe of this flow extended up a valley through the site of present-day Eight OClock Gorge. The relative age of the Road End Gap and Eight OClock Gorge units is unknown.

*In the remaining part of this chapter, unit labels refer to units shown on Maps 1 through 10 (fig. 9) rather than to units shown on the geologic map (pl. 1), unless otherwise noted. In all cases map labels on Maps 1 through 10 are similar to labels on the geologic map but are generalized to include minor units such as basal facies, intrusive phases, multiple flows, and flow-top zones. For example, crf in Maps 1 through 10 includes flows cr1, cr2, cr3, cr4, and cr5 on the geologic map, as well as intercalated parts of crb on that map.

Minor faulting occurred next, followed by erosion. A fault that may have been ancestral to the Four OClock Hill fault (which was formed during doming) occurred at this time. Map 2 (fig. 9) depicts the paleogeology and paleotopography after faulting and erosion of the Road End Gap and Eight OClock Gorge units.

The flow of Meadow Dam (cmf), which is a hornblende trachybasalt, and the tuff (ctb) and flow (ctf) of Two OClock Gap, which is a pyroxene trachyandesite, were erupted next (fig. 9, Map 3). The Meadow Dam flow had its source about 3/4 miles southwest of the rim of the present crater. A small volcanic dome, with a relief of about 300 feet, was extruded over the vent for this unit. This dome presently forms a high hill south of Meadow Dam. A lobe of the flow extended up a valley through the site of present-day Eight OClock Gorge. The tuff (ctb) of Two OClock Gap formed a thin blanket on top of nearby rocks. It apparently had its source near present-day Outer Hill. The flow (ctf) of Two OClock Gap formed a small volcanic dome, about 100 feet high, over its vent, which is located near the southeast end of present-day Lion Ridge. The flow did not extend beyond the small dome.

The Upper Two OClock Gap fault was formed some time during or after eruption of the tuff and flow of Two OClock Gap. If it was formed after the eruption, then minor erosion occurred to cause a thinning of the tuff on the upthrown, or southwestern, side of the fault. Map 3 (fig. 9) depicts the paleogeology and paleotopography after faulting and erosion, if it occurred, of the Two OClock Gap tuff and flow.

The flow of Annex Ridge (caf), a hornblende trachyandesite, was erupted next as a high, viscous dome (fig. 9, Map 4). The vent for this flow is located somewhere southeast of the rim of the present crater, perhaps beneath

present-day Annex Ridge. A small vent, occupied by an intrusive body labeled cis on the geologic map (pl. 1), may have been a local source for this flow near the southern part of the rim of the present crater. The relief on the volcanic dome was about 500 feet.

The flow of Buffalo Ridge (cbf), a hornblende trachyandesite, was erupted next from a vent now exposed on Buffalo Ridge (fig. 9, Map 5). In addition to this vent, a minor vent, occupied by a dike labeled cic on the geologic map (pl. 1), may have been a local source for this flow inside the limits of the present crater. This flow apparently formed a volcanic dome, with a relief of about 200 feet, over the vent exposed on Buffalo Ridge. The flow pinched out against the steep side of the Annex Ridge dome to the east. A low tongue of the flow apparently extended well up a valley northeast of present-day Eight OClock Gorge, as a jumbled block of the flow is found today in deposits on the north flank of the Fort Rock dome.

The flow of Lion Ridge (clf), a hornblende trachyandesite, was erupted next from vents located near the eastern and northeastern margins of the present crater (fig. 9, Map 6). A small vent, occupied by a plug labeled cie on the geologic map (pl. 1), may have been a local source for this flow inside the limits of the present crater. The flow moved downhill from its main vents, which were located on relatively high ground, and formed a shallow pool against the volcanic domes of the Buffalo Ridge and Annex Ridge flows. This flow apparently covered much of the area now occupied by the eroded Fort Rock dome, as rocks from this unit presently occur as clasts in beds of sedimentary breccia on several sides of the dome (fig. 10).

Following emplacement of the Lion Ridge flow, patches of the tuff and conglomerate of Hidden Pasture (ch) and undivided tuff (cu) were deposited

Figure 10. Map 8, Showing the Composition of the One OClock Wash Sedimentary Breccia at Various Places around the Fort Rock Dome. Clasts in the breccia are listed in order of most abundant to least abundant and are abbreviated as follows:

l clasts of Lion Ridge flow

b clasts of Buffalo Ridge flow

a clasts of Annex Ridge flow

t clasts of Two OClock Gap tuff and flow

r clasts of Road End Gap volcanic breccia and flow

p clasts of Precambrian rocks

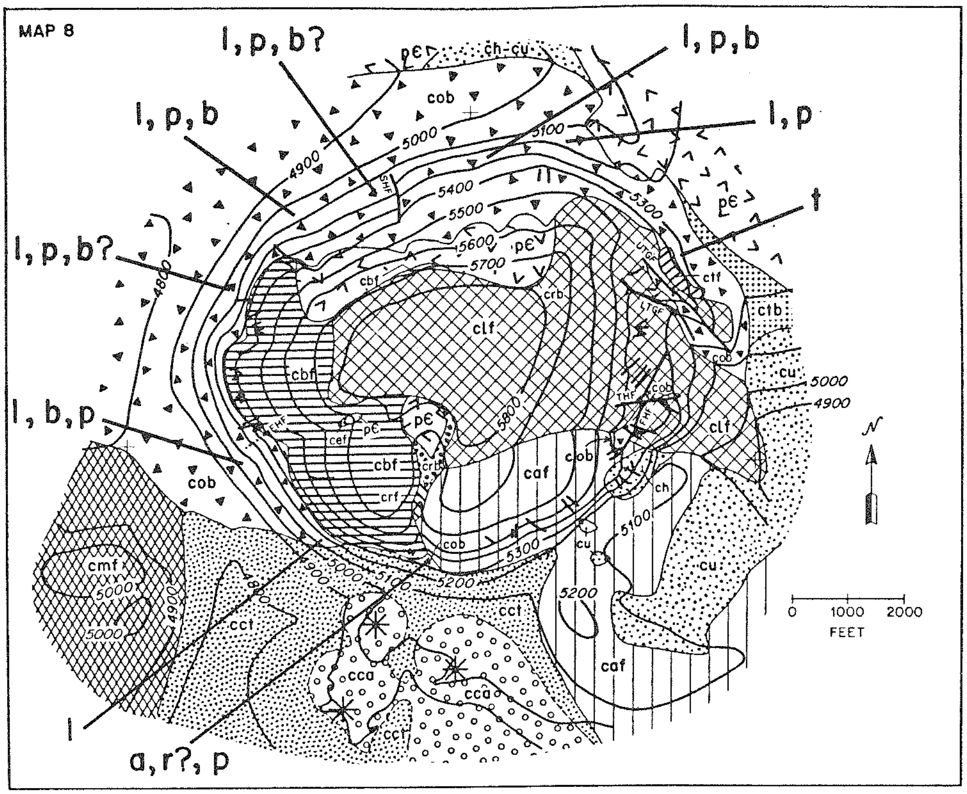
MAP 8
l, p, b?
l, p, b
l, p, b
l, p
l, p, b?
t
l, b, p
l
a, r?, p
cob
pЄ
ch-cu
clf
cbf
caf
cu
ctf
ctb
cmf
cct
cca
crf
crb
cef
ch
4800
4900
5000
5100
5200
5300
5400
5500
5600
5700
5800
SHF
UTGF
LTGF
THF
FHF
EHF
0
1000
2000
FEET
N

(fig. 9, Map 7). These units are trachyandesite in composition. One patch was deposited over a large area east and southeast of the present crater. Another was deposited north of the present crater. Ash and bombs in the deposit on the east and southeast appear to have come from a source in or near a large trachybasalt eruptive center east of the Fort Rock dome (fig. 3). Some ash may have come from vents now covered by the Cinder Basin tuff and agglomerate south of the dome. Ash in the deposit on the north may have come from the same source(s) or possibly from a vent now occupied by an intrusive shonkinite body, labeled cip on the geologic map (pl. 1), north of the Fort Rock dome.

Uplift of the Fort Rock dome followed the deposition of the Hidden Pasture tuff and conglomerate. Landsliding, or gravity thrusting signaled the beginning of the uplift. One large landslide block apparently broke away from a small outcrop of the Buffalo Ridge flow located near the north side of the present crater (fig. 9, Map 6). This block slid out over thin Hidden Pasture deposits, which probably initially covered the block (fig. 9, Map 7), and came to rest on top of these deposits at the site of present-day Noon Hill. A second large landslide block slid away from the northern edge of the Lion Ridge flow and now also rests on Hidden Pasture deposits in the east wall of Noon Gorge. This landslide block is, on its eastern end, contiguous with Lion Ridge flow that is in place.

As uplift continued, the sedimentary breccia of One OClock Wash (cab) was deposited on the flanks of the dome and the tuff (cct) and agglomerate (cca) of Cinder Basin were erupted on the south side of the dome (fig. 9, Map 8). Deposition of the breccia began earlier than eruption of the tuff and agglomerate, but throughout the last stages of uplift these units apparently

were being emplaced simul ously.

On the north side of the dome erosion proceeded rapidly, as volcanic rocks were undermined by weathering and erosion of poorly resistant, underlying Precambrian rocks. The One OClock Wash breccia is, therefore, relatively thick on this side of the dome. The initial concentration of clasts of Precambrian rocks in the detritus from the dome was high because the slopes here were initially underlain by Precambrian rocks. As uplift proceeded, volcanic rocks on the dome supplied most of the detritus, including disaggregated landslide blocks now seen as block patches in the breccia. As exposures of Precambrian rocks on the dome widened, clasts of Precambrian rocks again became abundant in the material eroded from the dome. On other sides of the dome, erosion proceeded more slowly because of mantling by resistant volcanic flows. The One OClock Wash sedimentary breccia is, thus relatively thin in these places. Drainages were cut slowly through the flows. Precambrian rocks were gradually exposed as inliers, and clasts of Precambrian rocks appeared in gradually increasing amounts in the detritus eroded from the dome. On the southeast side of the dome, breccia was not deposited or was deposited and removed before younger units were emplaced. In this location, the Annex Ridge flow is very thick and apparently resisted significant erosion.

The drainage pattern developed on the growing dome appears to have been ancestral to the pattern seen today. On the north side of the dome, where rocks were easily erodable, numerous drainages developed. Numerous drainages are seen in this area of the dome today. In locations where the dome was mantled by volcanic rocks, wide-spaced gorges were cut. From the clast content of the sedimentary breccia on the flank of the dome, it appears that one gorge was cut in the vicinity of present-day Eight OClock Gorge and

another in the vicinity of Six OClock Wash. None of the drainages on the dome were deeply entrenched, as there is no evidence today of old valleys in the rocks on the rim of the crater. Drainage profiles apparently were similar to the profile of the dome, that is, they were convex upward rather than concave upward. Such abnormal gradients could be explained if doming took place too rapidly for drainage gradients to keep pace. Progressively more rapid, or accelerated, doming is, in fact, suggested in figure 11. In this figure, a normal concave-upward profile forms first on a low dome but is unable to keep pace with uplift at some point in time and becomes convex upward.

The agglomerate (cca) of Cinder Basin was erupted from three vents south of the growing dome (fig. 9, Map 8). Tuff (cct) may have been erupted from the same vents at a slightly earlier time or from other vents now concealed by the Fault Canyon. These volcanic units were being erupted during the time that detritus from the south side of the dome was being washed southward. Interfingering of tuffaceous sedimentary breccia (not distinguished from tuff (cct) in Map 8) and volcanic units is now seen on the southern flank of the dome. The traces of ash found in the One OClock Wash sedimentary breccia may have come from vents for the Cinder Basin unit.

Both the One OClock Wash sedimentary breccia and the Cinder Basin tuff and agglomerate were deformed as the dome grew. The oldest beds were deformed the most. On present-day Noon Hill successively greater tilting of older beds in the One OClock Wash breccia is apparent. In addition to tilting and folding, faulting occurred. The Eight OClock Hill fault and the Eight OClock Gorge faults formed first as open fissures that were subsequently filled by sedimentary breccia. The Short Hill fault formed next. This fault offset a thick section of the One OClock Wash unit. Numerous relatively

Figure 11. Stream Profiles on an Accelerating Dome.

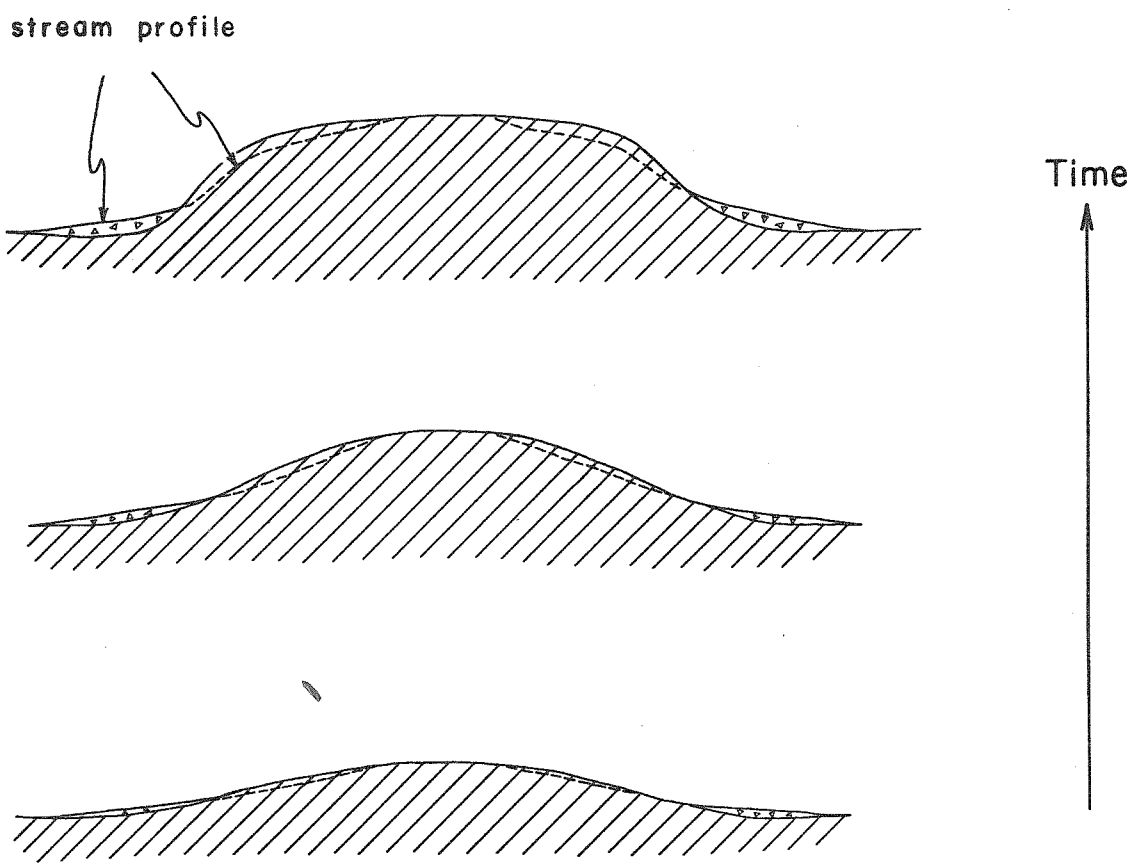
stream profile
Time

short radial faults on the west side of the dome probably formed during growth of the dome. The relatively long tangential faults on the east side of the dome, including the Upper and Lower Two OClock Gap faults and the Four OClock Hill fault, are of uncertain age but may have formed during uplift. The lack of a thick deposit of breccia on the northeast flank of Lion Ridge and the lack of clasts of the Lion Ridge flow in this breccia (fig. 10) could be explained if drainage from the dome were diverted to the southeast by in-facing fault scarps along the Upper and Lower Two OClock Gap faults (fig. 9, Map 8). A similar drainage diversion could have occurred along the Four OClock Hill fault, as there is no breccia on the southeast flank of Four OClock Hill (fig. 9, Map 8). It may be possible, on the other hand, to explain the lack of thick deposits of breccia on Lion Ridge and on Four OClock Hill as the result of retarded erosion due to resistant volcanic rocks or as the result of deposition and subsequent removal of breccia before the emplacement of younger units. Movement on the Upper Two OClock Gap fault, whatever its precise age, was in a direction opposite to pre-dome movement on this fault; rocks on its southwest side were dropped down. The Four OClock Hill fault may also represent reactivation of a pre-dome fault. Rocks on the north side of a pre-dome fault at its southwest end were downdropped; rocks on the northwest side of the Four OClock Hill fault were downdropped.

At the time when the Fort Rock dome had attained a topographic relief of about 1000 feet (fig. 9, Map 8) and a structural relief comparable to that seen today, the Fault Canyon flow (cff), an olivine-sanidine trachybasalt, was erupted on the southern flank (fig. 9, Map 9). The major vent for this flow is seen today at the head of Tyria Wash. Sills and dikes of this unit on Buffalo Ridge may have been small sources for the flow. A large lobe of

the flow extended to the north between the Fort Rock dome and the volcanic dome over the vent for the Meadow Dam flow. Most of the flow extended to the southwest and south. Nearly one tenth of a cubic kilometer of trachybasalt was erupted.

This flow apparently was erupted from beneath the dome, as the wall of the vent exposed at the head of Tyria Wash dips shallowly to the northeast beneath Buffalo Ridge. Major uplift of the dome halted after this flow was extruded, and some collapse may have even occurred. It is concluded from these facts that the magma which fed this flow was responsible for the uplift of the dome.

The relative subsidence of rocks toward the center of the dome that occurred along the Upper and Lower Two OClock Gap faults and the Four OClock Hill fault may represent collapse of the eastern section of the dome. Thus, a second plausible age for movement on these faults is the time during or after the extrusion of the Fault Canyon flow.

Eruption of the Fort Rock Creek Rhyodacite

Erosion of the Fort Rock dome continued after the eruption of the Fault Canyon flow. Clasts eroded from the dome were deposited on the flanks of the dome as the sedimentary breccia of Noon Gorge (fnb) which, because it also contains fragments of rhyodacite, is considered to be the basal unit of the Fort Rock Creek Rhyodacite. Widening exposures of Precambrian rocks on the dome contributed increasing quantities of Precambrian clasts to this deposit. On the north, the Lion Ridge flow (clf) was eroded southward to uncover the volcanic breccia (crb) of Road End Gap (fig. 9, Maps 9 and 10), clasts of which appear at the base of the Noon Gorge breccia on the north flank of the

dome. In the vicinity of present-day Eight OClock Gorge, Six OClock Wash, and Two OClock Gap, gorges on the dome deepened.

Mafic ash of at least two different compositions, trachybasalt and trachyandesite, was incorporated in the Noon Gorge breccia. Small amounts of this ash were sprinkled through the breccia as it accumulated, but occasionally discrete beds were deposited. A tuffaceous bed on the north flank of One OClock Hill contains ash and bombs of trachybasalt that may have been erupted from a vent beneath a hill of agglomerate located between 1/2 and 3/4 miles northwest of the dome. This tuffaceous bed is labeled fnt on the geologic map (pl. 1). Trachyandesite ash of unknown source was incorporated in beds, labeled fnc on the geologic map, on the southwest flank of the dome. In addition to mafic ash, small fragments of rhyodacite were included in trace amounts in the breccia. These clasts probably were erupted from the large rhyodacite eruptive center located 2-1/2 miles southwest of the dome in the Aquarius Mountains.

As eruption increased in frequency and volume at the large rhyodacite eruptive center, rhyodacite fragments were deposited in increasing quantities in the breccia, and pumice began to appear. Where more than trace amounts of these fragments occur in the breccia, the breccia is considered to be the basal unit (fob) of the Old Stage Road Member of the Fort Rock Creek Rhyodacite.

Ash flows were next erupted from the large rhyodacite center. One or more thin flows reached the Fort Rock dome followed by one or more massive flows which buried all terrane in the vicinity of the dome below an elevation of about 5150 feet. These flows constitute the ash-flow tuff (fot) of the Old Stage Road Member (fig. 9, Map 10). In places enough steam was trapped in the ash-flows to crystallize some of the pumice.

Deformation in the rocks on the flanks of the Fort Rock dome continued until after the ash flows were emplaced. Deformation included minor uplift, tilting, and faulting. The Noon Gorge sedimentary breccia probably was uplifted and tilted by a small amount, but uplift had apparently ceased by the time the Old Stage Road Member was laid down . Faulting occurred at several intervals. The One OClock Hill fault occurred during emplacement of the basal sedimentary breccia (fob) of the Old Stage Road Member. The Noon Gorge fault probably occurred at the same time. The scarps of these two faults created a small embayment in the north flank of the dome that was subsequently invaded by the ash flows. Continued(?) movement on the Lower Two OClock Gap fault may have occurred at about the same time as movement on the One OClock Hill fault. Such movement appears necessary to explain the presence of a small outcrop of the basal member (fob) of the Old Stage Road Member at a low elevation inside the present crater. (See pl. 1). The Wedge Basin fault occurred after the emplacement of the ash flows but caused only minor offset.

Following emplacement of the ash flows, massive ash and block falls(?) were erupted from the large rhyodacite center, together with occasional ash flows and volcanic mudflows of varying thicknesses and extent. The rocks erupted during this episode constitute the Three Sisters Butte Member of the Fort Rock Creek Rhyodacite.

A period of erosion followed eruption of the Three Sisters Butte Member during which a valley was carved in the site of present-day Fort Rock Creek. A volcanic mudflow(?) which now constitutes the breccia and conglomerate of the Crossing, subsequently filled this valley. This mudflow originated at the large rhyodacite eruptive center.

At intervals throughout the emplacement of the Fort Rock Creek Rhyodacite, movement occurred on the Fort Rock Creek fault and on the fault south of the present-day Three Sisters. Rocks moved up on the southwest side of the Fort Rock Creek fault and up on the south side of the fault near the Three Sisters. Units on the northeast and north sides of these faults, respectively, were either deposited in relatively greater thickness against the scarps of the faults or were protected from erosion compared to units on the upthrown sides.

Eruption of the Basalt of Buttox Hills

On the southeast side of the dome, following emplacement of ash-flow tuff and intrusion of a small body of rhyodacite (labeled fit on the geologic map (pl. 1)) a period of erosion occurred, and a thin bed of detritus from the Fort Rock dome was deposited. The basalt of Buttox Hills was erupted next. The major vent for this basalt lies beneath the northwest end of the Buttox Hills. A flow was fed from this vent and flowed away to the southeast. In addition, a long dike intruded the edge and flank of the dome in a radial northwest-southeast direction. A series of small plugs aligned with the northwest end of the dike intruded rocks deep inside the dome.

Eruption of Other Volcanic Rocks in the Region

Volcanic rocks that post-date the Fort Rock Creek Rhyodacite were emplaced in a number of locations in the region. These include the Peach Springs Tuff, the Mohon Mountain volcanics, and several minor intermediate and mafic dikes.

The Peach Springs Tuff originated as a regional Miocene ash flow that was emplaced in old drainages in an area extending from the east side of the Black Mountains, in western Arizona, to the Grand Wash Cliffs and south to

Trout Creek (Young and Brennan, in press). Prior to its emplacement on the western flank of the Aquarius Mountains, faulting occurred along a north-south fault located on the eastern edge of present-day Big Sandy Wash (fig. 3). This fault brought rocks of the Crater Pasture Formation up on the west and either formed a fault scarp against which rocks of the Fort Rock Creek Rhyodacite were emplaced or offset these rocks downward on the east. A period of erosion ensued before the Peach Springs Tuff was emplaced.

After emplacement of the Peach Springs Tuff, the Mohon Mountain volcanics were erupted south of the Aquarius Mountains (Young and Brennan, in press). A basalt flow at or near the base of these volcanics covered an extensive area south of the Fort Rock dome (fig. 3).

Miscellaneous dikes of intermediate and mafic volcanic rocks were intruded at several locations after emplacement of the Fort Rock Creek Rhyodacite. One and one-half miles north of the Fort Rock dome, andesite(?) dikes were formed which fed local flows on top of ash-flow tuff of the Fort Rock Creek Rhyodacite (fig. 3). Remnants of these flows form the cap rock of small buttes and mesas in this area today.

LATE GEOLOGIC HISTORY

Regional

Following emplacement of volcanic units in the region of the Fort Rock dome, renewed movement occurred on the Fort Rock Creek fault, the fault south of the Three Sisters, and the fault along the eastern edge of Big Sandy Wash. This movement, in all three cases, was in a direction opposite to earlier movement. The Fort Rock Creek fault moved down on the southwest; the fault south of the Three Sisters moved down on the south; and the fault along Big Sandy Wash moved down on the west.

Movement on the fault along Big Sandy Wash was part of an episode of faulting in which Basin and Range topography was being formed. Subsidence along this fault and along the fault at the base of the Grand Wash Cliffs to the north, which appears to be continuous with the Big Sandy fault, led to the formation of basins with interior drainage. Deposits such as the Muddy Creek deposits, of Miocene to Pliocene age near present-day Lake Mead, and the Big Sandy Formation, of Pliocene age (Sheppard and Gude, 1972) west of the Mohon Mountains, accumulated in these basins (Young and Brennan, in press).

An episode of significant erosion followed volcanism and faulting in the region and is continuing at the present. The deep canyons of Trout Creek, Cow Creek, Muddy Creek, and Fort Rock Creek have been cut during this episode. The volcano that was built over the vents of the large rhyodacite eruptive center southwest of the dome has been deeply dissected to produce the present-day Aquarius Mountains. This volcano probably was at one time as high as the volcano, still largely intact, that constitutes the Mohon Mountains to the south. The Fort Rock dome was deeply dissected during this episode. In addition, erosion in the region north and northeast of Cross Mountain occurred, and extensive deposits of gravel were laid down east of Fort Rock dome. These deposits are now being dissected and are preserved on terraces. This episode of erosion was associated with the formation of the present Colorado River drainage which began in early to middle Pliocene times (Young and Brennan, in press; McKee and McKee, 1972; Lucchitta, 1972).

Fort Rock Dome

About two-thirds of the volume of uplifted rocks in the Fort Rock dome, or about 2/3 cubic kilometer, was removed during this episode of erosion. Previous erosion of the dome, which is recorded in the deposits of sedimentary

breccia (cob, fnb, and fob) on the flanks of the dome, amounted merely to removing most of the relatively thin covering of volcanic rocks on the dome. The more recent episode of erosion resulted in carving of a crater-like depression on the dome.

The sequence of erosional events leading to the present crater on the dome, may have been somewhat as follows. As the volcanic rocks were stripped from the dome, drainages cut deeply into the less resistant Precambrian rocks beneath. Headward convergence of drainages apparently led frequently to stream capture. The two drainages most successful at stream capture appear to have been the drainages ancestral to Four OClock Wash and Five OClock Wash. These two drainages appear to have captured the headward parts of the drainage on the south side of the dome in the position of present-day Six OClock Wash and the drainage along Lower Two OClock Gap fault (see fig. 9, Map 10). It is likely that the headward part of the drainage ancestral to Eight OClock Gorge was also captured. Stream capture, thus, diverted drainage of more than half of the dome through two gorges on the southeastern side of the dome. Precambrian rocks in the center continued to be dissected along these two drainages. Drainage basins widened, converged on one another, and extended outward to the steeply dipping volcanic rocks in the monocline on the edge of the dome. The steeply dipping volcanic rocks formed an in-facing scarp around the drainage basins, and created the distinctive crater-like depression seen today in the southeastern half of the Fort Rock dome.

Lowering of the local base level for drainages on the northwestern half of the dome appears to have occurred, as deep gorges are now being cut in this area. Lowering of the local base level probably was caused by the incision of Fort Rock Creek on this side of the dome. Recent erosion of this half of the

dome is following the same course that erosion apparently followed in the southeastern half of the dome. The drainage through Eight OClock Gorge has already captured the headward parts of Nine OClock Wash and Ten OClock Wash. The drainage through Noon Gorge is presently about to capture the headward parts of One OClock Wash and the drainage on the west side of Noon Hill. Eight OClock Basin and Noon Basin are widening at the expense of terrane between them and at the expense of Crater Pasture, which constitutes the depression in the southeastern half of the dome. Crater Divide marks the present limit of encroachment of the young drainages in the northwest upon the older drainages in the southeast.

VIII. MECHANICS OF FORMATION OF THE FORT ROCK DOME

The Fort Rock dome apparently was created by a plug-like body of magma pushing its way toward the surface; this body arched overlying Precambrian rocks and a thin covering of volcanic extrusive rocks. In this chapter, an attempt is made to model this phenomenon mathematically. Precambrian rocks at the site of the Fort Rock dome are treated as a layer of viscous fluid of infinite lateral extent. The thin covering of volcanic extrusive rocks is ignored. On the bottom of the layer an axisymmetric pressure is applied, representing the pressure of a volcanic plug against the overlying rock. Analytic treatment of this problem is completely analogous to the treatment by N. A. Haskell (1935) of the depression of the earth's crust due to loading by glacial ice. Instead of applying pressure to the surface of a semi-infinite fluid, as was done in Haskell's treatment, we consider a fluid bounded by two surfaces with pressure applied to the bottom surface.

FORMULATION OF THE PROBLEM

Deformation in the Precambrian rocks at Fort Rock dome consisted of movement of parcels of rock along numerous faults. These parcels are fractions of a meter to tens of meters across, as determined from the spacing of small unmapped faults on the dome (fig. 8). On the flank of the dome some parcels are as large as 300 meters across, as determined from the spacing of subparallel mapped faults (pl. 1), but

these larger parcels probably moved, to some extent, as assemblages of smaller parcels. The radius of the dome is a little over one kilometer; one kilometer will be used as a characteristic length in this analysis. As the size of the parcels in the Precambrian rocks generally is much smaller than the characteristic length in this problem, the first assumption in the formulation of the problem will be

Assumption 1. Applicability of Continuum Mechanics. The Precambrian rocks will be approximated by a continuum and will be treated by continuum mechanics.

The second assumption will be

Assumption 2. Use of Viscous Rheology. The Precambrian rocks will be modeled as a viscous substance.

Other choices of rheology include elastic and plastic rheologies. Clearly, an elastic substance would be an unsatisfactory choice because permanent deformation is seen in the rocks on the dome. A plastic substance might be a reasonable choice except for the mathematical complexity of dealing with it (see Nadai, 1950, p. 401-404). There are also viscous-like substances which undergo steady creep at constant load (see Nadai, 1950, p. 416-418). For these substances,

$$\text{Stress} \propto (\text{Rate of strain})^m \qquad 0 \leq m \leq 1 \ ;$$

whereas for a viscous substance,

$$\text{Stress} \propto \text{Rate of strain}$$

Without knowledge of the actual rheology of the rocks underlying the dome, it is preferable, at least for the initial investigation, to use the simple, linear rheology of a perfectly viscous substance. The

writer is further influenced in this choice by the fact that an analytic treatment of a problem similar to the one at hand is already available in the literature, namely, that of Haskell (1935).

The equations of motion and continuity for an incompressible, perfectly viscous fluid are

$$\frac{d\underline{v}}{dt} = -\frac{1}{\rho}\nabla p + \frac{\eta}{\rho}\nabla^2\underline{v} + \frac{1}{\rho}\underline{f} \qquad (1)$$

$$\nabla \cdot \underline{v} = 0 \qquad (2)$$

where $\underline{v}$ is velocity (vector quantities are underlined), ρ is density, p is pressure, η is viscosity, and $\underline{f}$ is a body force.

The next step in our formulation is

> Approximation 1. Linearization of Equations of Motion. The acceleration term, $d\underline{v}/dt$, in (1) will be neglected in the problem at hand.

This approximation is valid if the Reynolds number of the flow is small (Landau and Lifshitz, 1959, p. 63)*. The Reynolds number, Re, is given by

$$\mathrm{Re} = \rho \frac{LV}{\eta}$$

---

*In general, only the term $(\underline{v}\cdot\nabla)\underline{v}$ in the expression, $d\underline{v}/dt = (\partial\underline{v}/\partial t) + (\underline{v}\cdot\nabla)\underline{v}$, is neglected in flow at small Reynolds number. In the problem at hand $|\underline{v}| \sim L/T$, $\partial/\partial t \sim 1/T$, and $\nabla \sim 1/L$, where L is a characteristic length and T is a characteristic time, e.g., the time of formation of the dome. In the expression for $d\underline{v}/dt$, both terms, $\partial\underline{v}/\partial t$ and $(\underline{v}\cdot\nabla)\underline{v}$, are thus of the same order of magnitude and both can be neglected.

where L and V are a characteristic length and a characteristic velocity, respectively, in the problem. Viscosities for geologic solids (Haskell, 1935) range from 10^{10}poises to 10^{27}poises. Velocities involved in the formation of Fort Rock dome might range from centimeters per year to kilometers per year. Using the highest velocity and lowest viscosity, the largest Reynolds number for Fort Rock dome is of the order, 10^{-7}; hence, the approximation that is made is reasonable.

It should be noted that after making Approximation 1, the viscosity term in (1) must be balanced solely by pressure and body-force terms. Furthermore, since the acceleration term has been dropped, eqs. (1) and (2) are independent of time. If time-variant behavior of doming is to be studied, time must be introduced as a variable again at some point in the solution of the problem.

Equations (1) and (2) may now be written

$$\frac{\eta}{\rho} \nabla^2 \underline{v} = \frac{1}{\rho} \nabla p - \frac{1}{\rho} \underline{f} \tag{3}$$

$$\nabla \cdot \underline{v} = 0 \tag{4}$$

These equations must be solved in conjunction with boundary conditions, but before tractable boundary conditions can be stated, the problem must be rather severely idealized. The following model is adopted.

The Model (fig.12). The Precambrian rock will be modeled as a layer of viscous fluid of depth h and infinite lateral extent. This layer will rest on a semi-infinite basement of inviscid fluid, or magma. A plug-like intrusion of the layer will be modeled by an axisymmetric pressure distribution on its bottom surface.

Figure 12. Model Used in a Mathematical Formulation of Doming. Note that the coordinate system (r, θ, z) remains fixed in space for all t, whereas the surfaces $H(r,t)$ and $Z(r,t)$ will move.

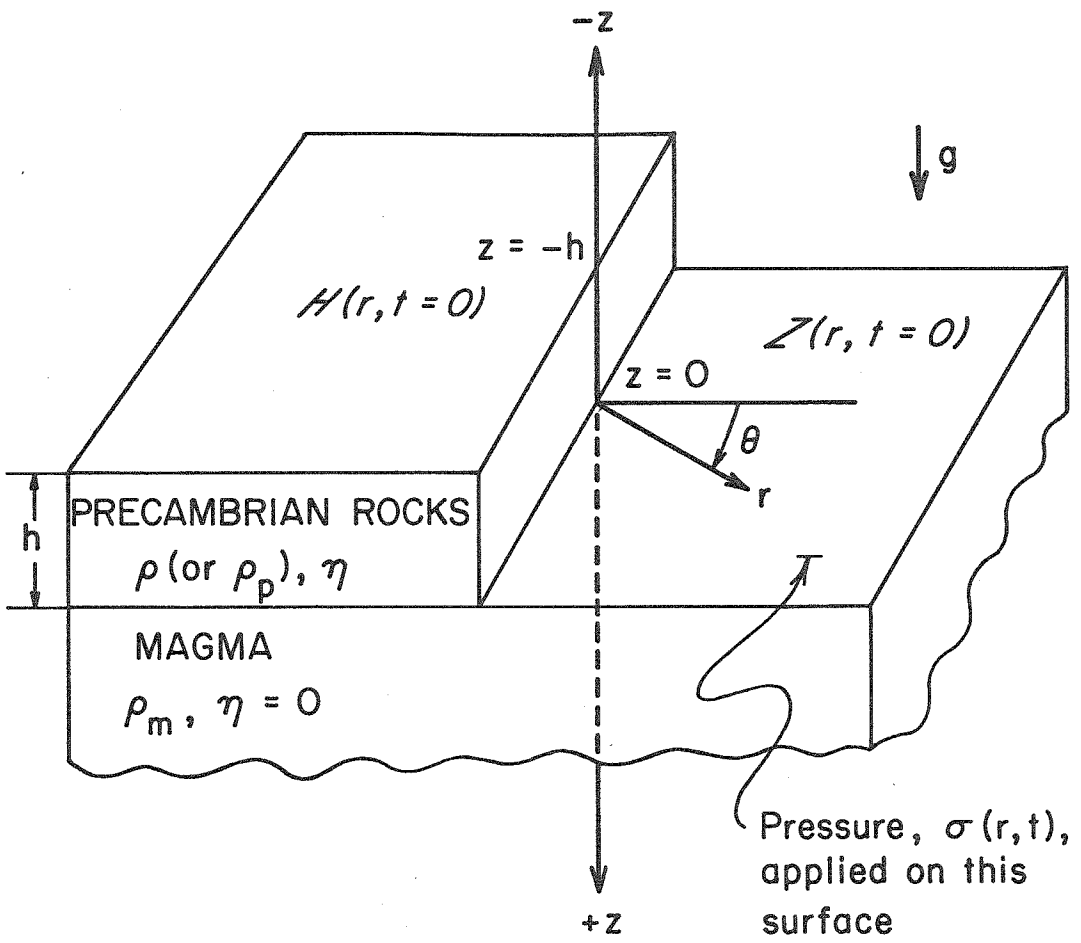
-z
g
z = -h
H(r, t = 0)
Z(r, t = 0)
z = 0
θ
r
h
PRECAMBRIAN ROCKS
ρ (or ρp), η
MAGMA
ρm, η = 0
T
Pressure, σ(r,t),
applied on this
surface
+z

In this model the thin layer of volcanic flows on the surface of the Precambrian rock is ignored. More importantly, the specification of a basement of inviscid magma everywhere beneath the layer of Precambrian rocks decouples these rocks from rocks below. If the actual magma chamber were a sill of infinite extent, decoupling would indeed occur at the base of the laryer of Precambrian rocks. If, however, the actual magma chamber were a more or less cylindrical plug, as is geologically reasonable in this case, decoupling would extend only to the edge of the plug and not beyond. In some sense, our ultimate choice of a Bessel-shaped pressure function to represent the intrusion at the bottom of the layer, acts to recouple the layer of Precambrian rocks to rocks below by preventing rocks in this layer from flowing away to infinity on either side of the dome. This feature will be discussed later. The representation of the process of intrusion as an axisymmetric pressure distribution makes no provision for stoping or injection of magma as dikes and apophyses. The intrusion is modeled simply as a concordant upwelling of magma, which was presumably the dominant process of intrusion during the formation of the Fort Rock dome. The early history of the plug, as it worked its way up to a depth h, is ignored in this model. This early history probably is not very important to doming, however; i.e., it will be shown later that doming caused by a plug at great depths is insignificant.

From this point forward the formulation and solution of the problem is completely analogous to that in Haskell (1935). A cylindrical coordinate system (r,θ,z) is located with its origin at the initial interface between the layer of Precambrian rocks and the basement of

magma (fig.12). Positive z is taken downward. (It would have perhaps been more convenient in the present treatment to have taken positive z upward.) In this coordinate system,

$$\frac{1}{\rho}\underline{f} = (0,0,g) \tag{5}$$

where g is the acceleration due to gravity. Pressure, p, may be written for convenience as

$$p \equiv \bar{p} + \rho g(z+h) \tag{6}$$

Assuming the problem has radial symmetry, that is, no dependence on azimuth, θ, eqs. (3), (4), (5), and (6) may be combined and expressed in cylindrical coordinates:

$$\frac{1}{r}\frac{\partial}{\partial r}\left(r\frac{\partial v_r}{\partial r}\right) - \frac{v_r}{r^2} + \frac{\partial^2 v_r}{\partial z^2} = \frac{1}{\eta}\frac{\partial \bar{p}}{\partial r} \tag{7}$$

$$\frac{1}{r}\frac{\partial}{\partial r}\left(r\frac{\partial v_z}{\partial r}\right) + \frac{\partial^2 v_z}{\partial z^2} = \frac{1}{\eta}\frac{\partial \bar{p}}{\partial z} \tag{8}$$

$$\frac{1}{r}\frac{\partial}{\partial r}(r\, v_r) + \frac{\partial v_z}{\partial z} = 0 \tag{9}$$

where v_r and v_z are components of velocity $\underline{v}$ in the r and z directions, respectively.

Boundary conditions are

$$\underline{v}^p \cdot \hat{n} = \underline{v}^a \cdot \hat{n} \qquad \text{upper surface} \tag{10a}$$

$$\underline{\underline{T}}^p \cdot \underline{\hat{n}} = \underline{\underline{T}}^a \cdot \hat{n} \tag{10b}$$

$$\underline{v}^p \cdot \hat{n} = \underline{v}^m \cdot \hat{n} \qquad \text{(11a)}$$

lower surface

$$\underline{\underline{T}}^p \cdot \hat{n} = \underline{\underline{T}}^m \cdot \hat{n} \qquad \text{(11b)}$$

where $\underline{\underline{T}}$ is the stress tensor, $\hat{n}$ is a unit vector normal to a boundary and the superscripts a, p, and m refer to air, Precambrian rocks, and magma, respectively. Equations (10a) and (11a) are referred to as kinematical boundary conditions; eqs. (10b) and (11b) are referred to as the dynamical boundary conditions. In cylindrical coordinates the stress terms, $\underline{\underline{T}}^a$, $\underline{\underline{T}}^p$, and $\underline{\underline{T}}^m$, are

$$\underline{\underline{T}}^a = 0 \qquad \text{(12)}$$

$$\underline{\underline{T}}^p = \begin{pmatrix} T_{rr} & T_{r\theta} & T_{rz} \\ T_{\theta r} & T_{\theta\theta} & T_{\theta z} \\ T_{zr} & T_{z\theta} & T_{zz} \end{pmatrix}$$

$$= \begin{pmatrix} -(\bar{p}+\rho g[z+h]) + 2\eta \dfrac{\partial v_r}{\partial r} & 0 & \eta\left(\dfrac{\partial v_r}{\partial z} + \dfrac{\partial v_z}{\partial r}\right) \\ 0 & -(\bar{p}+\rho g[z+h]) + 2\eta \dfrac{v_r}{r} & 0 \\ \eta\left(\dfrac{\partial v_z}{\partial r} + \dfrac{\partial v_r}{\partial z}\right) & 0 & -(\bar{p}+\rho g[z+h]) + 2\eta \dfrac{\partial v_z}{\partial z} \end{pmatrix} \qquad \text{(13)}$$

$$\underline{\underline{T}}^m = \begin{pmatrix} -\sigma & 0 & 0 \\ 0 & -\sigma & 0 \\ 0 & 0 & -\sigma \end{pmatrix} \tag{14}$$

where σ is the pressure applied by the magma to the bottom of the layer of Precambrian rock.

Let the equations of the upper and lower surfaces of the fluid be

$$z = H(r,t) - h \qquad \text{upper surface} \tag{15}$$

$$z = Z(r,t) \qquad \text{lower surface} \tag{16}$$

Now, Approximation 2 is made.

> Approximation 2: On the upper and lower surfaces, H and Z, let $\hat{n}$ be the vectors $(0,0,-1)$ and $(0,0,1)$, respectively.

This approximation clearly limits analytic study of the growth of the dome to its early stages, where the deformations, H and Z, are small compared to characteristic distances in the problem, such as the radius of the magma chamber. Using (12), (13), and (15) in (10b) gives

$$T_{rz} = \frac{\partial v_r}{\partial z}(r,z = H-h,t) + \frac{\partial v_z}{\partial r}(r,z = H-h,t) \tag{17}$$

$$T_{zz} = \bar{p}(r,z = H-h,t) + \rho g H - 2\eta \frac{\partial v_z}{\partial z}(r,z = H-h,t) = 0 \tag{18}$$

and using (13), (14), and (16) in (11b) gives

$$T_{rz} = \frac{\partial v_r}{\partial z}(r,z = Z,t) + \frac{\partial v_z}{\partial r}(r,z = Z,t) = 0 \tag{19}$$

$$T_{zz} - \rho gh = \bar{p}(r,z=Z,t) + \rho gZ - 2\eta \frac{\partial v_z}{\partial z}(r,z=Z,t) = \bar{\sigma} \quad (20)$$

where $$\bar{\sigma} \equiv \sigma - \rho gh \quad (21)$$

Equations (17) and (19) are statements that the shear stress, T_{rz}, must vanish on the boundaries; neither the air nor the magma can support the shear stresses that the Precambrian rocks can. Equations (18) and (20) are statements that the normal stress, T_{zz}, must not change across the boundaries. The upper surface is a free surface with zero applied normal stress, and the bottom surface has a normal stress $-\sigma(r,t)$ applied to it by the magma.

Equations (17)-(20) are simplified with the following approximation:

> Approximation 3. Evaluate all quantities in eqs. (17)-(20) except ρgH and ρgZ on the planes $z=-h$ and $z=0$ rather than on the actual surfaces $z = H-h$ and $z=Z$.

Haskell (1935) points out that this approximation is commonly made when one is dealing with small deformations of the surface of a fluid. When this approximation is made, the restoring force on the deformed fluid is simply gravity, which appears in the unaltered terms ρgH and ρgZ. The dynamical boundary conditions can now be stated,

$$\frac{\partial v_r}{\partial z}(r,-h,t) + \frac{\partial v_z}{\partial r}(r,-h,t) = 0 \quad (22)$$

$$\bar{p}(r,-h,t) + \rho gH(r,t) - 2\eta \frac{\partial v_z}{\partial z}(r,-h,t) = 0 \quad (23)$$

$$\frac{\partial v_r}{\partial z}(r,0,t) + \frac{\partial v_z}{\partial r}(r,0,t) = 0 \quad (24)$$

$$\bar{p}(r,0,t) + \rho g \mathcal{Z}\ (r,t) - 2\eta \frac{\partial v_z}{\partial z}\ (r,0,t) = \bar{\sigma}(r,t) \tag{25}$$

Using Approximation 2, eq. (10a) becomes

$$v_z^p(r,z = \mathcal{H} - h,t) = v_z^a(r,z = \mathcal{H} - h,t)$$

If radial velocities are small, as they will be for small deformations,

$$v_z^a(r,z = \mathcal{H} - h,t) = \frac{\partial}{\partial t}[\mathcal{H}(r,t)]$$

Therefore,

$$v_z(r,z = \mathcal{H} - h,t) \equiv v^p(r,z = \mathcal{H} - h,t) = \frac{\partial}{\partial t}\ [\mathcal{H}(r,t)] \tag{26}$$

Similarly, eq. (11a) gives

$$v_z(r,z = \mathcal{Z}\ ,t) = \frac{\partial}{\partial t}\ [\mathcal{Z}(r,t)] \tag{27}$$

Using Approximation 3, the kinematical boundary conditions become

$$v_z(r,-h,t) = \frac{\partial \mathcal{H}}{\partial t} \tag{28}$$

$$v_z(r,0,t) = \frac{\partial \mathcal{Z}}{\partial t} \tag{29}$$

Equations (7), (8), and (9) together with boundary conditions, eqs. (22), (23), (24), (25), (28), and (29), are the formal mathematical statement of the problem.

GENERAL SOLUTION FOR AN ARBITRARY AXISYMMETRIC APPLIED PRESSURE

The general solution of eqs. (7), (8), and (9) can be obtained using either transform methods or the method of separation of variables. This treatment follows Haskell (1935) and uses the method of separation of variables. Setting

$$v_r = R_1(r)\, Z_1(z) \tag{30}$$

$$v_z = R_2(r)\, Z_2(z) \tag{31}$$

$$\bar{p} = R_3(r)\, Z_3(z) \tag{32}$$

in eqs. (7), (8), and (9), and separating variables gives

$$\frac{1}{r}\frac{d}{dr}\left(r\frac{dR_1}{dr}\right) - \frac{R_1}{r^2} + \lambda^2 R_1 = 0 \tag{33}$$

$$\frac{1}{r}\frac{d}{dr}\left(r\frac{dR_2}{dr}\right) + \lambda^2 R_2 = 0 \tag{34}$$

$$R_3 = \kappa R_2 \tag{35}$$

where λ and κ are separation constants. Equations (33) and (34) are Bessel equations and have solutions

$$R_1 = A' J_1(\lambda r) + B' Y_0(\lambda r) \tag{36}$$

$$R_2 = C' J_0(\lambda r) + D' Y_0(\lambda r) \tag{37}$$

B' and D' must be zero in the problem at hand, in order that solutions remain finite at $r = 0$. The Z equations are

$$\frac{d^2Z_1}{dz^2} - \lambda^2 Z_1 = -\frac{\lambda}{\eta} Z_3 \tag{38}$$

$$\frac{d^2Z_2}{dz^2} - \lambda^2 Z_2 = \frac{1}{\eta} \frac{dZ_3}{dz} \tag{39}$$

$$\lambda Z_1 + \frac{dZ_2}{dz} = 0 \tag{40}$$

Eliminating Z_1 and Z_3 in eqs. (38) through (40) gives a fourth order equation for Z_2 ,

$$\frac{d^4Z_2}{dz^4} - 2\lambda^2 \frac{d^2Z_2}{dz^2} + \lambda^4 Z_2 = 0 \tag{41}$$

The solution to this equation is

$$Z_2 = e^{-\lambda z}(A'' + B''z) + e^{\lambda z}(C'' + D''z) \tag{42}$$

Using this solution in (39) and (40) gives

$$\begin{aligned} Z_1 = {} & e^{-\lambda z}\left[A'' - \frac{B''}{\lambda} + B''z\right] \\ & -e^{\lambda z}\left[C'' + \frac{D''}{\lambda} + D''z\right] \end{aligned} \tag{43}$$

$$Z_3 = 2\eta[B''e^{-\lambda z} + D''e^{\lambda z}] \tag{44}$$

Substituting (35), (36), (37), (42), (43), and (44) into (30), (31) and (32) gives

$$v_r/A' = J_1(\lambda r)[e^{-\lambda z}(A''-B''/\lambda+B''z) - e^{\lambda z}(C''+D''/\lambda + D''z)] \tag{45}$$

$$v_z/C' = J_0(\lambda r)[e^{-\lambda z}(A''+B''z) + e^{\lambda z}(C''+D''z)] \tag{46}$$

$$\bar{p}/\kappa = 2\eta\, J_0(\lambda r)[B''e^{-\lambda z} + D''e^{\lambda z}] \tag{47}$$

Substituting these expressions into the original unseparated equations, (7), (8), and (9), requires that $A' = C' = \kappa$. Equations (45) through (47) become

$$v_r = J_1(\lambda r)[e^{-\lambda z}(A - B/\lambda + Bz) - e^{\lambda z}(C + D/\lambda + Dz) \tag{48}$$

$$v_z = J_0(\lambda r)[e^{-\lambda z}(A + Bz) + e^{\lambda z}(C + Dz)] \tag{49}$$

$$\bar{p} = 2\eta\, J_0(\lambda r)[Be^{-\lambda z} + De^{\lambda z}] \tag{50}$$

where $A = \kappa A''$, $B = \kappa B''$, etc.

Equations (48), (49), and (50) contain four unknown constants. In addition, there are two unknown functions H and Z . Solutions for these six unknown quantities will come from the 6 boundary conditions, eqs. (22), (23), (24), (25), (28), and (29). Using eqs. (48) and (49) in (22) and (24) gives

$$\lambda A - B + \lambda C + D = 0 \tag{51}$$

$$Ae^{\lambda h} - Be^{\lambda h}(h + \tfrac{1}{\lambda}) + Ce^{-\lambda h} - De^{-\lambda h}(h - \tfrac{1}{\lambda}) = 0 \tag{52}$$

With the definitions,

$$f_1(\lambda) \equiv \frac{h}{e^{-2\lambda h} - 1} \tag{53}$$

$$f_2(\lambda) \equiv e^{-2\lambda h}\, f_1(\lambda) \tag{54}$$

$$F_1(\lambda) \equiv \frac{1}{\lambda} - f_1(\lambda) \tag{55}$$

$$F_2(\lambda) \equiv \frac{1}{\lambda} - f_2(\lambda) \tag{56}$$

eqs. (51) and (52) can be restated,

$$A = BF_1 - Df_2 \tag{57}$$

$$C = Bf_1 - DF_2 \tag{58}$$

Equations (48) through (50) now become

$$v_r = J_1(\lambda r)\ \{B(e^{-\lambda z}[F_1 - \frac{1}{\lambda} + z] - e^{\lambda z} f_1)$$
$$-D(e^{-\lambda z} f_2 - e^{\lambda z}[F_2 - \frac{1}{\lambda} - z])\}$$

$$v_z = J_o(\lambda r)\ \{B(e^{-\lambda z}[F_1 + z] + e^{\lambda z} f_1)$$
$$-D(e^{-\lambda z} f_2 + e^{\lambda z}[F_2 - z])\}$$

$$\overline{p} = 2\eta\, J_o(\lambda r)\ \{Be^{-\lambda z} + De^{\lambda z}\}$$

Equations (23) and (25) can now be applied using functions of the form

$$v_r = \int_0^\infty d\lambda\, J_1(\lambda r)\{B(e^{-\lambda z}[F_1 - \frac{1}{\lambda} + z] - e^{\lambda z} f_1)$$
$$-D(e^{-\lambda z} f_2 - e^{\lambda z}[F_2 - \frac{1}{\lambda} - z])\} \tag{59}$$

$$v_z = \int_0^\infty d\lambda\, J_o(\lambda r)\{B(e^{-\lambda z}[F_1 + z] + e^{\lambda z} f_1)$$
$$-D(e^{-\lambda z} f_2 + e^{\lambda z}[F_2 - z])\} \tag{60}$$

$$\overline{p} = 2\eta \int_0^\infty d\lambda\, J_o(\lambda r)\ \{Be^{-\lambda z} + De^{\lambda z}\} \tag{61}$$

We obtain

$$2\eta \int_0^\infty \lambda\, d\lambda\, J_0(\lambda r)\, \{B(e^{\lambda h}[F_1 - \bar{h}] - e^{-\lambda h} f_1) - D(e^{\lambda h} f_2 - e^{-\lambda h}[F_2 + h])\} + \rho g H = 0 \qquad (62)$$

$$2\eta \int_0^\infty \lambda\, d\lambda\, J_0(\lambda r)\, \{B(F_1 - f_1) - D(f_2 - F_2)\} + \rho g Z = \bar{\sigma}(r,t) \qquad (63)$$

Note that a lower limit of 0 rather than $-\infty$ is chosen for λ in the above integrals. This choice is arbitrary and is valid only if a solution can be found which fits all boundary conditions. The constants B and D will have to be functions of time to satisfy (62) and (63). Differentiating (62) and (63) with respect to time, the remaining boundary conditions, eqs. (28) and (29), can be used to obtain

$$\int_0^\infty \lambda\, d\lambda\, J_0(\lambda r)\, \{2\eta \frac{\partial B}{\partial t}(e^{\lambda h}[F_1 - h] - e^{-\lambda h} f_1) + \frac{\rho g}{\lambda} B(e^{\lambda h}[F_1 - h] + e^{-\lambda h} f_1) - 2\eta \frac{\partial D}{\partial t}(e^{\lambda h} f_2 - e^{-\lambda h}[F_2 + h]) - \frac{\rho g}{\lambda} D(e^{\lambda h} f_2 + e^{-\lambda h}[F_2 + h])\} = 0 \qquad (64)$$

$$\int_0^\infty \lambda\, d\lambda\, J_0(\lambda r)\, \{2\eta \frac{\partial B}{\partial t}(F_1 - f_1) + \frac{\rho g}{\lambda} B(F_1 + f_1) - 2\eta \frac{\partial D}{\partial t}(f_2 - F_2) - \frac{\rho g}{\lambda} D(F_2 + f_2)\} = \frac{\partial \bar{\sigma}}{\partial t} \qquad (65)$$

The following definitions will prove convenient:

$$m_1(\lambda) \equiv 2\eta(e^{\lambda h}[F_1 - h] - e^{-\lambda h} f_1) \qquad (66a)$$

$$m_2(\lambda) \equiv \frac{\rho g}{\lambda}(e^{\lambda h}[F_1 - h] + e^{-\lambda h} f_1) \qquad (66b)$$

$$m_3(\lambda) \equiv -2\eta(e^{\lambda h} f_2 - e^{\lambda h}[F_2 + h]) \tag{66c}$$

$$m_4(\lambda) \equiv -\frac{\rho g}{\lambda}(e^{\lambda h} f_2 + e^{-\lambda h}[F_2 + h]) \tag{66d}$$

$$m_5(\lambda) \equiv 2\eta(F_1 - f_1) \tag{66e}$$

$$m_6(\lambda) \equiv \frac{\rho g}{\lambda}(F_1 + f_1) \tag{66f}$$

$$m_7(\lambda) \equiv -2\eta(f_2 - F_2) \tag{66g}$$

$$m_8(\lambda) \equiv -\frac{\rho g}{\lambda}(F_2 + f_2) \tag{66h}$$

$$n_1 \equiv m_3 m_5 - m_1 m_7 \tag{66i}$$

$$n_2 \equiv m_3 m_6 + m_4 m_5 - m_1 m_8 - m_2 m_7 \tag{66j}$$

$$n_3 \equiv m_4 m_6 - m_2 m_8 \tag{66k}$$

Reduced expressions for these quantities are listed in Table 8.

Using definitions (66a-h), eqs. (64) and (65) can be rewritten

$$\int_0^\infty \lambda\, d\lambda\, J_o(\lambda r)\{(m_1 \frac{\partial}{\partial t} + m_2)B + (m_3 \frac{\partial}{\partial t} + m_4)D\} = 0 \tag{67}$$

$$\int_0^\infty \lambda\, d\lambda\, J_o(\lambda r)\{(m_5 \frac{\partial}{\partial t} + m_6)B + (m_7 \frac{\partial}{\partial t} + m_8)D\} = \frac{\partial \bar{\sigma}}{\partial t} \tag{68}$$

The Hankel integral formula can be applied to (67) and (68). This formula is (Bateman, 1953, p. 73), using a zeroth order Bessel function,

$$f(\lambda') = \int_0^\infty r\, dr\, J_o(\lambda' r) \int_0^\infty \lambda\, d\lambda\, J_o(\lambda r)\, f(\lambda) \tag{69}$$

Multiplying both sides of (67) and (68) by the operator

TABLE 8. Reduced Expressions for Various Mathematical Quantities

$$f_1 \equiv \frac{h}{e^{-2\lambda h} - 1}$$

$$f_2 \equiv e^{-2\lambda h} f_1$$

$$F_1 \equiv \frac{1}{\lambda} - f_1$$

$$F_2 \equiv \frac{1}{\lambda} - f_2$$

$$G \equiv \left[1 + \frac{4(\lambda h)^2 e^{-\lambda h}}{e^{\lambda h}(1 - e^{-2\lambda h})^2 - 4(\lambda h)^2 e^{-\lambda h}}\right]^{1/2}$$

$$H \equiv 1 - \frac{2\lambda h}{1 + 2\lambda h - e^{-2\lambda h}}$$

$$K_1 = \frac{\rho g}{2\eta \lambda} G$$

$$K_2 = -\frac{\rho g}{2\eta \lambda} G$$

$$K_3 = \frac{\rho g}{2\eta\lambda} H$$

$$m_1 \equiv \frac{2\eta}{\lambda} e^{\lambda h}\left[\frac{1 - e^{-2\lambda h}(1 - 2\lambda h)}{1 - e^{-2\lambda h}}\right]$$

$$m_2 \equiv \frac{\rho g}{\lambda^2} e^{\lambda h}$$

$$m_3 \equiv \frac{2\eta}{\lambda} e^{-\lambda h}\left[\frac{1 + 2\lambda h - e^{-2\lambda h}}{1 - e^{-2\lambda h}}\right]$$

$$m_4 \equiv -e^{-2\lambda h} m_2$$

TABLE 8 - Continued

$$m_5 \equiv e^{\lambda h} m_3$$

$$m_6 \equiv e^{-\lambda h} m_2$$

$$m_7 \equiv e^{-\lambda h} m_1$$

$$m_8 \equiv -e^{-\lambda h} m_2$$

$$n_1 \equiv -\left(\frac{2\eta}{\lambda}\right)^2 \left[e^{\lambda h}(1 - e^{-2\lambda h}) - \frac{4(\lambda h)^2 e^{-\lambda h}}{1 - e^{-2\lambda h}}\right]$$

$$n_2 \equiv 0$$

$$n_3 \equiv \frac{(\rho g)^2}{\lambda^4} e^{\lambda h}(1 - e^{-2\lambda h})$$

$$P_1 \equiv \frac{\eta}{G\lambda} e^{-\lambda h}\left[\frac{1 - G(1 + 2\lambda h) - e^{-2\lambda h}(1 - G)}{1 - e^{-2\lambda h}}\right]$$

P_2 is equal to P_1 with G replaced by -G

$$P_3 \equiv -\frac{1}{H - G}\left[\frac{1 + G(1 - 2\lambda h) - e^{2\lambda h}(1 + G)}{1 + 2\lambda h - e^{-2\lambda h}}\right]$$

P_4 is equal to P_3 with G replaced by -G

$\int_0^\infty r\,dr\,J_0(\lambda' r)\cdot$, it is seen that the expressions in braces in those equations correspond to f in the formula. Therefore,

$$[m_1(\lambda')\frac{\partial}{\partial t} + m_2(\lambda')]B(\lambda',t) + [m_3(\lambda')\frac{\partial}{\partial t} + m_4(\lambda')]D(\lambda',t) = 0 \quad (70)$$

$$[m_5(\lambda')\frac{\partial}{\partial t} + m_6(\lambda')]B(\lambda',t) + [m_7(\lambda')\frac{\partial}{\partial t} + m_8(\lambda')]D(\lambda',t) =$$

$$\int_0^\infty r\,dr\,J_0(\lambda' r)\frac{\partial \bar{\sigma}(r,t)}{\partial t} \quad (71)$$

λ' will be redesignated λ in eqs. (70) and (71), and $Q(\lambda,t)$ will be defined as

$$Q(\lambda,t) \equiv \int_0^\infty r\,dr\,J_0(\lambda r)\frac{\partial}{\partial t}\bar{\sigma}(r,t) \quad (72)$$

Eliminating D and using definitions (66) and (72) gives an equation for B ,

$$(\frac{\partial^2}{\partial t^2} + \frac{n_2}{n_1}\frac{\partial}{\partial t} + \frac{n_3}{n_1})\cdot B = X_1 \quad (73a)$$

where $$X_1 \equiv \frac{1}{n_1}(m_3\frac{\partial}{\partial t} + m_4)\cdot Q \quad (73b)$$

Equation (73a) has the general solution (Wayland, 1957, p. 75 ff.),

$$B = e^{K_2 t}\int_0^t dt'\, e^{(K_1-K_2)t'}\int_0^{t'} dt''\, e^{-K_1 t''}X_1 + L_1(\lambda)\,e^{K_1 t} + L_2(\lambda)e^{K_2 t}\ ,\ K_1 \neq K_2 \quad (74)$$

where K_1 and K_2 are roots of the equation

$$K^2 + \frac{n_2}{n_1} K + \frac{n_3}{n_1} = 0 \tag{75}$$

and $L_1(\lambda)$ and $L_2(\lambda)$ are constants in time which must be determined from initial conditions. D can be determined from (70),

$$\left(\frac{\partial}{\partial t} + \frac{m_4}{m_3} \right) D = X_2 \tag{76a}$$

where

$$X_2 \equiv - \frac{1}{m_3} \left(m_1 \frac{\partial}{\partial t} + m_2 \right) \cdot B \tag{76b}$$

Equation (76a) has the general solution,

$$D = e^{K_3 t} \int_0^t dt' \, e^{-K_3 t'} X_2 + L_3(\lambda) \, e^{K_3 t} \tag{77}$$

where

$$K_3 \equiv - \frac{m_4}{m_3} \tag{78}$$

and $L_3(\lambda)$ is another constant in time which must be determined from initial conditions. Using Table 8 and eqs. (75) and (78), one finds

$$K_1 = \frac{\rho g}{2\eta\lambda} G \tag{79}$$

$$K_2 = - \frac{\rho g}{2\eta\lambda} G \tag{80}$$

$$K_3 = \frac{\rho g}{2\eta\lambda} H \tag{81}$$

where

$$G \equiv \left[1 + \frac{4(\lambda h)^2 e^{-\lambda h}}{e^{\lambda h}(1 - e^{-2\lambda h})^2 - 4(\lambda h)^2 e^{-\lambda h}} \right]^{1/2} \tag{82}$$

$$H \equiv 1 - \frac{2\lambda h}{1 + 2\lambda h - e^{-2\lambda h}} \tag{83}$$

Integrating (74) by parts, the final expression for B is

$$B = \frac{1}{n_1}\int_0^\infty r\,dr\,J_o(\lambda r)\cdot$$

$$\left\{ m_3\bar{\sigma} + e^{K_1 t}\left[-\left(\frac{m_3\frac{\partial\bar{\sigma}}{\partial t}(r,0)}{K_1 - K_2} + P_1\,\bar{\sigma}(r,0)\right)\right]\right.$$

$$+ e^{K_2 t}\left[\left(\frac{m_3\frac{\partial\bar{\sigma}}{\partial t}(r,0)}{K_1 - K_2} + P_1\,\bar{\sigma}(r,0)\right)\right.$$

$$- m_3\bar{\sigma}(r,0)$$

$$+ (P_1[K_1 - K_2] + m_3K_2)\int_0^t dt'\,e^{-K_2t'}\,\bar{\sigma}$$

$$\left.\left. + P_1(K_1-K_2)K_1\int_0^t dt'\,e^{(K_1-K_2)t'}\int_0^{t'} dt''\,e^{-K_1t''}\bar{\sigma}\right]\right\}$$

$$+ L_1e^{K_1t} + L_2e^{K_2t} \qquad (84)$$

where use was made of the first of the definitions below,

$$P_1 \equiv \frac{m_3K_1 + m_4}{K_1 - K_2} \qquad (85a)$$

$$P_2 \equiv \frac{m_3K_2 + m_4}{K_2 - K_1} \qquad (85b)$$

$$P_3 \equiv -\frac{1}{m_3}\left(\frac{m_1K_1 + m_2}{K_1 - K_3}\right) \qquad (85c)$$

$$P_4 \equiv -\frac{1}{m_3}\left(\frac{m_1K_2 + m_2}{K_2 - K_3}\right) \qquad (85d)$$

Reduced expressions for these quantities are listed in Table 8. D can similarly be expressed in final form,

$$D = \frac{1}{n_1}\int_0^\infty r\,dr\,J_0(\lambda r)\cdot$$

$$\Bigg\{ -m_1\bar{\sigma} + e^{K_1 t}\left[-P_3\left(\frac{m_3\frac{\partial\bar{\sigma}}{\partial t}(r,0)}{K_1-K_2} + P_1\,\bar{\sigma}(r,0)\right)\right]$$

$$+ e^{K_2 t}\left[P_4\left(-m_3\bar{\sigma}(r,0) + \frac{m_3\frac{\partial\bar{\sigma}}{\partial t}(r,0)}{K_1-K_2} + P_1\bar{\sigma}(r,0)\right)\right]$$

$$+ e^{K_3 t}\left[P_3\left(\frac{m_3\frac{\partial\bar{\sigma}}{\partial t}(r,0)}{K_1-K_2} + P_1\bar{\sigma}(r,0)\right)\right.$$

$$\left. - P_4\left(-m_3\bar{\sigma}(r,0) + \frac{m_3\frac{\partial\bar{\sigma}}{\partial t}(r,0)}{K_1-K_2} + P_1\bar{\sigma}(r,0)\right)\right]$$

$$+ m_1\bar{\sigma}(r,0)$$

$$- m_1\left[\frac{P_1(K_1-K_2)}{m_3} - \frac{m_3P_4}{m_1}(K_2-K_3) + K_3\right]\int_0^t dt'\,e^{-K_3t'}\,\bar{\sigma}$$

$$- P_1(K_1-K_2)K_1\frac{m_1}{m_3}\int_0^t dt'\,e^{(K_1-K_3)t'}\int_0^{t'} dt''\,e^{-K_1t''}\,\bar{\sigma}$$

$$+ P_4(K_2-K_3)(P_1[K_1-K_2]+m_3K_2)\int_0^t dt'\,e^{(K_2-K_3)t'}\int_0^{t'} dt''e^{-K_2t''}\bar{\sigma}$$

$$+ P_1P_4(K_2-K_3)(K_1-K_2)K_1\int_0^t dt'e^{(K_2-K_3)t'}\int_0^{t'} dt''e^{(K_1-K_2)t''}$$

$$\times\int_0^{t'''} dt'''\,e^{-K_1t'''}\,\bar{\sigma}\,\Bigg]\Bigg\}$$

$$+ P_3L_1e^{K_1t} + P_4L_2e^{K_2t} + (L_3 - P_3L_1 - P_4L_2)e^{K_3t} \qquad (86)$$

Equations (59), (60) and (61) together with eqs. (84) and (86) constitute the formal solution of the problem.

DOMING BY A BESSEL-SHAPED PRESSURE DISTRIBUTION

The fluid representing the Precambrian rock will be considered to be initially at rest. The magmatic driving pressure, $\bar{\sigma}$, applied to the bottom of the fluid will be modeled as

$$\bar{\sigma}(r,t) = \sigma_0 J_0(\alpha r) H(t-0^+) \tag{87}$$

where σ_0 is an arbitrary pressure;

$$\alpha = \frac{\alpha_0}{a} \tag{88}$$

where $J_0(\alpha_0) = 0$ and a is an arbitrary radius; and $H(t-0^+)$ is a Heaviside step function whose values are

$$H(t-0^+) = \begin{cases} 0 , & t \leq 0 \\ 1 , & t > 0 \end{cases} \tag{89}$$

Equation (87) represents turning on at time $t>0$ a Bessel-shaped pressure distribution on the bottom of the layer of fluid. A Bessel function was chosen for mathematical convenience. A more appealing choice from the point of view of the geology of the dome would be a cylindrical pressure distribution, where the driving pressure is equal to σ_0 within a circle, $r=a$, on the bottom of the layer and is equal to zero everywhere outside the circle. Such a driving pressure is represented by

$$\bar{\sigma}(r,t) = \sigma_0 H(a-r) H(t-0^+)$$

Unfortunately, this function causes the integrals in eqs. (59) through (61) to blow up at their lower limits. This problem is presumably due to the fact that this cylindrical driving pressure exerts a net force

on the layer; it throws the layer out of equilibrium and is therefore inadmissible as a boundary value. A Bessel function, on the other hand, exerts no net force on the layer and can be used in this problem. The central peak of the Bessel function, $J_o(\alpha r)$, which has a radius of a, is of primary interest here. The wings of this function at $r > a$ are not of primary concern, although they do have an important effect on the answer.

Substituting (87) into (84) and (86) and noting that $\bar{\sigma}(r,0) = \frac{\partial \bar{\sigma}}{\partial t}(r,0) = 0$, one finds

$$B = \frac{\sigma_o}{n_1} \int_0^\infty r\, dr\, J_o(\lambda r)\, J_o(\lambda r)(P_1 e^{K_1 t} + P_2 e^{K_2 t}) + L_1 e^{K_1 t} + L_2 e^{K_2 t} \qquad t > 0 \qquad (90a)$$

$$B = L_1 e^{K_1 t} + L_2 e^{K_2 t} \qquad t \leq 0 \qquad (90b)$$

$$D = \frac{\sigma_o}{n_1} \int_0^\infty r\, dr\, J_o(\lambda r)\, J_o(\lambda r) \cdot$$

$$(P_1 P_3 e^{K_1 t} + P_2 P_4 e^{K_2 t} - [P_1 P_3 + P_2 P_4 + m_1]\, e^{K_3 t})$$

$$+ P_3 L_1 e^{K_1 t} + P_4 L_2 e^{K_2 t} + (L_3 - P_3 L_1 - P_4 L_2)\, e^{K_3 t} \qquad t > 0 \qquad (91a)$$

$$D = P_3 L_1 e^{K_1 t} + P_4 L_2 e^{K_2 t} + (L_3 - P_3 L_1 - P_4 L_2) e^{K_3 t} \qquad t \leq 0 \qquad (91b)$$

It can be shown, using Table 8, that in (91a)

$$P_1 P_3 + P_2 P_4 + m_1 \equiv 0 \qquad (91c)$$

The constants L_1, L_2, and L_3 in eqs. (90a) through (91b) can be determined from the condition that the fluid be initially at rest. Three relationships are needed. The first relationship comes from (71) and the remaining two come from any of eqs. (59) through (61). The procedure will only be outlined here. One first substitutes (86) and (84) into (71), sets $t = 0$, and uses eq. (87). The resulting equation is of the form

$$aL_1 + bL_2 + cL_3 = 0 , \quad a \neq b \neq c \tag{92}$$

Secondly, one substitutes (90b) and (91b) with $t = 0$ into eqs. (59), (60), and (61) and sets those equations equal to 0. The resulting equations are of the form

$$0 = \int_0^\infty d\lambda \, R_i(\lambda,r) \, \{(L_1 + L_2) \, S_i(\lambda,z) + L_3 T_i(\lambda,z)\}$$

where R_i, S_i, and T_i are distinct functions. These equations require that

$$L_1 + L_2 = 0 \tag{93}$$

$$L_3 = 0 \tag{94}$$

Equations (92) through (94) determine that

$$L_1 = L_2 = L_3 = 0 \tag{95}$$

Finally, (59) through (61) can be expressed

$$V_r = \frac{\sigma_o}{n_1\alpha} J_1(\alpha r) \{(P_1 e^{K_1 t} + P_2 e^{K_2 t})(e^{-\alpha z}[F_1 - \frac{1}{\alpha} + z] - e^{\alpha z} f_1)$$

$$- (P_1 P_3 e^{K_1 t} + P_2 P_4 e^{K_2 t})(e^{-\alpha z} f_2 - e^{\alpha z}[F_2 - \frac{1}{\alpha} - z])\} \quad (96)$$

$$V_z = \frac{\sigma_o}{n_1\alpha} J_o(\alpha r) \{(P_1 e^{K_1 t} + P_2 e^{K_2 t})(e^{-\alpha z}[F_1 + z] + e^{\alpha z} f_1)$$

$$- (P_1 P_3 e^{K_1 t} + P_2 P_4 e^{K_2 t})(e^{-\alpha z} f_2 + e^{\alpha z}[F_2 - z])\} \quad (97)$$

$$\overline{p} = \frac{2\eta\sigma_o}{n_1\alpha} J_o(\alpha r) \{(P_1 e^{K_1 t} + P_2 e^{K_2 t}) e^{-\alpha z}$$

$$- (P_1 P_3 e^{K_1 t} + P_2 P_4 e^{K_2 t}) e^{\alpha z}\} \quad (98)$$

where the properties have been used (Morse and Feshbach, 1953, p. 764)

$$\alpha \int_0^\infty r\, dr\, J_o(\lambda r)\, J_o(\alpha r) = \delta(\alpha - \lambda) \quad \text{(Dirac delta function)}$$

and

$$\int_{\omega_1}^{\omega_2} d\lambda\, f(\lambda)\, \delta(\alpha - \lambda) = \begin{cases} f(\lambda), & \omega_1 < \alpha < \omega_2 \\ 0, & \alpha < \omega_1 \text{ or } \omega_2 < \alpha \end{cases}$$

Equations (28) and (29) now give

$$H = \int_0^t dt\, v_z(r,-h,t) = \frac{\sigma_o e^{-\alpha h}}{n_1 \alpha^2} J_o(\alpha r) \{ (e^{K_1 t} - 1)\frac{P_1(e^{2\alpha h} - P_3)}{K_1}$$

$$+ (e^{K_2 t} - 1)\frac{P_2(e^{2\alpha h} - P_4)}{K_2}\} \quad (99)$$

$$Z = \int_0^t dt\, v_z(r,0,t) = \frac{\sigma_o}{n_1\alpha^2} J_o(\alpha r) \{(e^{K_1 t} - 1)\frac{P_1(1 - P_3)}{K_1} + (e^{K_2 t} - 1)\frac{P_2(1 - P_4)}{K_2}\} \qquad (100)$$

Note that in eqs. (96) through (100), the quantities f_1, f_2, F_1, F_2, K_1, K_2, n_1, P_1, P_2, P_3 and P_4 are now functions of α rather than λ .

It is convenient for purposes of calculation to express eqs. (96) through (100) in terms of dimensionless variables. The following definitions will be used:

$$\hat{r} \equiv \frac{r}{a} \; ; \quad \hat{z} \equiv \frac{z}{h} \qquad (101a)$$

$$\gamma \equiv \alpha h = \alpha_o \frac{h}{a} \qquad (101b)$$

$$\tau \equiv K_1 t = -K_2 t = \frac{\rho g}{2\eta\alpha} Gt = \frac{\rho g h}{2} (\frac{t}{\eta}) \cdot (\frac{G}{\gamma}) \qquad (101c)$$

$$\hat{f}_1 \equiv \frac{f_1}{h} \; ; \quad \hat{f}_2 \equiv \frac{f_2}{h} \; ; \quad \hat{F}_1 \equiv \frac{F_1}{h} \; ; \quad \hat{F}_2 \equiv \frac{F_2}{h} \qquad (101d)$$

$$\hat{n}_1 \equiv (\frac{\alpha}{2\eta})^2 n_1 \qquad (101e)$$

$$\hat{P}_1 \equiv \frac{\alpha}{\eta} P_1 \; ; \quad \hat{P}_2 \equiv \frac{\alpha}{\eta} P_2 \qquad (101f)$$

$$\hat{v}_r \equiv \frac{4\eta}{\sigma_o h} v_r \; ; \quad \hat{v}_z \equiv \frac{4\eta}{\sigma_o h} v_z \; ; \quad \hat{p} \equiv \frac{2}{\sigma_o} \bar{p} \qquad (101g)$$

One obtains

$$\hat{v}_r = \frac{J_1(\alpha_o \hat{r})}{\hat{n}_1} \left\{ \hat{P}_1 \left[e^{\tau - \gamma \hat{z}} (\hat{F}_1 - \frac{1}{\gamma} + \hat{z} - P_3 \hat{f}_2) - e^{\tau + \gamma \hat{z}} (\hat{f}_1 - P_3 [\hat{F}_2 - \frac{1}{\gamma} - \hat{z}]) \right] \right.$$

$$\left. + \hat{P}_2 \left[e^{-\tau - \gamma \hat{z}} (\hat{F}_1 - \frac{1}{\gamma} + \hat{z} - P_4 \hat{f}_2) - e^{-\tau + \gamma \hat{z}} (\hat{f}_1 - P_4 [\hat{F}_2 - \frac{1}{\gamma} - \hat{z}]) \right] \right\} \tag{102}$$

$$\hat{v}_z = \frac{J_0(\alpha_o \hat{r})}{\hat{n}_1} \left\{ \hat{P}_1 \left[e^{\tau - \gamma \hat{z}} (\hat{F}_1 + \hat{z} - P_3 \hat{f}_2) + e^{\tau + \gamma \hat{z}} (\hat{f}_1 - P_3 (\hat{F}_2 - \hat{z}]) \right] \right.$$

$$\left. + \hat{P}_2 \left[e^{-\tau - \gamma \hat{z}} (\hat{F}_1 + \hat{z} - P_4 \hat{f}_2) + e^{-\tau + \gamma \hat{z}} (\hat{f}_1 - P_4 [\hat{F}_2 - \hat{z}]) \right] \right\} \tag{103}$$

$$\hat{p} = \frac{J_0(\alpha_o \hat{r})}{\hat{n}_1} \{ \hat{P}_1 [e^{\tau - \gamma \hat{z}} + e^{\tau + \gamma \hat{z}} P_3] + \hat{P}_2 [e^{-\tau - \gamma \hat{z}} + e^{-\tau + \gamma \hat{z}} P_4] \} \tag{104}$$

$$H = \frac{\sigma_o}{\rho g} J_0(\alpha_o \hat{r}) \{ [e^{\tau} - 1] \Omega_{H1}(\gamma) + [1 - e^{-\tau}] \Omega_{H2}(\gamma) \} \tag{105a}$$

where

$$\Omega_{H1}(\gamma) = \hat{P}_1 (e^{2\gamma} - P_3) e^{-\gamma} / 2\hat{n}_1 G \tag{105b}$$

$$\Omega_{H2}(\gamma) = \hat{P}_2 (e^{2\gamma} - P_4) e^{-\gamma} / 2\hat{n}_1 G \tag{105c}$$

$$Z = \frac{\sigma_o}{\rho g} J_0(\alpha_o \hat{r}) \{ [e^{\tau} - 1] \Omega_{Z1}(\gamma) + [1 - e^{-\tau}] \Omega_{Z1}(\gamma) \} \tag{106a}$$

where

$$\Omega_{Z1}(\gamma) = \hat{P}_1 (1 - P_3) / 2\hat{n}_1 G$$

$$\Omega_{Z2}(\gamma) = \hat{P}_2 (1 - P_4) / 2\hat{n}_1 G \tag{106c}$$

It can be shown graphically that $\Omega_{H1} = \Omega_{H2}$ (fig. 13).

Figure 13. Amplitude Factors, Ω_{H1}, Ω_{H2}, Ω_{Z1}, and Ω_{Z2}.

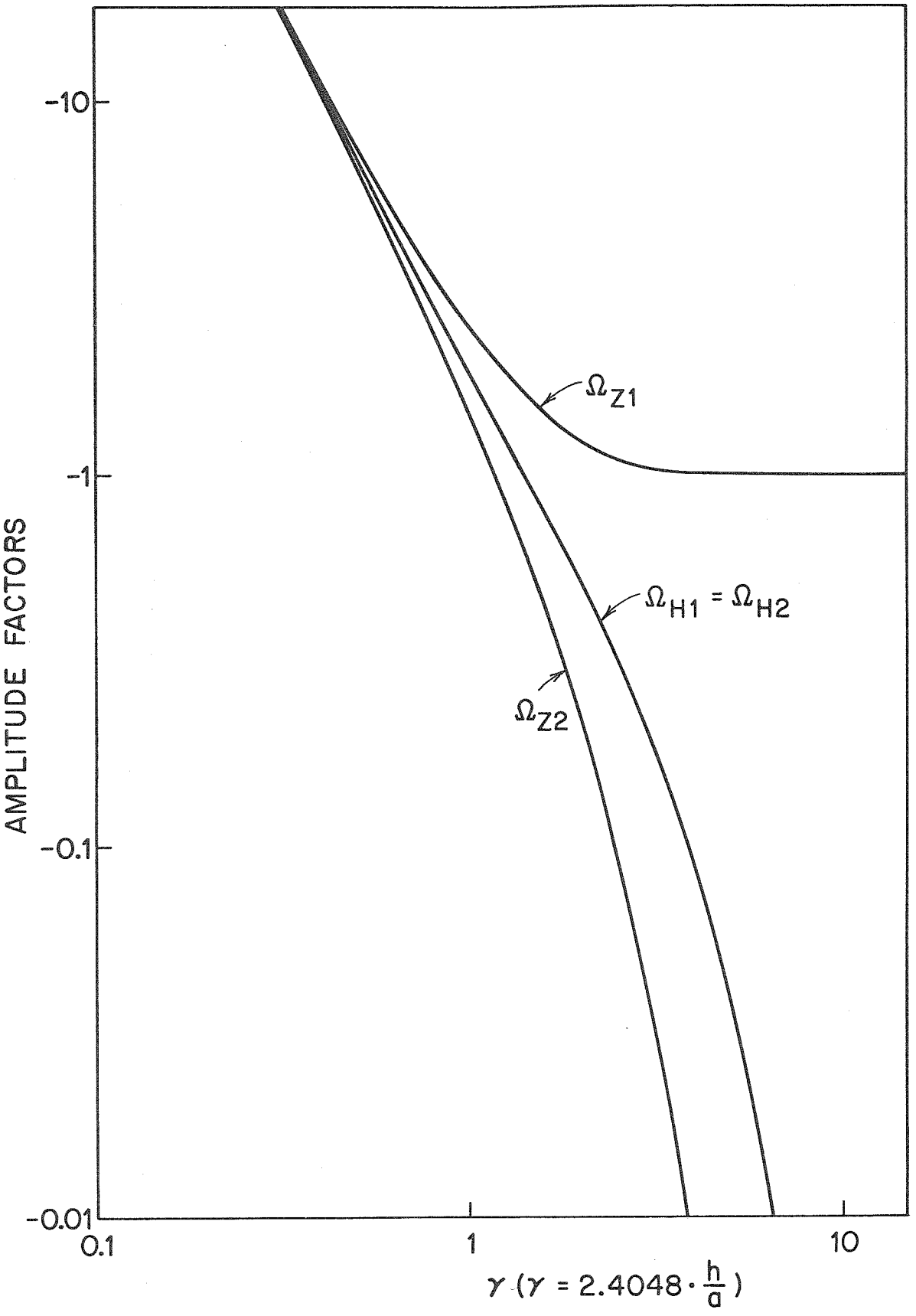
-10
-1
-0.1
-0.01
0.1
1
10
AMPLITUDE FACTORS
Ω_{Z1}
$\Omega_{H1} = \Omega_{H2}$
Ω_{Z2}
γ ($\gamma = 2.4048 \cdot \frac{h}{a}$)

EXAMINATION OF THE SOLUTION

Boundary Conditions

Dynamical boundary conditions on the upper surface of the fluid require that $T_{rz} = 0$ and $T_{zz} = 0$ (eqs. (17) and (18)). On the lower surface they require that $T_{rz} = 0$ and $T_{zz} = \sigma$ (eqs. (19) and (20)). These conditions were approximated in two steps. First, normals, $\hat{n}$, to the surfaces H and Z were approximated by the unit vectors $(0,0,\pm 1)$. (Approximation 2). Secondly, certain terms in the expressions for the boundary conditions were evaluated on surfaces $z = 0$ and $z = -h$, rather than on surfaces $z = Z$ and $z = H-h$ (Approximation 3). The resulting expressions for the dynamical boundary conditions are eqs. (22) through (25).

The first approximation, Approximation 2, is good for small distortions, where distortion is formally defined as $H(\hat{r}=0)/a$* or $Z(\hat{r}=0)/a$. For a distortion of, say, 0.1, $\hat{n}$ will be, on the average, $(0.1,0,\pm 1)$. True stress on the boundaries might thus differ from stress given by the model by as much as $0.1\sigma_o$, where σ_o is used here as a characteristic stress in the medium.

In order to examine the second approximation, Approximation 3, one must compare the sizes of errors in the approximated terms in eqs. (22) through (25) with the sizes of all terms in those equations. Using (102) through (106) to estimate errors, it can be demonstrated that for small distortions, $H(\hat{r}=0)/a$ and $Z(\hat{r}=0)/a$, the errors in $\bar{p}$ and $\partial v_z/\partial z$ in eqs. (23) and (25) are individually as large as the

* For convenience, the quantities $H(\hat{r} = 0)/a$, $Z(\hat{r} = 0)/a$, $H(\hat{r} = 0)/h$, and $Z(\hat{r} = 0)/h$, will be considered positive quantities in the remainder of this chapter.

terms $\rho g H$ and $\rho g Z$ but are of opposite sign and largely cancel one another. As distortions are increased the cancellation becomes worse until eventually the errors are additive. The net result of Approximation 3 is seen in Table 9. In Table 9, stresses on the upper and lower surfaces of the fluid, given by (22) through (25) (or by (109) through (112), below), are tabulated for $\frac{\rho g h}{2}(\frac{t}{\eta})$ = 0.1 and 0.5, $\frac{\sigma_o}{\rho g h}$ = 0.5, and h/a = 1. Values of $Z(\hat{r}=0)/a$ (and $H(\hat{r}=0)/a$) corresponding to the two values of $\frac{\rho g h}{2}(\frac{t}{\eta})$, 0.1 and 0.5, are of order 0.01 and 0.1, respectively. It is seen that for the smaller value of $\frac{\rho g h}{2}(\frac{t}{\eta})$, and smaller distortion, the model fits closely the proper dynamical boundary conditions. For the larger value of $\frac{\rho g h}{2}(\frac{t}{\eta})$, stresses commonly differ from their correct value by $0.1\sigma_o$, but differences as high as $0.5\sigma_o$ are seen.

Thus, for distortions of 0.1 and smaller, the model fits the proper dynamical boundary conditions with errors in stress of the order of $0.1\sigma_o$ and smaller. Insofar as the model fits these boundary conditions, it will be physically meaningful; i.e., it will be a faithful reproduction of doming in a viscous fluid. For larger distortions, it is not clear how the model would correlate with real doming. Mathematically, there are no limits on the solution, however, and domes as large as desired can be treated.

Functions H and Z

The function H is the displacement of the surface of the fluid, and the function Z is the displacement of the base of the fluid, which is the roof of the magma chamber. These functions are expressed in

TABLE 9. Stresses on the Upper and Lower Surfaces of the Fluid. $\sigma_o/\rho gh = 0.5$, and $h/a = 1$.

	$\hat{r} \longrightarrow$	0.0 (center of dome)	0.25	0.5	0.75	1.0 (edge of dome)
				$\frac{\rho gh}{2}\left(\frac{t}{\eta}\right) = 0.1$		
T_{zz}/σ_o	upper	-0.60410	-0.00310	-0.00122	-0.00015	-0.00000
	lower	-2.98313	-2.89877	-2.66470	-2.33719	-2.00000
T_{rz}/σ_o	upper	0.0	-0.02595	-0.03265	-0.01882	-0.00000
	lower	0.0	0.05579	0.07369	0.04541	0.00000
				$\frac{\rho gh}{2}\left(\frac{t}{\eta}\right) = 0.5$		
T_{zz}/σ_o	upper	-0.15962	-0.11876	-0.04487	-0.00529	-0.00000
	lower	-2.47103	-2.49109	-2.47932	-2.30842	-2.00000
T_{rz}/σ_o	upper	0.0	-0.20543	-0.24359	-0.12984	-0.00000
	lower	0.0	0.23801	0.37622	0.29578	0.00000

terms of the variables r, γ, and the quantity $\frac{\rho g h}{2}(\frac{t}{\eta})$, which appears in the exponent τ in eqs. (105a) and (106a). γ is the ratio of the layer thickness, h, to the plug radius, a, multiplied by α_o, or 2.4048. $\frac{\rho g h}{2}(\frac{t}{\eta})$ is the ratio of maximum hydrostatic pressure to viscosity, multiplied by time.

Dependence on Radius. H and Z are the same functions of $\hat{r}$; that is, the undulations on the surface of the fluid have the same radial dimensions as those on the roof of the magma chamber below. None of the upward broadening of features is seen that one would expect from, say, a cylindrical driving pressure. The fact that the radial dimensions remain unchanged from bottom to top in the model arises from the wings of the Bessel-shaped driving pressure. These wings prevent fluid from flowing off the top of the dome to infinity. Such flow would serve to broaden the dome and lessen its height. Instead, the wings intersperse areas of positive and negative v_r such that there is no net mass transport. In fact, as a test of the solution, mass should be conserved inside the first node of v_r. That is,

$$\rho \int_0^{\frac{\beta_o}{\alpha_o} a} 2\pi r \, dr[Z - (H - h)] \stackrel{?}{=} \rho\pi \left(\frac{\beta_o}{\alpha_o} a\right)^2 h \qquad (107)$$

where β_o is the first zero of J_1. It is straightforward to demonstrate that eq. (107) is true.

Amplitudes. Figure 14 is a plot of amplitudes $H(\hat{r}=0)/\frac{\sigma_o}{\rho g}$ and $Z(\hat{r}=0)/\frac{\sigma_o}{\rho g}$ versus γ, as described by eqs. (105a) and (106a); two

Figure 14. Amplitude of the Dome, $H(\hat{r}=0)/\frac{\sigma_o}{\rho g}$, and the Magma Chamber, $Z(\hat{r}=0)/\frac{\sigma_o}{\rho g}$.

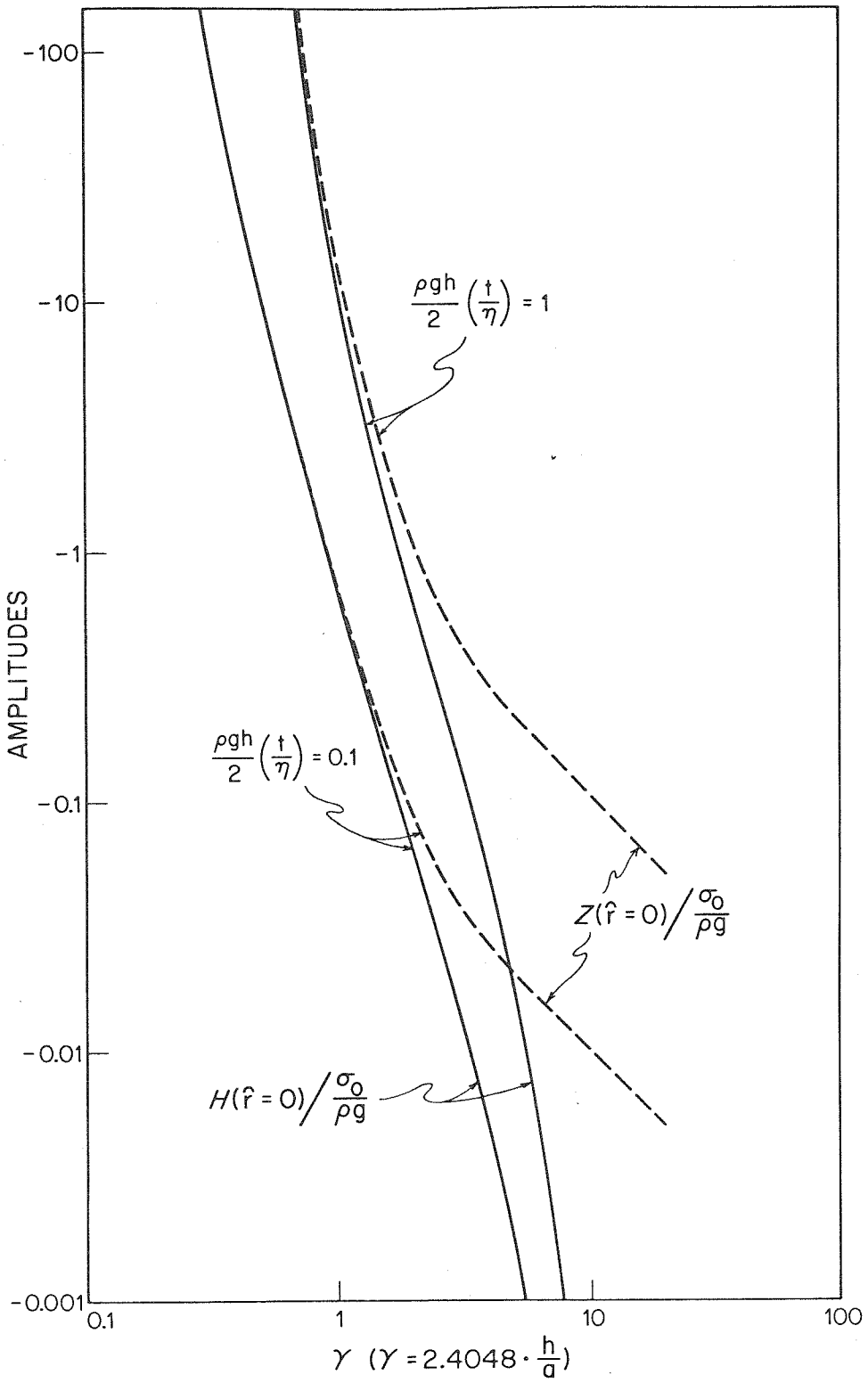
-100
-10
-1
-0.1
-0.01
-0.001
AMPLITUDES
0.1
1
10
100
γ (γ = 2.4048 · h/a)
ρgh/2 (t/η) = 1
ρgh/2 (t/η) = 0.1
Z(r̂ = 0) / σ0/ρg
H(r̂ = 0) / σ0/ρg

values of the quantity $\frac{\rho g h}{2}(\frac{t}{\eta})$ in the exponent τ are chosen for these plots, 0.1 and 1. There appear to be points of inflection in both curves of $H(\hat{r}=0)/\frac{\sigma_o}{\rho g}$ which occur at or near $\gamma = 2.4048$ or $\frac{h}{a} = 1$. As a result of these points of inflection, the curves, $H(\hat{r}=0)/\frac{\sigma_o}{\rho g}$ and $Z(\hat{r}=0)/\frac{\sigma_o}{\rho g}$, converge for values of $\frac{h}{a}$ smaller than 1 and diverge for values larger than 1. Thus, the amplitude of the dome converges to the amplitude of the arched roof of the magma chamber as the layer is made thinner than $h = a$ and it becomes negligible compared to the amplitude of the roof as the layer is made thicker than $h = a$.

Critical Values of h/a and $\frac{\rho g h}{2}(\frac{t}{\eta})$. Critical values of the parameters h/a and $\frac{\rho g h}{2}(\frac{t}{\eta})$ are defined as those values at which the largest dome distortion, $H(\hat{r}=0)/a$, occurs. In the Fort Rock dome, this distortion was significant, but the magma did not arch its way all the way to the original surface of the land so as to form a core inside the dome. Thus, if one wishes to examine a class of domes into which the Fort Rock dome falls, it would be defined as follows: $H(\hat{r}=0)/a$ must be greater than, say, 0.1, and $Z(\hat{r}=0)/h$ must be less than 1.

Figure 15 and a derivative figure, figure 16, are useful in determining critical values of h/a and $\frac{\rho g h}{2}(\frac{t}{\eta})$ for domes like the Fort Rock dome. In figure 15, $H(\hat{r}=0)/a$ divided by $\sigma_o/\rho g h$ is plotted versus γ. In addition, $Z(\hat{r}=0)\cdot\frac{1}{h} / (\frac{\sigma_o}{\rho g})\cdot\frac{1}{h}$ is repeated from figure 14. Six values of $\frac{\rho g h}{2}(\frac{t}{\eta})$ are used for the plots. The limits $H(\hat{r}=0)/a > 0.1$ and $Z(\hat{r}=0)/h < 1$ are shown for two limiting values

Figure 15. Amplitude of the Magma Chamber; Dome Distortion; and Allowable Limits for the Formation of Domes like the Fort Rock Dome. Dashed curves are $(Z(\hat{r}=0)/h)\cdot(\frac{1}{\sigma_o/\rho gh})$ versus γ for various values, 0.001, 0.01, etc. of $\frac{\rho gh}{2}(\frac{t}{\eta})$. This quantity is the same as $Z(\hat{r}=0)/\frac{\sigma_o}{\rho g}$ in figure 14, which is the amplitude of the magma chamber. Solid curves are $(H(\hat{r}=0)/a)\cdot(\frac{1}{\sigma_o/\rho gh})$ versus γ for various values of $\frac{\rho gh}{2}(\frac{t}{\eta})$. This quantity is the dome distortion. For convenience, the plotted quantities are considered positive in this figure and in figure 16. Domes like the Fort Rock dome are formed in a region where $Z(\hat{r}=0)/h$ is less than 1 and $H(\hat{r}=0)/a$ is greater than 0.1, at a given relative driving pressure, $\sigma_o/\rho gh$. The allowable limits for formation of such domes are shown for two extreme values, 0.033 and 3.3, of the relative driving pressure.

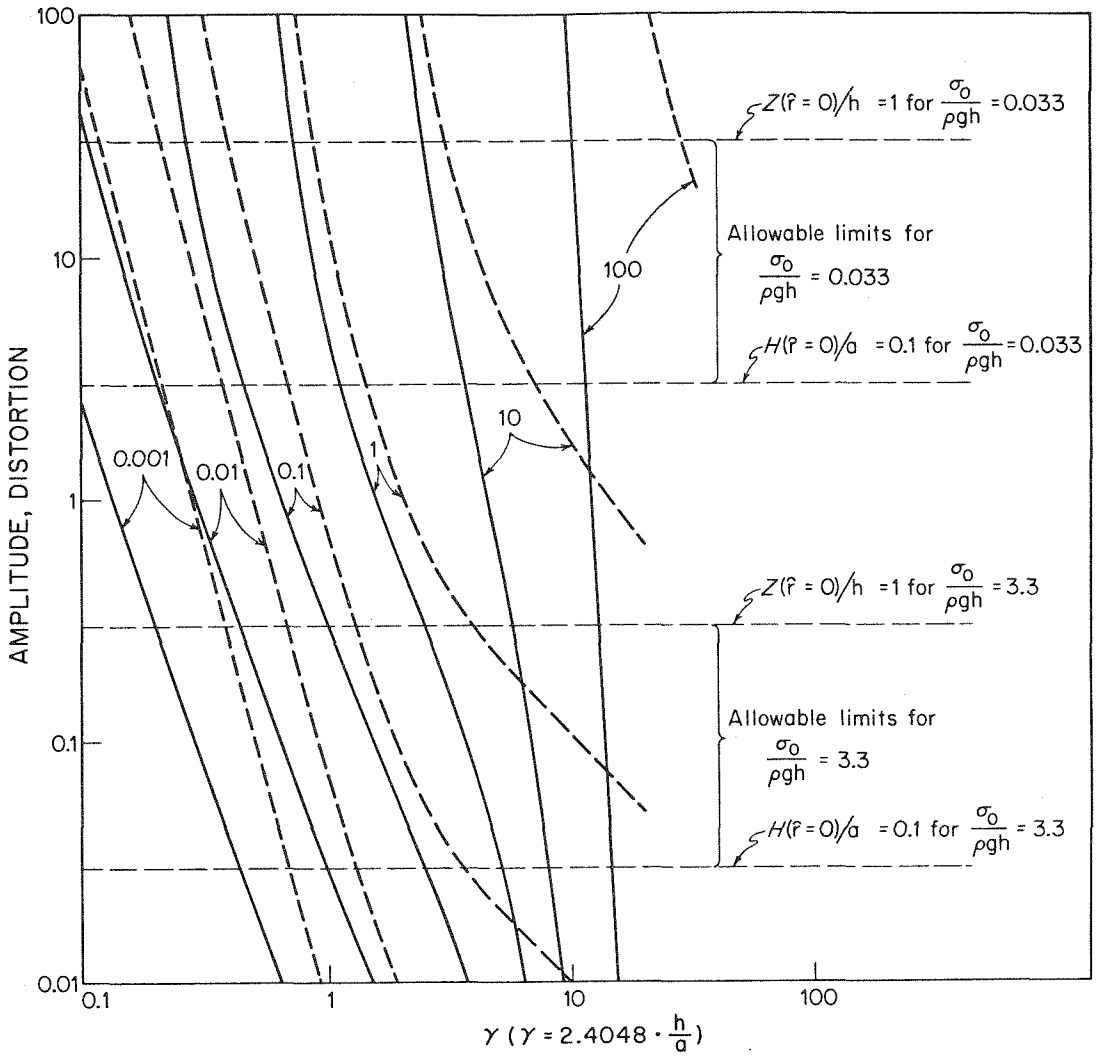
100
10
1
0.1
0.01
AMPLITUDE, DISTORTION
0.1
1
10
100
γ (γ = 2.4048 · h/a)
Z(r̂ = 0)/h =1 for σ0/ρgh =0.033
Allowable limits for σ0/ρgh = 0.033
H(r̂ = 0)/a =0.1 for σ0/ρgh =0.033
Z(r̂ = 0)/h =1 for σ0/ρgh =3.3
Allowable limits for σ0/ρgh = 3.3
H(r̂ = 0)/a =0.1 for σ0/ρgh = 3.3
0.001
0.01
0.1
1
10
100

of the relative driving stress, $\frac{\sigma_o}{\rho g h}$, 0.033 and 3.3. The limiting values of this quantity are discussed below (p. 263). Figure 16 is a reproduction of figure 15 with the elimination of all but certain segments of the curves in that figure for clarity. In addition, regions have been shaded where domes are created which satisfy the conditions that $H(\hat{r}=0)/a$ be greater than 0.1 and $Z(\hat{r}=0)/h$ be less than 1. At the lower limit of $\frac{\sigma_o}{\rho g h}$, 0.033, maximum distortions for domes of interest occur when $\frac{\rho g h}{2}(\frac{t}{\eta})$ is 1 and γ ranges from 0.9 to 1.1. Corresponding values of h/a range from 0.37 to 0.45. At the upper limit of $\frac{\sigma_o}{\rho g h}$, 3.3 maximum distortion for domes of interest has shifted to $\frac{\rho g h}{2}(\frac{t}{\eta}) = 0.1$ and $h/a = 0.55$ to 1.0 . For intermediate, reasonable values of $\frac{\sigma_o}{\rho g h}$, maximum dome distortions occur around $\frac{\rho g h}{2}(\frac{t}{\eta}) = 1$ with h/a ranging from about 0.5 to 1.5 . For example, the unshaded triangle in figure 16 represents the region of maximum dome distortion for $\frac{\sigma_o}{\rho g h} = 0.5$, which is a value used below in calculations of velocities and stresses. Here h/a ranges from .7 to 1.25 . One concludes that critical values of $\frac{\rho g h}{2}(\frac{t}{\eta})$ and h/a , or values where maximum dome distortions occur, exist near $\frac{\rho g h}{2}(\frac{t}{\eta}) = 1$ and $h/a = 1$.

The existence of critical values of $\frac{\rho g h}{2}(\frac{t}{\eta})$ and h/a can be understood as follows. For relatively thin layers, where $\frac{h}{a} << 1$, the time interval, t , during which doming occurs must be short or the fluid viscosity, η , must be high to prevent the magma from arching through the layer and violating the condition that $Z(\hat{r}=0)/h < 1$; therefore $\frac{\rho g h}{2}(\frac{t}{\eta})$ must be small. Dome distortions

Figure 16. Critical Values of h/a and $\frac{\rho g h}{2}(\frac{t}{\eta})$. This figure is a reproduction of figure 15 with parts of various curves omitted for clarity. Shaded triangles are regions where domes like the Fort Rock dome are formed at the two extreme values, 0.033 and 3.3, of the relative driving pressure, $\sigma o/\rho g h$. The unshaded triangle is a region where such domes are formed at a relative driving pressure of 0.5. Critical values of h/a and $\frac{\rho g h}{2}(\frac{t}{\eta})$ occur where triangles attain the greatest height within a given set of allowable limits for $Z(\hat{r}=0)/h$ and $H(\hat{r}=0)/a$.

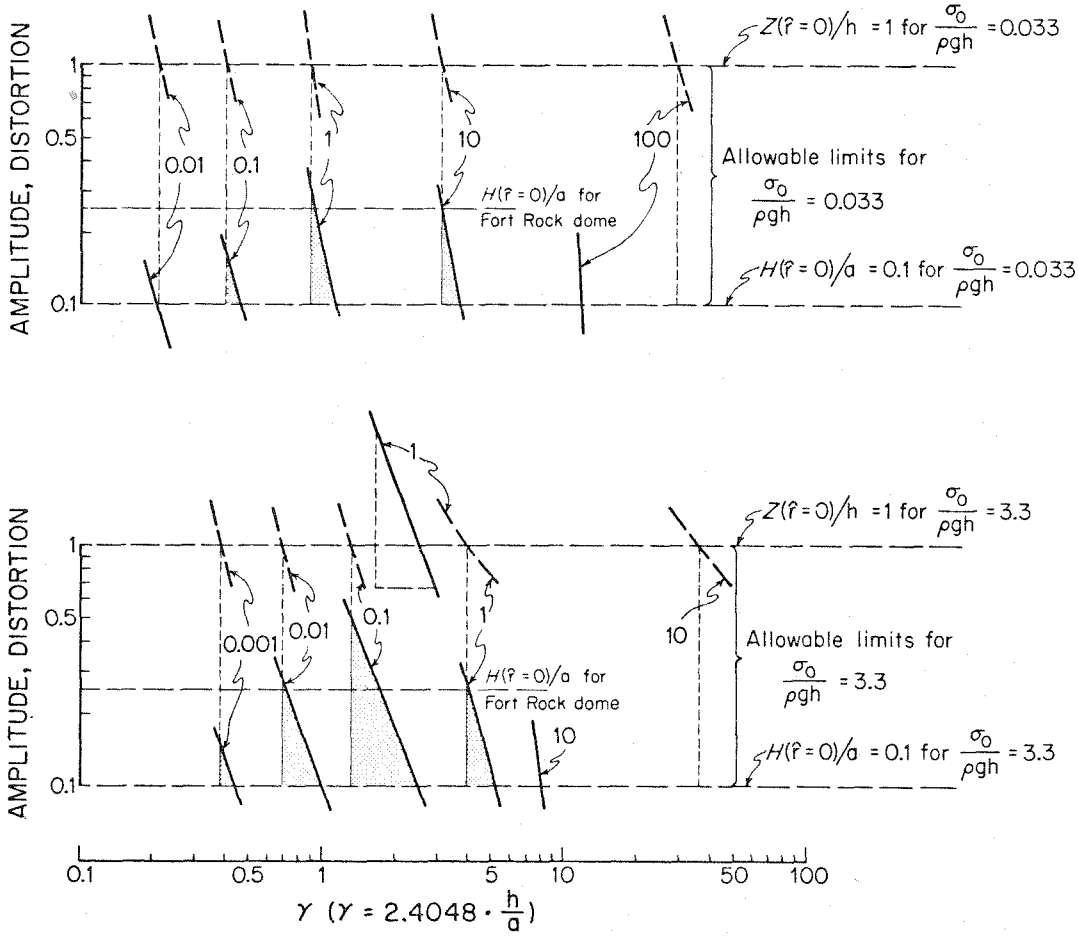
AMPLITUDE, DISTORTION
1
0.5
0.1
0.01
0.1
1
10
100
H(r̂ = 0)/a for Fort Rock dome
Z(r̂ = 0)/h = 1 for σ0/ρgh = 0.033
Allowable limits for σ0/ρgh = 0.033
H(r̂ = 0)/a = 0.1 for σ0/ρgh = 0.033
AMPLITUDE, DISTORTION
1
0.5
0.1
0.001
0.01
0.1
1
10
H(r̂ = 0)/a for Fort Rock dome
Z(r̂ = 0)/h = 1 for σ0/ρgh = 3.3
Allowable limits for σ0/ρgh = 3.3
H(r̂ = 0)/a = 0.1 for σ0/ρgh = 3.3
0.1
0.5
1
5
10
50
100
γ (γ = 2.4048 · h/a)

produced in these thin layers are small for $Z(\hat{r}=0)/h < 1$, since the shape of the dome is closely similar to that of the arched roof of the magma chamber and the latter has low distortion. For relatively thick layers, at the other extreme, where $h/a \ll 1$, the time interval, t, must be long or the viscosity, η, must be low to allow significant penetration by the magma; $\frac{\rho g h}{2}(\frac{t}{\eta})$ must, therefore, be large. Dome distortions are also small here, because a long time interval or a low viscosity permits fluid to flow away from the dome, making it flatter. Maximum dome distortions occur at intermediate values of time, viscosity, and h/a such that $\frac{\rho g h}{2}(\frac{t}{\eta}) \sim 1$ and $h/a \sim 1$. Near these critical values, factors tending to cause low dome distortions are minimized.

Since the mathematical model of doming is strictly applicable only to small values of $H(\hat{r}=0)/a$ and $Z(\hat{r}=0)/a$, there are problems with the above argument for the existence of critical values of h/a and $\frac{\rho g h}{2}(\frac{t}{\eta})$. Behavior of the model for $Z(\hat{r}=0)/h$ near 1, which is one of the limits used, may not be physically reasonable in most cases. It is possible, however, to make a strict argument for the existence of critical values of h/a and $\frac{\rho g h}{2}(\frac{t}{\eta})$ for a class of domes with much smaller dome distortions, $H(\hat{r}=0)/a$, magma-chamber amplitudes, $Z(\hat{r}=0)/h$. The limits, 0.1 and 1, appearing in the requirements, $H(\hat{r}=0)/a > 0.1$ and $Z(\hat{r}=0)/h < 1$, can be simultaneously reduced to smaller values; i.e., in figure 16, the horizontal limits

for a given value of $\frac{\sigma_o}{\rho g h}$ can be slid downward together, maintaining their original separation. It could be required, for example, that $H(\hat{r}=0)/a > 0.01$ and $Z(\hat{r}=0)/h < 0.1$ for $\frac{\sigma_o}{\rho g h} = 0.033$. The model is probably physically reasonable for these limits. Critical values of h/a and $\frac{\rho g h}{2}(\frac{t}{\eta})$ exist for these limits and are about the same as those stated above, namely $h/a \sim 1$ and $\frac{\rho g h}{2}(\frac{t}{\eta}) \sim 1$, as can be seen in figure 16. It is inferred herein, from the relative insensitivity of critical values to the movement of limits, that the values, $h/a = 1$ and $\frac{\rho g h}{2}(\frac{t}{\eta}) = 1$, are critical values for the class of domes that includes Fort Rock dome.

Gilbert (1880, p. 81 ff), using a very approximate method, came to a conclusion regarding the creation of a laccolith which is similar to one of the conclusions stated above. He concluded that a laccolith with significant distortion cannot be formed unless its diameter is of the order of the thickness of overlying rock. One of the conclusions above is that h/a has to be near 1, that is, a dome of significant distortion cannot be produced unless the magma which causes it intrudes to within one radius of the surface.

Acceleration. Figure 13 shows Ω_{H1} and Ω_{H2} to be equal. Equation (105a) may therefore be rewritten as

$$H = \frac{\sigma_o}{\rho g} J_0(\alpha_o r)\, \Omega_{H1} \cdot 2 \sinh \tau \qquad (108a)$$

or

$$H = \frac{\sigma_o}{\rho g} J_0(\alpha_o r)\, \Omega_{H1} \cdot 2 \sinh\left(\frac{\rho g h}{2}\left(\frac{G}{\gamma}\right)\frac{t}{\eta}\right) \qquad (108b)$$

All time derivatives of eq. (108b) are positive; therefore doming in the model is an accelerating process. This acceleration is caused by the fact that the driving pressure remains constant as the layer of fluid is progressively thinned by doming. The dome will continue to grow without bound unless some other process is introduced to stop it at some point. Processes for halting doming are discussed below.

Velocities and Stresses

Velocities in the deforming layer of fluid, given by (102) and (103) are shown for $\sigma_o/\rho g h = 0.5$, $h/a = 1$ and $\frac{\rho g h}{2}\left(\frac{t}{\eta}\right) = 0.1$ and 0.5 (fig. 17). Maximum vertical velocity is seen at $\hat{r} = 0$, as is expected. Maximum radial velocity is small compared to maximum vertical

Figure 17. Velocities in the Layer of Fluid. Velocity, in units of $\frac{\sigma_o h}{4\eta}$, is shown at a number of points in the deforming layer of fluid for $\frac{\rho g h}{2}(\frac{t}{\eta}) = 0.1$, indicated by O's, and $\frac{\rho g h}{2}(\frac{t}{\eta}) = 0.5$, indicated by X's. The upper and lower surfaces of the fluid are shown for these two values of $\frac{\rho g h}{2}(\frac{t}{\eta})$. In calculating velocities in this figure, values of $\frac{\sigma_o}{\rho g h} = 0.5$ and $h/a = 1.0$ were used.

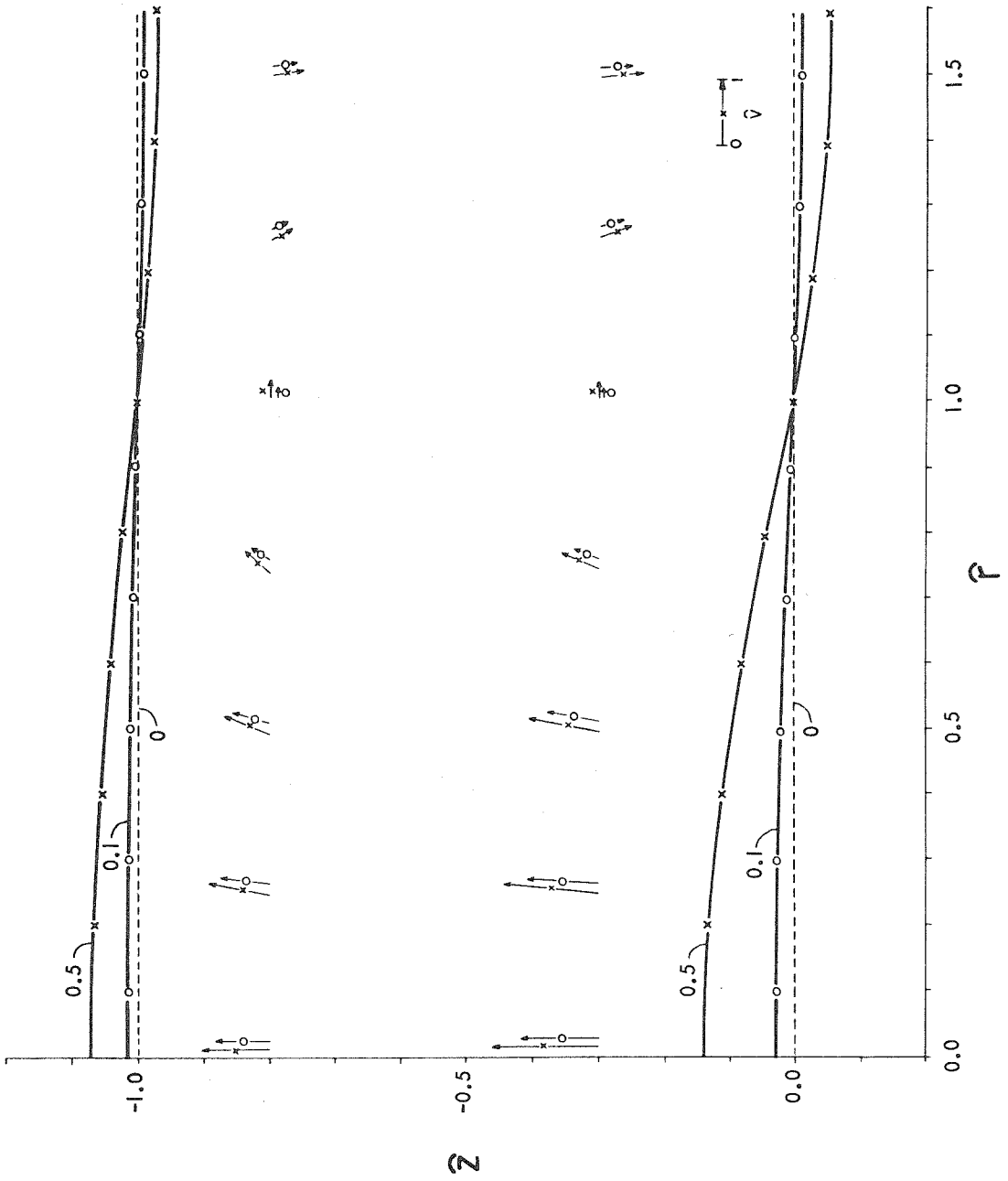
0.5
0.1
0
-1.0
-0.5
0.0
0.5
1.0
1.5
Z
r
$\hat{v}$

velocity and is realized near $\hat{r} = 0.75$. Note that velocity is purely vertical at the center of the dome and purely radial at the edge of the dome; the edge of the dome, for purposes here, is defined as $\hat{r} = 1$. Vertical velocity decreases with height whereas radial velocity increases. Both vertical and radial velocities increase with increasing $\frac{\rho g h}{2}(\frac{t}{\eta})$.

These trends in velocity can be understood in a heuristic fashion. Vertical velocity is imparted to the fluid by the upward push of the magma chamber, and a dome is created. Radial velocity arises from material flowing outward in response to gravity. This outward flow is highest laterally in the layer where slopes on the dome and magma chamber are the steepest, near $\hat{r} = 0.75$. In terms of depth within the layer, flow is highest at the surface of the dome, which is stress-free. Outward flow of material tends to reduce the height of the dome relative to the height of the magma chamber.

Gradients in the velocity components give rise to stresses (eq. (13)). Using eqs. (102) through (104) and the definitions (101a) through (101g), the stresses can be expressed,

$$
\begin{aligned}
T_{rr}/\sigma_o = & -\frac{\rho g h}{\sigma_o}(\hat{z}+1) \\
& - \frac{J_o(\alpha_o \hat{r})}{2\hat{n}_1}\Big\{\hat{P}_1\Big[e^{\tau-\gamma\hat{z}}(2-\gamma[\hat{F}_1+\hat{z}-P_3\hat{f}_2]) \\
& \qquad + e^{\tau+\gamma\hat{z}}(\gamma\hat{f}_1+P_3[2-\gamma(\hat{F}_2-\hat{z})])\Big] \\
& \qquad + \hat{P}_2\Big[e^{-\tau-\gamma\hat{z}}(2-\gamma[\hat{F}_1+\hat{z}-P_4\hat{f}_2]) \\
& \qquad\quad + e^{-\tau+\gamma\hat{z}}(\gamma\hat{f}_1+P_4[2-\gamma(\hat{F}_2-\hat{z})])\Big]\Big\}
\end{aligned}
$$

$$- \frac{J_1(\alpha_o \hat{r})}{2\hat{n}_1 \alpha_o \hat{r}} \gamma \left\{ \hat{P}_1 \left[e^{\tau-\gamma\hat{z}} (\hat{F}_1 - \frac{1}{\gamma} + \hat{z} - P_3 \hat{f}_2) \right.\right.$$
$$\left. - e^{\tau+\gamma\hat{z}} (\hat{f}_1 - P_3 [\hat{F}_2 - \frac{1}{\gamma} - \hat{z}]) \right]$$
$$+ \hat{P}_2 \left[e^{-\tau-\gamma\hat{z}} (\hat{F}_1 - \frac{1}{\gamma} + \hat{z} - P_4 \hat{f}_2) \right.$$
$$\left.\left. - e^{-\tau+\gamma\hat{z}} (\hat{f}_1 - P_4 [\hat{F}_2 - \frac{1}{\gamma} - \hat{z}]) \right] \right\} \qquad (109)$$

$$T_{\theta\theta}/\sigma_o = - \frac{\rho g h}{\sigma_o} (\hat{z} + 1)$$
$$- \frac{J_o(\alpha \hat{r})}{2\hat{n}_1} \{ \hat{P}_1 [e^{\tau-\gamma\hat{z}} + e^{\tau+\gamma\hat{z}} P_3]$$
$$+ \hat{P}_2 [e^{-\tau-\gamma\hat{z}} + e^{-\tau+\gamma\hat{z}} P_4] \}$$
$$+ \frac{J_1(\alpha_o \hat{r})}{2\hat{n}_1 \alpha_o \hat{r}} \gamma \left\{ \hat{P}_1 \left[e^{\tau-\gamma\hat{z}} (\hat{F}_1 - \frac{1}{\gamma} + \hat{z} - P_3 \hat{f}_2) \right.\right.$$
$$\left. - e^{\tau+\gamma\hat{z}} (\hat{f}_1 - P_3 [\hat{F}_2 - \frac{1}{\gamma} - \hat{z}]) \right]$$
$$+ \hat{P}_2 \left[e^{-\tau-\gamma\hat{z}} (\hat{F}_1 - \frac{1}{\gamma} + \hat{z} - P_4 \hat{f}_2) \right.$$
$$\left.\left. - e^{-\tau+\gamma\hat{z}} (\hat{f}_1 - P_4 [\hat{F}_2 - \frac{1}{\gamma} - \hat{z}]) \right] \right\} \qquad (110)$$

$$T_{zz}/\sigma_o = - \frac{\rho g h}{\sigma_o} (\hat{z} + 1)$$
$$- \frac{J_o(\alpha_o \hat{r})}{2\hat{n}_1} \gamma \left\{ \hat{P}_1 \left[e^{\tau-\gamma\hat{z}} (\hat{F}_1 + \hat{z} - P_3 \hat{f}_2) \right.\right.$$
$$\left. - e^{\tau+\gamma\hat{z}} (\hat{f}_1 - P_3 [\hat{F}_2 - \hat{z}]) \right]$$
$$+ \hat{P}_2 \left[e^{-\tau-\gamma\hat{z}} (\hat{F}_1 + \hat{z} - P_4 \hat{f}_2) \right.$$
$$\left.\left. - e^{-\tau+\gamma\hat{z}} (\hat{f}_1 - P_4 [\hat{F}_2 - \hat{z}]) \right] \right\} \qquad (111)$$

$$T_{rz}/\sigma_o = T_{zr}/\sigma_o$$

$$= \frac{J_1(\alpha_o \hat{r})}{2\hat{n}_1} \left\{ \hat{P}_1 \left[e^{\tau-\gamma\hat{z}}(1 - \gamma[\hat{F}_1 + \hat{z} - P_3\hat{f}_2]) \right.\right.$$
$$\left. - e^{\tau+\gamma\hat{z}}(\gamma\hat{f}_1 + P_3[1 - \gamma(\hat{F}_2 - \hat{z})]) \right]$$
$$+ \hat{P}_2 \left[e^{-\tau-\gamma\hat{z}}(1 - \gamma[\hat{F}_1 + \hat{z} - P_4\hat{f}_2]) \right.$$
$$\left.\left. - e^{-\tau+\gamma\hat{z}}(\gamma\hat{f}_1 + P_4[1 - \gamma(\hat{F}_2 - \hat{z})]) \right] \right\} \qquad (112)$$

These stresses are tabulated for $\sigma_o/\rho gh = 0.5$, $h/a = 1$ and $\frac{\rho gh}{2}(\frac{t}{\eta}) = 0.1$ (Table 10).

Positive values of the normal stresses, T_{rr}, $T_{\theta\theta}$, and T_{zz}, refer to tension and negative values to compression (fig. 18). Positive values of T_{rr}, radial stress, and $T_{\theta\theta}$, tangential stress, are encountered in lens-shaped regions which underlie the surface of the dome (Table 10). The positive-T_{rr} region has a radius of between $\hat{r} = 0.75$ and $\hat{r} = 1.00$; the positive-$T_{\theta\theta}$ region has a radius between $\hat{r} = 1.00$ and $\hat{r} = 1.25$. Both regions reach depths at their centers of nearly three-tenths of the distance to the original base of the layer. (Note that $\hat{z} = 0.0$ and $\hat{z} = -1.0$ in Table 10 do not refer to the roof of the magma chamber and the surface of the dome. The latter surfaces are shown in figure 17. A maximum value of T_{rz}, which is a shear stress, is seen in the vicinity of $\hat{r} = 0.75$. Equations (22) and (24) require, of course, that T_{rz} be zero on the surfaces $\hat{z} = 0.0$ and $\hat{z} = -1.0$ such that the maximum value of this stress occurs deep within the layer of fluid.

TABLE 10. Stresses in the Layer of Fluid. Note that $\hat{z}$ and $\hat{r}$ are normalized coordinates in a fixed coordinate system (fig. 12). The top of the layer of fluid was initially at $\hat{z} = -1.0$; the bottom was initially at $\hat{z} = 0.0$. The configuration of the dome for parameter values, $\frac{2}{3}\rho gh(t/\eta) = 0.1$, $\sigma_o/\rho gh = 0.5$, and $h/a = 1$, can be seen in fig. 17. These values were used in calculating the stresses tabulated below. $\hat{r} = 1.5933$ is the radius of the first trough of the Bessel function, J_o, which describes the shape of the dome.

T_{rr}/σ_o

$\hat{z}$ \ $\hat{r}$ →	0.0 (center of dome)	0.25	0.5	0.75	1.0 (edge of dome)	1.25	1.5	1.59333 (center of trough)
-1.0	0.82096	0.73542	0.50250	0.18622	-0.12820	-0.35553	-0.45394	-0.45024
-0.9	0.37436	0.31378	0.14890	-0.07483	-0.29686	-0.45963	-0.52497	-0.52171
-0.8	-0.01843	-0.04026	-0.17401	-0.32798	-0.48002	-0.59012	-0.63198	-0.62833
-0.7	-0.37756	-0.40462	-0.47794	-0.57658	-0.67776	-0.74022	-0.76206	-0.75745
-0.6	-0.72067	-0.77489	-0.77318	-0.82374	-0.87108	-0.90083	-0.90418	-0.89825
-0.5	-1.06412	-1.06570	-1.06939	-1.07242	-1.07137	-1.06357	-1.04819	-1.04076
-0.4	-1.42469	-1.41156	-1.37647	-1.32572	-1.27004	-1.21994	-1.18380	-1.17484
-0.3	-1.82092	-1.77013	-1.70533	-1.63703	-1.46302	-1.36064	-1.29957	-1.28926
-0.2	-2.27470	-2.21970	-2.06561	-1.96023	-1.84537	-1.47425	-1.38184	-1.37058
-0.1	-2.81323	-2.72480	-2.48275	-2.14996	-1.81070	-1.54649	-1.41335	-1.40189
0.0	-3.47124	-3.33624	-2.96729	-2.46189	-1.95048	-1.55844	-1.37172	-1.36126

$T_{\theta\theta}/\sigma_o$

$\hat{z}$ \ $\hat{r}$ →								
-1.0	0.82096	0.76145	0.64747	0.36855	0.12821	-0.07080	-0.10043	-0.21106
-0.9	0.37436	0.33346	0.22067	0.08296	-0.10311	-0.24143	-0.32584	-0.34099
-0.8	-0.01843	-0.04901	-0.11473	-0.21417	-0.31998	-0.40990	-0.44751	-0.47903
-0.7	-0.37759	-0.39934	-0.42405	-0.47311	-0.52724	-0.57637	-0.61252	-0.62171
-0.6	-0.72067	-0.72046	-0.72053	-0.72265	-0.72892	-0.74076	-0.75809	-0.76565
-0.5	-1.06412	-1.05121	-1.01652	-0.97091	-0.92863	-0.90282	-0.90148	-0.90759
-0.4	-1.42469	-1.39774	-1.32458	-1.22612	-1.12694	-1.06224	-1.03994	-1.04417
-0.3	-1.82092	-1.77734	-1.65665	-1.48741	-1.33698	-1.21572	-1.17005	-1.17169
-0.2	-2.27470	-2.21049	-2.03520	-1.79571	-1.65463	-1.37204	-1.28859	-1.28594
-0.1	-2.81323	-2.72263	-2.47483	-2.13475	-1.78631	-1.52240	-1.39137	-1.38124
0.0	-3.47124	-3.34039	-3.00397	-2.53232	-2.04952	-1.67017	-1.47351	-1.45364

T_{zz}/σ_o

$\hat{z}$ \ $\hat{r}$ →								
-1.0	-0.06996	-0.06360	-0.04680	-0.02360	-0.00000	0.01831	0.02742	0.02814
-0.9	-0.25885	-0.25012	-0.22622	-0.23340	-0.20300	-0.17409	-0.16121	-0.16019
-0.8	-0.57446	-0.55804	-0.51687	-0.45895	-0.40000	-0.35428	-0.33153	-0.32974
-0.7	-0.88312	-0.85810	-0.78967	-0.69566	-0.60000	-0.52580	-0.48889	-0.48597
-0.6	-1.21452	-1.17730	-1.07773	-0.94006	-0.80000	-0.69136	-0.63732	-0.63305
-0.5	-1.56006	-1.51068	-1.37520	-1.14923	-1.00000	-0.85321	-0.78021	-0.77443
-0.4	-1.91135	-1.84850	-1.67655	-1.44035	-1.20000	-1.01356	-0.92083	-0.91350
-0.3	-2.25879	-2.18232	-1.97553	-1.69017	-1.40000	-1.17402	-1.06297	-1.05412
-0.2	-2.58693	-2.50248	-2.26316	-1.93449	-1.60000	-1.34055	-1.21150	-1.20130
-0.1	-2.88754	-2.79144	-2.52657	-2.18746	-1.80000	-1.51467	-1.37320	-1.36198
0.0	-3.12713	-3.02755	-2.75509	-2.38084	-2.00000	-1.70459	-1.55756	-1.54604

T_{rz}/σ_o

$\hat{z}$ \ $\hat{r}$ →								
-1.0	0.0	-0.00000	-0.00000	-0.00000	-0.00000	-0.00000	-0.00000	-0.00000
-0.9	0.0	0.08659	0.11393	0.13281	0.11855	0.07691	0.02111	0.00000
-0.8	0.0	0.11235	0.19515	0.22749	0.20307	0.13174	0.03616	0.00000
-0.7	0.0	0.14519	0.25219	0.29394	0.26242	0.17025	0.04673	0.00000
-0.6	0.0	0.16702	0.29011	0.33218	0.30188	0.19585	0.05375	0.00000
-0.5	0.0	0.17888	0.31070	0.36241	0.32351	0.20988	0.05760	0.00000
-0.4	0.0	0.18052	0.31356	0.36552	0.32629	0.21168	0.05810	0.00000
-0.3	0.0	0.16624	0.28896	0.34247	0.30589	0.19845	0.05447	0.00000
-0.2	0.0	0.14065	0.24431	0.28479	0.25422	0.16493	0.04527	0.00000
-0.1	0.0	0.08770	0.15233	0.17767	0.15851	0.10283	0.02822	0.00000
0.0	0.0	-0.00000	-0.00000	-0.00000	-0.00000	-0.00000	-0.00000	-0.00000

Figure 18. Definition of Stresses in a Cylindrical Coordinate System. Stresses are drawn in their positive directions on an element of volume. Stresses, $T_{\theta r}$, $T_{r\theta}$, $T_{\theta z}$, and $T_{z\theta}$, which are not encountered in the model, are omitted. The downward direction in the model is toward the top of the page.

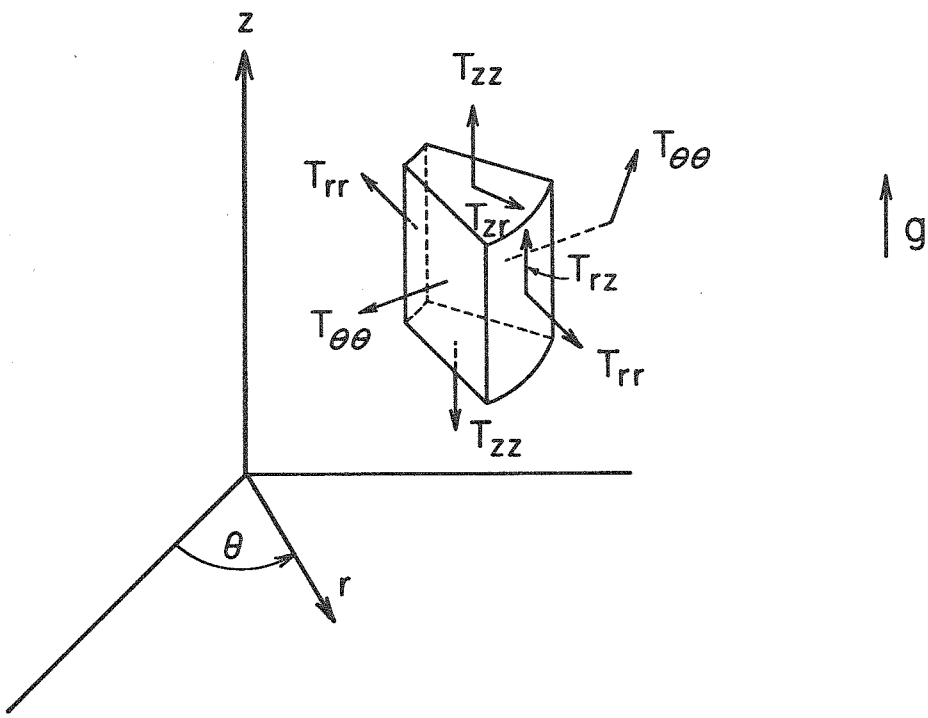
z
T_{zz}
$T_{\theta\theta}$
T_{rr}
T_{zr}
T_{rz}
$T_{\theta\theta}$
T_{rr}
T_{zz}
g
θ
r

The stress distribution given in Table 10 can be used to determine planes of maximum shear in the layer of fluid. "Shear" is used here to mean the derivative of velocity with respect to distance. Since shear in a given plane is proportional to shear stress across that plane, it is sufficient to determine planes of maximum shear stress. It can be shown (Anderson, 1942, p. 9; Jaeger, 1956, p. 17) that planes of maximum shear stress are inclined at angles of 45^{o} to the directions of the maximum and minimum principal stresses. To find these planes, it is therefore necessary to convert the stresses given in Table 10 to principal stresses.

Let Cartesian coordinates, x, y, and z, be referred to an origin at a point, O , in a medium, and let T_{xx}, T_{yy}, etc. be components of a Cartesian stress tensor in this coordinate system. At O, one can define a stress quadric given by (Bullen, 1963, p. 11)

$$T_{xx}x^2 + T_{yy}y^2 + T_{zz}z^2 + 2T_{xy}xy + 2T_{xz}xz + 2T_{yz}yz = \text{constant} \quad (113)$$

The form of this equation does not change upon rotation of the coordinate axes (Bullen, loc. cit.); i.e., when x, y, and z are changed to x', y', and z' , T_{xx}, T_{yy}, etc. are changed to $T_{x'x'}$, $T_{y'y'}$, etc. It follows from the theory of quadric surfaces (Thomas, 1961, p. 492,ff) that a rotation of coordinate axes can be found whereby the coefficients of the cross terms, namely $2T_{xy}$, $2T_{xz}$, and $2T_{yz}$, are zero. The stresses described in this particular coordinate system are purely normal stresses and are called principal stresses.

In the coordinate system used in the model, stresses, T_{rr}, $T_{\theta\theta}$, T_{zz}, and T_{rz}, encountered at point 0, which we locate in the plane $\theta = 0$ (fig. 19), are identical to Cartesian stresses, T_{xx}, T_{yy}, T_{zz}, and T_{xz}, respectively, described in a coordinate system located at 0 with the x-axis lying in the plane $\theta = 0$, the y-axis perpendicular to this plane, and the z-axis parallel to the z-axis in the model. In the plane $\theta = 0$, one can thus write

$$T_{rr}x^2 + T_{\theta\theta}y^2 + T_{zz}z^2 + 2T_{rz}xz = \text{constant} \tag{114}$$

The coordinate rotation, $x,y,z \rightarrow x',y',z'$ required to eliminate the T_{rz} cross term is about the y-axis, since there are no cross terms involving the y coordinate. This rotation has a magnitude, α, given by (Thomas, 1961, p. 493)

$$\tan 2\alpha = \frac{2T_{rz}}{T_{rr} - T_{zz}} \tag{115}$$

The principal stresses are (Thomas, loc. cit.)

$$T_{rr}\cos^2\alpha + 2T_{rz}\cos\alpha \sin\alpha + T_{zz}\sin^2\alpha \tag{116a}$$

$$T_{rr}\sin^2\alpha - 2T_{rz}\sin\alpha \cos\alpha + T_{zz}\cos^2\alpha \tag{116b}$$

$$T_{\theta\theta} \tag{116c}$$

If we denote by P the algebraically largest of the principal stresses, by R the algebraically smallest of the principal stresses, and by S the maximum shear stress, then it can be shown (Anderson, 1942, p. 9) that

Figure 19. Coordinate System Used to Describe Principal Stresses in the Layer of Fluid. Note that the downward direction in the model is toward the top of the page.

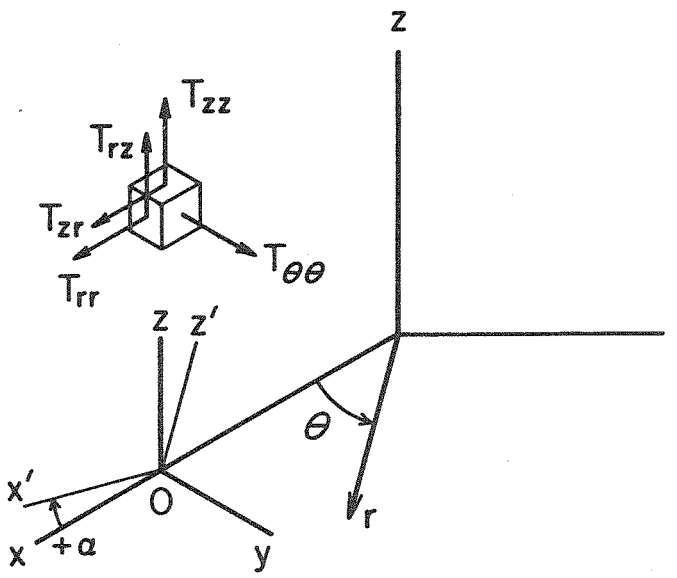
z
T_{zz}
T_{rz}
T_{zr}
$T_{\theta\theta}$
T_{rr}
z z′
θ
x′
O
x +α
y
r


g

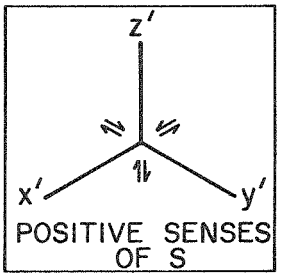
z′
x′
y′
POSITIVE SENSES
OF S

$$S = \frac{P - R}{2} \tag{117}$$

The planes on which maximum shear stress, S , are encountered are parallel to the direction of the intermediate principal stress and are inclined at 45^{o} to the directions of the maximum and minimum principal stresses, P and R .

Using values of T_{rr}, $T_{\theta\theta}$, T_{zz}, and T_{rz} from Table 10 in eqs. (115) through (117), one obtains values for α and S which are shown in Table 11. Positive senses of α and S are indicated in figure 19. The direction of the intermediate principal stress axis is also shown in Table 11. The numeral 1 indicates it is parallel to the x'-axis; 2 indicates it is parallel to the y'-axis, and 3 indicates it is parallel to the z'-axis. The combination, 1 2, indicates that principal stresses in the x'- and y'-directions are equal.

It is apparent from Table 11, that the principal-stress system is oriented parallel to the coordinate system of the model at $\hat{r} = 0$, which is the center of the dome, and on the horizons $\hat{z} = 0.0$ and $\hat{z} = -1.0$, which are near the bottom and top of the layer of fluid. Elsewhere in the layer, the principal-stress system departs from this orientation by an angle which becomes successively larger in a radial direction. At $\hat{r} = 1.0$, which is the edge of the dome, this angle exceeds 45^{o} everywhere except very near the base of the layer.

Maximum shear stress is highest at the point ($\hat{r} = 0$, $\hat{z} = -1.0$), which is near the top of the dome. On the horizon, $\hat{z} = -1.0$, the maximum shear stress decreases from its highest value at $\hat{r} = 0$ to a minimum at the edge of the dome. At horizons deeper than $\hat{z} = -0.8$,

TABLE II. Inclination , α, of Principal Stress System; Maximum Shear Stress, S/σ_o; and Direction of Shear Planes in Principal Stress System. α, S/σ_o, and direction of shear planes are calculated from stresses given in Table 10.

ζ ⟶	0.0 (center of dome)	0.25	0.5	0.75	1.0 (edge of dome)	1.25	1.5	1.59333 (center of trough)
Inclination ,α, of principal stress system (degrees)								
-1.0	0.0	0.001	0.001	0.004	89.994	89.999	90.000	90.000
-0.9	0.0	6.128	14.381	29.581	56.113	75.844	86.690	90.000
-0.8	0.0	12.126	24.351	36.970	50.573	65.915	83.233	89.999
-0.7	0.0	16.316	29.141	39.276	48.946	61.100	80.557	89.999
-0.6	0.0	18.509	31.154	40.121	48.357	59.068	79.029	89.999
-0.5	0.0	19.411	31.906	40.422	48.147	58.308	78.368	89.999
-0.4	0.0	19.796	32.214	40.544	48.063	57.996	78.080	89.999
-0.3	0.0	20.376	32.667	40.721	47.941	57.538	77.639	89.998
-0.2	0.0	22.425	34.153	41.286	47.549	56.032	76.005	89.998
-0.1	0.0	34.565	40.723	43.589	45.966	49.356	62.713	89.995
0.0	0.0	89.998	89.995	89.984	0.023	0.005	0.001	0.000
Maximum shear stress, S/σ_o								
-1.0	0.44539	0.41256	0.32212	0.19607	0.12820	0.18891	0.24067	0.23918
-0.9	0.33661	0.31531	0.25805	0.18587	0.13670	0.16217	0.18311	0.18076
-0.8	0.27801	0.27353	0.25975	0.23672	0.20697	0.17681	0.15452	0.14530
-0.7	0.25277	0.26924	0.29647	0.29995	0.26493	0.20120	0.14435	0.13574
-0.6	0.24693	0.27742	0.32764	0.34315	0.30367	0.22210	0.14385	0.13260
-0.5	0.24797	0.28551	0.34646	0.36709	0.32548	0.23476	0.14585	0.13316
-0.4	0.24333	0.28325	0.34761	0.36999	0.32816	0.23550	0.14375	0.13067
-0.3	0.21893	0.25925	0.32348	0.34653	0.30751	0.21910	0.13024	0.11757
-0.2	0.15761	0.19543	0.26293	0.28720	0.25523	0.17796	0.09645	0.08464
-0.1	0.03716	0.09382	0.15404	0.17778	0.15860	0.10403	0.03464	0.01995
0.0	-0.17203	-0.15935	-0.17442	-0.07573	-0.04952	0.07297	0.09296	0.09238
Direction of shear planes in principal stress system								
-1.0	12	1	1	1	1	2	2	2
-0.9	12	1	1	1	1	2	2	2
-0.8	12	2	2	2	2	2	2	2
-0.7	12	2	2	2	2	2	2	2
-0.6	12	2	2	2	2	2	2	2
-0.5	12	2	2	2	2	2	2	2
-0.4	12	2	2	2	2	2	2	2
-0.3	12	2	2	2	2	2	2	2
-0.2	12	2	2	2	2	2	2	2
-0.1	12	2	2	2	2	2	2	2
0.0	12	3	3	3	3	2	2	2

normal shear | reverse shear

maximum shear stress increases from $\hat{r} = 0$ to a maximum near $\hat{r} = 0.75$.

Shear planes are parallel to the x'-direction in a lens-shaped region underlying the surface of the dome and extending somewhat beyond $\hat{r} = 1.0$ and somewhat below $\hat{z} = -0.9$. Near the center of the dome, where the x'-direction plunges shallowly, these planes have a more or less radial strike and a dip of a little more than 45^{o}. At the edge of the dome, where the x'-direction plunges steeply, they have subradial strikes and steep dips. Everywhere beyond the lens-shaped region, except near the base of the fluid, the shear planes are parallel to the y'-direction. These planes have tangential strikes and shallow to steep dips.

Senses of displacement on the planes of shear can be determined by referring to figure 19. On planes parallel to the x'-direction, shear is a mixture of strike-slip and dip-slip relative motion. The sense of displacement is such that for positive S and α less than 90^{o} the downthrown side is away from the center of the dome and the dip-slip component represents normal shear; the terms normal and reverse are used here as they are in describing faults. On planes parallel to the y'-direction, shear is purely dip-slip. The sense of displacement is such that on the steeper-dipping of the conjugate shear planes, the downthrown side is away from the center of the crater for positive S and for α less than 90^{o}. On both conjugate shear planes the shear is normal for positive S and α less than 45^{o}; it is reverse for positive S and α between 45^{o} and 90^{o}. Planes parallel to the z'-direction occur only in a thin lens-shaped region at the horizon,

$z = 0.0$ and are not of interest in this discussion. In Table 11 a line has been drawn to separate the region of normal shear from the region of reverse shear beneath the dome.

The following summarizes shear in the model:

a) The highest shear occurs near the top of the dome. At lower horizons, maximum shear occurs near $\hat{r} = 0.75$.

b) Shear planes which have radial to subradial strikes, and dips steeper than 45^{o} are seen in a lens-shaped region underlying the surface of the dome. Shear planes in deeper regions and those in the region beyond the dome have tangential strikes and shallow to steep dips.

c) Senses of displacement on all shear planes with dips greater than 45^{o} are such that the downthrown side is away from the center of the dome.

d) The region from the center of the dome to the edge of the dome is characterized by normal shear; whereas the region beyond the edge of the dome is characterized by reverse shear.

PROCESSES FOR HALTING DOMING

In the model, doming continues at an accelerating rate. Acceleration is caused by the fact that the pressure applied to the base of the layer is constant as the layer is thinning above it. There are at least two processes by which the pressure applied by the magma can be made to decrease, with the result that doming is decelerated or halted completely. These processes are the formation of a vent and the solidification of the magma.

Formation of a Vent

Let us examine pressures encountered in two different cases, Case I and Case II, where a magma fills a cylindrical chamber in Precambrian rock (fig. 20). In Case I, the chamber is completely surrounded by Precambrian rock; in Case II, the chamber is connected by a tube to the surface. In both cases the wall of the cylinder is considered to be infinitely rigid, such that all interaction between magma and Precambrian rock takes place at the top and bottom of the cylinder. In Case I, the stress, T_{zz}, at the top of the magma chamber, $z = 0$, can be written (eq. (13))

$$T^p_{zz}(z=0) = -\rho_p g h + T^p_{zz}{}'(z=0) \tag{118a}$$

$$T^m_{zz}(z=0) = -\sigma \tag{118b}$$

where superscripts and subscripts p and m refer to Precambrian rocks and magma, respectively. $T^p_{zz}{}'$ includes all non-hydrostatic stresses. At the bottom of the magma chamber, $z = \ell$,

$$T^p_{zz}(z=\ell) = -\rho_p g(\ell+h) + T^p_{zz}{}'(z=\ell) \tag{119a}$$

$$T^m_{zz}(z=\ell) = -(\sigma + \rho_m g \ell) \tag{119b}$$

Equating stresses at the top of the magma chamber

$$\sigma = \rho_p g h - T^p_{zz}{}'(z=0) \tag{120}$$

Comparing this equation with (21) and (87), it is clear that

Figure 20. Cylindrical Magma Chambers in Precambrian Rock. Case I, unvented; Case II, vented.

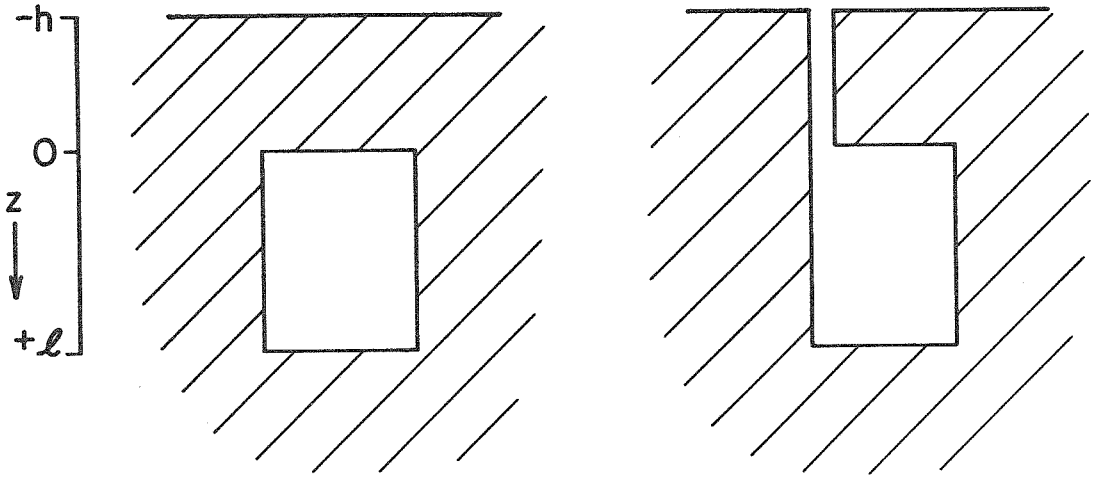

Case I

Case II

$$\sigma_o = -T^{p}_{zz}{}'(z=0) \tag{121}$$

where dependence on radius is ignored in this treatment. Equating stresses at the bottom of the magma chamber,

$$\sigma = g\ell(\rho_p - \rho_m) + \rho_p gh - T^{p}_{zz}{}'(z=\ell) \tag{122}$$

Let

$$\sigma_\ell \equiv -T^{p}_{zz}{}'(z=\ell) \tag{123}$$

Substituting eqs. (120), (121),and (123) into (122) gives

$$\sigma_o = g\ell(\rho_p - \rho_m) + \sigma_\ell \tag{124}$$

Owing to the fact that the magma is buoyed upward, $T^{p}_{zz}{}'(z=\ell)$ will be a tensile, or positive stress; by eq. (123) σ_ℓ will be negative. The maximum value σ_o can have is therefore,

$$\sigma_{o_{max}} = g\ell(\rho_p - \rho_m) \tag{125}$$

As rock strength in tension is considerably lower than rock strengthin compression, equilibration is likely to take place more rapidly at the bottom of the magma chamber than at the top, and σ_ℓ will remain small. Equation (125) is, therefore, probably a good approximation to σ_o.

In Case II, flow of magma through a tube to the surface is permitted. This flow is considered to be inviscid. Velocities in the magma are assumed to be small compared to velocities in the tube, and the magma can be treated hydrostatically. Bernoulli's equation

requires that

$$\sigma = \frac{1}{2}\rho_m v^2 + \rho_m gh \tag{126}$$

where v is the velocity of the magma as it leaves the vent. Substituting this expression in (120) and (122) and using (121) and (123) gives

$$\sigma_o = -gh(\rho_p - \rho_m) + \frac{1}{2}\rho_m v^2 \tag{127}$$

$$\sigma_\ell = -g(h+\ell)(\rho_p - \rho_m) + \frac{1}{2}\rho_m v^2 \tag{128}$$

The eruption velocity, v, will drop at a rate determined by the size of the vent and how fast the walls of the magma chamber collapse inward to maintain the flow. The rate of collapse is determined by the viscosity of the Precambrian rock and the pressures σ_o and σ_ℓ. Hypothetical graphs of σ_o and σ_ℓ versus time have been constructed (fig. 21), assuming that σ_ℓ is initially zero and that v falls off smoothly with time after formation of a vent at $t = t_o$. Two examples are given, example A and example B. For the curves of example A, the velocity is presumed to drop rapidly after formation of a vent owing to either a large vent opening or a slow rate of collapse of the magma chamber. Equations (127) and (128) predict sharp drops in both σ_o and σ_ℓ in this case. These pressures will conceivably level off at a point in time where the collapse of the magma chamber, which these pressures induce, can maintain a constant flow out of the tube. Doming will continue, although at a lesser acceleration than previously, until time t_1, after which collapse, corresponding to a negative value of

Figure 21. Hypothetical Graphs of σ_o and σ_ℓ Versus Time. A vent is formed at t_o; the vent is closed at t_2. See text for further explanation.

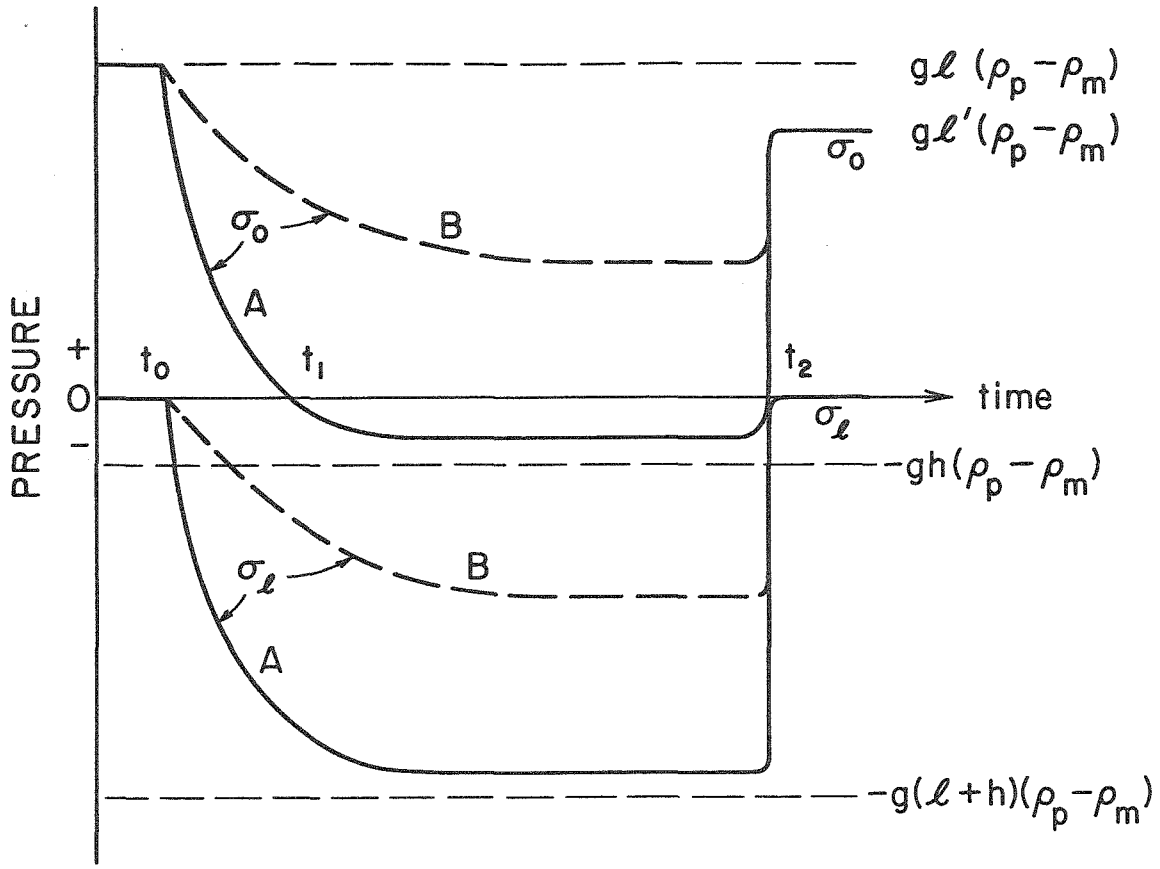
PRESSURE
+
0
-
t_0
t_1
t_2
time
$g\ell\ (\rho_p-\rho_m)$
$g\ell'(\rho_p-\rho_m)$
σ_0
σ_0
B
A
σ_ℓ
$-gh(\rho_p-\rho_m)$
σ_ℓ
B
A
$-g(\ell+h)(\rho_p-\rho_m)$

σ_o , will occur. For curves of example B, the velocity drops much less rapidly than for curves of example A, owing to either a small vent opening or a high rate of collapse of the magma chamber. Doming will continue indefinitely in this case at an acceleration less than acceleration prior to venting. In both examples A and B, σ_ℓ is negative and would induce collapse of the base of the magma chamber. Although the wall of the magma chamber has been considered rigid for the sake of analysis, it too will presumably collapse.

At time t_2 (fig. 21), the vent is closed and pressures will rise to their pre-vent values again with the exception that

$$\sigma_o = g\ell'(\rho_p - \rho_m)$$

where ℓ' is less than ℓ owing to magma loss through the vent. Doming will continue for t greater than t_2, but at a somewhat lesser acceleration than prior to venting.

If the flow of the magma through the vent tube is viscous, backpressure in the tube due to magmatic viscosity would supplant dynamic backpressure, $\frac{1}{2}\rho v^2$, and would presumably lead to slower drops in pressures after venting than those discussed above (fig. 21).

Solidification of the Magma

If the density difference $(\rho_p - \rho_m)$ in eq. (125) decreases, σ_o will decrease. It can be shown that if the density of the crystallized magma is about equal to the density of the Precambrian rocks, then

$$(\rho_p - \rho_m) \simeq \frac{\rho_c f_\ell}{\rho_\ell/(\rho_c - \rho_\ell) + f_\ell} \simeq \frac{\rho_c}{\rho_\ell}(\rho_c - \rho_\ell)\, f_\ell \qquad (129)$$

where ρ_c is the density of the crystallized magma, ρ_ℓ is the density of the liquid magma, and f_ℓ is the fraction of the mass of the magma which is liquid. (The quantity $(\rho_c - \rho_\ell)/\rho_\ell$ will be less than about 0.1). According to (125) and (129), σ_o is roughly proportional to the fraction of the magma which is liquid.

The time required to crystallize a magma gives an upper limit on the duration of doming. In order to calculate the time required for crystallization, suppose that crystallization proceeds inward from the walls of the magma chamber. The magma chamber will be modeled as a dike of half-width equal to its radius. A dike will, of course, cool more slowly than a cylindrical magma chamber; hence, the following calculation should give an exaggerated upper limit on the time involved in cooling. If the country rock is initially at zero temperature and the magma is intruded at its melting point and does not convect, then the interface $X(t)$ between the crystal growth on the wall and the liquid magma moves (Carslaw and Jaeger, 1959, p. 288-89) as

$$X = 2\lambda(\kappa t)^{1/2} \tag{130}$$

where λ is given by

$$\lambda e^{\lambda^2}(1 + \operatorname{erf} \lambda) = \frac{c\,\theta_m}{L\pi^{1/2}} \tag{130a}$$

assuming thermal properties of the country rock and solidified magma are similar. In these equations, κ and c are, respectively, the thermal diffusivity and specific heat of the country rock; L is the latent heat of fusion of the magma; θ_m is the temperature of the magma; and

t is time. Choosing values of

$$X = 1 \text{ km}$$

$$\kappa = 0.01 \text{ cm}^2/\text{sec}$$

$$c = 0.20 \text{ cal/g}$$

$$L = 100 \text{ cal/g}$$

$$\theta_m = 1000^{\circ}\text{C}$$

it is found that λ is about 0.5 (Carslaw and Jaeger, 1959, Fig. 38) and that

$$t = 31{,}700 \text{ years}$$

This time will be somewhat high for the magma beneath Fort Rock dome for three reasons. The first involves the simplified geometry assumed in this heat-flow model, as was mentioned above. The second is the probability that the magma was convecting rather than static and was hence able to transfer heat more rapidly. The third is the possibility that solidification took place by crystal settling rather than by outward growth of crystals from the walls. In the latter case temperature gradients adjacent to the magma would be higher and heat conduction faster than would be the case if a growing layer of crystals intervened between the magma and wall rock. (See Irvine, 1970, p. 1059). The above considerations would probably not change t by as much as an order of magnitude, however.

EXAMINATION OF THE FORT ROCK DOME IN LIGHT OF THE MODEL

Dimensions and Volumes of the Dome and Magma Chamber

The uplift map (fig. 6) shows the amplitude of the dome to be about 900 feet or about 0.25 kilometer. The average radius is about 3500 feet, or a little over 1 kilometer. The volume of uplifted rock in the dome, as calculated from this map is 0.19 cubic miles or 0.79 cubic kilometers.

The only actual measurement of the magma chamber that can be made is a lower limit on its volume. The Fault Canyon flow is interpreted as an extruded part of this magma. The volume of this flow calculated from Maps 8 and 9 (fig. 9) is 0.019 cubic miles. An estimated additional volume of 0.003 cubic miles lies to the southeast of the area covered by Maps 8 and 9. The total volume of this flow is thus estimated to be 0.022 cubic miles, or about 0.092 cubic kilometers.

Limits can also be set on the dimensions of the magma chamber using the mathematical model and geologic considerations. It was noted earlier (fig. 14) that the amplitude of the dome is always smaller than the amplitude of the arched roof of the magma chamber. For a dome and magma chamber with the same radii, then, the volume of uplifted rock in the dome will always be smaller than the volume of magma occupying the arched roof region of the magma chamber. Assuming the radii of Fort Rock dome and its underlying magma chamber are similar, the volume of uplifted rock in the dome should be a lower limit on the

volume of magma in the chamber below. This limit, 0.79 cubic kilometers, is about ten times higher than the limit previously set by measuring the volume of the extruded rock. Assuming the magma chamber is cylindrical and that its radius is 1 kilometer, its minimum length, ℓ, corresponding to a lower limit on its volume of 0.79 cubic kilometers, is 0.25 kilometer. The thickness of the earth's crust in this area would presumably represent the maximum length this magma chamber could have. The crustal thickness can be calculated from the depth and dip of the Moho discontinuity at Seligman, Arizona (Johnson, 1967); the thickness is around 33 kilometers at Fort Rock dome.

Limits on the distance of the magma chamber below the present land surface can be inferred from the model. Using the dimensions of the dome stated above, $H(\hat{r}=0)/a$ for the dome is $\frac{900 \text{ feet}}{3500 \text{ feet}}$ or about 0.25. Referring to figure 16, the maximum and minimum values of γ for this distortion are 3.0 and 0.7 and occur at the upper limit, $\sigma_o/\rho gh = 3.3$. These values of γ correspond to values of h/a of 1.25 km and 0.29 km. As the amplitude of the arched roof of the magma chamber is always greater than the amplitude of the dome, Z must be greater than 900 feet or 0.25 kilometer. This minimum value of Z subtracted from the maximum layer thickness, gives 1 kilometer as the greatest distance below the original land surface at which one will encounter the magma chamber at Fort Rock dome. Using an elevation of 5000 above sea level as the elevation of the original (pre-dome) land surface (fig. 9, Map 7), the minimum elevation of the top of the magma chamber is presently 1700 feet above sea level. The top of

the magma chamber may, of course, be encountered at any elevation up to that of the original land surface, (or, for that matter, at any elevation below the present surface). In cross section B-B' (pl. 2), the top of the magma is pictured at an elevation of 3500 feet.

Driving Pressure

The relative driving pressure, $\sigma_o/\rho gh$, can be expressed, using eq. (124) and assuming σ_ℓ is small, as

$$\frac{\sigma_o}{\rho_p gh} \simeq \left(\frac{\rho_p - \rho_m}{\rho_p}\right) \frac{\ell}{h} \qquad (131)$$

where, as before, the subscripts p and m refer to Precambrian rocks and magma, respectively. In evaluating this expression, 2.84 grams per cubic centimeter is chosen for ρ_p, and 2.54 grams per cubic centimeter is chosen for ρ_m. The former value is the average crustal density (Stacey, 1969, p. 287) and is in accord with common densities of metamorphic rocks such as amphibolites and schists (Clark, 1966, p. 26). A magma density of 2.54 grams per cubic centimeter is arrived at by choosing a density of 2.70 grams per cubic centimeter, which is at the low end of the range of densities for basalt (Clark, loc. cit., p. 20), and correcting for volumetric thermal expansion, using an estimated average coefficient of $50 \times 10^{-6}/^{o}C$, (see Clark, loc. cit., p. 93). Using these numbers, the fractional density difference between the basement rocks and magma is about 0.1. If the critical value of h/a for Fort Rock is chosen, namely h/a = 1, then h = 1 kilometer. Limiting values of the relative driving pressure can now

be obtained using limiting values of ℓ . For ℓ = 0.25 kilometer, $\frac{\sigma_o}{\rho_p gh}$ = 0.025; for ℓ = 33 kilometers, $\frac{\sigma_o}{\rho_p gh}$ = 3.3 . Limiting values of of $\frac{\sigma_o}{\rho_p gh}$ = 0.033 and 3.3 were used in figures 15 and 16. A value of $\frac{\sigma_o}{\rho_p gh}$ = 0.033 corresponds to a driving pressure , σ_o, of about 0.01 kb. A value of $\frac{\sigma_o}{\rho_p gh}$ = 3.3 corresponds to a pressure , σ_o , of about 1 kb. A value of $\frac{\sigma_o}{\rho_p gh}$ = 0.5 was used in calculating velocities and stresses (fig. 17 ; Table 9 through 11). This value corresponds to a driving pressure , σ_o , of about 0.15 kb.

Effective Viscosity of Highly Fractured Precambrian Rock

If the value of the quantity $\frac{\rho gh}{2}(\frac{t}{\eta})$ has a value A , then

$$\eta = \frac{t}{A}\frac{\rho gh}{2} \qquad (126)$$

An upper limit on the time, t , involved in the formation of Fort Rock dome has been established as 31,700 years. A value of $H(r=0)/a$ = 0.25 for the dome requires that A be, at the smallest, 0.01 (fig. 16). Therefore an upper limit on viscosity, η , is

$$\eta = 1.4 \times 10^{22} \text{poises} \qquad \underline{\text{upper limit}}$$

where we have used ρ = 2.84 grams per cubic centimeter and h = 1 kilometer. Since the time of formation of the dome will probably not differ by an order of magnitude from 10^4 years and since the critical value of A is 1 for Fort Rock dome, a probable value of the viscosity, η , is

$$\eta = 4.4 \times 10^{20} \text{poises} \qquad \underline{\text{probable value}}$$

The viscosity given here is the effective viscosity for highly fractured Precambrian basement rocks underlying Fort Rock dome.

For comparison, Haskell (1935) obtains an effective kinematic viscosity, η/ρ , of 2.9×10^{21} square centimeters per second for viscous flow in the earth's mantle during the post-glacial rebound in Fennoscandia. Using a density of 3 grams per cubic centimeter for the mantle; the mantle's viscosity would, thus, be about 10^{22} poises. The physics of flow are, of course, much different in the Fort Rock dome than they are in the earth's mantle. In the dome, "flow" takes place by movement along numerous fractures in the rocks. Temperatures and pressures are low. In the mantle, temperatures are high and pressures are enormous. It is perhaps reasonable that the effective viscosity of rocks in the dome should be lower than that of rocks in the mantle, but the fact that they differ by only a factor of about 20 is surprising.

Faults and Breccia Lenses

Two assumptions about material properties are inherent in an assumption of perfect viscosity for the fluid in the mathematical model. The first is an assumption of zero yield strength, or continuous failure. The second is an assumption that stress is proportional to the strain rate. In the Fort Rock dome, rock is so thoroughly fractured that it is conceivable that the effective rock strength was indeed small compared to stresses developed. Of course, some doming must have occurred before the rock became thoroughly fractured. The response of fractured rock to stress is, of course, unknown. The

assumption of a linear stress-rate-of-strain relationship is an approximation at best. Without understanding the physics of doming at Fort Rock, the best one can hope to do is examine structure in the dome to see if it is consistent with structure predicted by the model. In particular, are shear features in the dome, e.g., faults and lenses of breccia, similar to shear features in the model?

Mapped faults on the Fort Rock dome include radial to subradial faults, tangential faults, and gravity-thrust faults bounding some landslide blocks. The latter faults are not of interest in this discussion. Both radial and tangential faults are steep-dipping in all places where attitudes can be determined. Faults on the north side of the dome involve block rotations (fig. 7). Radial faults on the west and south sides of the dome probably involve relative movement perpendicular to contact planes, which dip steeply. These faults, therefore, show a combination of dip-slip and strike-slip movement. Faults similar to these are also seen on the north flank of Three OClock Hill. Tangential faults on the east side of the dome are apparently derived from pre-dome structures. The Upper Two OClock Gap fault is definitely a reactivated pre-dome fault, and the Four OClock Hill fault may represent renewed movement on a pre-dome fault on Four OClock Hill. The Eight OClock Gorge faults, on the other hand, are tangential reverse faults which occurred during doming.

Steep-dipping, subradial planes of combined normal and strike-slip shear are generated in the model near the edge of the dome (Table II). Displacement is such that on shear planes which are not quite radial the downthrown side occurs on the side of the plane away

from the center of the crater. This sense of displacement is seen on at least parts of all faults on the north side of the dome, with the exception of the One OClock Hill fault (pl. 1). On the latter fault the downthrown side is toward the center of the dome. The Three OClock Hill fault is also an exception. The sense of displacement predicted by the model is , seen on virtually all faults on the west and south sides of the crater and on faults on the north side of Three OClock Hill.

Tangential shear is not generated in the model except at deep horizons beneath the dome. It is encountered (Table 11) below a horizon of $\hat{z} = -0.9$. For an optimum, or probable, layer thickness of h = 1 kilometer, this horizon is about 650 feet below the original surface of the land at the Fort Rock dome and would be found at an elevation of about 4350 feet above sea level. The sense of displacement on these deep tangential shear planes in the model is opposite that of the Upper and Lower Two OClock Gap faults and the Four OClock Hill fault. The fact that tangential faults occur at the surface of Fort Rock dome and are of the wrong sense of displacement when compared with the model leads one to suspect that a different stress regime from that used in the model was responsible for them. These faults may represent collapse of the dome, which is brought about by venting of the magma, or they may represent uneven uplift due to some irregularity in the magma chamber below. Collapse is perhaps the simplest and most appealing interpretation from the standpoint of the model. On the other hand, one interpretation from the standpoint of geologic history (p. 189) is that these faults are not primarily

collapse features but were active throughout doming with the senses of displacement such that blocks toward the center of the crater were relatively down. Irregularities in the magma chamber during doming might have developed because of the fact that the Upper Two OClock Gap fault and possibly the Four OClock Hill fault are structures which predate the formation of the dome.

Tangential reverse shear is predicted by the model everywhere beyond the edge of the dome, or beyond $\hat{r} = 1.0$. The Eight OClock Gorge faults are tangential reverse faults which lie about on the edge of the dome. They appear to be consistent with the predicted shear.

In addition to faults shown on the map, abundant small faults, with displacements of inches to feet, and lenses of open, unmineralized breccia are found throughout the dome and were apparently caused by doming. The spatial density of the faults and maximum thickness of breccia lenses is apparently greatest near a radius of about 2500 feet (fig. 8), which would correspond to $\hat{r} = r/a = \frac{2500 \text{ feet}}{3500 \text{ feet}} \simeq 0.7$. Most measurements of fault densities and breccia lenses were made at an elevation of about 5100 feet, which is only about 100 feet above the average level of the pre-dome ground surface. For purposes here, we shall consider that these measurements were made at a horizon, $\hat{z} = -1.0$.

The model predicts (Table 11) the highest maximum shear stress, $S = 0.45\sigma_o$, at $\hat{r} = 0$ and $\hat{z} = -1.0$. S drops to less than a third of this value, $0.13\sigma_o$, at $\hat{r} = 1.0$ and $\hat{z} = -1.0$. One might expect the spatial density of faults and maximum thickness of breccia lenses in the Fort Rock dome to reflect maximum shear stresses, in that higher

values of these quantities would be found where S is higher. If this assumption is correct, it is clear that these quantities do not follow the pattern predicted by the model for $\hat{z} = -1.0$. The pattern in the dome actually resembles closely a pattern predicted by the model for horizons $\hat{z} = -0.7$ and deeper, which would be found beneath Fort Rock dome at an elevation of 4000 feet above sea level and lower.

The discrepancy between the fault and breccia pattern in the dome and the pattern of maximum shear predicted by the model might be explained in one of four ways. First, the assumption of a correlation between S and fault density or breccia thickness may be wrong. Secondly, stress patterns predicted by the model in Tables 9 through 11 for $\frac{\rho g h}{2}(\frac{t}{\eta}) = 0.1$ may be much different from those encountered at a value of $\frac{\rho g h}{2}(\frac{t}{\eta}) = 1$, which is appropriate for the Fort Rock dome. Thirdly, the geometry of applied stress beneath the Fort Rock dome might have been different from the smooth Bessel-shaped geometry used in the model. Fourthly, the actual rheology of rocks underlying the Fort Rock dome might lead to a somewhat different pattern of deformation from that arising from the viscous rheology in the model. Examining stresses generated in the model for values of $\frac{\rho g h}{2}(\frac{t}{\eta})$ slightly higher and slightly lower than 0.1 reveals that spatial patterns of stress remain similar, but that the difference between stress maxima and minima decreases slightly for higher stress values; thus, the second explanation above is unlikely. Either the third or fourth explanation seems most likely. The concentration of deformation toward the edge of Fort Rock dome, including the existence of a sharp monocline, suggests, on one hand, that the magma chamber below may

have sharp corners. On the other hand, a nonlinear rheology, such as one characterized by creep, might produce such deformation without requiring sharp corners on the magma chamber. In a nonlinear rheology, there is a tendency for deformation to concentrate into narrow zones (Yokobori, 1964).

Open breccia is formed during normal faulting and in cases of strike-slip faulting where normal stress across the fault plane is less than hydrostatic pressure (Anderson, 1942, p. 18). The existence of lenses of open breccia in Fort Rock dome is thus consistent with the regime of normal shear predicted beneath the dome by the model.

History of Doming

Uplift at the Fort Rock dome was rapid prior to extrusion of the Fault Canyon flow. Abnormal stream gradients appear to have existed on the dome (fig. 9, Maps 8 through 10) and units of massive sedimentary breccia were deposited on the flanks of the dome. It is possible that doming was actually accelerating as is suggested in figure 11; acceleration is predicted by the model.

Halting of uplift of the Fort Rock dome is most conspicuously related to extrusion of the Fault Canyon flow. Little, if any, continued doming is needed to explain attitudes within units on the flanks of the dome that are younger than this flow. Collapse may have, in fact, occurred. The radial faults on the north side of the dome occurred largely after extrusion of the Fault Canyon flow, but it is difficult to determine whether they represent collapse of certain segments on the dome's periphery or lagging behind of these segments

during continued doming. Except for the One OClock Hill fault, all of these faults are consistent with (continued) doming as described by the model. The Upper and Lower Two OClock Gap fault and the Four OClock Hill fault are, on the other hand, inconsistent with doming as described by the model. Either doming was irregular in these areas or these faults represent collapse.

Crystallization of the Magma

The Fault Canyon flow is interpreted to be an extrusive part of the magma which caused doming. The flow may not, however, be a representative sample of the magma. At the time of vent formation, the Fault Canyon flow was between 12 percent and 38 percent crystallized. The sum of olivine phenocrysts and colorless cores of pyroxene phenocrysts in the rock is 12 percent (see p. 98); the sum of all mafic minerals in the rock is 38 percent, the rest of the rock being essentially sanidine, which is last to crystallize. The body of magma beneath the dome, on the other hand, may have been much more highly crystallized if extensive crystal settling had taken place. In this case, the Fault Canyon flow may be representative only of the liquid fraction of the magma which occupied the upper part of the magma chamber.

According to the model, uplift of the Fort Rock dome would be expected to continue after the vent for the Fault Canyon flow was plugged. Acceleration would be proportional to the fraction of the magma that was still liquid. Continued doming was, however, small in magnitude. If the Fault Canyon flow is representative of the magma, a great deal of crystallization must have taken place shortly after the

flow was extruded. If the flow is representative only of the upper liquid fraction of the magma, then that fraction was probably relatively small at the time of venting.

SUMMARY

The mathematical model that is developed in this chapter is a description of viscous doming which is physically reasonable for $H(\hat{r} = 0)/a$ or $Z(\hat{r} = 0)/a$, equal to 0.1 or smaller. In this range of distortion the model fits proper boundary conditions to a good approximation and behaves in an expected fashion. For distortions greater than 0.1 the correlation of the model to real doming in a viscous fluid is uncertain.

The model is applied to the Fort Rock dome, where the dome distortions, $H(\hat{r} = 0)/a$, is 0.25, in order to make order-of-magnitude arguments for certain quantities of interest. Within a range of $Z(\hat{r} = 0)/h$ and $H(\hat{r} = 0)/a$ defined to include Fort Rock dome, it was found that values of the quantities h/a and $\frac{\rho g h}{2}(\frac{t}{\eta})$ which produce the largest domes remain close to 1 over a wide range of driving pressure, $\sigma_0/\rho gh$. Assuming that these "critical" values are more or less correct for the Fort Rock dome, a "layer" thickness, h, and a probable effective viscosity η for the fractured Precambrian rocks beneath the dome are calculated. For a radius, a, of 1 kilometer, the layer thickness is 1 kilometer. This thickness is the depth of the magma chamber when doming began to be felt significantly at the surface. For a time, t, of the order of 10^4 years, the time required to crystallize the magma beneath the dome, an effective viscosity for the fractured

Precambrian rocks is calculated to be 4.4×10^{20} poises. An upper limit on the layer thickness, h , was found to be about 1.25 kilometers, from which it was concluded that the maximum depth to the present top of the magma chamber is 1 kilometer; the top may lie anywhere above this depth. Geologic arguments set lower and upper limits on the length of the magma chamber at 0.25 kilometers and 33 kilometers, respectively. Corresponding limits on the driving pressure are estimated to be 0.01 kilobar and 1 kilobar.

In the model, planes of maximum shear are generated which are consistent with most mapped faults on the Fort Rock dome. Near the surface of the dome in the model, these planes are radial to subradial and steep-dipping and show a combination of normal and strike-slip shear. Deep beneath the dome, they are tangential and show normal shear. Beyond the edge of the dome they are tangential and show reverse shear. Several tangential faults on the east side of Fort Rock dome are inconsistent with shear planes generated in the model and either represent collapse of the dome, following a venting of the magma or reflect some irregularity in the magma chamber at depth. The spatial density of numerous unmapped faults of small displacement in Fort Rock dome follows a pattern which appears inconsistent with the pattern of maximum shear stresses given by the model. This discrepancy can be explained if either the magma chamber beneath Fort Rock dome had sharp corners or the rocks underlying the dome had a nonlinear rheology, e.g., a rheology characterized by creep.

According to the model, doming is an accelerating process which can be halted by formation of a vent or solidification of the magma causing the uplift. Upon formation of a vent, doming decelerates, and

collapse occurs in some cases. After the vent is sealed, doming continues at a lesser acceleration until the magma solidifies. In Fort Rock dome most of this predicted sequence of events is seen. Doming was rapid and may well have been accelerating prior to extrusion of the Fault Canyon flow. Following extrusion of this flow, little if any continued doming is indicated and some collapse may have occurred. From the lack of significant continued doming, it is concluded that either solidification of the magma was rapid after extrusion of the Fault Canyon flow, or the magma was largely solidified at the time of extrusion.

REFERENCES CITED

Anderson, C. A., 1967, Precambrian wrench fault in central Arizona: U.S. Geol. Survey Prof. Paper 575-C, p. C60-C65.

Anderson, C. A., Blacet, P. M., Silver, L. T., and Stern, T. W., 1971, Revision of Precambrian stratigraphy in the Prescott-Jerome area, Yavapai County, Arizona: U. S. Geol. Survey Bull. 1324-C, 16 p.

Anderson, C. A., and Creasey, S. C., 1958, Geology and ore deposits of the Jerome area, Yavapai County, Arizona: U. S. Geol. Survey Prof. Paper 308, 184 p.

Anderson, C. A., Scholz, E. A., and Strobell, J. D., Jr., 1955, Geology and ore deposits of the Bagdad area, Yavapai County, Arizona: U. S. Geol. Survey Prof. Paper 278, 103 p.

Anderson, E. M., 1942, The dynamics of faulting and dyke formation: London, Oliver and Boyd, 191 p.

Barnes, W. C., (revised and enlarged by Granger, B. H.), 1960, Arizona place names: Tuscon, Univ. of Ariz. Press, 519 p.

Bateman, H., Erdelyi, A., (ed.), and others, 1953, Higher transcendental functions: New York, McGraw Hill, v. II, 396 p.

Boyce, J. M., 1972, The structure and petrology of the older Precambrian crystalline rocks, Bright Angel Canyon, Grand Canyon, Arizona: masters thesis, Northern Arizona University, 88 p.

Bullen, K. E., 1963, An introduction to the theory of seismology: Cambridge University Press, 381 p.

Carslaw, H. S., and Jaeger, J. C., 1959, Conduction of heat in solids: London, Oxford Univ. Press, 2nd ed., 510 p.

Clark, S. P., 1966, Handbook of physical constants: Geol. Soc. America Mem. 97, 587 p.

Damon, P. E., 1964, Correlation and chronology of ore deposits and volcanic rocks: Tuscon, Univ. of Ariz., Geochronology Labs., Ann. Prog. Rept. No. COO-689-42 to the Research Div., U.S. Atomic Energy Comm., 117 p.

_____ 1968, Correlation and chronology of ore deposits and volcanic rocks: Tuscon, Univ. of Ariz., Geochronology Labs., Ann. Prog. Rept. No. COO-689-100 to the Research Div., U.S. Atomic Energy Comm. p. 48-52.

Davis, W. M., 1931, The Peacock Range, Arizona: Geol. Soc. America Bull. 41, p. 293-313.

Elston, D. P., Grommé, C. S., and McKee, E. H., 1973, Precambrian polar wandering and behavior of the earth's magnetic field from stratified rocks of the Grand Canyon Supergroup, Arizona: Geol. Soc. America, Abs. with Programs, v. 5, p. 611.

Fenneman, N. M., 1931, Physiography of western United States: New York, McGraw Hill, 1st ed., 534 p.

Gilbert, G. D., 1880, Report on the geology of the Henry Mountains: Washington, U.S. Govt. Printing Office, 2nd ed., 170 p.

Green, C. R., and Sellers, W. D., 1964, Arizona climate: Tuscon, Univ. of Ariz. Press, 503 p.

Haskell, N. A., 1935, The motion of a viscous fluid under a surface load: Physics, v. 6, p. 265-269.

Hobbs, S. W., 1944, Tungsten deposits in the Borina district and in the Aquarius Range, Mohave County, Arizona: U.S. Geol. Survey Bull. 940-I, p. 247-264.

Irvine, T. N., 1970, Heat transfer during solidification of layered intrusions. I. Sheets and Sills: Canadian Jour. of Earth Sci., v. 7, p. 1031-1061.

Jaeger, J. C., 1956, Elasticity, fracture, and flow: New York, Wiley, 152 p.

Johnson, L. R., 1967, Array measurements of P velocity in the upper mantle: Jour. Geophys. Research, v. 72, p. 6309-6325.

Koons, E. D., 1948, Geology of the eastern Hualpai Reservation (Arizona): Plateau, v. 20, p. 53-60.

_____ 1964, Structure of the eastern Hualpai Indian Reservation: Ariz. Geol. Soc. Digest, v. 7, p. 97-114.

Krieger, M. H., 1965, Geology of the Prescott and Paulden quadrangles, Arizona: U. S. Geol. Survey Prof. Paper 467, 127 p.

Krieger, M. H., 1967, Reconnaissance geologic maps of the Turkey Canyon, Camp Wood, Simmons, Iron Springs, and Sheridan Mountain quadrangles, Yavapai County, Arizona: U. S. Geol. Survey, Misc. Geol. Investigations, Maps I-501 through I-505.

Landau, L.D., and Lifschitz, F.M., 1959, Fluid Mechanics: London, Pergamon Press, 536p.

Lucchita, I., 1972, Early history of the Colorado River in the Basin and Range Province: Geol. Soc. America Bull., v. 83, p. 1933-1948.

Maxon, J. H., 1961, Geologic history of the Bright Angel quadrangle, in Geologic map of the Bright Angel quadrangle: Grand Canyon Natural History Assoc., 2nd. ed., revised 1966.

McKee, E. H., and Anderson, C. A., 1971, Age and chemistry of Tertiary volcanic rocks in north-central Arizona and their relation to the Colorado Plateaus: Geol. Soc. America Bull, v. 82, p. 2767-2782.

McKee, E. D., and McKee, E. H., 1972, Pliocene uplift of the Grand Canyon region -- time of drainage adjustment: Geol. Soc. America Bull, v. 83, 1923–1931.

McKee, E. D., Wilson, R. F., Breed, W. J., and Breed, C. S., 1964 Evolution of the Colorado River: Flagstaff, Arizona, Museum of Northern Arizona.

Morse, P.M., and Feshbach, H., 1953, Methods of theoretical physics: New York, McGraw Hill, part I, 997 p.

Nadai, A., 1950, Theory of flow and fracture in solids: New York, McGraw Hill, v. I, 2nd. ed., 572 p.

Noble, L. F., and Hunter, J. F., 1916, a reconnaissance of the Archean complex of Granite Gorge, Grand Canyon, Arizona: U. S. Geol. Survey Prof. Paper 98-I, p. 95-113.

Nockolds, S. R., 1954, Average chemical compositions of some igneous rocks: Geol. Soc. America Bull., v. 45, p. 1007–1032.

Pasteels, P., and Silver, L. T., 1965, Geochronologic investigations in the crystalline rocks of the Grand Canyon, Arizona: Geol. Soc. America Special Paper 87, p. 124.

Rascoe, J., 1968, Old Arizona treasures: Fort Davis, Texas, Frontier Book Company, 120 p.

Ross, C. S., and Smith, R. L., 1961, Ash-flow tuffs: their origin, geologic relations, and identification: U. S. Geol. Survey Prof. Paper 366, 81 p.

Sauck, N. A., and Sumner, J. S., 1970, Residual aeromagnetic map of Arizona: Tuscon, Univ. of Ariz., Dept. of Geosciences.

Sheppard, R.A.,and Gude, A. J., 1972, Big Sandy Formation near Wikieup, Mohave County, Arizona: U. S. Geol. Survey Bull. 1354-C, p. 1-10.

Shoemaker, E. M., Elston, D. P., Squires, R. L., and Abrams, M. J., in press, Bright Angel and Mesa Butte fault systems of northern Arizona: Plateau.

Stacey, F. D., 1969, Physics of the Earth: New York, Wiley, 324 p.

Thomas, G. B., 1961, Calculus and Analytic Geometry: Reading, Mass., Addison-Wesley, part I, 602 p.

Wayland, H., 1957, Differential equations applied in sciace and engineering: New York, D. van Nostrand, 353 p.

Williams, H., 1936, Pliocene volcanoes of the Navajo-Hopi country: Geol. Soc. America Bull., v. 47, p. 111.

Williams, H., Turner, F. J., and Gilbert, C. M., 1954, Petrography: San Francisco, W. H. Freeman, 406 p.

Wilson, E. D., Moore, R. T., and Cooper, J. R., 1969, Geologic map of Arizona: Ariz. Bur. of Mines and U. S. Geol. Survey.

Yokobori, T., 1964, The strength, fracture, and fatigue of materials: Gröningen, Netherlands, P. Noordhoff, 372 p.

Young, R. A., 1966, Cenozoic geology along the edge of the Colorado Plateau in northwestern Arizona: Ph.D. thesis, Washington University, 167 p.

Young, R. A., and Brennan, W. J., in press, The Peach Springs Tuff: its relation to the structural evolution of the Colorado Plateau and the origin of the Colorado River in Mohave County, Arizona: Geol. Soc. America Bull.

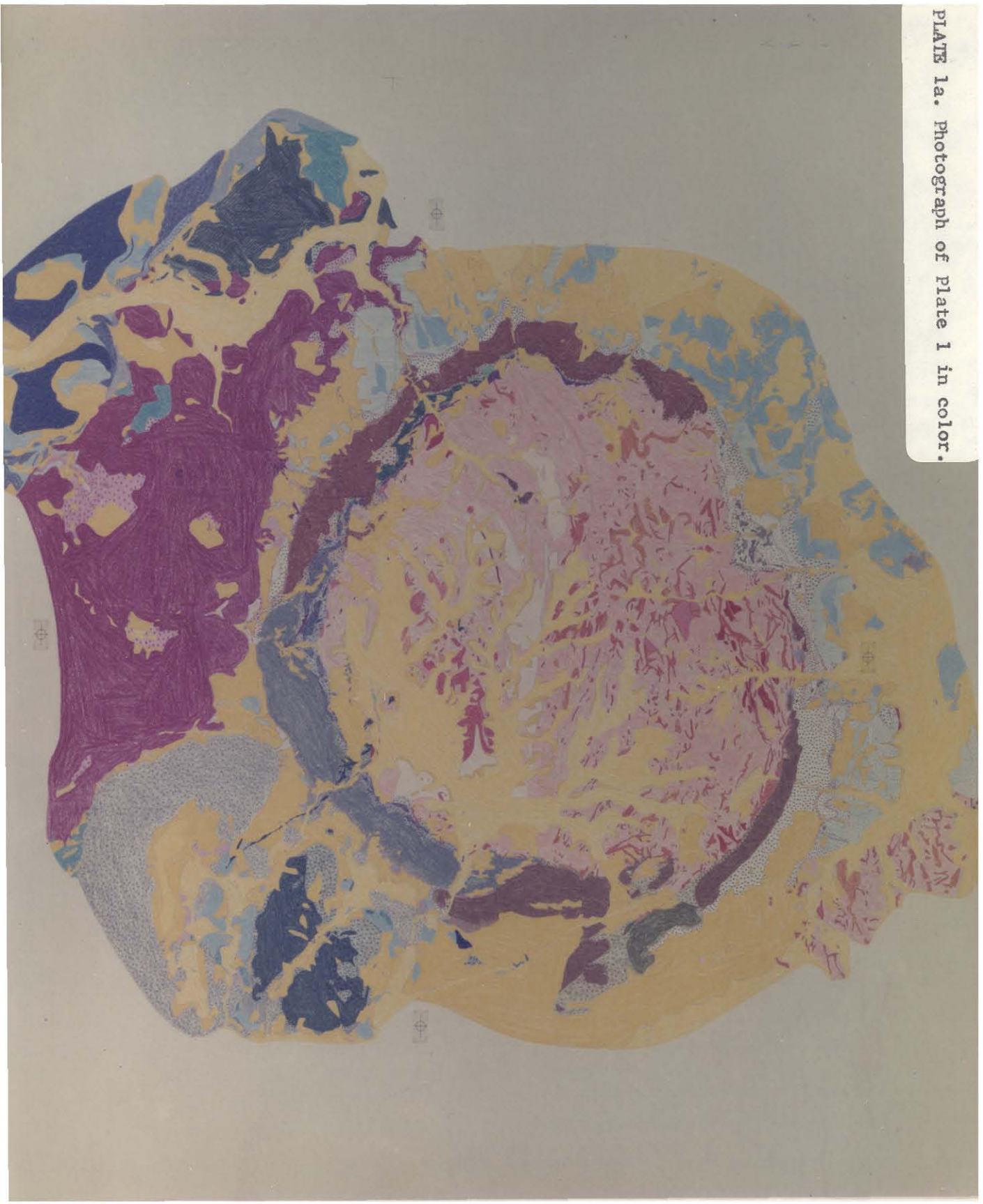

PLATE 1a. Photograph of Plate 1 in color.